Julius-Maximilians-Universität Würzburg

Fakultät für Biologie

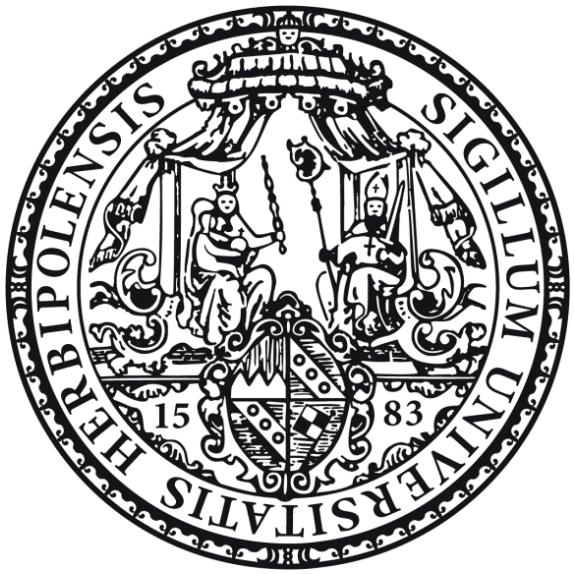

Characterization of Murine GL261 Glioma Models for Oncolytic Vaccinia Virus Therapy

Dissertation

Zur Erlangung des naturwissenschaftlichen Doktorgrades der Julius-Maximilians-Universität Würzburg

vorgelegt von Christina Kober
aus Altburg

Würzburg, 2015

Eingereicht am: _____

Mitglieder der Promotionskommission:

Vorsitzender: _____

Erstgutachter: _____
Prof. Dr. A. A. Szalay

Zweitgutachter: _____
Prof. Dr. T. Dandekar

Tag des Promotionskolloquiums: _____

Doktorurkunde ausgehändigt am: _____

„Nicht die Dinge und Ereignisse selbst kann ich verändern, wohl aber das Licht in dem ich sie betrachte“

(Marc Aurel)

Table of Contents

Zusammenfassung

Glioblastoma multiforme (GBM) ist eine der häufigsten und bösartigsten Formen von Hirntumoren im Erwachsenenalter und trotz intensiver Forschung ist die Prognose für GBM mit einer durchschnittlichen Überlebenszeit von 12-15 Monaten sehr schlecht. Die Behandlung von GBM wird durch multiple Faktoren erschwert: Das aggressive und infiltrative Wachstum des Tumors in das Hirnparenchym, die histologische Heterogenität der Tumormasse, die Lage des Tumors innerhalb des Gehirns, die Infiltration des Tumors mit Mikroglia/Makrophagen und die Funktion und Morphologie der Blut-Hirn-Schranke. Es gibt eine Anzahl alternativer Behandlungsmöglichkeiten, die in präklinischen und klinischen Studien für GBM untersucht werden, wobei eine dieser Methoden die onkolytische Virustherapie ist. Ein onkolytisches Virus ist dadurch definiert, dass es sich selektiv in Krebszellen repliziert, normale Körperzellen und Gewebe aber unversehrt bleiben. Ein äußerst vielversprechender Kandidat für die onkolytische Virustherapie ist das Vaccinia-Virus. Es ist sehr gut charakterisiert, repliziert sich im Zytoplasma der Wirtszelle und es können große DNA-Fragmente in das Virusgenom inseriert werden. Oftmals existiert eine große Diskrepanz zwischen der onkolytischen Effektivität, welche in Zellkultur für ein bestimmtes Modell festgestellt werden kann und den Ergebnissen im Mausmodell. Sie spiegelt sich auch in einer verminderten therapeutischen Effektivität in aktuellen klinischen Studien wider. Dies legt den Schluss nahe, dass physiologische Aspekte des Tumor-Mikromilieus und Abwehrmechanismen des Wirts das therapeutische Potenzial des Virus verringern können. Aus diesem Grund sind weiterführende präklinische Studien notwendig, um die Mechanismen zu verstehen, die zu einer verminderten Wirksamkeit der Therapie führen. Der Anteil und die Zusammensetzung von Immunzellen variiert sehr stark zwischen verschiedenen Krebsarten und Patienten und wird zunehmend als Biomarker angewendet. Grundlage dieser Arbeit war, dass eine erfolgreiche Virustherapie bei GBM ein umfangreiches Verständnis der Tumorbiologie, des Tumormikromilieus und des Immunsystems erfordert.

In Zellkultur wurde zunächst gezeigt, dass sich LIVP 1.1.1, ein attenuiertes wildtypisches VACV-Isolat, in der murinen GL261 Gliom-Zelllinie in Zellkultur repliziert und dass das Virus effizient zum Absterben der Zellen führt. Im nächsten Schritt wurde die Replikationseffizienz von LIVP 1.1.1 durch einen vergleichenden Ansatz in murinen GL261-Gliomen im Mausmodell untersucht. Für diese Studien wurden immunkompetente C57BL/6 wildtypische Mäuse und immundefiziente Mausstämme mit unterschiedlichem genetischem Hintergrund, C57BL/6 athymisch und Balb/c athymisch, verwendet. Zudem wurden unterschiedliche Tumor-Lokalisationen, subkutan und

intrakranial/orthotop, analysiert. Es wurde gezeigt, dass ausschließlich im subkutanen Tumormodell der Balb/c athymischen Mäuse eine effektive Replikation der Viren stattfand. In allen anderen Modellen kam es nicht zur produktiven Vermehrung der Viruspartikel über die initial applizierte Virusdosis hinaus. Konsistent dazu wiesen alle subkutanen Tumormodelle ein sehr aggressives Tumorwachstum auf, wobei eine signifikante Wachstumsverzögerung durch das Virus ausschließlich in Balb/c athymischen Mäusen erreicht werden konnte. Da sich der Virustiter bereits einen Tag nach Infektion signifikant zwischen den Mausmodellen unterschied, konnte davon ausgegangen werden, dass die Unterschiede bereits vor Infektion bestanden. Es erfolgte eine detaillierte Charakterisierung des Tumormikromilieus der subkutanen Tumormodelle mittels Biomarker-Analyse, einem Immunzell-Profiling sowie einer immunhistochemischen Charakterisierung des Tumors. Dadurch konnte gezeigt werden, dass die Implantation derselben Tumorzellen in unterschiedliche Mausstämme zur Entwicklung eines komplett unterschiedlichen Tumormikromilieus mit einer individuell variierenden Zusammensetzung von Immunzellen führt, mit den größten Unterschieden zwischen immunkompetenten und immundefizienten Mäusen. Die wildtypischen C57BL/6-Mäuse wiesen eine starke proinflammatorische Signatur im Vergleich zu den athymischen Mäusen auf. Des Weiteren zeigte die Studie signifikante Unterschiede in der MHCII-Expression. Die prominenteste Expression konnte in wildtypischen C57BL/6-Mäusen detektiert werden, gefolgt von C57BL/6 athymischen Mäusen und schließlich Balb/c athymischen Mäusen. Im weiteren Verlauf wurde analysiert, wodurch die phänotypischen Veränderungen in den GL261-Zellen, verbunden mit der Hochregulierung von MHCII, in den subkutanen Tumoren der wildtypischen C57BL/6 Mäusen ausgelöst wurden und welche Konsequenzen dies für die virale Infektion dieser Zellen hat. Stimulationsexperimente in Zellkultur zeigten, dass es auf GL261-Zellen nach Stimulation mit IFN-γ zu einer zeit- und dosisabhängigen Erhöhung von MHCII kommen kann und diese GL261-Zellen im Folgenden zwar infiziert wurden, aber keine produktive virale Replikation stattfand. Durch einen direkten Vergleich von wildtypischen C57BL/6-Mäusen und C57BL/6-IFN-γ-Knockout Mäusen konnte IFN-γ eindeutig als verantwortlicher Faktor im Tumormikromilieu identifiziert werden, welcher für die Reduktion des Virustiters und für die Hochregulierung von MHCII in den wildtypischen C57BL/6-Mäusen verantwortlich ist. Dabei war der durch endogenes IFN-γ ausgelöste anti-virale Effekt reversibel und konnte durch zeitweise Kultivierung in Zellkultur aufgehoben werden.

Des Weiteren wurden Gründe für die Hemmung der viralen Replikation und der Eliminierung des Virus in den orthotopen Gliom-Modellen aufgeklärt. In einem ersten Schritt wurden hierzu immunhistochemische Analysen von Mikroglia und Astrozyten in nicht-infizierten sowie PBS-

oder LIVP 1.1.1-infizierten GL261-Tumoren in wildtypischen C57BL/6-Mäusen durchgeführt. Dabei konnte gezeigt werden, dass die intratumorale Menge und Verteilung der Gliazellen in diesen Tumoren unabhängig von der Vaccinia-Virus-Applikation war und die Gliazellen vielmehr als Reaktion auf den Tumor selbst verstärkt rekrutiert wurden. Basierend auf diesem Ergebnis wurden die drei beteiligten Hauptzelltypen, Gliomzellen, Mikroglia und Astrozyten, im Detail untersucht. Dafür wurde die Replikation von LIVP 1.1.1 in GL261-Gliomzellen, in der Mikrogliazelllinie BV-2 und der Astrozytenzelllinie IMA 2.1 verglichen. Es konnte gezeigt werden, dass im Vergleich zur starken Replikation in GL261-Zellen, BV-2- sowie IMA 2.1-Zellen, nur eine sehr schwache, nicht-produktive Replikation von LIVP 1.1.1 zuließen. Direkte Ko-Kultivierungsversuche von BV-2- und GL261-Zellen wiesen darauf hin, dass Mikrogliazellen um die Aufnahme der Viruspartikel mit den Tumorzellen konkurrieren. Des Weiteren zeigten Apoptose/Nekrose-Studien, dass das Vaccinia-Virus LIVP 1.1.1 unterschiedliche Eigenschaften des Zelltods in den unterschiedlichen Zellen auslösen kann. So wiesen BV-2-Mikroglia verstärkte Charakteristika der Apoptose auf während in GL261-Tumorzellen nekrotische Eigenschaften überwogen. Im Falle von BV-2- und IMA 2.1-Zellen wurde zusätzlich der von Makrophagen bekannte M1-Phänotyp (klassisch aktiviert; anti-tumor Aktivität) oder M2-Phänotyp (alternativ aktiviert; pro-tumor Aktivität) in Hinblick auf die VACV LIVP 1.1.1 Infektion untersucht: In BV-2-Zellen mit M1-Phänotyp konnte eine weitere Reduktion der viralen Infektion festgestellt werden. Die Infektion von IMA-2.1-Zellen war unabhängig vom induzierten Phänotyp. Die Applikation von BV-2-Zellen mit M1-Phänotyp auf organotypische Schnittkulturen mit implantierten GL261-Tumoren resultierte in einer reduzierten Infektion der BV-2-Zellen mit LIVP 1.1.1 und im Gegenzug in einer verstärkten Infektion der GL261-Tumorzellen.

Zusammenfassend konnte gezeigt werden, dass die GL261-Tumore durch den immunologischen und genetischen Hintergrund der Umgebung geprägt wurden. Es konnte ein Modell entwickelt werden, welches das Prinzip der personalisierten Medizin widerspiegelt: In den subkutanen oder orthotopen GL261-Tumoren in unterschiedlichen Mausstämmen entwickelte sich ein individuelles Tumormikromilieu mit einer unterschiedlichen Zusammensetzung an Immunzellen welche unterschiedlich auf die onkolytische VACV Therapie ansprachen.

In einem zusätzlichen Projekt wurde, basierend auf Genexpressionsdaten und bioinformatischer Auswertung (Dr. J. Reinboth, Dr. A. Cecil), die biologische Funktion des anti-apoptotischen Faktors AVEN hinsichtlich der onkolytischen Virustherapie mit dem VACV GLV-1h68 analysiert. Für diese Studie wurden vier humane Zelllinien unterschiedlichen histologischen Ursprungs (888-MEL, 1936-MEL, GI-101A, HT-29) untersucht. Neben einem Vergleich der Replikationseffizienz des VACV GLV-1h68 und der VACV-vermittelten Zelllyse dieser Zellen wurde gezeigt, dass AVEN,

auf Basis der RNA- und Proteinebene, in allen untersuchten Zellen exprimiert wird. Außerdem wurde am Beispiel von HT-29 und 1936-MEL in Zellkultur gezeigt, dass die Herunterregulierung von AVEN durch siRNA in diesen Zellen zu einer Erhöhung der apoptotischen Eigenschaften und einer Abnahme der VACV Infektion führt. Die Ergebnisse dieser Zellkulturstudien liefern wichtige Erkenntnisse für die Entwicklung zukünftiger genetisch veränderter VACV, welche eine erhöhte therapeutische Wirksamkeit *in vivo* aufweisen sollten.

Summary

Glioblastoma multiforme (GBM) is one of the most frequent and most malignant form of brain cancer in adults. Despite extensive research the prognosis is very poor with a median survival time of 12-15 months. Difficulties associated with treatment of GBM are the highly aggressive and infiltrative nature of the tumor into the brain parenchyma, the histological heterogeneity of the tumor mass, the location within the brain, the infiltration of the tumor with microglia/macrophages and the function as well as the morphology of the blood brain barrier. There is a broad range of alternative treatment options studied in preclinical and also clinical trials for GBM. One of those is oncolytic virotherapy, defined as the use of replication-competent viruses that selectively infect, replicate in and destroy cancer cells while leaving normal, non-transformed cells and tissues unharmed. Vaccinia virus (VACV) is a favorable candidate for oncolytic virotherapy due to its great safety potential and due to its biology as a double-stranded DNA virus with the unique characteristic to only replicate in the cytoplasm without integration into the host genome. Although oncolytic viruses can kill tumor cells grown *in vitro* with high efficiency, they often exhibit reduced replication capacity *in vivo* which results in a low therapeutic efficiency in clinical trials. These findings suggest that physiological aspects of the tumor microenvironment and host defense mechanisms do decrease the virus' therapeutic potential and continued preclinical research aimed to understand and overcome virus inhibitory physiological aspects are required. The percentage and composition of immune cells varies between cancer types and patients and is investigated more and more as a biomarker in several studies. Making oncolytic virotherapy successful for GBM, it is necessary to understand the individual tumor biology as well as the interaction with the tumor microenvironment and the immune system.

In a first approach it was demonstrated by standard viral plaque assay that the attenuated VACV wild-type isolate LIVP 1.1.1 was able to replicate within the murine GL261 glioma cell line *in vitro* and the cell line was susceptible for virus-mediated cell killing. Afterwards, the replication efficacy of LIVP 1.1.1 in murine GL261 gliomas was characterized in a comparative approach *in vivo*. For this, immunocompetent C57BL/6 wild-type (wt) mice and immunodeficient mouse strains of different genetic background C57BL/6 athymic and Balb/c athymic mice were used. In addition, different tumor locations subcutaneous and intracranial/orthotopic were analyzed. The results revealed viral replication exclusively in Balb/c athymic mice with subcutaneous tumors but in none of the other models.

Consistently, all subcutaneous tumor models were characterized by rapid and aggressive tumor growth and a significant tumor growth delay after VACV LIVP 1.1.1 injection was only detected in Balb/c athymic mice with subcutaneous tumors. As the virus titer differed significantly already one day post infection the differences seem to exist already before virus infection. Therefore, a detailed characterization of the tumor microenvironment of the subcutaneous tumor models at the time of infection was performed. The experimental setup consists of a mouse immune-related biomarker analysis, a detailed immune cell profiling and an immunohistological analysis. The study showed that implantation of the same tumor cells in different mouse strains resulted in a completely different tumor microenvironment with a distinct composition of immune cells. Highest differences were detected between immunodeficient and immunocompetent mice. Further, C57BL/6 wt mice showed a highly proinflammatory signature. Additionally, the study showed major differences in the expression of MHCII. Strongest MHCII expression was detected in C57BL/6 wt, followed by C57BL/6 athymic and at least Balb/c athymic tumors. In the following, the reasons and influence on viral replication of the phenotypic change associated with the upregulation of MHCII on GL261 tumor cells in subcutaneous tumors of C57BL/6 wt mice were analyzed. The results revealed that indeed GL261 glioma cells can upregulate MHCII after stimulation with IFN-γ in a time- and dose-dependent manner. Replication analysis revealed that GL261 cells pre-incubated with IFN-γ are infected with LIVP 1.1.1, but the detected virus titer was significantly lower than in cells without stimulation. By a direct comparison between C57BL/6 wt and C57BL/6 IFN-γ knockout mice endogenous IFN-γ levels were indeed identified to upregulate MHCII on GL261 tumor cells and to reduce viral replication in C57BL/6 wt mice. Analysis of single cell suspensions of tumor homogenates of C57BL/6 and Balb/c athymic mice as control showed that the endogenous IFN-γ-mediated anti-tumor effect was a reversible effect. Furthermore, reasons for the inhibition of virus replication and elimination of virus particles in both orthotopic glioma models were elucidated. In a first step immunohistochemical analysis of microglia and astrocytes was investigated in non-, PBS- and LIVP 1.1.1-infected orthotopic GL261 gliomas in C57BL/6 wt mice. It was shown that intratumoral amounts and distribution of $Iba1^+$ microglia and $GFAP^+$ astrocytes in these tumors was independent from intratumoral VACV injection but a consequence of the tumor itself. Based on these findings the three cell types, glioma cells, microglia and astrocytes, were analyzed in detail. For this, virus replication and virus-mediated cell death of GL261 glioma cells, BV-2 microglia and IMA2.1 astrocytes were compared. It was detected that in contrast to the GL261 glioma cells, replication was barely detectable in BV-2 and IMA2.1 cells. Direct co-culture experiments between microglia and glioma cells revealed that microglia compete for virus

uptake in cell culture. Apoptosis/necrosis studies showed that VACV causes different cell death characteristics in different cell types. BV-2 cells showed apoptotic characteristics after VACV infection while GL261 cells showed signs of necrotic cell death. Additionally, in the case of BV-2 and IMA 2.1 cells the classically activated M1-phenotype (tumor inhibitory activity) and alternatively activated M2-phenotype (tumor promoting activity) initially described for macrophages were analyzed in terms of VACV LIVP 1.1.1 infection: In BV -2 cells with M1-phenotype a further reduction of viral replication and inhibition of cell lysis was detected. Infection of IMA 2.1 cells was independent of the phenotype. Application of BV-2 microglial cells with M1-phenotype onto organotypic slice cultures with implanted GL261 tumors resulted in reduced infection of BV-2 cells with LIVP 1.1.1, whereas GL261 cells were significantly infected.

Taken together, it was demonstrated that the analyzed GL261 tumors were imprinted by the immunologic and genetic background in which they grow. The experimental approach applied in this thesis can be used as suitable model which reflects the principles of personalized medicine: GL261 glioma cells implanted subcutaneously or orthotopically into Balb/c athymic, C57BL/6 athymic or C57BL/6 wt mice formed individual tumor microenvironments that respond to oncolytic virotherapy with different outcomes.

In an additional project, based on gene expression data and bioinformatic analyses (Dr. J. Reinboth, Dr. A. Cecil), the biological role and function of the anti-apoptotic factor AVEN was analyzed with regard to oncolytic VACV therapy. For this study, four human cell lines of different histologic origin (888-MEL, 1936-MEL, GI-101A, HT-29) and the VACV GLV-1h68 were used. Besides a comparison of the replication efficacy of GLV-1h68 and VACV-mediated cell killing of these cell lines, it was shown that AVEN- based on RNA and protein levels was expressed in all analyzed cells. Further, paradigmatically analyzed for HT-29 and 1936-MEL, the knockdown of AVEN by siRNA in cell culture resulted in an increase of apoptotic characteristics as measured by FACS analysis and Western blot and a decrease of VACV infection. The findings of these cell culture studies provide essential insights for future virus development, carrying a siRNA gene on a very late promoter which is assumed to increase the therapeutic efficiency *in vivo*.

1 Introduction

1.1 Cancer

Cancer is a heterogeneous group of malignant diseases that can affect any part of the body and that are still one of the world's leading causes of illness and mortality [1–4].

1.1.1 Cancer incidence, development and characteristics

In 2012, worldwide 14.1 million new cancer cases were registered, 32.6 million people were suffering from cancer within 5 years of diagnosis and 8.2 million people died as a consequence of cancer [1–3]. Lung, breast and colorectal cancer were the most frequently diagnosed types of cancer, the most common causes of cancer related deaths were lung, liver and stomach cancer [2]. The incidence of new cancer patients is expected to rise over the next two decades from 14.1 million cases in 2012 to 22 million cases [3]. Despite extensive research, most adult cancers are still not curable [2]. Besides approaches for an earlier detection and diagnosis of the disease, one major challenge for scientists and clinicians is to overcome the "robustness" of the disease that leads to therapy resistance and failure. For this, an in depth understanding of the processes of tumor development, the biology of the tumor and its interaction with the tumor microenvironment and immune system is essential [5].

From an evolutionary and ecological sight of view Merlo *et al.* [6] describe cancer as a *"disease of clonal evolution within the body"* or *"a microcosm of evolution"* where cells that acquired an accumulation of mutations in genes responsible for *e.g.* cell cycle control are in a contest for capabilities and space, evasion of the immune system and colonization to further organs [7].

The process of tumorigenesis (Figure 1a) that describes the transformation of a normal cell into a malignant cancer cell is a multistage process consisting of tumor initiation, tumor progression and metastasis [8–10]. Critical for cancer development are alterations in so-called "cancer related genes", that have been found in almost all kinds of human tumors and that in total make up more than 1% of the human genome [11].

Based on their opposite function on cell proliferation and control, cancer genes are divided into two classes: Proto-oncogenes normally stimulate cell growth and are hyperactivated during tumor development to oncogenes. Tumor suppressor genes inhibit cell division under healthy conditions and are inactivated in cancer cells [4, 9, 12, 13]. There are different mechanisms that can lead to changes in the cancer cell genome including single mutations in specific genes,

amplifications or deletions of larger parts of the genome, rearrangements of chromosomes (*e.g.* "Philadelphia chromosome") or epigenetic modifications such as DNA methylation [9, 12–15].

The process when normal cells obtain a first mutational hit resulting in enhanced proliferation or improved survival is termed the initiation phase of tumorigenesis [8, 9]. In most cases one mutation is insufficient and most cancers require at least four to five critical mutations for tumor progression [13, 14, 16, 17]. The specific and multiple genetic mutations in colon carcinoma were analyzed for the first time by Vogelstein *et al.* [16].

Only a very rare group of tumors (~5-10%) are caused by germline mutations whereas 90-95% are caused by somatic mutations due to various environmental and lifestyle factors. There are three different types of carcinogens: physical carcinogens such as ultraviolet or ionizing radiation, chemical carcinogens such as aflatoxin or tobacco smoking and biological carcinogens like chronic, virus or bacterial infections as well as dietary factors such as obesity [18, 19].

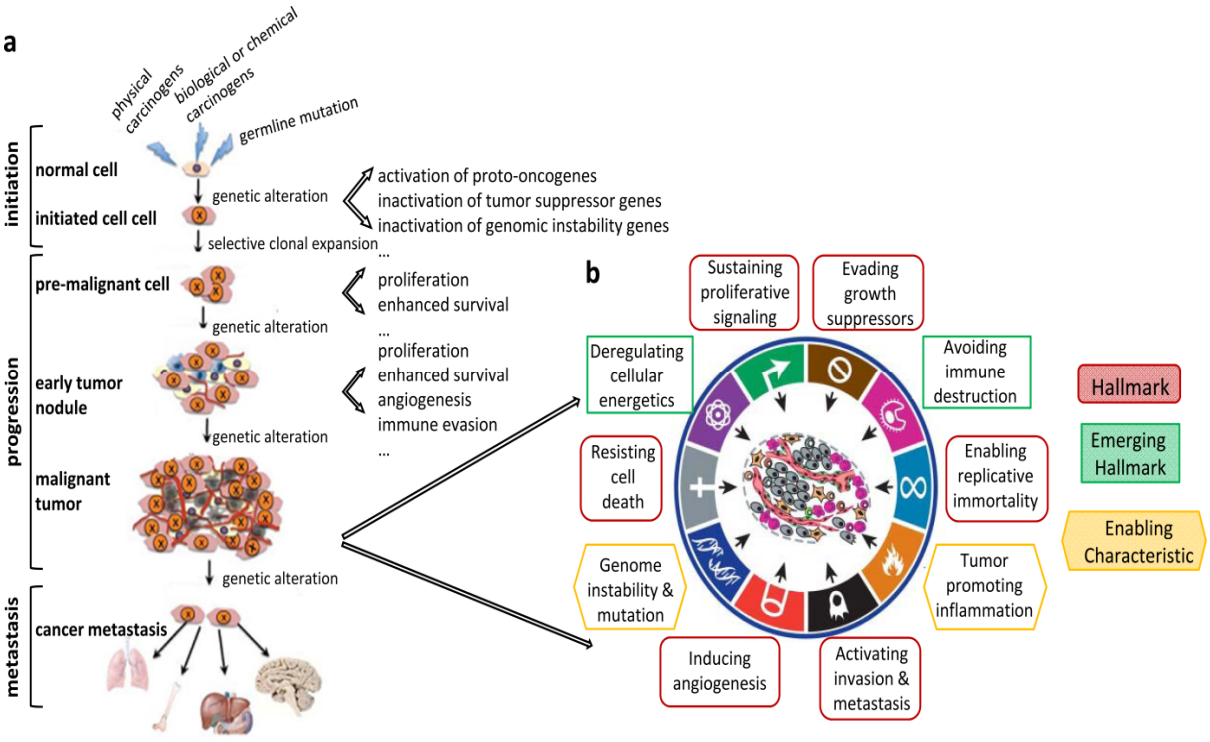

Figure 1: The process of neoplastic transformation and the definition of cancer based on the hallmarks of cancer according to Hanahan and Weinberg [20]**.**

The process of cancer development **(a)** was modified from [8]. It represents the stages of tumorigenesis including initiation, progression and metastatic disease. Mutations in the cancer cells (light brown) are marked with a "x" and are caused by physical, chemical, biological carcinogens or germline mutations (blue arrows). Immune cells in blue, endothelial cells in dark brown and blood vessels in red are depicted. The characteristics of neoplastic, malignant tumors **(b)** were modified from [20]. The six established hallmarks of cancer by Hanahan and Weinberg are marked in red, emerging hallmarks are marked in blue and enabling characteristics are marked in yellow.

Great research efforts have been made to identify the cancer-initiating cells within a malignancy. As reviewed by Visvader *et al.* [21] to pass the oncogenic mutations on to the cells progeny in tissues with high cellular turnover, the tumor initiating cell might be a stem cell, a tissue stem cell, or an early progenitor cell. However, also more restricted progenitor cells or differentiated cells were identified as initiator cells in other types of cancer *e.g.* in basal cell carcinomas or medulloblastoma [21].

Although there are a huge number of various mutated genes in cancer cells, the number of affected pathways that are critical for tumor development is much smaller. Examples include maintenance of genetic integrity, cell cycle check-point controls, DNA repair mechanisms, cell death pathways, cellular metabolism, migration, angiogenesis and immune response [9, 22]. In 2000, Hanahan and Weinberg [17] enunciated six hallmark capabilities that are acquired during tumorigenesis and that in a comprehensible manner, characterize malignant tumors (Figure 1b). Based on these, malignant tumors are characterized by sustained proliferative signals, evasion of growth suppressors, enabling of replicative immortality, activation of invasion and metastasis, induction of angiogenesis as well as resistance to cell death [17, 20]. In 2011, two additional "emerging" hallmarks that are not yet completely generalized and validated were included to the definition of cancer: The deregulation of cellular metabolism and the evasion of immunological destruction by T- and B-lymphocytes as well as natural killer cells (NK cells). Additionally, genomic instability increasing the risk for tumor promoting mutations and an inflammatory environment support the six established and the emerging hallmarks as enabling ones [20].

1.1.2 Tumor heterogeneity

Tumor heterogeneity is an important aspect of cancer taking place on different levels. It is one explanation for cancer robustness and the variable outcome of therapeutic responses [5, 23]. Large scale sequencing studies have demonstrated that each tumor is characterized by an individual genetic signature with a unique pattern of mutations [24]. In literature, four mechanisms are described leading to tumor heterogeneity: Mutations forcing genomic instability, epigenetic modifications supporting genomic instability, stochastic protein dynamics and interactions with the tumor microenvironment [5, 6, 25].

Intertumoral heterogeneity represents differences between patients with tumors of the same lineage. Consequences are *e.g.* variations in the molecular profile, the morphology of the tumor cells or the expression of specific antigens on the tumor cell surface [21].

Intratumoral heterogeneity defines phenotypic differences of cancer cells within an individual tumor and include but are not limited to factors such as cellular morphology, expression of antigens, growth factors, receptors, as well as the proliferative, immunogenic or metastatic potential of cancer cells [5, 21]. One example is the broad expression range of estrogen receptors on breast cancer cells [21, 26, 27].

1.1.3 Tumor microenvironment and its cellular components

Malignant tumor cells are imbedded into the tumor microenvironment depicted in Figure 2a. The tumor microenvironment comprises the extracellular matrix (ECM) consisting of proteoglycans, hyaluronic acid, fibrous proteins and stromal cells. The cellular subsets of the tumor microenvironment include mesenchymal cells like fibroblasts, cells of the vascular system like endothelial cells and diverse cell types of the innate and adaptive immune system. The different cell types interact and communicate directly or indirectly in an autocrine or paracrine manner via secretion of humoral factors such as hormones, cytokines and chemokines [reviewed in 9, 22, 28, 29]. The tumor microenvironment not only contributes to intratumoral heterogeneity but also is described to be crucial during all steps of tumorigenesis [9, 28]: During tumor development far-reaching alterations not only take place in malignant tumor cells, but also in the tumor microenvironment and are subject to continuous dynamic changes (Figure 2a) [29, 30].

In the following section, a short overview about the main characteristics of the individual cell types and their role in the modulation of the tumor microenvironment (Figure 2b) will be provided.

In healthy tissues, **fibroblasts** are responsible for ECM maintenance by controlling ECM component synthesis and degradation. Fibroblasts have a crucial role in the regulation of epithelial differentiation, inflammation and are activated in case of tissue injury and wound healing [30, 31]. Fibroblasts recruited and activated in the tumor microenvironment are termed cancer-associated fibroblasts (CAFs) and differ from normal fibroblasts [28, 29]. They are a heterogeneous population of cells representing several characteristics of embryonic fibroblasts or mesenchymal progenitors [29]. One major population of activated CAFs are myofibroblasts that express smooth muscle actin [9, 22, 30, 31]. In the tumor microenvironment, CAFs are responsible for major changes in the ECM like upregulation of ECM synthesis or modification of ECM proteins [30]. CAFs interact with tumor cells and immune cells by release of several growth factors and chemokines and are described to promote tumor growth, inflammation, angiogenesis and infiltration [29–31].

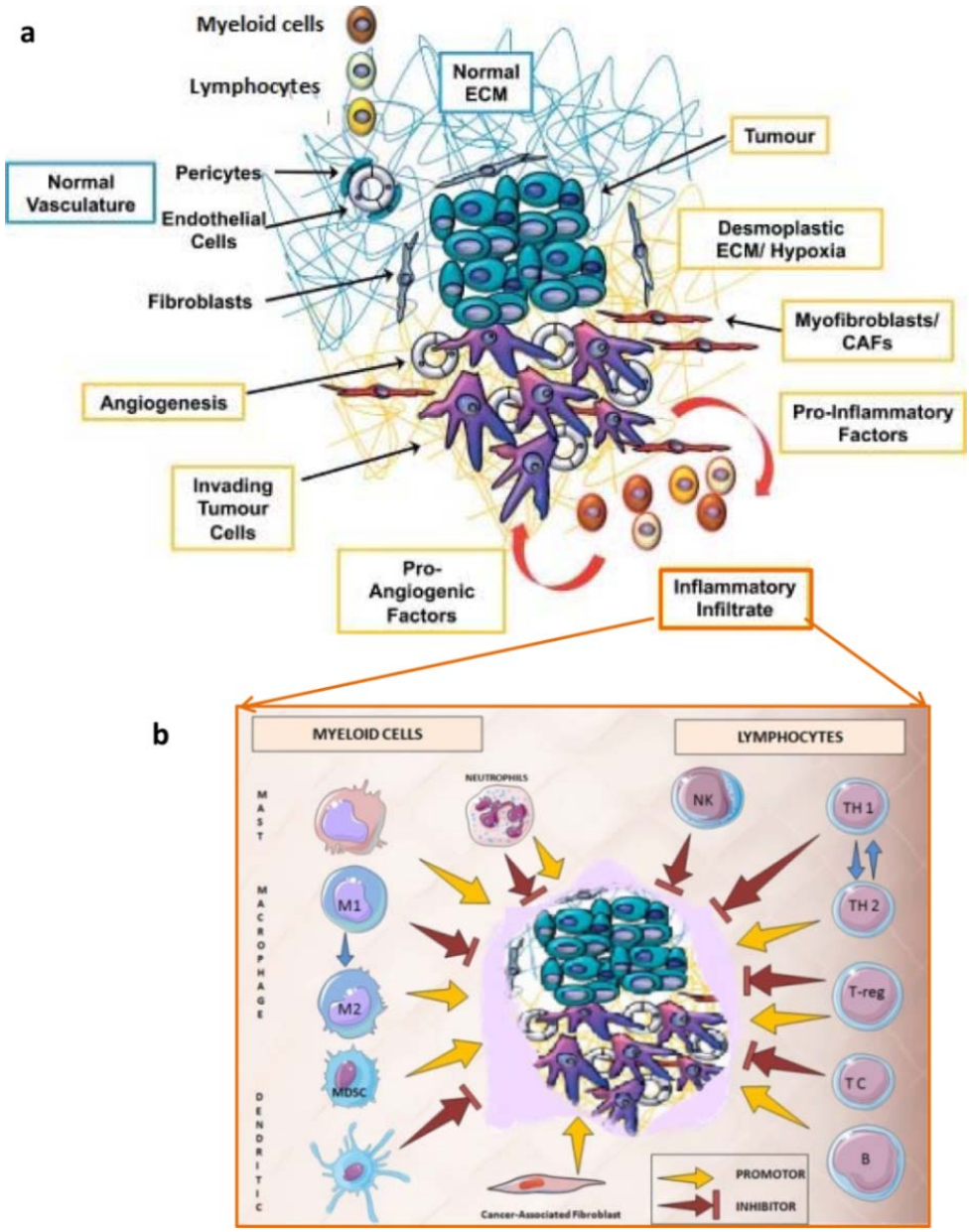

Figure 2: Overview of the components of the tumor microenvironment. In addition to transformation and modification of neoplastic cells during cancer development, major changes take place in the tumor microenvironment **(a; modified from** [29]**)**. Tumor promoting (yellow) and tumor suppressive (red) effects of cells of the myeloid and lymphocytic lineage on tumor development and progression **(b; modified from** [28]**).**

Proliferation and expansion of malignant tumor cells beyond 2-4 mm^3 lead to induction of a tumor-associated neovasculature required for the supply with nutrients or oxygen and the evacuation of metabolic waste products and carbon dioxide by a process called angiogenesis [9, 30, 32]. The process of blood vessel formation is reviewed by Bergers and Benjamin [33]. The development of new vessels arises from pre-existing capillaries or post-capillary venules. In the initial phase, **pericytes** detach, blood vessels dilate and the ECM is degraded. By a process called "angiogenic switch" normally quiescent **endothelial cells** of the tissue vasculature become

activated and migrate into the perivascular space towards angiogenic stimuli and start to proliferate. Following the adherence of the endothelial cells, the basement membrane is formed, pericytes are recruited and attach. In addition, bone marrow-derived vascular progenitor cells that have migrated towards angiogenic stimuli *e.g.* vascular endothelial growth factor (VEGF), hepatocyte growth factor (HGF) are integrated into the tumorigenic vasculature [20, 33]. In contrast to the normal vasculature, the balance between pro- and antiangiogenic factors in tumors is shifted toward the pro-angiogenic side resulting in a continuous development of new vessels. However, tumor vasculature is not comparable with the vasculature in healthy tissues. The tumor vasculature displays characteristics such as leakiness, tortuousness, dead ends or chaotic organization [20, 32, 33].

One major component of the tumor microenvironment is the immune cell infiltrate. It is established that the composition of immune cells varies between tumor types but also between patients suffering from the same tumor type [34, 35]. In the tumor microenvironment immune cells of the innate immune system of the myeloid lineage (macrophages, dendritic cells (DCs), mast cells and neutrophils) as well as lymphocytes as part of the adaptive immune system (NK cells, B-lymphocytes, T-lymphocytes such as T-helper cells (T_H), regulatory T cells (T_{Regs}) or memory T cells are present [34].

Macrophages originate from monocytes and can be classically activated (M1) or alternatively activated (M2) dependent on the micromilieu. Exposure of monocytes with cytokines of T_H1 cells like interferon gamma (IFN-γ), tumor necrosis factor alpha (TNF-α) or microbial products like lipopolysaccharide (LPS) induce the M1 phenotype. Monocytes polarized by cytokines of T_H2 cells like interleukin- (IL-) -4, -5, -6, -13 become M2 macrophages. M1 macrophages can be characterized by high expression levels of major histocompatibility complex II (MHCII), production of IL-12, TNF-α, and nitric oxide (NO), killing of intracellular pathogens and antitumoral activity. M2 macrophages express arginase, mannose receptor CD206, high levels of immunosuppressive cytokines like IL-10, tumor growth factor beta (TGF-β) and VEGF but express low levels of proinflammatory cytokines like MHCII, IL-12 and TNF-α. M2 macrophages are responsible for parasite killing, tissue remodeling and act as tumor promotors. They have a crucial role in immune evasion mechanisms of tumors and angiogenesis [29, 36]. Macrophages recruited into the tumor microenvironment are defined as tumor-associated macrophages (TAMs). They are either recruited from the bone marrow or already present in the original stroma. Dependent on the tumor milieu, TAMs are polarized into a phenotype comparable with M1 or M2 macrophages [28]. In most cases TAMs may be biased towards an M2 phenotype with additional characteristics of M1 macrophages [30]. They are often recruited to hypoxic and

necrotic areas [29]. Besides T-lymphocytes, TAMs are the most frequent immune cell type in the tumor microenvironment. TAMs promote tumorigenesis, angiogenesis, invasion and metastasis. Tumors that are heavily infiltrated with TAMs are often associated with poor prognosis [8]. A recent review by Gordon [85] proposes several additional macrophage activation and deactivation phenotypes, suggesting a high complexity and plasticity of the monocyte/macrophage cell lineage.

Neutrophils are cells with a short life time that have antimicrobial functions. In tumors, similar to macrophages, they can be polarized into N1 or N2 phenotypes by diverse TGF-β concentrations with tumor promoting or inhibiting functions. N1 neutrophils support the activation of $CD8^+$ cytotoxic T-lymphocytes and DCs and thus anti-cancer immunity. N2 neutrophils produce angiogenic factors and ECM degrading enzymes and promote tumor progression [30, 37].

Myeloid-derived suppressor cells (MDSCs) are a heterogeneous population of cells that combine characteristics of macrophages ($CD11b^+$ $Ly6C^{high}$ $Ly6G^{low}$) and neutrophils ($CD11b^+Ly6G^{high}$ $Ly6C^{low}$) [38]. MDSCs promote tumorigenesis: Amongst other functions, they are highly immunosuppressive by inhibiting the functions of *e.g.* NK cells, B-lymphocytes, DCs or T_{Regs}. In addition they enhance angiogenesis and metastasis [28, 30].

As major antigen-presenting cells in the tumor microenvironment, **DCs** represent the link between the innate and adaptive immune system [28, 38, 39]. As professional antigen-presenting cells, DCs interact and prime recruited T-lymphocytes *e.g.* in the lymphoid organs [28, 39]. In the tumor microenvironment the functions of DCs may be inefficient. It is described that tumor-associated DCs have down-regulated MHC molecules and do not efficiently present antigens on their surface. Several molecules in the tumor microenvironment such as VEGF, IL-6, macrophage colony-stimulating factor (M-CSF) or IL-10 are responsible for an altered differentiation of DCs resulting in an immature phenotype with impaired functions [38].

NK cells inhibit tumor formation. They kill altered cancer cells by secretion of perforin, independent of antigen presentation on the surface of the target cells. In addition they interact with DCs, macrophages, T-lymphocytes and endothelial cells [28, 40].

The role of T- and B-lymphocytes recruited into the tumor microenvironment is complex and can be tumor promoting or suppressing dependent on their effector functions. The function of **$CD3^+CD4^+$ T_H cells** is dependent on the ratio of their particular subtype (T_H1 or T_H2) [28, 30]. T_H1 cells inhibit tumor formation by enhancing cancer immunosurveillance [28]. T_H1-type cytokines such as IL-2 and IFN-γ promote cellular immunity by activating cytotoxic and phagocytic functions in cytotoxic $CD3^+CD8^+$ T-lymphocytes, NK cells, and macrophages [41]. In contrast, T_H2

cells support tumor promotion amongst others by secretion of molecules that polarize macrophages into the M2 phenotype [30]. In addition, T_H2-type cytokines stimulate humoral immune responses and down-regulate tumor-specific immunity [41]. **B-lymphocytes** that normally control humoral immunity can change the T_H1/T_H2 ratio and thus support tumor promotion. **Cytotoxic $CD3^+CD8^+$ T-lymphocytes** have tumor suppressive effects as they can kill cancer cells after interaction between their MHCII molecules and tumor antigens [28]. **$CD4^+CD25^+FoxP3^+$ T_{Regs}** are a T helper cell type with immune suppressive characteristics. T_{Regs} mediate immune evasion mechanisms and create an immune suppressive tumor microenvironment. By secretion of TGF-β and IL-10 the activity of $CD4^+$, $CD8^+$ or NK cells is inhibited. In addition, these cells function as competitive sink for IL-2 and other inflammatory cytokines by expression of a heterotrimeric receptor with higher affinity than the dimeric receptor for this molecule. T_{Regs} interact with antigen-presenting cells by cell surface receptors such as cytotoxic T-lymphocyte-associated protein 4 (CTLA-4), programmed cell death protein 1 (PD-1), or glucocorticoid-induced tumor necrosis factor receptor related protein (GITR) resulting in a suppressive immune environment.

Clinical trials using inhibitors for CTLA-4 or PD-1 have shown promising results with regression of the tumor burden and induction of an effective antitumor response [38]. Besides the tumor promoting role by interference with the immune surveillance system, T_{Regs} are described to inhibit tumorigenesis in inflammatory cancer types [28].

Besides the amount of individual immune cell populations within the tumor microenvironment especially the cytokine and chemokine expression profiles are crucial for the sensitive equilibrium between antitumor immunity and proinflammatory, tumor promoting activities of the immune system (Figure 3) [8, 36, 42]. Independent of their source, different inflammatory mediators can either promote (*e.g.* IL-1, -6, -17, -23) or inhibit (IL-12, TNF-related apoptosis-inducing ligand (TRAIL), IFN-γ) tumor development and progression. This is mediated by activation of downstream transcription factors such as nuclear factor kappa-light-chain-enhancer of activated B cells (NF-ƙB), signal transducer and activator of transcription (STATs) or caspases. Factors such as TRAIL, FasL, TNF-α, epidermal growth factor receptor ligands (EGFRL), TGF-β, IL-6 may also have direct effects on tumor cell survival and growth [8, 42]. Such an interplay is schematically represented in Figure 3 and the role of individual cytokines, chemokines and their particular signal transduction pathways are reviewed in detail in [8, 42–46].

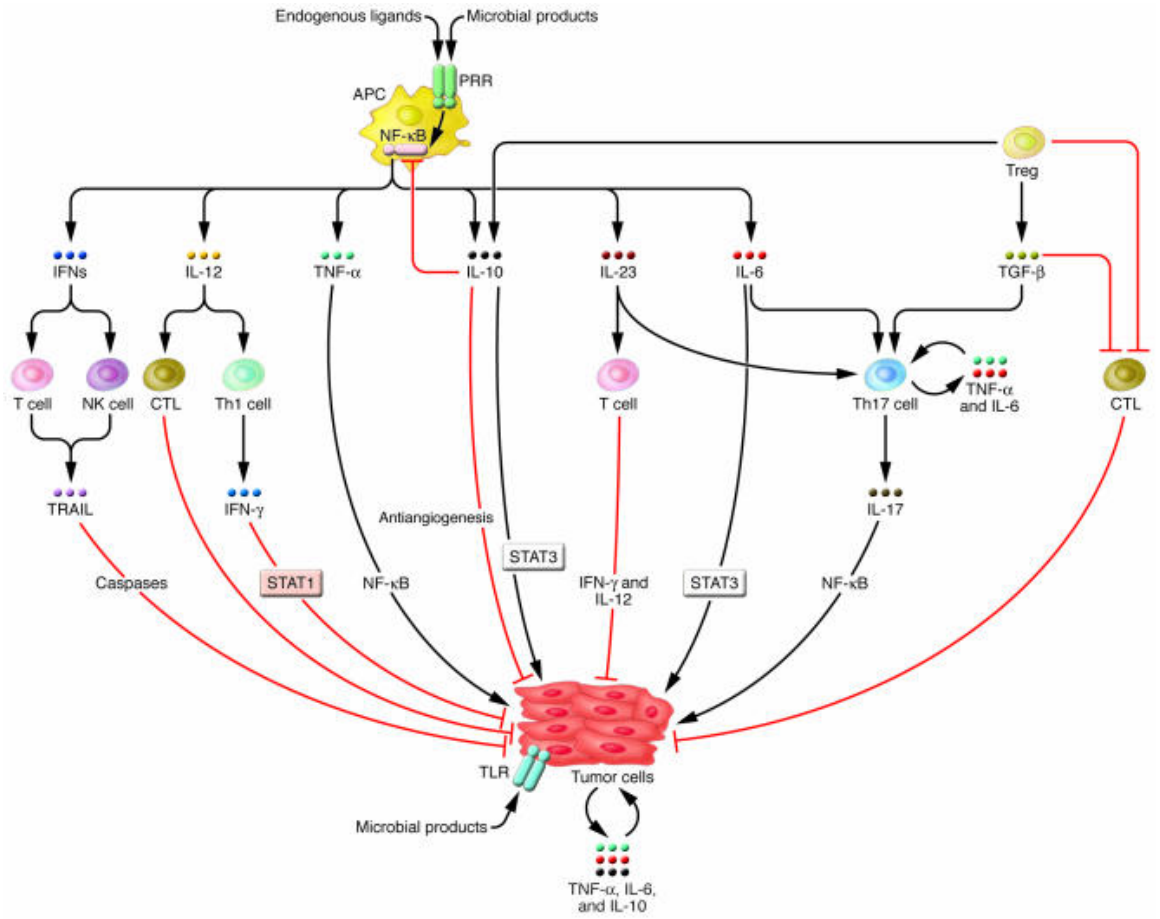

Figure 3: Effects of various cytokines and cell types in the tumor microenvironment on tumor cells (adapted from [42]**).** Activated myeloid cells are a major source for proinflammatory and anti-inflammatory cytokines. Cytokines can have direct effects on tumor cells and can stimulate the functions of tumor-infiltrating immune cells such as T_H1 cells, NK cells, T_{Regs}, and T_H17 cells. Possible interactions are depicted.

1.1.4 Cancer immunity - from the concept of immunoediting to the immune score

The concept of cancer immunoediting by Dunn and Schreiber [47] unifies the dual role of the host immune system on tumor development: On the one hand the tumor suppressive functions and on the other side the ease of tumor progression by sculpting the immunogenic phenotype of developing tumors and thereafter [48–50]. The concept is defined as dynamic process of three independent or consecutive phases termed elimination, equilibrium and escape and it is depicted in Figure 4 [50, 51].

The elimination phase represents a modernized description of the cancer immunosurveillance theory first defined by Burnet and Thomas [52, 53] which is characterized by the recognition and elimination of transformed cells by innate and adaptive immune cells and their respective effector molecules [47]. By studies in different mouse models, the following cell types and effector molecules were identified to be crucial for tumor cell elimination: $CD4^+$ T-cells, γδ T-

cells, NKT-cells, and NK cells as well as perforin, TRAIL, IFN-γ, IFN-α/β, and IL-12. The process and the role of the individual components are reviewed by Vesely *et al.* [54]and Dunn *et al.* [51].

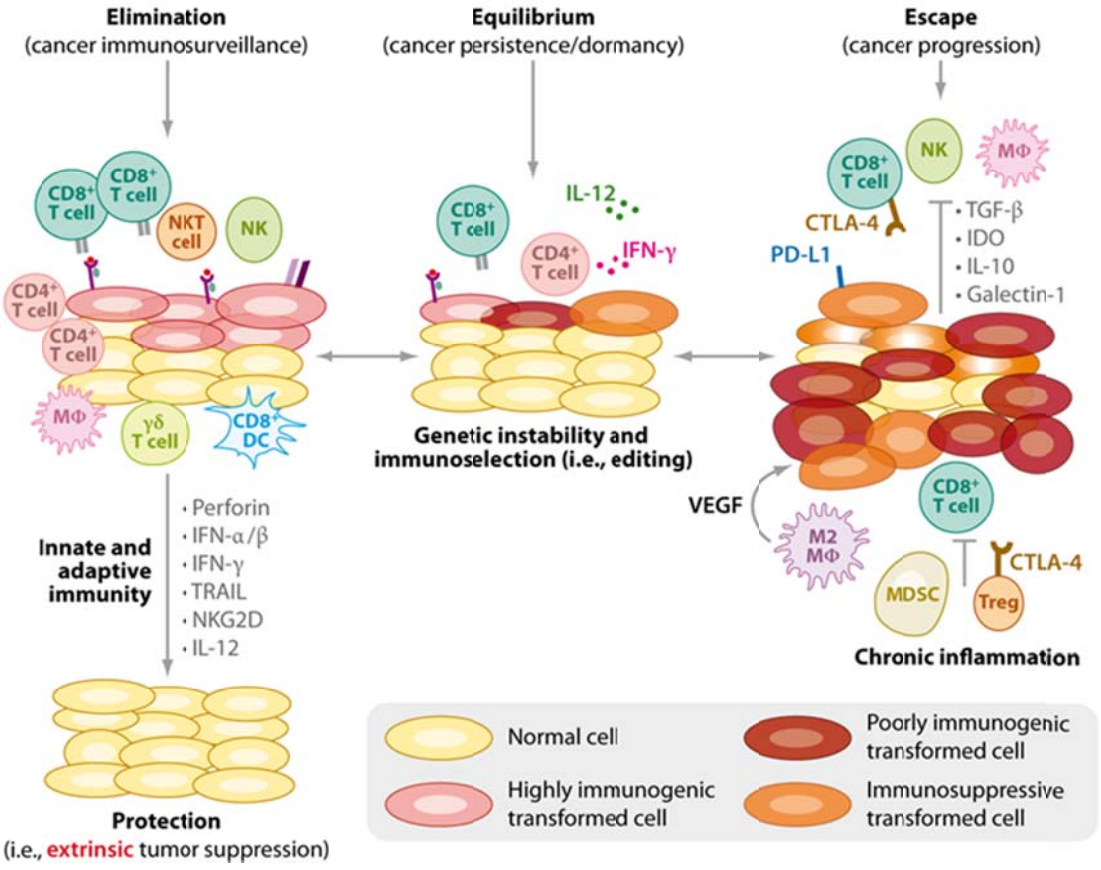

Figure 4: Overview of the three phases of cancer immunoediting: elimination, equilibrium and escape (adapted from [54]**).** Shown are the cell types (macrophages (MΦ), $CD8^+$ cytotoxic **T** cells, NKT cells, $CD4^+$ T cells, γδ T cells) and various molecular factors identified to be crucial for the particular phases and the transformation of normal cells (yellow) to subpopulations of poorly immunogenic (brown) or immunosuppressive tumor cells (orange).

In case that all tumor cells are destroyed during the elimination phase, cancer immunoediting ends at this point [47]. If the transformed tumor cells are not completely eliminated the surviving cells enter the equilibrium phase also known as tumor dormancy. In this phase the host immune system and the tumor cells are in a dynamic balance [47, 51, 55]. This period is the longest of the three phases. The tumor cells are exerted to a strong selection pressure induced by cells of the adaptive immune system and cytokines like IFN-γ. Many of the originally escaped tumor cells have been destroyed and tumor cell clones with reduced immunogenicity and increased resistance to immunologic recognition and control have been developed [47, 51, 54, 55].

The escape phase represents the uncontrolled proliferation of tumor cells that have undergone genetic and epigenetic changes during the equilibrium phase and that are thus insensitive for

immunologic detection and destruction [47, 54]. Mechanisms leading to tumor escape are reviewed in detail by Vesely *et al.* [54]. They include the selective pressure of the immune system on tumor cells and the destruction of antigen-positive and thus immunogenic tumor cells by $CD8^+$ T-lymphocytes. On the other side tumor cells have developed mechanisms to inhibit immunity. Examples are down-regulation of MHCII molecules and thus antigen presentation, upregulation of anti-apoptotic molecules and immunosuppressive molecules such as PD-L1 or FasL that directly kill $CD8^+$ T-lymphocytes. Secretion of molecules that promote an immunosuppressive microenvironment or inhibit cellular effector functions are further mechanisms [54].

In addition to the increased understanding of the interactions between immune and tumor cells within the tumor microenvironment major efforts have been made in correlating the level of immune infiltrates within tumors and the clinical outcome of patients. Data of large cohorts of human cancers have shown that immunophenotyping of tumors in addition to the classical staging system (AJCC/UICC-TNM) would provide additional prognostic and even predictive information. A prognostic biomarker is a marker that gives information about the course of disease without treatment, whereas a predictive biomarker identifies patients that most likely respond to a particular therapy [35]. Immune parameters that are associated with improved survival were characterized in the immune contexture initially described by Galon *et al.* [35, 56, 57]. The immune contexture is described as the type, functional orientation, density and location of adaptive immune cells within distinct tumor regions. In more detail, the density of $CD3^+$ T-lymphocytes, $CD8^+$ cytotoxic T-lymphocytes and $CD45RO^+$ memory T-lymphocytes and their location at the tumor center, invasive margin or tertiary lymphoid structures. Also included are T_H1-related inflammatory mediators such as (IFN-γ, T-bet, interferon regulatory factor 1 (IRF-1), IL-12), chemokines (chemokine (C-X3-C motif) ligand 1 (CX3CL1), chemokine (C-X-C motif) ligand 9, 10 (CXCL9, 10), chemokine (C-C motif) ligand 5, 2 (CCL5,2)), adhesion molecules (intercellular adhesion molecule 1 (ICAM1), vascular cell adhesion protein 1 (VCAM1)) and cytotoxic factors (granzymes, perforin, granulysin) [35, 58].

As a worldwide task force, the immunoscore is aimed to be incorporated into the traditional classification system [59]. The immunoscore is derived from the immune contexture but modified to a standardized, simple, quantitative, routine test. It is based on the lymphocyte populations (CD3/CD45RO, or CD3/CD8 or CD8/CD45RO) that are quantified in the tumor center and invasive margin ranging from immunoscore 0, with low densities of the cell types in both regions; to immunoscore 4, with high densities of the cell populations in both regions [35, 58] .

1.2 Glioblastoma multiforme (GBM) - the most aggressive brain tumor

The worldwide incidence rate of newly diagnosed brain and central nervous system tumors was 256,000 new cases in 2012. This number represents 2% of all diagnosed cancer cases. The mortality rate of this group of neoplastic diseases was 189,000 deaths and 2% of all cancer related deaths [60]. Brain tumors account for 85-90% of all central nervous system (CNS) tumors [61]. By the World Health Organization (WHO) classification of tumors of the CNS 2007 [62], primary brain tumors - arising in the CNS have been characterized according to the cells of phylogenetic origin into seven categories: neuroepithelial tumors, tumors of cranial and spinal nerves, tumors of the meninges, mesenchymal tumors, hematopoietic neoplasms, germ cell tumors and sellar tumors. In addition, there are secondary, metastatic brain tumors that have spread from other tissues into the CNS.

Glial tumors or gliomas account for 28% of all brain tumors and 80% of malignant brain tumors and arise from glial cells such as astrocytes, oligodendrocytes or ependymal cells or their less differentiated progenitors [63, 64]. Gliomas include astrocytomas, glioblastomas, oligodendrogliomas, ependymomas, and mixed forms [63].

In addition to the morphological grouping of gliomas by the WHO classification system, they are classified by four histological malignancy grades (I-IV) important for prognosis and choice of an adequate therapy [62]. The grades are defined by histological characteristics such as nuclear polymorphism, cellular density, mitotic activity, necrosis and endothelial proliferation. Increasing grades are associated with increased levels of dedifferentiation, anaplasia and aggressiveness [62, 65]. Lower grade gliomas are *e.g.* WHO grade I pilocytic astrocytoma and WHO grade II diffuse astrocytoma, oligodendroglioma as well as pleomorphic xanthoastrocytoma. Malignant high grade gliomas are anaplastic astrocytoma, oligodendroglioma, oligoastrocytoma (WHO grade III) as well as glioblastoma and its variants such as giant cell glioblastoma or gliosarcoma (WHO IV) [62]. Histological characteristics of grade III lesions are nuclear atypia and mitotic activity whereas additional characteristics of grade IV lesions are necrosis and microvascular proliferation [66].

Glioblastoma multiforme (GBM) is the most malignant form of gliomas and with 54.7% also the most common glioma. In addition, GBM represents the most frequent tumor type of all malignant CNS tumors, with 10,110 cases predicted in 2014 and 10,200 in 2015 in the USA. The relative survival of GBM is very low with only 5% of patients that survive five years after diagnosis and a median survival time of less than 15 month. The incidence of the disease is increasing with age and the median age of diagnosis is 64 years [63]. Besides increasing age,

male gender and white ethnicity, the exposure to ionizing radiation is verified as definitive risk factor [67, 68].

Clinical symptoms vary depending on the size and location of the tumor and affected brain structures [69]. In addition to focal symptoms such as aphasia, paraesthesia, hemiparesis, visual disturbances, mood- and personality changes, brain tumors are in most cases associated with increased intracranial pressure causing headaches, nausea, seizure, and a reduced level of consciousness [69, 70].

GBM is a highly invasive disease, infiltrating surrounding brain parenchyma and adjacent lobes and in many cases there is progression from one hemisphere into the other via the corpus callosum to form butterfly gliomas. [71]. The invasion is preferentially seen along white matter tracts or around neurons in the grey matter [72]. In contrast to other highly malignant diseases, hematogenous or lymphatic spread of glioblastoma outside the brain is very rare [73, 74].

GBM is highly heterogeneous showing additional characteristics such as microvascular proliferation, angiogenesis, endothelial hyperplasia, glomeruloid leaky vessels and tumor cell necrosis [71, 72]. In addition to the tumor as a whole, also the single tumor cells are highly heterogeneous. They can be monomorphic, highly variable in size and shape with granular or lipidized cytoplasm or hyperchromatic nuclei. Also giant cell formations with multiple cell nuclei can be found within the tumor [71]. The histological representation is depicted in Figure 5.

Most glioblastoma cases occur sporadic and only 5% of all primary tumors are associated with genetic disorders such as neurofibromatosis, tuberous sclerosis, Turcot syndrome, and von-Hippel Lindau disease [65, 75]. There is a great number of genetic alterations in tumor supressor genes, oncogenes and their receptors associated with GBM initiation and progression that are reviewed in detail by Bleeker *et al.* [76] and Ohgaki *et al.* [77].

GBM can be distinguished into two distinct disease subtypes: primary GBM that arises *de novo* by accumulation of a number of genetic alterations and without evidence of a less malignant tumor phenotype and secondary GBM that shows clinical, radiological, or histopathological evidence of a pre-existing lower grade type II or III glioma [73, 77]. Primary GBM is the most frequent type of GBM with more than 90%-95% of diagnosed GBM cases. It affects preferentially elder patients (mean age 59-62 years) and represents a more severe clinical outcome. Secondary GBM occur in younger patients (mean age 33-45 years) and as a consequence of the transformation process they develop slower and have a significant better median survival time [77, 78].

Primary and secondary GBM cannot be distinguished histologically, however, they have different genetic, epigenetic and proteomic profiles [77]. The development of primary and secondary GBM is shown exemplarily in Figure 5.

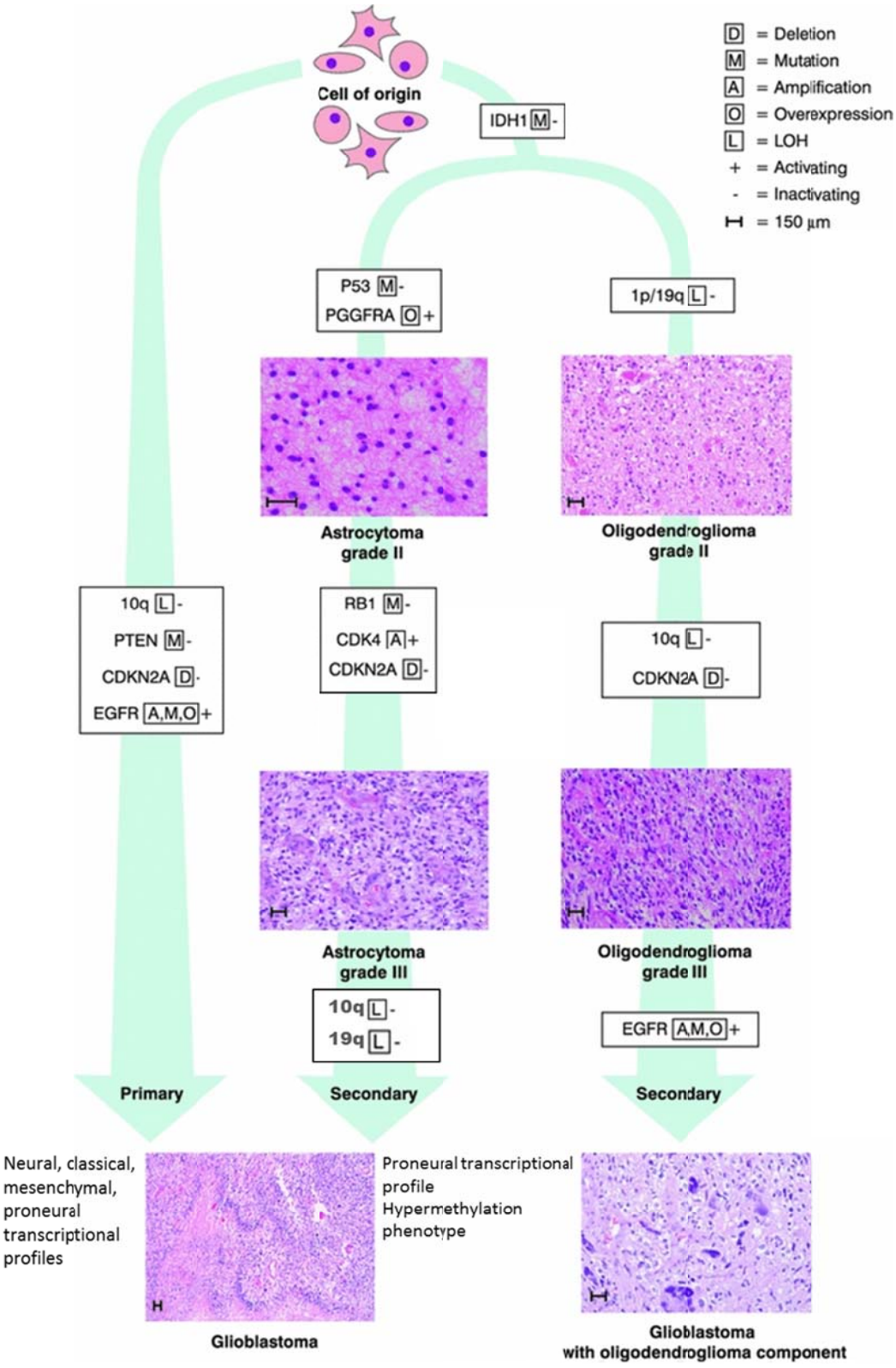

Figure 5: Schematic overview on histologic subtypes of gliomas and the genetic pathways leading to the development of primary and secondary GBM (adapted from [76]**).**

Primary GBM can be characterized by relatively high frequency of EGFR amplification as well as duplications in the proto-oncogene mouse double minute 2 homolog (MDM2) [76, 77]. A mutation often found in EGFR amplicons is the deletion of exon 2-7 resulting in the variant EGFRvIII [78, 79]. This mutation results in the constitutive activation of the receptor and thus down-regulation of p27 and activation of the phosphatidylinositol (3,4,5)-trisphosphate/mammalian target of rapamycin/protein kinase B (PIP3/mTor/AKT) pathway associated with cell proliferation and survival by inhibition of apoptosis [80]. Further, associated with primary GBM is the loss of heterozygosity (LOH) of chromosome 10q and p. A tumor supressor factor frequently deleted in primary GBM is the phosphatase and tensin homolog (PTEN) which physiologically inhibits the PIP3/AKT pathway and the cyclin-dependent kinase inhibitor 2A (CDKN2A or p16) that physiologically block the transition of G1 to S phase [76, 77].

Secondary GBM is characterized by high incidence of mutations in the p53 tumor supressor gene involving codons 248 and 273 or G:C→A:T mutations at CpG sites, overexpression of platelet-derived growth factor receptor (PDGFR), LOH 19q, LOH 22q and a-thalassemia/mental-retardation-syndrome-X-linked (ATRX) gene mutations [76, 77]. Recently identified by Parson *et al.* [81] were mutations in the IDH1 and IDH2 genes, that encode the isocytrate dehydrogenase 1 and 2 which are detected mainly in younger patients and in more than 80% of all secondary GBM cases. Mutations in IDH1 have been shown to be associated with a better prognosis of glioblastoma patients [82]. Analysis of multiple biopsies of the same patient revealed that IDH1/2 mutations are very early events in gliomagenesis and may affect a common glial precursor cell population. Those mutations occur before mutations of the p53 tumor supressor factor typical for lower grade astrocytomas or 1p/19q loss typical for development of oligodendroglioma [77, 83].

Gene expression studies of GBM samples revealed 4 transcriptional subclasses namely: classical, mesenchymal, proneural, and neural. Those subtypes are characterized by aberrations and diverse gene expression of EGFR, NF1, IDH1, and PDGFR and varying prognosis [84].

1.2.1 The tumor microenvironment of GBM

In addition to glioma cells and glioma stem cells, tumor associated non-malignant stromal cells (vascular and endothelial cells) and immune cells (microglia and peripheral immune cells) account for a significant proportion of the glioma tumor mass [85]. Those cells can be brain-resident or infiltrated into the brain [86]. As reviewed by Chen and Parney [87] and Kruse *et al*. [88] the intratumoral milieu of gliomas is highly immunosuppressive due to the interactions and functions of recruited immune and glial cells and the secretion and expression of various

cytokines, chemokines and growth factors. In the following, the role and interaction of glioma cells with microglia and astrocytes will be described in more detail.

1.2.1.1 Microglial cells in general and in the context of GBM

Microglia are the resident macrophages of the CNS and the main innate immune cells that are activated amongst others by infiltrating pathogens and tissue injury. As immune effector cells, microglia mediate both - innate as well as adaptive immunity [89–91]. Microglia account for 5-20% of all glial cells, but are in contrast to other glial cells such as astrocytes or oligodendrocytes, of mesenchymal/myeloid origin [91, 92]. Their precursor cells were derived from mesodermal hematopoietic cells that entered the developing brain during perinatal stages were they differentiated to microglial cells [91, 92]. There is no unique phenotypic marker profile for microglial cells but they can be classified by the following: $CD68^{+}$, $CD45^{low}$, $CD11b^{+}$, $CD11c^{high}$, $MHCII^{+}$, $CD14^{-}$, $Iba1^{+}$ and Griffonia simplicifolia isolectin B4 (ILB4) [92, 93].

According to their morphology, gene expression profile, and functional characteristics, microglia are classified into three stages: resting ramified, activated and amoeboid phagocytic. In their resting, quiescent state, microglial cells display an immobile ramified morphology with low expression of activation-associated molecules. During this stage present in the healthy adult CNS, they constantly monitor their environment. Under pathological conditions such as infections, trauma, ischemia, or neurodegenerative diseases microglial cells become activated in a highly regulated process. Reactive microglial cells are large cells with amoeboid morphology and are actively recruited to pathological lesions following chemotactic gradients. As part of the activation process there is an induction and change of surface molecules and receptors, intracellular enzymes, release of molecular factors and pro- and anti-inflammatory cytokines. In addition, similar to macrophages, microglial cells activate phagocytic capabilities for clearance of cellular debris, apoptotic cells, and pathogens. Another consequence of microglial activation is the upregulation of MHCI and II, co-stimulatory receptors (CD40, CD80, CD86) and thus presentation of antigens to T-lymphocytes and activation of the adaptive immune system [89, 92–94]. Similar to peripheral macrophages, also microglial cells can be polarized into a classical M1 or alternatively activated M2 phenotype reviewed by Colton *et al.* [95] and Saijo *et al.* [91] and depicted in Figure 6a.

Microglia and glioma infiltrating macrophages account for the predominant immune subset within malignant gliomas [96–98]. In a study of Morantz *et al.* [99] 11 human GBM samples were analysed and a mean average of tumor associated macrophages of 45% were assessed. In a study of Badie and Schartner [97] analysing experimental glioma models, they determined that

microglia ($CD11b^{+}/CD45^{dim}$) accounted for 13-34% and infiltrating macrophages ($CD11b^{+}/CD45^{high}$) accounted for 4.2–12%. Several studies propose a positive correlation between the number of microglia/macrophages and tumor stage and severity [92, 96, 99, 100].

Microglia/macrophages are recruited to the tumor side and proliferate within tumors due to local secretion of chemoattractants (monocyte chemotactic protein 1 and 3 (MCP-1 and -3)) and growth factors (*e.g.* granulocyte macrophage colony-stimulating factor (GM-CSF), and granulocyte colony-stimulating factor (G-CSF)) by glioma cells [86, 89, 101].

Contrary to the expectations, glioma infiltrating microglia/macrophages do not support an efficient anti-tumor immune response. However there is accumulating evidence that glioma cells silence immune properties and the release of proinflammatory cytokines by microglial cells and instead stimulate them to promote tumor growth, invasion and angiogenesis [89, 92, 102]. Another example for the described symbiosis and representative for the glioma-induced microglial phenotype is the study of Voisin *et al.* [102] which shows that microglia were in an activated state with phagocytic activity within the first 3 h of co-culture with C6 glioma cells but lost their phagocytic activity when they were in co-culture for more than 6 h. The polarization of glioma infiltrating microglia/macrophages into the alternative M2 phenotype was described by several groups and was reviewed by Li and Graeber [101]. As shown in Figure 6a, M-CSF and TGF-β are factors released by glioma cells that promote the polarization of microglia/macrophages into the M2 phenotype. This phenotype is amongst others associated with expression of the surface molecules CD204, CD163, increased expression of immunosuppressive molecules IL-10, TGF-β, and B7-H1, decreased phagocytic capacity, poor antigen presentation and inhibition of proinflammatory cytokines.

Microglia/macrophages within the tumor microenvironment secrete matrix metalloproteinases (MMPs) that facilitate invasion, as well as EGF and VEGF that promote tumor proliferation and angiogenesis [86, 89, 101]. Tumor-associated microglia/macrophages express EGFR and MET by which they receive signals (EGF, hepatocyte growth factor/scatter factor (HGF/SF)) from the tumor that further increase glioma growth and invasion [101]. Glioma cells release immune suppressive cytokines such as TGF-β, IL-10, and prostaglandin E2 (PGE2). Amongst other functions, those immune suppressive cytokines are known to down-regulate proinflammatory cytokines and antigen-presenting molecules such as MHCII on microglial cells and thus inhibit antigen-specific T-lymphocyte activation and differentiation of cytotoxic $CD3^{+}CD8^{+}$-T-lymphocytes. In addition to glioma cells also microglia/macrophages within the glioma microenvironment contribute to the immunosuppressed environment.

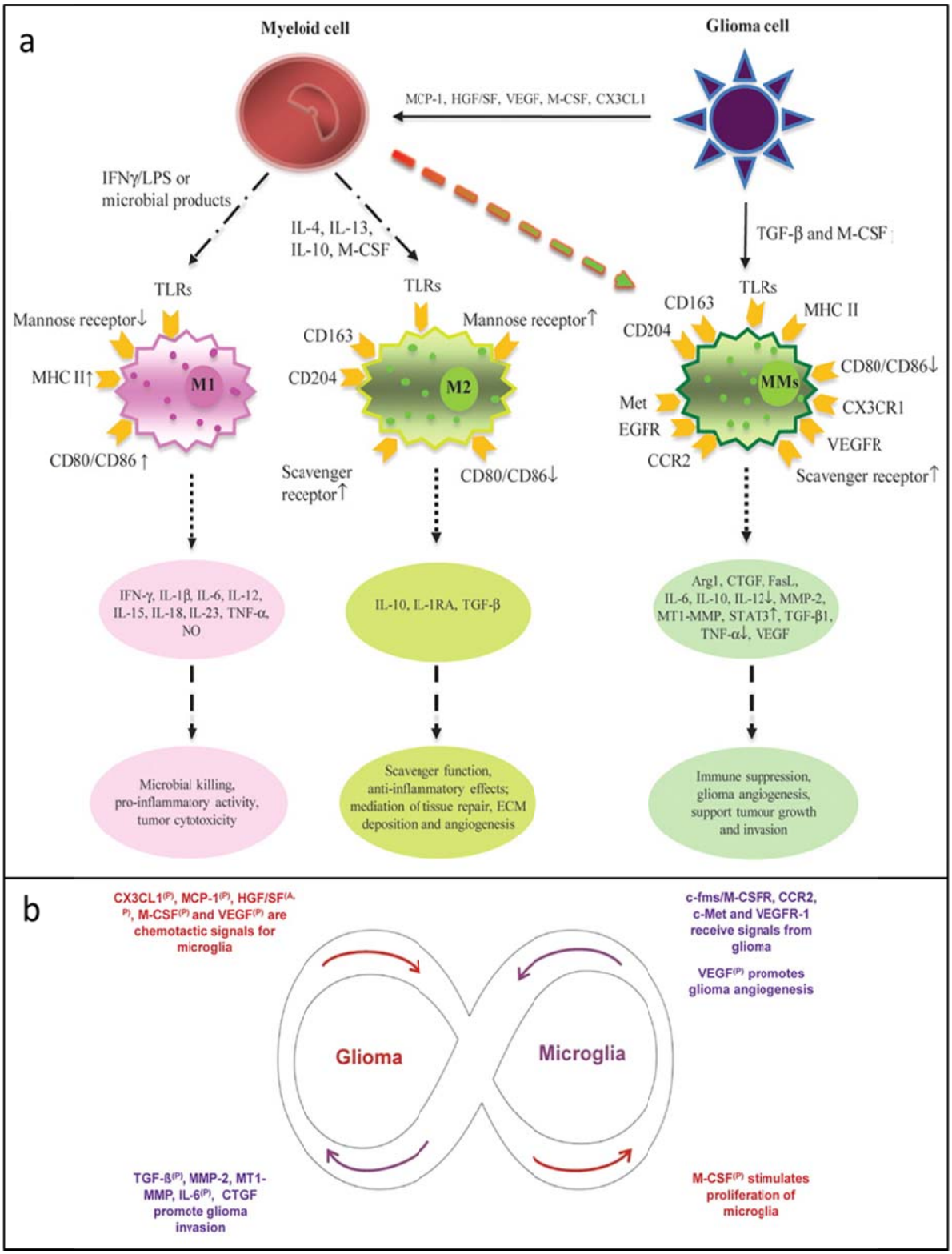

Figure 6: Overview of polarization states of microglia/macrophages and influence of glioma cells on polarization towards M2 phenotype (a) adapted and modified from [101]**.** Activated microglia exist in two polarization states in response to a particular microenvironment and dominance of either T_H1 or T_H2 cytokines - either a proinflammatory phenotype (classical activation) or an anti-inflammatory and reparative phenotype (alternative activation). Tumor-associated microglia can be polarized by glioma cells towards a M2 phenotype. **Interplay of glioma cells and microglial cells favoring tumor progression (b)** adapted and modified from [101]**.** The interaction is provided by several cytokines, chemokines and growth factors in a number of paracrine (p) and autocrine (a) loops.

Glioma infiltrating microglia/macrophages *e.g.* have been shown to express increased levels of B7-H1 and FASL both, immunosuppressive molecules that induces T-lymphocyte apoptosis [86, 89, 101]. The interplay between glioma associated microglia/macrophages and glioma cells is shown in Figure 6b and described in further detail in literature [86, 88, 89, 101].

1.2.1.2 Definition of astrocytes and their role in brain tumor microenvironments

Astrocytes are one of the most frequent cell types in the CNS (>50%) and a heterogeneous group of cells that differ in their morphology, development, metabolism, physiology and pathology [103–105]. Astrocytes have a star-shaped form with a central cell body and long processes that extend in all directions [103]. Astrocytes interact with almost all cell types in the CNS (neurons, oligodendrocytes, microglia, endothelia, and astrocytes themselves) [103]. They play a crucial role in the regulation and homeostasis of extracellular concentrations of potassium ions and neurotransmitters [104, 106]. In addition, astrocytes participate in synapse formation and plasticity and interact and communicate with neurons by release of gliotransmitters [104, 106]. Further, astrocytes regulate the blood brain barrier and have the ability to respond to immune and inflammatory activities in the CNS [103, 104, 106]. Astrocytes are activated in pathological situations [104, 107, 108]. Reactive gliosis is the response of astrocytes to tissue injury, infection or various diseases which can have beneficial or deleterious effects on neuronal function and survival. During neuroinflammation, activated astrocytes express diverse cytokines, chemokines, and their receptors [109, 110]. Jang *et al.* [110] showed, that activated astrocytes exhibit M1/M2-like characteristics with respect to pro- or anti-inflammatory gene expression, glial fibrillary acidic protein expression, and neurotoxic or neuroprotective activities.

Activation of microglia and astrocytes occur at different stages and times in several pathological situations (*e.g.* trauma, ischemia, Alzheimer's disease, epilepsy). Microglia are activated in the first instance and enable the activation of astrocytes by proinflammatory cytokines such as IL-1. On the other hand, activated astrocytes promote distant microglial activation via calcium waves, however, they can also inhibit microglial activities *e.g.* by down-regulation of NO and ROS [103].

In addition to microglia, astrocytes are also recruited to brain tumors or metastases in the brain. It has been shown that astrocytes are able to contribute to cancer progression by supporting tumor cell proliferation by secretion of various neurotrophic factors (*e.g.* TGF-α, TGF-β, stromal cell-derived factor-1 (SDF-1), glial cell-derived neurotrophic factor (GDNF), IL-6) and invasion by secretion of *e.g.* heparanase, pro-matrixmetalloproteinase 2 (pro-MMP2) and plasminogen activator (uPA) that are involved in the degradation of the extracellular matrix. Astrocytes also contribute to immune suppression by down-regulation of proinflammatory cytokines such as

TNF-α and suppression of MHCII and CD80 on tumor and microglial cells and thus impairing T-lymphocyte activation [85, 86]. In addition, by direct cell-cell contact via FAS-L/CD95L astrocytes induce apoptosis in T-lymphocytes infiltrating the CNS [86, 111].

1.2.2 Therapy of GBM

Despite decades of research and multimodal treatment regimen the prognosis for GBM is still very poor [112]. The standard of care for GBM starts with surgical resection, followed by a combination of radiotherapy and Temozolomide (TMZ) chemotherapy and finishes with adjuvant TMZ chemotherapy [113, 114]. Surgical resection is used as biopsy for diagnostic purposes and to minimize the tumor burden and thus symptoms associated with mass effect and edema. However, due to the infiltrative nature of the tumor complete surgical resection is almost impossible [69, 75]. In several clinical trials, summarized by Laperriere *et al.* [115] it has been shown that there is a significant survival benefit favouring post-operative radiotherapy compared with no radiotherapy.

Then, in a randomized clinical trial phase III with 573 patients in 2005, it was demonstrated that concomitant radio- and TMZ chemotherapy in contrast to radiotherapy alone significantly improved the median survival from 12.5 month to 14.6 month and increased the percentage of surviving patients 2 years after diagnosis from 11- 27% [69, 116]. In addition, studies showed that chemotherapy is more effective in younger patients and in particular in patients with promoter methylation of the DNA repair enzyme O6-methylguanine-DNA methyltransferase (MGMT) [65]. In these patients the 2-year survival rate of the standard treatment regimen further increase to 49% [117, 118].

The standard radiotherapy dose is 60 Gy divided in 30–33 fractions. In elder patients (>70 years) a lower radiation dose *e.g* 40-50 Gy and shorter treatment regimens were proven beneficial [113]. In the standard protocol, TMZ is administered daily during radiotherapy for at most 49 days, and for 5 days every 4 weeks for six cycles as adjuvant treatment [117].

TMZ is a DNA alkylating agent of the second-generation that induces thymine mispairing during DNA replication which results in tumor cell G2/M phase arrest and autophagy. It can be administered orally and is in contrast to many other chemotherapeutics able to cross the blood brain barrier. Thus it accumulates in the brain at high concentrations especially in highly angiogenic regions [114].

Despite slight advances in therapy for newly diagnosed GBM, almost all patients suffer tumor recurrence. Reasons for tumor recurrence include genetic heterogeneity of GBM, glioma stem

cells, the blood brain barrier that prevents most therapeutics to reach the tumor side, and the infiltrative nature of the tumor prohibiting complete surgical resection [112].

Due to the limited success of conventional therapy and thus poor prognosis of GBM, especially of recurrent diseases, there is an intensive search for and development of alternative therapeutical approaches in pre-clinical and clinical studies. These therapeutic modalities include molecular targeted therapy, immunotherapy, gene therapy and oncolytic virotherapy. They are of course associated with several advantages but also limitations and the efficiency needs to be demonstrated in randomized clinical control trials [119, 120].

The concept of molecular targeted therapy is the usage of monoclonal antibodies and low-molecular-weight inhibitors that are designed to specifically target growth factor receptors and their downstream effector molecules associated with the development of GBM [121–123]. Taken together, it can be noted, that these small molecular inhibitors in monotherapy or combination with radiotherapy and Temozolomide were not very successful. The risk of a systemic inhibition when combining multiple inhibitors in one therapeutical approach to block more than one signalling pathway must be seriously tested in the future [121, 124]. Promising target candidates are molecules associated with angiogenesis. Bevacizumab, a monoclonal therapeutic antibody against VEGF, which is currently tested in a randomized phase III clinical trial, is such an inhibitor of angiogenesis [69].

Another alternative therapeutical approach is immunotherapy which can be defined by the ability of the immune system to distinguish between malignant cells and healthy cells and to perform a specific anti-tumor immune response leaving normal cells and tissues unaffected. Current immunotherapeutic approaches for gliomas can be divided into three categories: immune priming (active immunotherapy), immunomodulation (passive immunotherapy), and adoptive immunotherapy [125]. The major limitations and an overview about immune therapeutic approaches for GBM currently under investigation on the level of preclinical and also clinical trials were reviewed in detail by Daga *et al.* [126], Rolle *et al.* [125], and Patel *et al.* [114].

Gene therapy includes the correction of altered genes in GBM, such as p53 (direct gene therapy) or the introduction of suicide genes such as the Herpes simplex virus thymidine kinase/ganciclovir (HSV-TK/GCV) system (indirect gene therapy) [120]. Oncolytic virotherapy will be discussed in more detail in 1.3.

1.3 Principles of oncolytic virotherapy

The observation of cancer regression especially haematological malignancies following virus infection dates back to the mid-1800s and beginning of the 20th century [127, 128]. Tumor

regressions were also reported following vaccination of patients suffering from cancer as shown in a female patient with cervical carcinoma after immunization with an attenuated rabies virus vaccine in 1912. The modern era of oncolytic virotherapy started in the 1990s with the possibilities to generate recombinant genetically modified viruses and an improved understanding of cancer genetics and virology in general [127, 129, 130].

Oncolytic viruses are defined as naturally occurring or engineered viruses that selectively infect, replicate in and kill tumor cells while healthy cells and tissues remain unharmed (Figure 7a) [131–134]. Viral progeny released from initially infected host cells are capable to infect neighboring tumor cells and spread throughout the tumor [130]. Advantageous are the multiplication of the initial virus dose and a local self-amplification of the therapeutic effect. Besides the direct cytopathic effects caused by efficient viral replication resulting in a mixture of apoptotic, necrotic or autophagic tumor cell death, the anti-tumor properties of oncolytic virotherapy are multimodal [134, 135]: Examples are inhibitory effects on the tumor vasculature, the release of cytotoxic cytokines upon virus infection by tumor-resident or infiltrating immune cells or the activity of virally encoded therapeutic transgenes [134, 136, 137].

Another aspect which has become increasingly important in recent years is the use of oncolytic viruses as cancer vaccines as reviewed by Woller *et al.* [134] and Bartlett *et al.* [135] and as depicted in Figure 7b. Virus-mediated tumor cell death causes immunogenic tumor cell debris. This tumor cell debris consists of tumor-associated antigens (TAAs), damage-associated molecular patterns (DAMPs), OV-derived pathogen-associated molecular patterns (PAMPs) and inflammatory cytokines that activate innate immune receptors and that are taken up by antigen-presenting cells such as macrophages and DCs. These antigen presenting cells induce a cytotoxic T-cell response directed against TAAs. In addition, oncolytic virus infection may turn the highly immune suppressive tumor microenvironment into a proinflammatory micromilieu favoring the anti-tumor immune response.

The natural selectivity of oncolytic viruses to infect and replicate in cancer cells is in most cases a consequence of the biology of the cancer cells themselves. They display aberrant signaling pathways affecting cell proliferation, protein and nucleotide synthesis, inhibition of apoptosis as well as inhibition and defects in IFN and other cellular innate immune signaling pathways as reviewed by Ilkow *et al.* [138]. In addition, some oncolytic viruses possess specificity for surface receptors highly upregulated on cancer cells or require conditions present in the tumor microenvironment such as hypoxia or angiogenesis [139].

Tumor selectivity can be further increased by genetic engineering of oncolytic viruses *e.g.* by modification of viral surface molecules or deletion of viral genes which are necessary for viral

replication in non-transformed cells but not in cancer cells [131, 139]. One such example is the deletion of the thymidine kinase (TK) gene locus. TK is required for synthesis of deoxythymidine monophosphate in DNA synthesis. Deletion of this gene results in viral dependence on the cellular TK the expression of which is higher in cancer than in normal cells [131]. As reviewed by Pol *et al.* [133] genetic modifications enhancing viral tumor selectivity take place at many different levels such as the transcriptional, posttranscriptional or translational level.

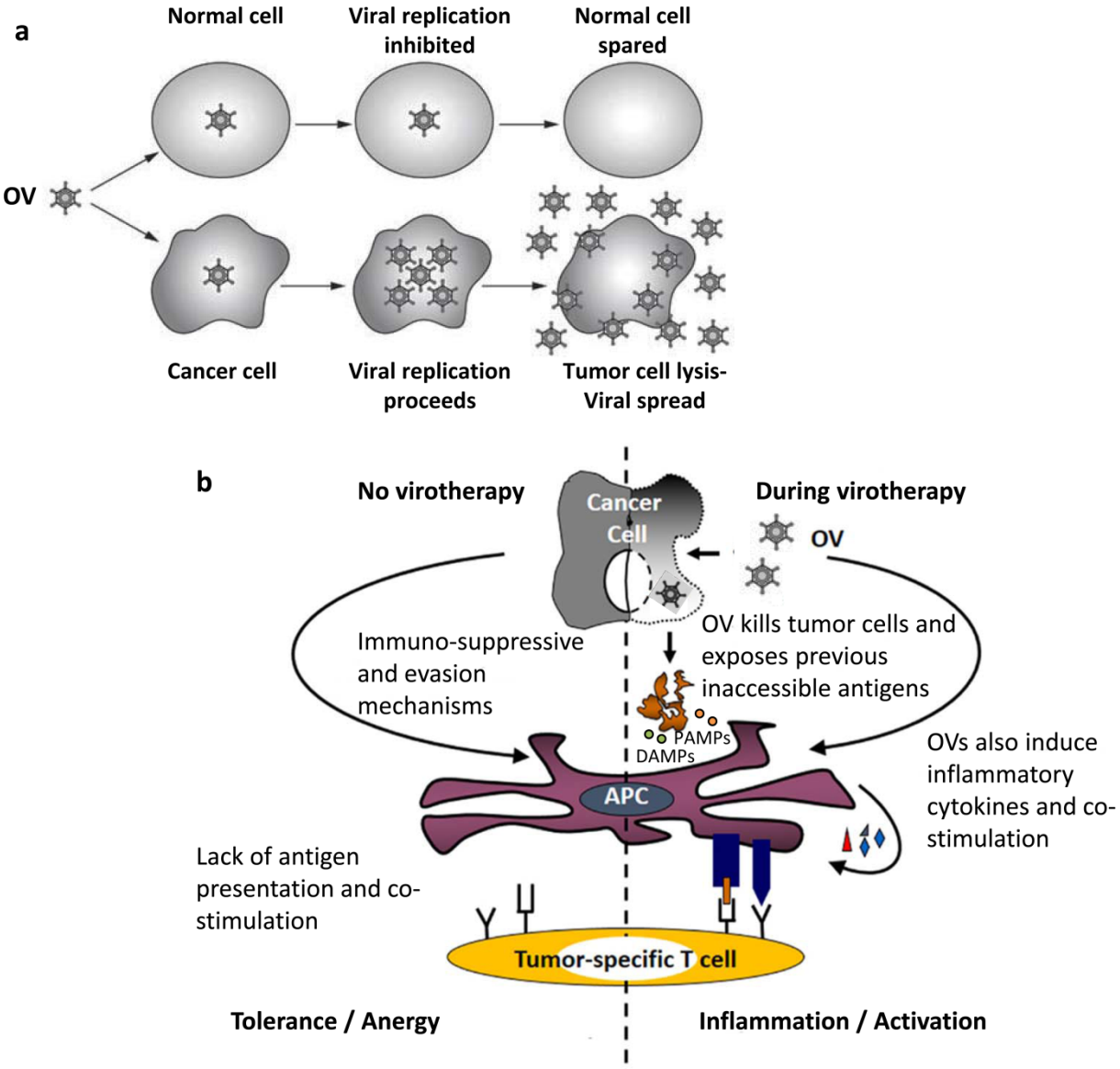

Figure 7: Schematic overview on the principle of oncolytic virotherapy (a) adapted from [127]. Oncolytic viruses (OVs) selectively infect tumor cells while normal cells result in an abortive infection. **OVs can function as tumor vaccines, activating innate and adaptive immunity and thus triggering indirect anti-tumor activity (b)** modified from [140].

An optimal oncolytic virotherapy and thus an optimal oncolytic virus is characterized by high tumor-selectivity, high efficiency, low toxicity to normal tissues, short replication cycles,

capability for intratumoral spread and systemic delivery, genetic stability, easy manufacturing and scale up, availability of antiviral drugs etc. [130].

To date a great number of virus families has been tested as cancer biotherapeutics in preclinical and also clinical trials in almost all types of cancer [139]. Examples are the families of rhabdoviridae (*e.g*. vesicular stomatitis virus, Maraba virus), poxviridae (*e.g.* vaccinia [VACV], myxoma), adenoviridae (*e.g*. adenovirus serotype 5, Colo-Ad1), paramyxoviridae (*e.g*. Newcastle disease virus, measles virus), togaviridae (*e.g*. Sindbis virus), herpesviridae (*e.g.* Herpes simplex virus-1 (HSV-1)), reoviridae (*e.g*. reovirus type III), picornaviridae (*e.g.* poliovirus, coxsackievirus), and parvoviridae (*e.g.* H1-parvovirus) [138].

An overview about the status of current clinical trials with oncolytic viruses and the first lessons learned from those are reviewed in detail by Russel *et al.* [129], Patel *et al.* [141], Bell *et al.* [142] and Pol *et al.* [133].

The adenovirus ONYX-015 (ONYX Pharmaceuticals, USA) has been one of the first oncolytic viruses in clinical trials targeting and selectively replicating in p53 negative cells [132, 141]. A derivative adenovirus H101 (Shanghai Sunway Biotech Co., Ltd) has been licenced in China for combination with chemotherapy in head and neck cancer, but not in Europe or in the US as the promising results could not be seen in further clinical trials.

Of great interest is the status of Talimogene laherparepvec T-VEC formerly known as OncoVEX$^{GM\text{-}CSF}$ (Amgen, Inc, USA) based on HSV-1 which has deletions in the viral genes ICP34.5 and ICP47 and expresses GM-CSF to enhance anti-tumor immune responses. This virus showed 16% durable response in a clinical phase III trial for late stage melanoma [129, 143]. In April 29th 2015 the FDA voted for approval of the dual-acting cancer vaccine/viral therapy in the US [144]. Another clinically relevant oncolytic virus is the reovirus REOLYSIN® (Oncolytics Biotech Inc., Canada) which is currently tested in clinical phase III for advanced squamous cell carcinoma of the head and neck in combination with chemotherapy. Promising early clinical results were obtained in phase I and I/II studies with vaccinia viruses *e.g*. GL-ONC1 (Genelux Corporation, USA) or JX-594 (Jennerex Biotherapeutics, Inc. USA) [129, 145]. GL-ONC1 which is based on GLV-1h68 in preclinical studies is a Lister vaccinia virus vaccine strain [146]. GLV-1h68 was constructed by insertion of the three reporter gene expression cassettes Renilla luciferase-Aequora green fluorescent fusion protein (RUC-GFP), β-galactosidase (LacZ), and β-glucuronidase (GusA) into the F14.5L (encoding WR53.5 protein an IMV transmembrane protein [147]), J2R (encoding thymidine kinase) and A56R (encoding hemagglutinin) loci of the LIVP viral genome, respectively [146]. Insertion of the reporter gene Ruc-GFP fusion allows visualization and identification of infected cells and tumor regression in real time offering theranostic

potential. GLV-1h68 was tested successfully in a great number of preclinical tumor models [148–155]. In the clinic, patients with therapy-resistant peritoneal carcinomatosis were treated with intraperitoneal doses of GL-ONC1 up to 4 times every 28 days. Although the data is not published in detail yet, the researchers stated that the doses were well tolerated and resulted in a reduction of malignant tumor cells in the ascites [145].

JX-594 was engineered from the Wyeth vaccine strain and is attenuated by TK disruption [156]. Similar to T-VEC, JX-594 expresses GM-CSF and additionally β-galactosidase as a marker gene. The clinical findings of this oncolytic VACV are reviewed in detail by Dave *et al.* [132].

Taken together, the early clinical experience with oncolytic viruses has largely been promising [130, 141, 157]. The application of replication-competent oncolytic viruses was generally safe, however, the strong anti-tumor effects and therapeutic efficiency observed in the preclinical studies need to be transferred to human patients so far. Possible factors limiting the success in the clinical setting are the following: Impaired diffusion of oncolytic viruses within neoplastic lesions, antiviral immune responses including the complement system, neutralizing antibodies and the development of therapy resistance [133, 142].

1.3.1 Vaccinia virus taxonomy and morphology

VACV is a member of the *Poxviridae* family. The family of *Poxviridae* is divided into two subfamilies dependent on the host species that becomes infected: *chordopoxvirinae* infecting vertebrates and divided into eight genera and *entomopoxvirinae* infecting insects, divided into three genera [158, 159]. The family of *Poxviridae* is a family of large (300 x 200 x 100 nm), brick-shaped virions with double-stranded DNA genomes (130,000–375,000 nucleotides) that in contrast to other DNA viruses remain in the cytoplasm for the whole infection and replication cycle [158, 160, 161]. Together with variola virus, the causative agent of smallpox disease in humans, VACV is the prototypic member of the *chordopoxvirinae*, with a double-stranded DNA genome of approximately 192 kb, encoding for more than 200 genes responsible for functions such as viral entry, transcription, DNA and RNA synthesis, virion assembly and host immune suppression [160, 162]. The most prominent VACV strains include Lyster, Wyeth, Copenhagen and Western Reserve [145, 163].

The infectious particles of VACV consist of a lipoprotein envelope surrounding a lateral body and a biconcave core containing the DNA genome and viral enzymes. The ends of the two DNA strands are connected with hairpin loops to one molecule. The essential and highly conserved genes within the family of *Poxviridae* are localized in the central part of the genome and those, which are not necessary for viral replication, are localized in the more peripheral regions. The

genome is further characterized by the absence of introns, short promoter sequences and many small open reading frames which allow the dense packaging of the 200 genes in the DNA molecule [158, 164].

1.3.2 VACV life cycle and morphogenesis

The VACV life cycle consist of the following steps: viral entry, early gene expression, uncoating, virus replication, intermediate and late gene expression, virus particle formation, maturation and finally virus release [162].

During the VACV life cycle there are four different infectious forms produced including intracellular mature virions (IMV), intracellular enveloped virions (IEV), cell-associated enveloped virions (CEV) and extracellular enveloped virions (EEV). They differ in the number of surrounding membranes, associated virus proteins, their frequency, function and localization [145, 165]. The most common and infectious forms are IMV and EEV [145]. They enter the host cell either at a neutral pH by direct fusion with the cellular membranes or at low acidic pH by an endosomal pathway via activation of micropinocytosis [145, 166, 167]. The mechanisms of attachment and initiation of micropinocytosis differ between the two infectious forms [166]. The viral proteins associated with attachment of IMVs to glycosaminoglycan or laminin on the cell membrane have been identified and include A26, A27, H3, and D8 [167, 168]. Independent from the process of virus attachment, the fusion is dependent on a complex of 11-12 non-glycosylated transmembrane proteins that are conserved in poxviruses [167].

When the core has entered the cytoplasm, it is transported further into central regions of the cell to the endoplasmic reticulum (ER) along microtubules [165]. Similar to other viruses, the gene expression of the individual gene classes (early, intermediate and late) in VACV is tightly regulated by a temporal cascade. Proteins required early for DNA replication, nucleotide biosynthesis or intermediate gene transcription are transcribed early and proteins required for virus assembly and morphogenesis are encoded by intermediate and late genes [161, 169]. Inside the core, together with the genome, all proteins *e.g.* a multi-subunit DNA-dependent RNA polymerase, early transcription factors, capping and methylating enzymes, and a poly(A) polymerase necessary for early gene transcription are packaged [162]. Early mRNAs that are detected as soon as 1 hour post infection (hpi) are released and translated in the cytoplasm of the host cell. They are responsible for uncoating of the core, the release of the parental DNA, DNA replication and protection of the host cell from immune responses [159, 162]. DNA replication starts within a few hpi and takes place in cytoplasmic virus factories [164, 168, 170]. Those viral factories are cytoplasmic infection-specific domains with uniform density surrounded

by cellular ER-derived membrane cisternae [168]. The replication of the VACV genome, which was released during the uncoating step, starts at both terminal sequences and takes place in form of multiple concatemers that are finally ripped into individual genomes [159]. Following replication, the transcription of intermediate and late genes starts [165]. In contrast to the early transcription, in the transcription process of intermediate and late genes also host-derived transcription factors are involved, in addition to the viral transcriptome [161]. The intermediate genes encode for regulatory proteins necessary for the transcription of late genes. The latter encode for structural and membrane proteins necessary for virus assembly and early transcription factors and enzymes that are part of the newly synthesized virus particles [165, 171]. Virion assembly starts in the area where virus replication took place. The process is associated with the formation of crescent-shaped single lipid bilayers and viral proteins that step by step become a spherical structure enclosing the virus core. Those structures are then called immature virions (IV) and the process is reviewed in detail by Liu *et al.* [168]. These IVs finally form IMVs by condensation of the core proteins [159]. IMVs are the first and simplest form of infectious VACV particles and are surrounded by a single lipid bilayer [145]. In most cases, they remain within the infected cells until cell lysis or they are transported via microtubules to the trans-Golgi network or to early endosomes where they become modified and surrounded by two additional membranes termed as IEVs. IEVs transported via microtubules to the plasma membrane and exposed at the cell surface are called CEVs. CEVs either support the formation of actin tails under the plasma membrane transporting virus particles to neighbouring cells or are released from the cell as EEVs [145, 169, 172].

1.3.3 The clinical history of VACV and its use as genetic vector and oncolytic agent

VACV has a long clinical history which dates back to the year 1798 and Edward Jenner's smallpox vaccination experiments using cowpox viruses [163, 173]. Due to the successful clinical history of VACV as vaccine virus during the worldwide smallpox eradication program which was completed in 1978, VACV is one of the most extensively studied viruses up to date [163, 173]. Beside its use as vaccine against influenza or HIV, VACV has been evaluated concerning its use in cancer therapy: it has been analysed as expression vector in gene therapy, as replication-competent oncolytic virus or as cancer vaccine with immunostimulatory properties [174].

There are a number of inimitable characteristics making VACV a promising candidate for prospective biotherapeutics: the first point which is an important safety issue is that VACV exclusively replicates in the cytoplasm of the host cell and thus does not integrate into the host genome [174]. Second, in comparison to other viruses, VACV has a fast replication cycle which is

normally completed after 24 h resulting in the release of up to 10,000 new virus particles, and also shows rapid and efficient cell lysis 48 to 72 hpi [175]. Third, due to great number of VACV viral promoters the timing and level of gene expression can be controlled [174]. In addition, VACV has a natural tropism for cancer cells however it can infect a large range of human tissues without causing severe illnesses [162, 176]. Due to the broad host range it can be studied in syngeneic animal models [174]. Another advantage is that VACV has a large genome which allows integration or manipulation of large exogenous DNA fragments and transgene expression [132]. Further, VACV is a highly immunogenic virus that not only causes oncolysis in malignant tumor cells but also induces a strong anti-tumor immune response by activation of T-lymphocytes. An important safety issue is the availability of antiviral drugs to treat possible side effects of an infection. [174]

Due to the great number of advantages, VACV has been used as oncolytic agent in this study. The oncolytic viruses LIVP 1.1.1 and GLV-1h68 used in all experiments are based on the Lister strain.

1.3.4 Oncolytic virotherapy of malignant gliomas

With respect to oncolytic vaccinia virus therapy and its effectiveness for high grade gliomas, anti-tumor effects and survival benefits were demonstrated in preclinical rodent models after combination therapy with the double-deleted vaccinia virus JX-594 with rapamycin or cyclophosphamide [177, 178]. Further, in an article recently published, it was demonstrated that focal irradiation followed by systemic administration of the VACV GLV-1h68 and LIVP 1.1.1 increased survival and preferential replication in a mouse glioma xenograft tumor model [179]. In a further study, systemic administration of the oncolytic vaccinia virus GLV-1h164 expressing an anti-VEGF antibody in combination with fractionated irradiation resulted in enhanced inhibition of tumor growth when compared to non-anti-VEGF expressing oncolytic virus GLV-1h68 [180].

In another study a BMP-4 overexpressing VACV (GLV-1h285) was found to target and better replicate in GBM initiating stem cell cultures. In addition, a lack of tumor recurrence in orthotopic xenograft models of GBM based on primary cancer stem cell lines compared to the parental virus strain was observed [181].

There is a great number of oncolytic viruses, such as HSV (HSV-1716 and G207), adenovirus (AdV-Onyx-015), Newcastle disease virus (NDV-MTH-68/ H, NDV-HUJ), reovirus (Reo V), H1 parvovirus (H1PV), measles virus, (MV-CEA) and poliovirus (PVS-RIPO) that have been or are currently tested in early clinical trials phase I/II for gliomas [130, 137, 157]. In total, 120 GBM

patients were treated with oncolytic viruses administered intratumorally or intravenously [182]. Initial clinical trials have been completed for HSV, adenovirus, reovirus and NDV [137]. In general, it was shown, that the tested oncolytic viruses were safe, with no maximum tolerated dose reached, and a certain level of anti-glioma activity was found in some of the patients [157]. However, the encouraging preclinical findings could not be translated to the clinic so far.

Factors responsible for limited efficiency in clinical glioma trials which need to be analyzed and improved are, amongst others, the delivery route (intracranial *vs.* intravenous), the use of carrier cells such as neural stem cells, mesenchymal stem cells, the intratumoral distribution and spread, the selective targeting of cancer initiating cells, the circumvention of the blood brain barrier, the role of the immunosuppressive microenvironment and resident brain and immune cells [137, 183]. Also combinational therapeutic approaches with established treatment modalities such as chemotherapy, radiotherapy or immunomodulatory/immuneinhibitory agents need further evaluation [183, 184].

1.4 Aims of the thesis

It has been demonstrated in clinical trials for most cancer types, including glioblastoma multiforme, that the application of replication-competent viruses is safe. However, the promising therapeutic effects observed in the preclinical studies still need to be confirmed in human patients [130, 157]. As described by Dey *et al.* [185], the choice of and search for an adequate preclinical model may help to overcome the dichotomy between preclinical and clinical findings. The concept of personalized medicine by screening cancer patients for best treatment options and thereby maximizing therapeutic outcome is a very successful approach which could improve oncolytic virotherapy, as well [186, 187].

The main topic of this thesis was thus, the characterization of various murine GL261 glioma models for oncolytic VACV therapy and in addition identifying prospective biomarkers.

- In the first instance, a comparative approach should be applied to analyse the replication efficacy and oncolytic potential of the VACV LIVP 1.1.1 in different murine GL261 glioma models. With this approach it was expected to identify potential microenvironmental factors that influence treatment success or failure and that might function as biomarkers in future clinical trials. Replication efficacy of LIVP 1.1.1 should be compared at different tumor locations, *i.e.* subcutaneous and orthotopic as well as in mice with different immunologic (immunocompetent and immunodeficient) and genetic backgrounds (C57BL/6 and Balb/c).

- Further, a detailed characterization of the tumor microenvironments of the subcutaneous GL261 tumor models (Balb/c athymic, C57BL/6 athymic and C57BL/6 wt) should be elaborated. For this, immunohistochemistry, FACS analysis, a biomarker profiling by RBM ELISA and depletion or substitution of relevant factors/cell types was to be conducted.

- There is not much knowledge about the susceptibility of glial cells to VACV infection and the consequences for oncolytic virotherapy of gliomas. Therefore, the impact of two distinct cell populations besides the tumor cells, namely microglia/macrophages and astrocytes should be analysed in the context of oncolytic VACV therapy for intracranial GL261 glioma models. Both cell types are described to be recruited to malignant gliomas or make up significant proportion of the tumor mass as in case for microglial cells [86, 188, 189]. Besides the *in vivo* analyses, different *in vitro* studies with two murine cell lines namely BV-2 microglia and IMA 2.1 astrocytes as well as organotypic brain slice cultures should be used to figure out whether these glial cells are susceptible to VACV infection and whether VACV infection of these cells does affect the therapeutic efficacy of LIVP 1.1.1 in the orthotopic GL261 glioma models.

In an additional project, the impact and role of the anti-apoptotic factor AVEN on VACV GLV-1h68 infection should be investigated with the help of different biological assays in cells of different human tumor cell lines (888-MEL, 1936-MEL, GI-101A, HT-29). AVEN as a potential target gene has been identified by J. Reinboth and A. Cecil (unpublished data) based on gene expression analysis and Boolean models.

2 Material

2.1 Chemicals, enzymes, kits

Table 1: List of chemicals and enzymes

Reagent	Manufacturer/supplier
1 kb DNA ladder	New England BioLabs, Frankfurt, Germany
100 bp DNA ladder	New England BioLabs, Frankfurt, Germany
Agarose Low Melt	AppliChem, Darmstadt, Germany
Acetic acid	Roth, Karlsruhe, Germany
Aceton	Roth, Karlsruhe, Germany
Agarose	Roth, Karlsruhe, Germany
Ammonium chloride (NH_4Cl)	Merck, Darmstadt, Germany
Ammonium persulfate (APS)	Merck, Darmstadt, Germany
β-Mercaptoethanol	AppliChem, Darmstadt, Germany
Bromophenol blue	Roth, Karlsruhe, Germany
Carboxymethylcellulose (CMC)	Sigma-Aldrich, Steinheim, Germany
Cinnamic acid	Sigma-Aldrich, Steinheim, Germany
Complete Mini protease inhibitors	Roche, Mannheim, Germany
Coomassie Brillant Blue G250	Serva Feinbiochemica, Heidelberg; Germany
Crystal violet	Sigma-Aldrich, Steinheim, Germany
DABCO	Roth, Karlsruhe, Germany
Dimethyl sulfoxide (DMSO)	Sigma-Aldrich, Steinheim, Germany
Disodium phosphate hydrate ($Na_2HPO_4x12H_2O$)	Merck, Darmstadt, Germany
DNTP-Mix	Fermentas, St. Leon-Rot, Germany
Ethylenediaminetetraacetic acid (EDTA)	Sigma-Aldrich, Steinheim, Germany
EDTA-NA_2	Roth, Karlsruhe, Germany
Ethanol (96%)	Chemical dispensing, University Würzburg, Germany
Ethanol (p.a.)	Riedel de Haen, Seelze, Germany
FITC-coupled Isolectin B4 (IB4)	Sigma-Aldrich, Steinheim, Germany
Fetal bovine serum (FBS)	PAA, Pasching, Austria
Gel loading dye blue (6x)	New England BioLabs, Frankfurt, Germany
Glycerol	Sigma-Aldrich, Steinheim, Germany
Glycine	Roth, Karlsruhe, Germany
Hoechst 33258	Sigma-Aldrich, Steinheim, Germany
Hydrogen peroxide (H_2O_2)	Sigma-Aldrich, Steinheim, Germany
Isotonic sodium chloride solution (0.9%)	Braun, Emmenbrücke, Switzerland

Isopropyl alcohol	Roth, Karlsruhe, Germany
Ketavet (10%)	Pharmacia GmbH, Berlin, Germany
Kynuric acid	Sigma-Aldrich, Steinheim, Germany
Luminol	Amersham, Freiburg, Germany
Magnesium chloride ($MgCl_2$)	Sigma-Aldrich, Steinheim, Germany
Metacam	Boehringer Ingelheim, Ingelheim, Germany
Methanol	Roth, Karlsruhe, Germany
Midori geen advanced DNA stain	Nippon Genetics Europe GmbH, Dueren, Germany
Monopotassium phosphate (KH_2PO_4)	Sigma-Aldrich, Steinheim, Germany
Monosodium phosphate (NaH_2PO_4)	Merck, Darmstadt, Germany
Mowiol 4-88	Roth, Karlsruhe, Germany
MTT 3-(4,5-Dimethylthiazol-2-yl)-2,5-diphenyltetrazolium bromide	Sigma-Aldrich, Steinheim, Germany
Myo-inositol	Sigma-Aldrich, Steinheim, Germany
N,N,N',N'-Tetramethylethylendiamin (TEMED)	Fluka, Buchs, Switzerland
PageRuler prestained protein ladder	Thermo Scientific, Karlsruhe, Germany
Paraformaldehyde	AppliChem, Darmstadt, Germany
Phosphate buffered saline (PBS)	PAA, Pasching, Austria
Phalloidin tetramethylrhodamine in MeOH (P-TRITC)	Sigma-Aldrich, Steinheim, Germany
Potassium bicarbonate ($KHCO_3$)	AppliChem, Darmstadt, Germany
Potassium chloride (KCl)	Merck, Darmstadt, Germany
Propidium iodide (PI)	Sigma-Aldrich, Steinheim, Germany
Pyruvic acid	PAA Laboratories, Pasching, Austria
Rotiporese®Gel 30	Roth, Karlsruhe, Germany
Saponin	Roth, Karlsruhe, Germany
Simvastatin	Sigma-Aldrich, Steinheim, Germany
Skimmed milk powder	Roth, Karlsruhe, Germany
Sodium azide (NaN_3)	Sigma-Aldrich, Steinheim, Germany
Sodium bicarbonate ($NaHCO_{3)}$	Merck, Darmstadt, Germany
Sodium chloride (NaCl)	Roth, Karlsruhe, Germany
Sodium deoxycholat	Roth, Karlsruhe, Germany
Sodium dodecyl sulfate (SDS)	Roth, Karlsruhe, Germany
Sodium hydroxide (NaOH)	Merck, Darmstadt, Germany
SiLentFect™ Lipid Reagent	Bio-Rad, München, Deutschland
ß-Mercaptoethanol	AppliChem, Darmstadt, Germany
Streptavidin-Cy3 (from *Streptomyces avidinii*)	Sigma-Aldrich, Steinheim, Germany
Sucrose	Roth, Karlsruhe, Germany
Tablet complete	Roche, Mannheim, Germany
Tissue Tek	LABART, Waldbüttelbrunn, Germany
Tripotassium phosphate (K_3PO_4)	Merck, Darmstadt, Germany
Trizma-base	Sigma-Aldrich, Steinheim, Germany

Tris-HCl pH 3.5-5	Roth, Karlsruhe, Germany
Triton X-100	Applichem, Darmstadt, Germany

Table 2: List of kits

Kit	Manufacturer/Supplier
RNeasy Mini Kit	Qiagen GmbH, Hilden, Germany
DNA-free™ Kit	Ambion, Austin, TX, USA
RevertAid™ First Strand cDNA Synthesis Kit	Fermentas, St. Leon-Rot, Germany
Transcriptor High Fidelity cDNA Synthesis Kit	Roche Diagnostics, Mannheim, Germany
si-RNA-27 Kit	OriGene, Rockville, USA
FITC Annexin V Apoptosis Detection Kit with 7-AAD	BioLegend Inc. San Diego, USA
Griess reagent system	Promega, Mannheim, Germany
Venor™GeM Mycoplasma Detection Kit	Minerva Biolabs GmbH, Berlin, Germany

2.2 Antibodies, oligonucleotides and enzymes

Table 3: List of primary antibodies for fluorescence microscopy and Western blot

Specificity	Clone	Source	Usage	Manufacturer/Supplier
α-arginase	H-52	rabbit	WB	Santa Cruz, Heidelberg, Germany
α-AVEN		rabbit	WB	Cell Signaling Technology, Danvers, USA
α-beta actin	AC-15	mouse	WB	Abcam, Cambridge, UK
α-caspase-3	H-277	rabbit	WB	Santa Cruz, Heidelberg, Germany
α-GAPDH	6C5	mouse	WB	Abcam, Cambridge, UK
α-GFAP		chicken	IF	Abcam, Cambridge, UK
α-caspase-9	H-277	rabbit	WB	Cell Signaling Technology, Danvers, USA
α-Iba-1		rabbit	IF	WAKO, Neuss, Germany
α-iNOS		rabbit	WB	Novus Biologicals, Cambridge, UK
α-mouse-CD68	FA-11	rat	IF	Abcam, Cambridge, UK
α-MHC class II (I-A/I-E)-biotin-conj.	M5/114.15.2	rat	IF	eBioscience, Frankfurt, Germany
α- MHC class II (I-A/I-E)	M5/114.15.2	rat	IF	eBioscience, Frankfurt, Germany
α-vaccinia virus		rabbit	WB,IF	Abcam, Cambridge, UK

Table 4: List of secondary antibodies for fluorescence microscopy and Western blot

Specificity	Conjugate	Source	Usage	Manufacturer/Supplier
α-rat IgG (H+L)	Cy3	donkey	IF	Jackson ImmunoResearch, Inc. West Grove, PA, USA
α-rat IgG (H+L)	Cy2	donkey	IF	Jackson ImmunoResearch, Inc. West Grove, PA, USA
α-chicken IgY(H+L)	Cy5	donkey	IF	Dianova, Hamburg, Germany
α-rabbit IgG (H+L)	Cy2	donkey	IF	Dianova, Hamburg, Germany

α-rabbit IgG (H+L)	Cy5	donkey	IF	Dianova, Hamburg, Germany
α-rabbit IgG (H+L)	Cy3	donkey	IF	Dianova, Hamburg, Germany
α-rabbit IgG (H+L)	HRP	goat	WB	Santa Cruz, Heidelberg, Germany
α-mouse IgG(H+L)	HRP	rabbit	WB	Abcam, Cambridge, UK

Table 5: List of conjugated antibodies for FACS analysis

Specificity	Conjugate	Clone	Isotype	Manufacturer/Supplier
α-CD3	PE	145-2C11	Hamster IgG	BD Bioscience Heidelberg, Germany
α-CD4	APC	GK1.5	Rat IgG2b	eBioscience, Frankfurt, Germany
α-CD8	FITC	53-6.7	Rat IgG2a	BD Bioscience Heidelberg, Germany
α-CD11b	APC	M1/70	Rat IgG2b	eBioscience, Frankfurt, Germany
α-CD11b	PE	M1/70	Rat IgG2b	BD Bioscience Heidelberg, Germany
α-CD11b	PerCP-Cy5.5	M1/70	Rat IgG2b	eBioscience, Frankfurt, Germany
α-CD11c	PE	N418	Hamster IgG	BioLegend, London, UK
α-CD11c	APC	N418	Hamster IgG	BioLegend, London, UK
α-CD14	PerCP	Sa2-8	Rat IgG2a	eBioscience, Frankfurt, Germany
α-CD16/CD32	-	93	Rat IgG2a	eBioscience, Frankfurt, Germany
α-CD19	PerCP-Cy5.5	6D5	Rat IgG2a	eBioscience, Frankfurt, Germany
α-CD45	PerCP-Cy5.5	30-F11	Rat IgG2b	eBioscience, Frankfurt, Germany
α-CD49b	APC	DX5	Rat IgM	eBioscience, Frankfurt, Germany
α-CD68	FITC	FA-11	Rat IgG2a	Serotec GmbH
α-CD206	FITC	C068C2	Rat IgG2a	BioLegend, London, UK
α-F4/80	APC	BM8	Rat IgG2a	eBioscience, Frankfurt, Germany
α-Gr1	FITC	RB6-8C5	Rat IgG2b	eBioscience, Frankfurt, Germany
α-Ly6c	PerCP-Cy5.5	AL-21	Rat IgM	BD Bioscience Heidelberg, Germany
α-Ly6G	PE	1A8	Rat IgG2a	BD Bioscience Heidelberg, Germany
α-MHCII	PE	M5/114. 15.2	Rat IgG2b	eBioscience, Frankfurt, Germany

Table 6: List of isotype controls for FACS analysis

Isotype Controls	Conjugate	Clone	Manufacturer/Supplier
Hamster IgG	APC	HTK888	BioLegend, London, UK
Rat IgG2a ƙ	PE	eBR2a	eBioscience, Frankfurt, Germany
Rat IgG2a ƙ	APC	eBR2a	eBioscience, Frankfurt, Germany
Rat IgG2a ƙ	PerCP-Cy5.5	eBR2a	eBioscience, Frankfurt, Germany
Rat-IgG2b ƙ	PE	eB149/10H5	eBioscience, Frankfurt, Germany
Rat-IgG2b ƙ	APC	eB149/10H5	eBioscience, Frankfurt, Germany
Rat-IgG2b ƙ	FITC	eB149/10H5	eBioscience, Frankfurt, Germany
Rat-IgG2b ƙ	PerCP-Cy5.5	eB149/10H5	eBioscience, Frankfurt, Germany
Rat-IgM ƙ	APC		eBioscience, Frankfurt, Germany
Rat-IgG1 ƙ	APC	EBRG1	eBioscience, Frankfurt, Germany

Table 7: List of synthetic oligonucleotides

Target	Sequence
human AVEN	forward 5'-GATTTCAGTGTCCTCCTTAG-3'
	reverse 5'-CCTTGCCATCATCAGTTCTC-3'
human GAPDH	forward 5'-GCCTTCCGTGTCCCCACTGC-3
	reverse 5'-CAATGCCAGCCCCAGCGTCA-3'
human β-Actin	forward 5'-CCTCTCCCA AGTCCACACAG-3'
	reverse 5'-CTGCCTCCACCC ACTC-3'

Table 8: List of enzymes

Enzyme	Manufacturer/Supplier
Benzonase	Merck, Darmstadt, Germany
Collagenase I	Sigma-Aldrich, Steinheim, Germany
DNase I	Calbiochem, Darmstadt, Germany
Phusion DNA Polymerase	Finnzymes, Espoo, Finland
Trypsin-EDTA	PAA, Pasching, Austria / Sigma-Aldrich, Steinheim, Germany

2.3 Laboratory equipment and other materials

Table 9: List of laboratory equipment

Equipment	Manufacturer/Supplier
Accuri C6 Cytometer	Accuri Cytometers, Inc. Ann Arbor, MI USA
Anesthetic device	Berthold Technologies, Bad Wildbad, Germany
Autoclip Wound Clip System	Harvard Apparatus, Holliston, USA
Axiovert 25 inverse microscope	Zeiss, Jena, Germany
Axiovert 40 CFL inverse microscope	Zeiss, Jena, Germany
Axiovert 200M inverse microscope	Zeiss, Jena, Germany
Biofuge fresco	Heraeus, Hanau, Germany
ChemiDox XRS^{+}	BioRad, Munich, Germany
Centrifuge 5804R	Eppendorf AG, Hamburg, Germany
Cryostat 2800 Frigocut	Leica Wetzlar, Germany
DNA gel electrophoresis chamber	BioRad, Munich, Germany
ELISA-Photometer Sunrise^{TM}	TECAN Group, Männedorf, Germany
FastPrep^{TM} 120 Cell Disruptor	Qbiogene, Germany
FastPrep Cell Disruptor	Thermo Scientific, Karlsruhe Germany
Gel documentation	PeqLab, Erlangen, Germany
GentleMACS Dissociator	Miltenyi Biotec, Bergisch Gladbach, Germany
HandyStep® S	BRAND, Wertheim, Germany
Horizontal electrophoresis chambers	BioRad, Munich, Germany
KL 1500 Compact Light Source	Schott, Mainz, Germany
Flow-Hood LaminAir	Kendro, Langenselbold, Germany
Leica VT1000S Vibratome	Leica Wetzlar, Germany

Leica MZ16 FA Stereo-Fluorescence microscope	Leica Wetzlar, Germany
Maestro *In Vivo* imaging system	CRI, US-Woburn
Megafuge 1.OR	Heraeus, Hanau, Germany
Mini-PROTEAN electrophoresis system	BioRad, Munich, Germany
Multipette® plus	Eppendorf, Hamburg, Germany
Neubauer counting chamber	Hartenstein, Würzburg, Germany
Refrigerator	Liebherr, Germany
Pipetboy comfort	INTEGRA Biosciences, Fenwald, Germany
PowerPac Basic Powersupply	BioRad, Munich, Germany
Semi-Dry Blot apparatus	Peqlab, Erlangen, Germany
Table centrifuge minispin	Eppendorf, Hamburg, Germany
Table shaker	Heidolph, Schwabach, Germany
T-Gradient Thermoblock PCR machine	Biometra, Göttingen, Germany
Thermomixer Comfort	Eppendorf, Hamburg, Germany
Sonifier Branson 450	Heinemann, Schwäbisch-Gmünd, Germany
Special accuracy weighing machine	Kern, Balingen-Frommern, Germany
Spectral confocal & multiphoton system Leica TCS SP2	Leica, Wetzlar, Germany
Stereotactic apparatus for small animals	Stoelting Europe, Dublin, Ireland

Table 10: List of consumption items

Consumption items	Manufacturer/Supplier
Alcohol swab	Servoprax GmbH, Wesel, Germany
Aseptic filter (0.2 µl and 0.45 µl)	Schleicher & Schuell, Dassel,Germany
Autoclips (wound clips)	Harvard Apparatus, Holliston, USA
Blotting paper	Hartenstein, Würzburg, Germany
Cannulae 25G, 27G	Braun, Emmenbrücke, Switzerland
Cell culture dishes (Cellstar® 100 mm; 145 mm)	Greiner, Frickenhausen, Germany
Cell culturing flasks (25 cm², 75 cm² and 175 cm²)	Greiner, Frickenhausen, Germany
Cell culture well plates (6-, 12-, 24-, 48-, 96-well)	Greiner, Frickenhausen, Germany/ Sarstedt, Nümbrech, Germany
Cell strainer/Nylon mesh filter (40 µm and 70 µm)	BD Biosciences, Erembodegem, Belgium
Cell scraper	SPL Lifesciences Inc., South Korea
Ceramic bead tubes (1.4 mm)	Peqlab, Erlangen, Germany
Combitips	Eppendorf AG, Hamburg, Germany BRAND GMBH + CO KG, Wertheim, Germany
Cotton tip swabs Eurotubo® (sterile)	I.A.S.A, Rubí, Spain
Cryo tubes	Greiner, Frickenhausen, Germany
Glassware	Schott, VWR, Brand
Gloves (Semperguard Latex)	Semperit, Wien, Austria
Hamilton syringe #701	Hartenstein, Wuerzburg, Germany
Insulin syringe-100 26 G x ½ in	Becton Dickinson, New Jersey,USA
Injekt® Solo	Braun, Emmenbrücke, Switzerland

Microscope cover glasses	Hartenstein, Würzburg, Germany
Microscope cover slides	Roth, Karlsruhe, Germany
M-tubes	Miltenyi Biotec, Bergisch Gladbach, Germany
Nitrocellulose transfer membrane (0.45 µm)	Hartenstein, Würzburg, Germany
SafeSeal tube (1.5 ml)	Sarstedt, Nümbrech, Germany
Sample tubes (0.5 ml, 1.5 ml, 2 ml)	Sarstedt, Nümbrech, Germany
Sample tubes (15 ml & 50 ml)	Greiner, Frickenhausen, Germany
Screw cap tubes (1.5 ml) and caps	Sarstedt, Nümbrech, Germany
Semi-porous membrane inserts (0.4 mm)	Millipore, Temecula, USA,
Serological pipet (5 ml, 10 ml, 25 ml, 50 ml)	Greiner, Frickenhausen, Germany
Shaver, Contura	Wella, Germany
Surgical scalpel Fig. 10, Fig. 15	Megro, Wesel, Germany
Syringe	Becton, Heidelberg, Germany
Parafilm	Hartenstein, Würzburg, Germany
PCR tube strips and cap strips (0.2 ml)	Hartenstein, Würzburg, Germany
Pipet tips (blue, white)	Anthos, Krefeld, Germany
Pipet tips (yellow)	Sarstedt, Nümbrech, Germany

Table 11: Software

Software	Function	Company
Adobe Photoshop CS5 (64 bit)	Image processing / editing	Adobe
Axiovision 4.8	Image acquisition (Axiovert 200M inverse microscope)	Zeiss
C Flow Plus 1.0.227.4	Analysis of FACS data	Accuri Cytometers
Image J	Image processing / editing (http://rsbweb.nih.gov/ij)	NIH
Image lab software 5.2	Image acquisition of DNA and RNA gels and Western blots	BioRad
Leica Confocal 2.16	Image acquisition (Leica TCS SP2)	Leica
Magellan	ELISA-Photometer	Tecan
Metamorph Imaging	Image acquisition (Leica MZ16 FA)	Leica
Microsoft Word 2010	Word processing	Microsoft
Microsoft Excel 2010	Spreadsheet analysis and statistics	Microsoft
Microsoft Power Point 2010	Presentations and figure preparation	Microsoft
WinLight	Bioluminescence-Imaging	Berthold

2.4 Media and supplements for cell culture

Table 12: List of media

Medium	Manufacturer/Supplier
DMEM High Glucose (4,5 g/L)	
Ham's F12	PAA, Pasching, Austria /

MEM with Earle's salts	Sigma-Aldrich, Steinheim, Germany
RPMI-Medium 1640 with phenol red	
RPMI-Medium 1640 without phenol red	

Table 13: List of buffers, supplements and stimulants

Reagents	Manufacturer/Supplier
1x Balanced salt solution (BSS)	Sigma-Aldrich, Steinheim, German
Fetal bovine serum (FBS)	PAA, Pasching, Austria
D-Glucose	Applichem, Darmstadt, Germany
Gentamycin	PAA, Pasching, Austria
Hepes (1 M)	PAA, Pasching, Austria
LPS, 026:B6 from E.coli	Sigma-Aldrich, Steinheim, German
Non-essential amino acids (100x)	PAA, Pasching, Austria
Normal horse serum	PAA, Pasching, Austria
Estradiol	Sigma-Aldrich, Steinheim, Germany
Phosphate buffered saline (PBS)	Sigma-Aldrich, Steinheim, German
Progesterone	Sigma-Aldrich, Steinheim, German
Recombinant human fibroblast growth factor (rh-FGF)	Millipore, Temecula, USA
Recombinant human interferon gamma (rh-IFN-γ)	Immunotools, Friesoythe, Germany
Recombinant murine interferon gamma (rm-IFN-γ)	Immunotools, Friesoythe, Germany
Recombinant murine interleukin 4 (rm-IL-4)	Immunotools, Friesoythe, Germany
Recombinant murine macrophage colony stimulating factor (rm-M-CSF)	Immunotools, Friesoythe, Germany
Recombinant murine granulocyte macrophage colony stimulating factor (rm-GM-CSF)	Immunotools, Friesoythe, Germany
Sodium bicarbonate solution (2.2 g/l)	Sigma-Aldrich, Steinheim, German
Sodium pyruvate ($C_3H_3NaO_3$) (100 mM)	Sigma-Aldrich, Steinheim, Germany
Stable Glutamine (200 mM)	Invitrogen, Karlsruhe, Germany
Penicillin / Streptomycin (100 U/ml)	Sigma-Aldrich, Steinheim, Germany

2.5 Cell lines and culture media

Table 14: List of cell lines

Cell line	Description	Source of supply
BV-2	raf/myc-immortalized murine neonatal microglia; most frequently used substitute for primary microglia [190, 191]	M. Karlstetter (University of Cologne, Germany)
CV-1	african green monkey kidney fibroblast cells	American Type Culture Collection (ATCC; Manassas, VA, USA)
DBTRG-05MG	human glioblastoma cell line	Leibniz Institute DSMZ

		(Braunschweig, Germany)
GI101A	human ductual breast adenocarcinoma cell line	A. Aller (Rumbaugh-Goodwin Institute for Cancer Research, Inc., FL, USA)
GL261	murine glioma cell line	A. Pagenstecher (University Hospital of Marburg, Germany) Authentication by the DSMZ
HT-29	human colorectal adenocarcinoma cell line (Duke's type B)	ATCC (Manassas, VA, USA9
IMA2.1	immortalized murine cortical astrocytes [192]	S. Schildknecht (University of Konstanz, Germany)
J774	murine macrophages	ATCC (Manassas, VA, USA)
U-87	human glioblastoma cell line	Cell Lines Service GmbH CLS (Eppelheim, Germany)
U-138-MG	human glioblastoma cell line	Leibniz Institute DSMZ (Braunschweig, Germany)
888-MEL	human melanoma cell line	F. M. Marincola (National Institutes of Health, Bethesda, MD, USA)
1936-MEL	human melanoma cell line	F. M. Marincola (National Institutes of Health, Bethesda, MD, USA)
42-MG-BA	human glioblastoma cell line	Leibniz Institute DSMZ (Braunschweig, Germany)

2.5.1 Composition of cell culture media

Culture medium	DMEM	500 ml
CV-1 / GL261 / BV-2 / IMA2.1	FBS (h.i.)	10%
	Penicillin/Streptomycin (100 U/ml)	1%
Culture medium	RPMI	500 ml
DBTRG-05MG / J774 / 888-MEL	FBS (h.i.)	10%

/ 1936-MEL	Penicillin/Streptomycin (100 U/ml)	1%
Culture medium	DMEM	500 ml
U-87 MG	FBS (h.i.)	10%
	Penicillin/Streptomycin (100 U/ml)	1%
	Non-essential amino acids (100x)	1%
	Stable glutamine (200 mM)	1%
Culture medium	MEM with Earle's salts	500 ml
U-138-MG	FBS (h.i.)	10%
	Penicillin/Streptomycin (100 U/ml)	1%
	Stable glutamine (200 mM)	1%
	Non-essential amino acids (100x)	1%
	Sodium pyruvate (100 mM)	1%
Culture medium	RPMI 1640 : MEM (1:1)	500 ml
42-MG-BA	FBS (h.i.)	20%
	Penicillin/Streptomycin (100 U/ml)	1%
Culture medium	RPMI	500 ml
HT-29	FBS (h.i.)	10%
	Penicillin/Streptomycin (100 U/ml)	1%
	Sodium bicarbonate solution (2.2 g/l)	1%
Culture medium	RPMI	500 ml
GI-101A	FBS (h.i.)	20%
	Penicillin/Streptomycin (100 U/ml)	1%
	Estradiol and Progesteron	5 ng/ml
	Sodium pyruvate (100 mM)	1%
	Hepes (1 M)	1%
Culture medium	DMEM/Ham's F12 (50:50)	500 ml
Organotypic slice cultures	Normal horse serum	24%
	Hepes (1 M)	2%
	D-Glucose (20%)	0.9%
	Gentamycin	0.1%
Infection medium	DMEM or RPMI	500 ml
(all cell lines)	FBS (h.i.)	2%
	Penicillin/Streptomycin (100 U/ml)	1%
	appropriate cell culture supplement	
Freezing medium	Culture medium	70%
(for all cell lines)	FBS (h.i.)	20%

	DMSO	10%

2.6 Composition of buffers and solutions

RBM tumor lysis buffer	Tris-HCl (pH 7.4)	50 mM
	EDTA (pH 7.4)	2 mM
	PMSF	2 mM
	Complete mini protease inhibitor	1 per 10 ml
Orthotopic implantation		
Anaesthesia solution	PBS	250 µl
(300 µl/30 g)	Ketamin (10%)	30 µl
	Xylazin (2%)	20 µl
Analgetic solution (100 µl)	PBS	96.7 µl
	Metacam (2 mg/ml)	3.3 µl
Immunohistochemistry		
10x PBS (1 l)	KCl	2 g
	KH_2PO_4	2 g
	Na_2HPO_4	11.5 g
	NaCl	80 g
	ddH_20	add to 1 l
1x PBS (1 l)	10x PBS	100 ml
	ddH_20	900 ml
4% PFA	4 g PFA dissolved in 80 ml warm ddH_20	
	add 1 N NaOH until solution clears	
	10x PBS	10 ml
	pH 7,4 (1 N HCl)	
	ddH_20	add to 100 ml
Mowiol 4-88	Glycerin	6 g
	Mowiol 4-88	2.4 g
	ddH_20	6 ml
	Tris-HCl (0.2 M; pH 8.5)	12 ml
	DABCO	25 mg/ml
Blocking/permeabilization	1x PBS	500 ml
solution	Triton X-100	0.3% (1.5 ml)
	FBS (h.i.)	5% (25 ml)
Western blot		

10% APS	APS	5 g
	ddH_2O	50 ml
	freeze aliquots at -20 °C	
Blocking solution	PBS-T /TBS-T	50 ml
	skimmed milk powder	2.5 g (4%)
Blotting buffer	Tris	5.85 g
	Glycine	2.7 g
	10% SDS	0.4 ml
	Methanol	200 ml
	ddH_2O	1 l
5 x Bradford Reagent	Coomassie brillant blue G250	50 mg
	Ethanol (96%)	25 ml
	Phosphoric acid (85%)	50 ml
	ddH_2O	25 ml
	solution was stirred for 15 min and sterile filtered bevor storage	
ECL	Cinnamic acid	90 mM (0,5 ml)
	Luminol	250 mM (1 ml)
	Tris-HCl, pH 8.5	1 M (20 ml)
	ddH_2O	200 ml
	before use add 3 µl H_2O_2 to 10 ml ECL reagent	
1x PBS-Tween /TBS-Tween	1 x PBS / 1x TBS	1 l
	Tween	1 ml (0.1%)
Lysis buffer	Tris-HCl (7.4)	50 mM
	NaCl	150 mM
	EDTA	1 mM
	Triton X-100	1%
	Sodium desoxycholate	1%
	SDS	0.1%
	Complete tablet	1 for 50 ml
10% SDS	SDS	5 g
	ddH_2O	50 ml
10X SDS-PAGE running buffer	Tris base	250 mM
	Glycine	1.92 M
	SDS	1%

	ddH_2O	1 l
4X SDS-PAGE sample buffer	Tris/HCl (pH 6.8)	62.5 mM
	Glycerol	10%
	SDS	2%
	ß-Mercaptoethanol	5%
	Bromophenol blue	1 crumb
	ddH_2O	16 ml
Stripping solution	NaCl (5M)	32 ml
	Acetic acid	10 ml
	ddH_2O	278 ml
10x TBS (pH 7.4)	Tris base	0.5 M (60.57 g)
	NaCl	1.5 M (87.6 g)
	ddH_2O	1 l
1.5 M Tris-HCl buffer (pH 8.8)	Tris base	90 g
	ddH_2O	0.5 l
	HCl/NaOH for pH adjustment	
0.5 M Tris-HCl buffer (pH 6.8)	Tris base	30 g
	ddH_2O	0.5 l
	HCl/NaOH for pH adjustment	
<u>MTT assay</u>		
MTT-solution	MTT dissolved in RPMI 1640 without phenol red and sterile filtrated (45 µm filter) before use	2.5 mg/m
1 N HCL in Isopropyl alcohol (100 ml)	HCl (100%)	10 ml (10%)
	Isopropyl alcohol	90 ml
<u>Standard viral plaque assay</u>		
CMC medium	Carboxymethylcellulose	7.5 g
	DMEM	500 ml
	FBS	5%
	Penicillin/Streptomycin	1%
Crystal violet staining solution	Crystal violet	1.3 g
	Ethanol (96%)	50 ml
	Formaldehyde (37%)	300 ml
	ddH_2O	650 ml

FACS analysis

Collagenase I solution	Collagenase I (stock: 244.9 U/ml) PBS	10.000 U/ml
DNAse I solution	DNAse I ddH_2O	5 MU/ml = 5000.000 U/ml
0.5 M EDTA (anti-coagulant)	EDTA ddH_2O NaOH pellets to reach a pH of 8.0 while stirring. Filter the solution with 0.45 µm filter before use.	186.1 g 800 ml ~20 g
Erythrocyte lysis buffer (10x)	NH_4Cl $KHCO_3$ EDTA-NA_2 ddH_2O	8.29 g 1.09 g 41 mg 100 ml
Permeabilization buffer	PBS FBS NaN_3, Saponin	50 ml 5% 0.1% 0.2

Organotypic brain slice culture

Ringer solution (pH 7.3)	KCl $MgCl_2$ D-Glucose $NaHCO_3$ NaH_2PO_4 Pyruvic acid Myo-inositol Kynuric acid $CaCl_2$	2.5 mM 1 mM 260 mM 26 mM 1.25 mM 2 mM 3 mM 1 mM 2 mM

Molecular biology

10x TBE buffer (pH 8.0)	Tris-base Boric acid 0.5 M EDTA	108 g 55 g 40 ml

2.7 Animals

Wild-type mice	
C57BL/6JOlaHsd (C57BL/6 wt) (Harlan Winkelmann, Borchen, Germany)	Inbred mouse strain
Immunodeficient mice	
B6.Cg/NTac-*FoxN1*^{nu} (C57BL/6 athymic nude) (Taconic Europe A/S (Lille Skensved, Denmark)	Foxn1nu mutation backcrossed to the C57BL/6NTac inbred strain for ten generations.
Hsd:Athymic Nude-Foxn1^{nu} (Balb/c athymic nude) (Harlan Winkelmann, Borchen, Germany)	Balb/c outbread mouse strain
Knockout mice	
B6.129S7-*Ifngtm1Ts*/J (C57BL/6 IFN-γ KO) (Charles River Laboratories (Sulzfed, Germany)	Congenic mutant strain with a targeted mutation (null/knockout) of IFN-γ.

Athymic nude mice are characterized by an autosomal recessive mutation of the *Foxn1*^{nu} locus on chromosome 11 resulting in a hairless (nude) phenotype and aphasia of the thymus. Due to the abnormal thymus these mice do not have mature T cells or cytotoxic effector cells and thus do not show graft rejection after xenotransplantation which makes them an ideal model for oncological research.

All animals were ordered at the age between 4-5 weeks for orthotopic implantation of tumor cells or at the age between 5-6 weeks for subcutaneous implantations.

All animals were kept in small groups of 2 to 7 animals with a 12 hour day night rhythm by dimmed light in sterile cages. Animal studies were performed in accordance with the government of Unterfranken (Wuerzburg, Germany, protocol number Az. 55.2-2531.01-30/12 and AZ 55.2-2531.01-62/11).

2.8 Oncolytic viruses

The replication-competent VACVs used in this study were constructed and provided by the Genelux Corporation San Diego, USA.

LIVP 1.1.1 was isolated from a wild-type stock of the VACV vaccine strain LIVP originated from the Lister strain (Institute of Viral Preparations, Moscow, Russia). LIVP 1.1.1 represents a “native” virus without genetic manipulations. Sequence analysis revealed a naturally occurring disruption of the thymidine kinase (TK) gene locus (Chen, N.G. personal communication). Consequences of a TK gene deletion in VACVs are a preferential replication in dividing cells such

as tumor cells resulting in enhanced tumor specificity and reduced virulence [193, 194]. Toxicity and efficiency of LIVP 1.1.1 was tested in various cell lines in cell culture and *in vivo* [179, 195].

GLV-2b372 is a virus construct derived from the parental LIVP 1.1.1 virus strain, carrying the TurboFP635 expression cassette under the control of the vaccinia synthetic early/late promoter at the TK locus.

GLV-1h68 was constructed by inserting three reporter gene expression cassettes namely *Renilla luciferase – Aequorea green fluorescent protein (RUC-GFP) fusion, β-galactosidase (LacZ), and β-glucuronidase (GusA*) into the *F14.5L* (encoding WR53.5 protein an IMV transmembrane protein), *J2R* (encoding thymidine kinase) and *A56R* (encoding hemagglutinin) loci of the LIVP viral genome, respectively [146].

3 Methods

3.1 General cell culture techniques

3.1.1 Cultivation of adherent growing cells

To ensure sterile conditions for all cell culture works, experiments were performed under a laminar flow hood. Biological equipment and all materials were autoclaved before use. Antibiotics such as penicillin G/streptomycin were added into the medium to avoid bacterial infection and FBS was heat inactivated (30 min, 56 °C).

For expansion of adherent growing cells, they were cultured in 175 cm^2 cell culturing flasks in ~40 ml of the appropriate pre-warmed culture media under constant conditions of 37 °C in a 100% humidified 5% CO_2 incubator until reaching confluence.

Proliferating cells were passaged regularly to avoid multilayer formation. For this, culture medium was removed from the flask and the cells were washed once with 5 ml 1x BSS to get rid of floating and dead cells. Cells were then subsequently trypsinized with 5 ml trypsin/EDTA for 4-7 min depending on the cell line in the 37 °C CO_2 incubator. After detachment of cells, trypsin was inhibited by addition of 5 ml culture medium containing the trypsin inhibitors Ca^{2+} and Mg^{2+}. The required amount of cell suspension was then transferred to a new flask containing 40-50 ml of fresh culture medium. The same procedure was performed for cell harvesting.

As the cells consume the nutrients of the cell culture media, and metabolic substances and dead cells accumulate over time, media needed to be refreshed all three or four days depending on the cell line. An exhaustion of the media was indicated by a color change from red to yellow, due to a pH indicator in the medium.

3.1.2 Centrifugation of cells

Centrifugation was carried out under standard conditions unless otherwise noted in a centrifuge model Biofuge fresco for 3 min at 1,500 rpm at 20 °C.

3.1.3 Determination of the cell number and determination of cell viability

To determine the cell number for a particular cell culture experiment, a Neubauer counting chamber was used. A coverslip was placed over the counting surface, which consisted of a grid of 4 big corner squares which were divided into 16 small squares until Newton's Rings were visible. 10 µl of the cell suspension were pipetted under the coverslip. Cells were counted in a row of

four small squares in each of the four corner squares (1 mm^2), using an Axiovert inverted microscope. The cell count per milliliter was calculated by multiplication of the cell number counted in the 16 small squares with the chamber factor of 1 x 10^4.
Cell viability was tested by using the trypan blue exclusion test. For this, equal amounts of cell suspension and trypan blue were mixed, incubated for 1 min at room temperature and pipetted onto the Neubauer chamber. For distinguishing between live and dead cells, cell suspension was mixed 1:1 with trypan blue. Dead cells appeared blue. The dilution factor of 2 needed to be considered.

3.1.4 Thawing and freezing of cells

For storage in liquid nitrogen (-196 °C), expanded cells with 80-90% confluence were harvested by trypsin treatment. Afterwards cells were counted and the required amount of cell suspension (usually 1x10^6 or 5x10^6 cells/cryotube) calculated and centrifuged. The cell pellet was resuspended in 1 ml freezing medium (culture medium (70%), DMSO (10%) and FBS (20%)) and then transferred to cryotubes. Cryotubes were stored overnight at -80 °C in a freezing box and were then transferred to liquid nitrogen.
For thawing of cells, an aliquot of cells was taken out from the liquid nitrogen (-196 °C) tank, quickly defrosted under a running tap and the cells subsequently transferred to a 75 or 175 cm^2 cell culturing flask containing fresh culture medium. The medium was changed the other day.

3.1.5 Test for cell proliferation and confluence

To determine the optimal cell number for different cell culture experiments, a confluence test was performed in 24- or 6-well plates. For this purpose, cell concentrations ranging from 1x10^4 to 4x10^5 cells/well were seeded in duplicate and monitored on consecutive days. For example for the infection of cells in cell culture, cells should be 90-95% confluent.

3.1.6 Mycoplasma detection

Mycoplasms are small parasitic bacteria (< 1 µm) that are often found as contamination in cell cultures. They can cause severe damage, as they are able to change the metabolism, growth or general vitality of infected cells. Due to their small size they are very difficult to detect by microscopy. The cell lines used in this study were tested for mycoplasms by the Venor™GeM Mycoplasma Detection Kit which is a PCR-based test system. The test was performed according to the manufactures instructions.

3.1.7 Stimulation and polarization of cells in cell culture

Cell lines (*e.g.* GL261, BV-2, IMA2.1) were seeded in wells of a 24- or 6-well plate in medium with 2% FBS supplemented with either 10 ng/ml recombinant murine (rm)-IL-4, rm-IFN-γ, 1 µg/ml lipopolysaccharide (LPS), rm-IFN-γ + LPS, 100 ng/ml basic fibroblast growth factor (bFGF) or 10 ng/ml recombinant human (rh)-IFN-γ for 24-72 hours (h). In addition, to determine a time and concentration dependency, other concentrations such as 30, 60 and 100 ng/ml rm-IFN-γ were used for stimulation of GL261 cells for 24 and 72 h. As a control, cells without (w/o) stimulation were used.

Further, GL261 cells were stimulated with Simvastatin (concentration range 0.1-10 µM) or in a combination of both 10 ng/ml IFN-γ + Simvastatin (0.1-10 µM) for 40 h or 72 h. Prior to application, Simvastatin purchased in its inactive lactone form (prodrug form) needed to be activated into the biologically active β-hydroxy acid form [196]. According to Sadeghi *et al*. [197] and Leung *et al.* [198], 25 mg Simvastatin was dissolved in 625 µl ethanol (99%) and mixed with 937 µl 0.1 M NaOH. The solution was incubated for 2 h at 50 °C. The pH value was adjusted to 7.2 and by adding sterile NaCl (0.9%) solution to reach 12.5 ml in total, a concentration of 5 mM was adjusted. The solution was sterile filtered and 400 µl aliquots were frozen at -20 °C.

The pre-stimulated cells were finally analyzed for MHCII expression by FACS analysis (described in 3.6.1) or were infected with LIVP 1.1.1 at an MOI of 0.1 or 1.0 to determine the virus titer by standard viral plaque assay (3.2.3) or virus-mediated toxicity by MTT assay (3.1.8). After infection, cells were either cultured with culture medium or in culture medium supplemented with the particular stimulants.

3.1.8 MTT assay

The MTT [3-(4,5-dimethylthiazol-2-yl)-2,5-diphenyltetrazolium bromide]-assay is a bioassay used to determine cell proliferation and survival *e.g*. after viral infections or after stimulation with particular cytokines. The assay is based on the metabolic reduction of the yellow tetrazolium ring into the blue-colored end product formazan. The underlying mechanism of the metabolic reduction involves NADH-dependent enzymes of the endoplasmic reticulum and to a lesser extent succinate that act as an electron donor through the mitochondrial succinate dehydrogenase [199].

Cells were plated and cultured in 24-well plates until 80-90% confluence and infected with the VACV LIVP 1.1.1 or GLV-1h68 as described in (3.2.1) at different MOIs (multiplicity of infection). Cell viability was determined 24, 48, 72 and 96 hours post viral infection (hpi). For this purpose,

culture medium was replaced by 500 µl sterile filtrated MTT solution (2.6). After an incubation time of 2 h at 37 °C in the 5% CO_2 incubator the MTT-solution was carefully removed from the wells and the plates stored at -20 °C until all time points were taken. For each time point and condition the experiment was performed in triplicate. The color reaction and thus the cell viability was measured after adding 400 µl 1 N HCl diluted in isopropyl alcohol which lysed the cells resulting in a release of the blue formazan crystals. The solution was transferred to a 96-well plate in triplicates (100 µl/well). The optical density was measured at a wavelength of 570 nm in an ELISA-reader. Uninfected cells were used as positive control, defined as 100% viable.

3.1.9 siRNA knockdown of AVEN in cell culture

For AVEN gene knockdown, a si-RNA-27 kit (OriGene) containing three unique human AVEN-27mer siRNA duplexes (Locus ID 57099) and a Trilencer-27 universal scrambled negative control siRNA duplex in combination with SiLentFect™ Lipid Reagent were used.

According to the manufacturer's instructions, siRNA duplexes (control and target specific duplex) were reconstituted in 100 µl RNAase-free Duplex Buffer resulting in a concentration of 20 µM. Samples were vortexed, centrifuged and heated for 2 min at 94 °C. The heating step guarantees, that the oligos will be completely duplexed. Before usage, samples needed to cool down to room temperature. The hydrated duplexes were stored at -20 °C.

For siRNA transfection of the AVEN gene, cells were cultured for 24 h in wells of a 6-well plate to 50-60% confluence. SiLentFect™ Lipid Reagent (5 µl/well) and siRNA (15 µM/well scrambled control or 3x5 µM/well of specific AVEN siRNA duplexes) were mixed in 100 µl serum-free medium and incubated at room temperature for 20 min. As a control, a sample with SiLentFect™ Lipid Reagent but without siRNA duplex was used. Cells were incubated for 4 h with 1 ml of serum-free medium and the SiLentFect™/siRNA (si-control/si-AVEN) mixture. Afterwards 1 ml serum-containing medium was added and cells were cultivated for 48 or 72 h (final concentration of the siRNA 37.5 nM). Transfected cells were used for RT-PCR, Western blot experiments, FACS analysis or cells were infected with the VACV GLV-1h68.

3.2 Virological technics

3.2.1 Infection of monolayer cultures wit VACV LIVP 1.1.1 or GLV-1h68

For infection of adherent cells in cell culture, cells should be 90-95% confluent. To determine the required amount of the respective VACV stock, cells of two wells were harvested by trypsinization and counted. The mean value of the cell number was used to calculate the

required amount of the virus stock in µl. For infection of cells with different MOIs the following formula has been used:

$$\textit{Amount of viral stock (µl) for z wells} = \frac{\textit{(Cell number x MOI) x number of wells (z)}}{\textit{viral titer (pfu/µl)}}$$

The viral titer of the VACV stocks was known and was defined as plaque forming units (pfu)/ml. Before the viral stocks could be used, the virus aliquots were thawed in a 37 °C water bath and sonicated two times for 30 s with a 30 s break at 2-3 °C to avoid virus aggregate formation.
For infection, culture medium was removed from the respective wells and the calculated viruses at specific doses were mixed with 300 µl infection medium/24-well or 1 ml infection medium/6-well and pipetted into the wells. The plates were incubated for 1 h at 37 °C in a humidified 5% CO_2 incubator. During the incubation time, plates were moved up and down from time to time to achieve a uniform viral distribution. After the incubation time, infection medium was replaced with 1 ml of fresh culture medium.

3.2.2 Replication analysis

To measure the replication capacity of LIVP 1.1.1 or GLV-1h68 in the different cell lines, cells were seeded and cultured in 24-well plates until 90-95% confluence and infected as described in 3.2.1 using different MOIs. The virus inoculum (infection medium) was collected and stored at -80 °C as reference value. 2, 24, 48, 72, 96 hpi, supernatants of the samples were collected and stored at -80 °C. Cells were washed with 1x BSS, trypsinized with 500 µl trypsin/EDTA and after detachment the reaction was stopped with 500 µl culture medium. Samples were centrifuged at 3,000 rpm for 3 min. Cell pellets were resuspended in 1 ml PBS and also stored at -80 °C. Prior to analysis by standard viral plaque assay, three freeze and thaw cycles in liquid nitrogen were accomplished. Experiments were performed in triplicates.

3.2.3 Standard viral plaque assay

The standard viral plaque assay is a biological assay to determine the viral titer of a sample, defined as plaque forming unit (pfu) per milliliter.
For this, a 100% confluent monolayer of CV-1 cells was infected with serial dilutions of a virus stock/sample: CV-1 cells were seeded in 500 µl CV-1 culture medium at cell densities of $6x10^4$ cells/well for 2 days, $4x10^4$ cells/well for 3 days or $2x10^4$ cells/wells for 4 days, respectively. Prior to use, the virus was sonicated two times for 30 s with a 30 s break in the middle and serial

dilutions were prepared in CV-1 infection medium. 250 µl of the viral dilutions were pipetted onto the CV-1 cells. For accuracy, every dilution was used in duplicate. After an incubation time of 1 h at 37 °C in the 5% CO_2 incubator 1 ml semi-solid CMC medium which restricts viral spread from the initial infected cell to neighboring cells was added to the wells and the plates were incubated further for 48 h. After the incubation time 250 µl crystal violet were added to the wells that were stained for 24-48 h at room temperature.

Plaque formation finally is a result of cell lysis after viral infection of cells within the cell monolayer that can be seen virtually after staining. It is assumed that one infectious particle infects one cell and therefore forms one plaque [200]. To determine the number of plaques (unstained areas), the wells were washed with H_20 and dried. Wells with 10-100 plaques were counted and used for the statistical analysis. The virus titer (pfu/ml) of the virus samples was calculated using the following formula:

$$\textit{virus titer (pfu/ml)} = \frac{\textit{number of plaques (pfu)}}{\textit{dilution factor x infection volume (ml)}}$$

The replication capacity in percentage (%) was calculated by the following formula:

$$\textit{Replication capacity (\%)} = \frac{\textit{actual viral load (pfu)}}{\textit{virus inoculum (pfu)}} \textit{ x 100\%}$$

The initial virus inoculum / infection medium was set 100%.

3.3 Animal experiments

3.3.1 Subcutaneous (s.c.) implantation of GL261 glioma cells

For implantation of subcutaneous tumors 5-6 week old female Balb/c athymic nude, C57BL/6 athymic nude, C57BL/6 wt, or C57BL/6 IFN-γ KO mice were used.

GL261 glioma cells were grown in cell culture flasks to 80% confluence and prepared as followed: Cells were harvested by trypsinization. Afterwards, the cell suspension was centrifuged and the pellet washed twice with the same volume of PBS. After the second washing step, cells were counted and the cell pellet was resuspended in an adequate volume of PBS.

$1x10^6$ GL261 cells in a volume of 100 µl were implanted into the right hint of the mice using an insulin syringe. Prior to implantation the injection side was disinfected with an Alco-prep to avoid bacterial side infections.

Tumor growth was monitored by measuring the tumors twice a week with a digital caliper from two directions (length and width). The tumor volume was calculated using the following formula:

Tumor volume (mm^3) = length (mm) x width $(mm)^2$ x 0.52

In addition to measurement of the tumor volume, mice were weighed twice a week. The net body weight was calculated using the following formula:

Net body weight (g) = body weight (g) – tumor weight (g)

3.3.2. Orthotopic implantation of GL261 glioma cells

GL261 glioma cells were grown to 80% confluence. Cells were harvested, washed twice with PBS, counted and resuspended in an adequate volume of PBS (injection volume 3 µl / mouse). For each mouse a 10-fold approach in a separate aliquot was prepared. $1x10^5$ cells/mouse were implanted.

For intracranial implantation of GL261 cells, 4-5 week old female Balb/c athymic nude and C57BL/6 wt mice were used. An anesthesia solution (2.6; 10 µl/g mouse weight) was injected intraperitoneal (i.p.) into the mice. The depth of the anesthesia was monitored by checking the toe pinch reflex and corneal reflex.

When animals were unresponsive, the dorsal head surface was disinfected with an Alco-prep and the skin incised at the midline. The exposed area was blotted dry with a sterile cotton swab. Afterwards, mice were placed in a small animal stereotactic apparatus (Stoelting). They were fixed through nose and ear bars that were part of the stereotactic apparatus. Then, the coordinates for the injection side which were 1 mm anterior and 2 mm right to the bregma were determined and a small burr hole was made with a cannula.

The Hamilton syringe containing the cell suspension was then placed over the burr hole and inserted to a 3 mm depth from the scull surface. Cell suspension was injected slowly at 0.5 µl/min to avoid intracranial pressure and the needle was left for another minute within the hole. After the injection, the syringe was slowly removed (1 mm/min) to avoid ascending of cells through the needle track.

Afterwards the skull was disinfected with H_2O_2 and closed with one or two surgical staples. Mice were then injected (s.c.) with 80 µl analgetic solution in case of C57BL/6 wt mice or 100 µl analgetic solution (2.6) in case of Balb/c athymic nude mice and placed in a fresh cage in front of an infrared heater until awakening. Mice were monitored daily and twice a week the body weight of the mice was measured, as weight loss in this model is described in literature as an indicator for progressive disease.

3.3.3 Intratumoral injection of LIVP 1.1.1 into subcutaneous or orthotopic tumors

Mice with subcutaneous tumors at a size of about 250 mm^3 were injected intratumorally (i.t.) with a single dose of $5x10^6$ pfu LIVP 1.1.1 in 100 µl PBS. The control group was injected with a single dose of 100 µl PBS. For infection, mice were anesthetized with isoflurane (3.3.4). Injection sites were disinfected with Alco-preps before, to avoid side infections.

Mice with orthotopic tumors were injected with $5x10^6$ pfu LIVP 1.1.1 in 3 µl PBS over a period of ~0.5 µl/min into the former implantation site. Mice were treated similar as for the tumor cell implantation. The tumor formation was confirmed by MRI in corporation with Dr. T. Basse-Lüsebrink at the Department of Experimental Physics of the University of Würzburg.

3.3.4 Anesthesia of mice with isoflurane

Isoflurane is an inhalational anesthesia in gaseous phase which acts as muscle relaxant and which is also analgetic. For induction of the anesthesia, mice were put into an induction chamber and isoflurane was initiated at a concentration of 2.5%. Anesthesia was maintained at a concentration of 2-2.5% through a nosecone during the experimental procedure.

3.3.5 Harvesting of tumors and organs

Animals were euthanized by CO_2 inhalation. Tumors and organs such as the ovaries, liver, kidneys, spleen, lung and the brain were dissected at different time points. Tumors were either stored at -80 °C for immunohistochemical analysis (3.5) or tumors and organs were homogenized for determination of viral titers by standard viral plaque assay (3.3.6), RBM ELISA (3.3.8), FACS analysis (3.6.3) or cell culture experiments.

3.3.6 Preparation of tissue homogenates for standard viral plaque assay

Organs and tumors were dissected, weighed and transferred into ceramic bead tubes containing 1 ml of ice cold PBS. The tissues were mechanically homogenized with a FastPrep FP120 Cell Disruptor at a speed of 6,000 for 30 s, repeated two times. Afterwards, the samples were sonicated once and then centrifuged at 13,000 rpm for 4 min. The supernatants were then transferred into new tubes. During the whole process the organs were kept on ice. The viral titer per organ or tumor was finally determined by standard viral plaque assay and calculated in proportion to the organ/tumor weight.

3.3.7 Clodronate depletion

C57BL/6 wt mice were implanted subcutaneously with $1x10^6$ GL261 cells. When tumors reached a size between 200-400 mm^3, mice were i.p. injected on three consecutive days with 200 µl clodronate liposomes or PBS. On day 4 after these injections, tumors were i.t. injected with LIVP 1.1.1 ($5x10^6$ pfu) and analyzed by standard viral plaque assay and FACS analysis.

3.3.8 RBM ELISA

To prepare tumor lysates at the day of infection (d 0) five Balb/c athymic, C57BL/6 wt and athymic mice with subcutaneous GL261 tumor were sacrificed. Tumors were dissected, crushed and resuspended in 9 volumes of ice cold RBM lysis buffer (2.6) and lysed in a gentleMACS Dissociator using M-Tubes. Tumor samples were centrifuged at 13,000 rpm for 5 min at 4 °C and supernatants were analyzed by Myriad RBM (Austin, USA) for an immune-related protein antigen profiling (RodentMAP® v. 3.0).

3.3.9 Simvastatin treatment

Simvastatin was activated as described in (3.1.7). C57BL/6 wt mice were implanted subcutaneously with $1x10^6$ GL261 cells. On day 1, 3, 7, 9, 13, 15 and 17 post implantation (dpimp) mice were injected i.p. with 20 mg/kg body weight Simvastatin according to Leung *et al.* [198] and Müller *et al.* [201]. On day 21 LIVP 1.1.1 was injected i.t. One day post LIVP 1.1.1 injection, FACS analysis and replication analysis were performed.

3.4 Organotypic brain slice cultures (OSCs)

3.4.1 Preparation of OSCs

OSCs as three-dimensional (3D) cell culture systems maintain the cryoarchitecture and physiological cell-cell and cell-matrix interactions of the original tissues in contrast to conventional two-dimensional (2D) cultures [202]. As they are a helpful tool to mimic *in vivo* conditions *ex vivo* they represent an option to reduce the number of animal experiments [203]. OSCs are used in a great number of cell biological, biochemical or electrophysiological studies *e.g.* cell migration, tumor formation, drug application or virus infection [189, 203–207].

The protocol for the preparation of organotypic brain slice cultures was adapted from previously published research articles [203, 205, 208].

Brains from 2-3 month old (adult) or 3-15 day old (young) C57BL/6 wt mice were removed and immediately immersed in ice-cold Ringer solution (2.6). To stabilize the brains during the cutting process, they were embedded in 4% low melting agarose. The embedded brains were trimmed and glued with the caudal side onto the cutting table of a vibratome. Brains were cut in coronal slices of 250 µm, collected and kept in ice-cold Ringer solution for 1 h. During this time, sterile semi-porous membrane inserts with a pore diameter of 0.4 mm were inserted into 6-well plates and incubated with 1 ml sterile OSC culture medium at 37 °C and 5% CO_2.

Using a small brush, agarose residues were removed and up to four brain slices were placed onto one pre-incubated semi-porous membrane insert. Brain slices from the cerebral cortex (area shown in Figure 8a) were cultivated at the air-liquid interphase in 1 ml culture medium per well at 37 °C under 5% CO_2 as depicted in Figure 8b. Medium was changed every other day. Viability of brain slices was assessed using PI staining.

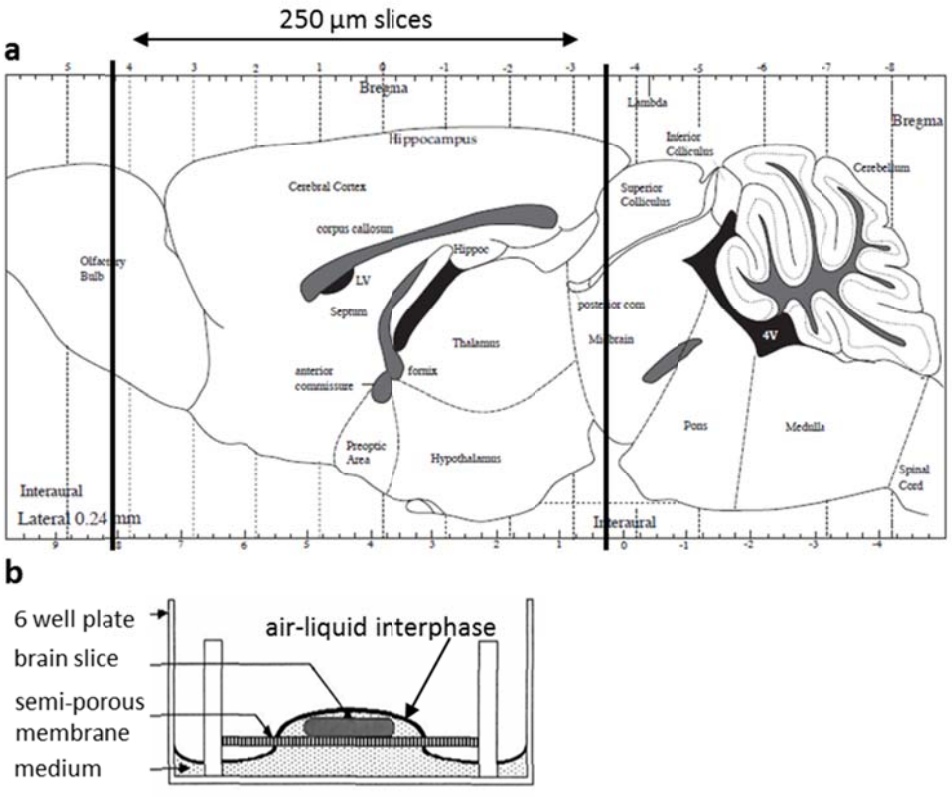

Figure 8: (a) Sagittal diagram of a mouse brain adapted from Paxinos *et al.* [209], highlighting the area between neocortex and cerebellum, that was used for preparation of brain slices. **(b)** Schematic representation of the culture method of brain slices on semi-porous membrane inserts in 6-well plates adapted from Bergold *et al.* [210].

3.4.2 Implantation of tumor cells into OSCs

Using a Hamilton syringe, $1x10^4$ U87-MG-RFP or GL261-RFP cells in a volume of 1 µl PBS were implanted into OSCs, 7 days after slice preparation. Medium was changed directly after the implantation and then every other day. Glioma growth and invasion was evaluated using a Leica MZ16 FA Stereo-Fluorescence Microscope 1 day post implantation and every second day following that.

3.4.3 Viral replication in OSCs

Prior to infection of the brain slices, medium was removed from the wells and replaced by 1 ml infection medium. For infection of brain slices (5 slices per 6-well), that were cultured for 7 days, $5x10^6$ or $1x10^7$ pfu VACV diluted in 50 µl infection medium were prepared. 10 µl virus solution per slice was pipetted. The cultures were incubated for 3 h at 37°C. After the incubation time, 1 ml culture medium was added into the wells and slices were cultured further for 24 to 72 h.
For determination of the virus titer, slices were transferred into ceramic bead tubes containing 1 ml of ice cold PBS at appropriate time points. The slices were mechanically homogenized with a FastPrep FP120 Cell Disruptor at a speed of 6,000 for 30 s, repeated two times. Afterwards, the samples were sonicated once and then centrifuged at 13,000 rpm for 4 min. The supernatants were then transferred into new tubes. The viral titer per slice was finally determined by standard viral plaque assay.

3.4.4 Polarization of BV-2 cells and application onto OSCs

Semi-confluent BV-2 cells were stimulated with either 10 ng/ml rm-IFN-γ or 10 ng/ml rm-IL-4 for 24 h. As a control unstimulated BV-2 cells were used. BV-2 cells were harvested, washed once and then applied directly onto the OSCs implanted with tumor cells. BV-2 microglial cells were applied in a volume of 2 µl PBS at a density of $1x10^5$. Slices were further cultured for 24 to 48 h.

3.5 Immunohistochemical analyses

3.5.1 Immunohistochemistry of tumor cryosections

Mice were sacrificed by CO_2 inhalation and tumors were excised and snap frozen in liquid nitrogen.
Afterwards the tumors were fixed in 4% paraformaldehyde/PBS overnight, followed by 3-4 washing steps with PBS for 3 to 4 h in total. The tumors were then dehydrated by incubating in a

10% sucrose/PBS solution for 3-4 h followed by incubation in a 30% sucrose/PBS solution over night. Afterwards the samples were put into a mixture of Tissue Tek and PBS (1:1) for 3-4 h and finally embedded in Tissue Tec. The samples were sectioned in a Cryostat 2800 Frigocut at a thickness of 10 µm.

Slides were fixed in ice-cold acetone for 10 min and afterwards stained with appropriate antibody solutions in single stainings or co-stainings for 1 h at RT. The following primary antibodies (1:100) were used: rat anti-mouse MHC class II (I-A/I-E) or anti-mouse MHC class II (I-A/I-E) functional grade biotin and rat anti-mouse CD68. After 3 washing steps with PBS, sections were labeled with secondary antibodies (1:200) and Hoechst 33258 (1:200) to stain cell nuclei for 1 h at RT. In the experiments the following secondary antibodies have been used: AffinityPure donkey anti-rat-Cy3/Cy2 or Streptavidin-Cy3 (from *Streptomyces avidinii)* in buffered aqueous solution. After three washing steps (10 min each) and an ethanol step (1 min) the slides were mounted in Mowiol 4-88.

Images were taken at an Axiovert 200M inverse microscope and edited with the software program Axiovison 4.8.2. For quantification, 10 images per tumor slice (five images from tumor rim and five from tumor center) were taken at a magnification of 20x with identical settings. RGB-Images were converted into 8-bit grey scale images and the fluorescence intensities of CD68 and MHCII stainings were measured by Image J and represent the average brightness of staining related pixels.

3.5.2 Immunohistochemistry of tumor agarose sections

Mice were sacrificed by CO_2 inhalation and brains with and without brain tumors were excised and snap frozen in liquid nitrogen. Brains were fixed over night at 4 °C in 4% paraformaldehyde/PBS (pH 7.4). Afterwards brains were rinsed with PBS and finally embedded in 5% low-melting agarose. The samples were cut in 100 µm sections using a Leica VT1000S Vibratome. Before staining, the sections were incubated with blocking/permeabilization solution for 1 h. The sections were labeled with the primary antibodies for 12-15 h. The following primary antibodies were used: rabbit anti-Iba-1 (1:500), anti-MHCII (I-A/I-E) functional grade biotin (1:100), chicken anti-GFAP (1:1,000) and rabbit anti-VACV (1:100). Sections stained with IB4-FITC (1:100) were incubated for additional 24 h. After the sections were rinsed three times with PBS, they were incubated with the secondary antibodies (1:200) for 5 h. As secondary antibodies Streptavidin-Cy3, donkey anti-rabbit-Cy5, donkey anti-rabbit-Cy2, donkey anti-rabbit-Cy3 and donkey anti-chicken-Cy5 were used. Nuclei were labeled with Hoechst 33342. Then, sections were washed with PBS and mounted onto glass slides in Mowiol 4-88.

The fluorescent-labeled preparations were examined using a MZ16 FA Stereo-Fluorescence microscope (Leica) equipped with a digital CCD camera (DC500, Leica). The Iba-1-Cy5 staining was converted to a green signal by Photoshop CS5.

For quantification of the fluorescence intensity, 3 brain tumors per treatment conditions, in duplicate staining were analyzed. RGB images were converted into 8-bit gray scale with an intensity range from 0-255 with Photoshop CS5. The fluorescence intensity and the tumor areas were determined with Image J. The fluorescence intensities of Iba-1 and GFAP were calculated as ratio to the tumor area (dotted lines).

3.5.3 Immunohistochemistry of OSCs

Using a small brush, sections were transferred into 48-well plates and fixed with 4% paraformaldehyde in PBS, pH 7.4, for 16 h at 4 °C. Following three washing steps in PBS for 15 min each, slices were blocked for 1 h with 5% FBS in PBS supplemented with 0.3% Triton X-100. Afterwards slices were incubated for 3 days at 4 °C with primary antibodies diluted in blocking solution with continuous orbital shaking. For the study, the following antibodies have been used: chicken anti-GFAP (1:100), rabbit anti-Iba-1 (1:100), FITC-coupled *Griffonia simplicifolia* Isolectin B4 (IB4; 1:50) and rabbit anti-Vaccinia (1:100).

After three washing steps in PBS (10 min each), slices were incubated with specific fluorescence-labeled secondary antibodies donkey anti-rabbit-Cy2 (1:200) and donkey anti-chicken-Cy5 (1:200) for 4 h at room temperature. Hoechst 33342 (1:200) was used to stain cell nuclei. After three final washing steps (10 min each) in PBS the slices were mounted onto glass slides and embedded in Mowiol 4-88 mounting medium. Images were taken under a MZ16 FA Stereo-Fluorescence microscope equipped with a digital CCD camera and at a TCS SP2 confocal microscope. Digital images (1024 x 1024 pixel RGB-color images) were processed with Photoshop CS5 and merged to yield pseudo-colored images.

3.6 Flow cytometry (FACS) analyses

At flow cytometry (FACS) analysis, single cells are transported in a laminar flow which passes a laser beam and allows the simultaneous measurement of various properties of individual cells. Such properties are *e.g.* the relative particle size (forward scatter-FSC), the relative granularity or internal complexity (sideward scatter-SSC) and also the relative fluorescence intensity. There is a coupled optical-electronic system which determines how the cell scatters the incident light and emits fluorescence. The emitted light is guided via mirrors to detectors and is quantified there. A complex analysis is possible by "gating", defining of specific populations.

3.6.1 Sample preparation and staining of cultured cells

Cells were cultured in 24-well plates according to the conditions described in 3.1.7. Cells were trypsinized with 300 µl trypsin/EDTA until all cells were detached and the reaction was stopped by adding 600 µl of culture medium. Cell suspensions and supernatants were centrifuged at 2,000 rpm for 4 min, 4 °C. The supernatants were removed and cells were stained with 200 µl PBS + 2% FBS and 0.2 µl labeled monoclonal antibody anti-MHCII-PE for 30-45 min at 4 °C. Experiments were performed in triplicate and repeated twice.

3.6.2 Apoptosis studies and cell cycle analyses

For cell cycle analyses and detection of DNA fragmentation (sub-G1 phase) a method described by Krysko *et al*. [211] and Darzynkiewicz *et al*. [212] was used. Cell pellets were resuspended in a solution of 100 µl PBS + 2% FBS and 5 µl PI. The pellets were then frozen in liquid nitrogen and thawed at 37 °C prior to measurement. For the flow rate the option “slow” was chosen.
To distinguish apoptotic from necrotic cells, a FITC Annexin V Apoptosis Detection Kit with 7-AAD was used according to the manufacturer’s instructions: Cells were washed once with PBS, resuspended in 100 µl Annexin V Binding Buffer supplemented with 2 µl FITC-Annexin V and 2 µl of 7-AAD cell viability staining solution. In addition, the combination of Annexin V-APC and PI was used. Experiments were performed in triplicate and repeated twice.
Another method to distinguish apoptotic cells from necrotic cells is a PI exclusion assay. Based on the status of membrane damage the uptake kinetics of PI differ and healthy (PI-negative), apoptotic (PI-dim) and necrotic (PI-bright) cells can be differentiated [213, 214]. For this, cells were stained with 1 µl PI 5 min before measurement at room temperature and were then subsequently analyzed.

3.6.3 Preparation of single-cell suspensions

Mice (C57BL/6 wt, C57BL/6 athymic, Balb/c athymic or C57BL/6 IFN-γ-KO mice) were sacrificed by CO_2 inhalation at different times (d0, 1 dpi or end stage disease).
As described by Gentschev *et al.* [154] single-cell suspensions were prepared as follows: Tumors were minced and transferred into 50 ml tubes containing 5 ml RPMI media + 2% FBS + 150 µl collagenase I + 5 µl DNase I solution (2.6) and were incubated for 40 min at 37 °C. Afterwards cells were passed through a 70 µm nylon mesh filter. The suspension was centrifuged at 1,000 rpm for 10 min and washed once with 20 ml PBS + 2% FBS. For tumors at end stage disease, the suspension was treated once with 1x erythrocyte lysis buffer to get rid of red blood cells. Edema

fluid was taken before, using an insulin syringe. Edema fluid was then treated similar to the minced tumor tissues.

Spleen were dissected and passed through a nylon mesh filter. Cells were incubated for 10 min at 37 °C in 20 ml RPMI media + 2% FBS + 150 µl collagenase I + 5 µl DNase I solution. Cells were centrifuged at 1,000 rpm for 10 min and resuspended in 10 ml 1x erythrocyte lysis buffer and incubated for 10 min at room temperature. Afterwards, the suspension was centrifuged and washed once before staining.

Blood was taken by cardiac puncture and subsequently mixed with 0.5M EDTA solution. 0.1 ml blood/2 ml 1x erythrocyte lysis buffer (2.6) was incubated for 10 min at room temperature. The samples were then centrifuged at 1,200 rpm for 5 min and washed twice before staining.

3.6.4 Staining of single-cell suspensions

Cell suspensions were blocked with purified anti-mouse CD16/CD32 antibody (1µl/1x10^6 cells) for 30 min at 4 °C to block non-specific stainings. Cells were then stained in appropriate antibody solutions for 40 min at 4 °C. The following monoclonal anti-mouse antibodies were used in this study: CD3-PE, CD4-APC, CD8-FITC, CD11b-APC, CD11b-PE, CD11b-PerCP-Cyanine5.5, CD14-PerCP, Ly6c-PerCP-Cy5.5, Gr1-FITC, CD49b-APC, CD19-PerCP/Cy5.5, CD11c-Pe, CD11c-APC, Ly6G-PE, CD45-PerCP-Cy5.5, MHCII-PE and F4/80-APC. The following isotype controls have been used: Rat-IgG2aκ-PE/APC/FITC/PerCP-Cy5.5, Rat-IgG2bκ-PE/APC/FITC/PerCP-Cy5, Hamster-IgG-APC, Rat-IgM-APC and Rat-IgG1-APC.

For intracellular stainings, cells were fixed with 2% paraformaldehyde/PBS solution for 15 min at room temperature under continuous agitation. The reaction was stopped with PBS + 2% FBS. Afterwards CD206-FITC or CD68-FITC were diluted in permeabilization buffer in the appropriate concentration and stained for 1 h at 4 °C. Prior to the analysis, cells were washed once and resuspended in an appropriate volume of PBS + 2% FBS.

3.6.5 FACS analyses of stained cells

Stained cells were analyzed using an Accuri C6 Cytometer and FACS analysis software CFlow Version 1.0.227. For each measurement, 10,000 events per sample were analyzed. The core size was set 25 and the threshold at 500,000. The flow rate was adjusted between 50 and 60. The following filter-combinations in the four detectors FL-1 to FL-4 were used: filter 533 to detect FITC, filter 585/40 to detect PE, filter 675 (25) to detect APC and filter 670 LP to detect PerCP and PerCP-Cy5.5. Cell debris was excluded from the measurements by defining a proper gate for the cell population of interest by using FSC and SSC. For each antibody combination a single staining

and an isotype control were prepared as controls and for compensation of the fluorescence signals. Double stainings were conducted to avoid false positive or unspecific results. Calculated percentages below 1% were defined as not detectable (n.d.).

3.7 Protein analytical methods

3.7.1 Sample preparation of cultured cells

For detection and quantification of specific proteins in cell lysates, cells were cultured in 6-well plates, washed once with PBS, harvested with a cell scraper and transferred into a 1.5 ml tube. After centrifugation at 2,000 rpm for 5 min, the pellet was resuspended in 150 µl lysis buffer. For disruption of the cell membranes, the samples were frozen for 30 min at -20 °C followed by 2 cycles of sonication for 30 sec at 4 °C. Cell debris was excluded by centrifugation for 10 min at 10,000 rpm and the supernatant was collected. The protein concentration was determined with 1x Bradford-Reagent. For removal of unsheared nucleic acids that make the samples highly viscose and gel loading difficult, 1 µl benzonase was added and incubated for 10 min at 37 °C. Supernatants were mixed with 4x SDS sample buffer and incubated for 5 min at 95 °C prior to SDS PAGE or storage at -20 °C.

3.7.2 Sodium dodecyl sulfate polyacrylamide gel electrophoresis (SDS PAGE)

Proteins of the cell lysates were separated according to their electrophoretic mobility, dependent on charge, molecular weight and conformation, by sodium dodecyl sulfate polyacrylamide gel electrophoresis (SDS PAGE). Bigger proteins generally move slower through the gaps in the gel and need wide meshed gels to migrate faster. Smaller proteins are generally faster as they can move more freely. These characteristics are responsible for the separation of the proteins over time. For preparation of the SDS PAGE a “Mini-PROTEAN electrophoresis system” from BioRad was used. The gels were prepared as described in the table below with polyacrylamide concentrations between 10 and 14% dependent on the molecular weight of the proteins.

Sufficient amounts for two gels

	Separating gel			Stacking gel
chemical	10%	12%	14%	4.3%
ddH_2O (ml)	4.88	4.08	3.23	3.05
1.5 M Tris/HCl pH 8.8 (ml)	3	3	3	
0.5 M Tris/HCl pH 6.8 (ml)				1.25
Acrylamide (30%) (µl)	4	4.8	5.6	650
SDS (10%)(µ)l	120	120	120	50
TEMED (µl)	30	30	30	30
APS (10%) (µl)	150	150	150	150
total	12.18	12.18	12.18	5.18

The separation gel was poured between two glass plates after APS and TEMED were added for polymerization and overlaid with isopropyl alcohol. After polymerization, isopropyl alcohol was removed and the stacking gel was poured over the separation gel and a comb was inserted. The polymerized gel was transferred to a horizontal electrophoresis chamber. The comb was removed and the gel overlaid with 1x SDS running buffer. The protein samples mixed with 4x SDS sample buffer were denatured by incubation at 95 °C for 5 min prior to application onto the gel. 20 µl of the protein sample per well was transferred. A PageRuler prestained protein ladder as size standard was included. The separation was carried out at 120 V for 1-2 h.

3.7.3 Western blotting, immunodetection and “stripping”

To enable antibody detection, all proteins needed to be transferred from the polyacrylamide gel onto a nitrocellulose membrane using a semi-dry blotting apparatus (BioRad). For this the polyacrylamide gel was placed above the nitrocellulose membrane between 2 layers of blotting paper soaked with blotting buffer to vertically relay the electric current and thus draw the proteins from the gel onto the membrane. The transfer appeared at a constant electric current according to the following formulae:

Amperage [mA] = length x width x number of membranes x 0.8

Following electrophoresis, the membrane was incubated for 1 h in blocking solution at room temperature to saturate unspecific binding sites. After a washing step in 1x TBS-T or 1x PBS-T the membrane was incubated with the primary antibody (Table 3) over night at 4 °C or for 2-3 h at room temperature. Afterwards the membrane was rinsed 3-4 times and incubated for 1 h with the HRP-labeled secondary antibody directed against the Fc-part of the primary antibody (Table 4). After three washing steps the membrane was incubated with enhanced chemiluminescence

(ECL) reagent for 1 min prior to detection using the BioRad Detektor ChemiDox XRS$^+$. In this system, the enzyme HRP acts as a catalyst for the oxidation of luminol to 3-aminopthalic acid.
To exhibit its luminescence, luminol must be activated first by adding an antioxidant such as hydrogen peroxide. Oxidation of luminol finally triggers light emission.
α-actin or α-GAPD were used as internal controls to check whether similar amounts of the proteins were applied to all lanes.

It is possible to re-use a Western blot after the chemiluminescence reaction to analyze more than one specific protein on the same membrane. For this, the blot needs to be relieved "stripped" from the bound antibodies to enable a new antibody to bind.
For this, the membrane was incubated with stripping solution for 30 to 45 min at room temperature. Afterwards the blot was rinsed 5 times with ddH_2O and neutralized with 1 M Tris-HCl (pH 8.0) for 20 min. After the neutralization, the blot was rinsed 5 times with ddH_2O and 1 time with TBS-T before it was used for another antibody staining as described above.

3.7.4 Griess assay

The colorimetric Griess assay which was first described in 1879 is a method to determine nitric oxide (NO) production in various biological samples *e.g.* plasma, urine or cell culture media [215, 216]. NO is a crucial physiological effector molecule synthesized by different highly regulated nitric oxide synthases (NOS) in diverse biological systems including immunological or neuronal tissues [215]. Due to the short half-life of NO, nitrite (NO_2^-) a stable breakdown product of NO, as a surrogate marker is measured in the Griess assay [215]. The Griess reagent system (Promega, Germany) according to the manufacturer's instructions is based on a diazotization reaction where NO_2^- is treated with sulfanilamide a diazotizing reagent in acidic medium to form a transient diazonium salt. This product then reacts with a coupling reagent, N-1-naphthyl-ethylenediamine dihydrochloride (NED), to form a stable azo-compound. The purple color of the end product allows detection with high sensitivity (detection limit 2.5 µM).
Supernatant of the samples of interest were collected at appropriate time points and stored at -20 °C until use. The assay was performed as described by the manufacturer's instructions: The sulfanilamide solution and NED solution were equilibrated to room temperature prior to use. 50 µl of the samples were pipetted into wells of a 96-well flat-bottom enzymatic assay plate in duplicates. Afterwards, 50 µl of sulfanilamide solution were added using a multichannel pipet. After an incubation time of 5-10 min at room temperature in the dark, 50 µl NED solution were added to the wells with a multichannel pipet. During an incubation time of 5-10 min at room temperature in the dark, a color formation to magenta became visible.

In parallel, a nitrite standard reference (100 µM to 1.56 µM) was prepared and treated similar to the experimental samples on the same plate. The absorbance was measured within 30 min at a wavelength of 550 nm.

Absorbance and concentration values of the NO_2^- standard were plotted as a X-Y diagram in Excel to generate a standard reverence curve. Based on this curve and the absorbance values of the experimental samples, the NO_2^- concentration of the experimental samples could be calculated.

3.8 Reverse transcription polymerase chain reaction (RT-PCR)

RT-PCR is used for qualitative detection of RNA expression. The following steps are necessary for successful RT-PCR: Following RNA isolation (3.8.1) and inactivation of desoxyribonucleases (3.8.2) the RNA template is converted into a complementary DNA (cDNA) by specific RNA-dependent DNA polymerases (reverse transcriptases; 3.8.3). The synthesized cDNA is finally used as template for amplification of specific gene sequences by PCR reaction using specific primers (3.8.4). The PCR products are finally analyzed by agarose gel electrophoresis (3.8.5).

3.8.1 Isolation of RNA from adherent cancer cells

Cells were grown in 6-well plates or cell culture dishes (100 mm). In case of knockdown of AVEN, cells were treated as described in (3.1.9). Cells were washed once with PBS, harvested with a cell scraper and centrifuged at 2,000 rpm for 5 min. The pellet was stored at -20 °C. For total RNA isolation, the RNeasy Mini Kit (Qiagen GmbH) was used according to the manufacturer's instructions. In brief, the RLT buffer was prepared by adding 10 µl β-mercaptoethanol per milliliter of buffer. 350 µl RLT buffer was pipetted onto the cell pellet and resuspended by pipetting up- and down several times. The suspension was transferred to RNA shredder columns and centrifuged for 2 min at 13,000 rpm in a Biofuge fresco. Afterwards, 1 volume of 70% ethanol was added to the suspension and mixed. The total volume was then transferred to a RNeasy spin column and centrifuged for 30 s at 10,000 rpm. The flow-through was discarded and 700 µl RW1-buffer was added to the column followed by centrifugation at 8,000 rpm for 30 s. The flow-through was discarded and 500 µl RPE buffer was pipetted onto the column and centrifuged at 8,000 rpm for 30 s. This step was repeated but the centrifugation took place at 8,000 rpm for 2 min. For elution of the RNA, the column was transferred to a new 1.5 ml collection tube and 40 µl RNAse free H_2O was added. Centrifugation was performed at 13,000 rpm for 1 min.

3.8.2 DNase treatment to remove genomic DNA

Genomic DNA was excluded from the samples using DNA-free™ Kit (Ambion). According to the manufacturer's instructions, 4 µl 10x DNase 1 buffer and 1 µl recombinant Dnase I were pipetted to the RNA (40 µl) and mixed. After an incubation step at 37 °C for 30 min, 4.4 µl DNase Inactivation Reagent was added and mixed. The mixture was incubated for 2 min at room temperature and centrifuged at 13,000 rpm for 1.5 min. The supernatant containing the RNA was transferred into a new 1.5 ml tube. The amount of RNA was measured with a Nanodrop.

3.8.3 Synthesis of cDNA by reverse transcription

Total RNA was converted to cDNA using the RevertAid™ First Strand cDNA Synthesis Kit (Fermentas) according to the manufacturer's instructions. 1 µg template RNA diluted in RNase free H_2O to 10 µl were mixed with 1 µl RevertAid™ M-MuLV Reverse Transcriptase and 9 µl mastermix. The mastermix exemplarily for 10 samples was composed of 40 µl 5x Reaction Buffer, 10 µl RiboLock™ RNase Inhibitor, 20 µl 10 mM dNTP mix and 10 µl random hexamer primer.

The samples were incubated in a T-Gradient Thermoblock PCR machine (Biometra) for 5 min at 25 °C followed by a synthesis step at 42 °C for 60 min and the reaction was terminated by heating at 70 °C for 5 min.

Alternatively, the Transcriptor High Fidelity cDNA Synthesis Kit (Roche Diagnostics) has been used according to the manufacturer's instructions. 1 µg template RNA and 2 µl random hexamer primer were mixed and filled up to 11.4 µl with RNase free H_2O. The template-primer mixture was denatured by heating for 10 min at 65 °C in the PCR cycler. Afterwards the tube was cooled on ice. Following this step, 4 µl 5x Reaction Buffer, 0.5 µl Protector RNase Inhibitor, 2 µl 10 mM dNTP mix, 1 µl DTT and 1.1 µl Transcriptor High Fidelity Reverse Transcriptase were added, mixed carefully and incubated for 30 min at 50 °C. The reaction was stopped by heating at 85 °C for 5 min.

3.8.4 Polymerase chain reaction (PCR)

For amplification of human AVEN [217], human β-actin and human GAPDH [218] sequences, a PCR was performed using specific primers listed in Table 7. In brief, for 1 sample 5 µl Phusion buffer, 0.5 µl specific primer (sense and antisense), 1.5 µl $MgCl_2$ (50 mM), 1 µl Phusion DNA Polymerase, 10.4 µl PCR grade H_2O and 5 µl cDNA were properly mixed. The PCR reaction was run in a T-Gradient Thermoblock PCR machine (Biometra) under the following conditions: 98

°C/1 min, followed by 30 cycles of 98 °C/15 s, 56 °C/15 s, 72 °C/5 s) and a 72 °C/5 min step. In the first step at 98 °C, the double stranded DNA is separated into two single strands. This step is followed by an annealing step (56 °C) where specific primers bind to the single DNA strands. The temperature in this step is primer-dependent. In the elongation step (72 °C), the DNA polymerase binds to the template and uses dNTPs to synthesize the complementary strand starting at the specific primers. The elongation time is dependent on the size of the amplified DNA fragment. The reaction ends with a final elongation step, where unfinished strands are completed.

3.8.5 Agarose gel electrophoresis

For separation of DNA fragments based on their size, horizontal agarose gel electrophoresis is used. Based on the size of the DNA fragments an agarose concentration of 1.5% diluted in TBE buffer was chosen for experiments performed in this work. For visualization of the nucleic acids bands Midori Green Advanced DNA stain has been used (4 µl per 100 µl agarose solution). It emits green fluorescence (~530 nm) when it is bound to DNA. A DNA ladder was added to the gel prior to running to identify the size of DNA fragments in base pairs (bp). A total of 20 µl per sample was loaded onto the gel. Prior to gel loading, 6x gel loading dye blue was added to the samples. As DNA molecules are negatively charged, they migrate in the electric field to the plus pole through the agarose polymer network. Larger molecules need more time than smaller molecules for the same distance which allows the fractionation of the DNA bands. DNA gels were analyzed using a ChemiDox XRS$^+$ (Biorad) or a gel documentation system from Peqlab. According to (http://home.arcor.de/d-kraus/lab/ImageJ_Western_blots.html; 2015/16/01) the intensity of the DNA fragments was determined using ImageJ.

3.9 Statistical analysis

To determine significance between 2 independent groups and normal distribution, a 2-tailed t-test with unequal variances was used (Excel 2010 for Windows). P values were defined as follows *p<0.05, **p<0.01, ***p<0.001.

Power analysis was performed using the software G*Power. The optimal sample size (n = 17) to detect a difference of d= 1.02 for the viral replication in C57BL/6 wt and C57BL/6 IFN-γ KO mice was calculated to assure an adequate power to detect statistical significance. A power of 80% and an α-level of 0.05 has been used in the present experiment.

For calculating boxplot diagrams, a template from Vertex42 LLC has been used.

4 Results

Part 1: Characterization of murine GL261 glioma models for oncolytic vaccinia virus therapy

[The majority of the results in part 1 have been published in the research article Kober et al. [219]*, "Intratumoral INF-γ triggers an anti-viral state in GL261 tumor cells: A major hurdle to overcome for oncolytic vaccinia virus therapy of cancer" and in the research article Kober et al.* [220]*., "Microglia and astrocytes attenuate the replication of the oncolytic vaccinia virus LIVP 1.1.1 in murine GL261 gliomas by acting as vaccinia virus traps."]*

4.1 Analysis of the replication capacity of LIVP 1.1.1 in murine GL261 glioma models

Cancer formation is associated with a close interaction of malignant tumor cells and the microenvironment consisting of a composition of various cell types such as endothelial cells, fibroblasts, immune cells, blood and lymph vessels, as well as cytokines and chemokines [35, 58]. The percentage and composition of immune cells varies between cancer types and among patients [34, 35]. This link between the immune status of a tumor and the clinical outcome is investigated as a biomarker in several studies and great effort is performed to introduce the "Immunoscore" as an additional cancer classification system [34, 35, 59]. Possible mechanisms resulting in a diverse immune cell infiltration and activation of a particular tumor microenvironment include the genetic background of the host, genetic polymorphism of cytokine receptors and the genetics of the tumor itself and are reviewed in "An immunologic portrait of cancer" by Ascierto *et al.* [221]. It was assumed that the advancement of a successful oncolytic virotherapy for GBM requires a detailed understanding of the individual tumor biology, as well as the interaction with the tumor microenvironment and the immune system. A comparative approach with different tumor locations (subcutaneous and orthotopic) as well as different immunologic (wild-type and immunodeficient) and genetic backgrounds (C57BL/6 athymic nude and Balb/c athymic nude

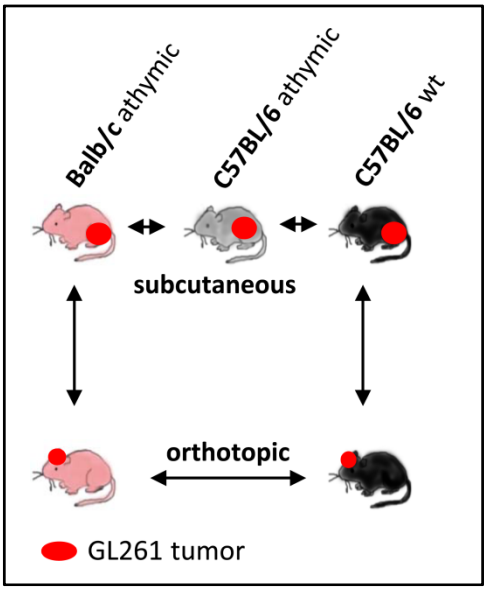

Figure 9: **Experimental design**

mice) as experimental setup (Figure 9) was designed. By using this approach, the replication capacity and oncolytic potential in murine GL261 gliomas was analyzed. In addition, it was expected to identify potential microenvironmental factors, which may influence treatment success or failure.

4.1.1 GL261 glioma cells are susceptible to VACV LIVP 1.1.1 infection under cell culture conditions

The potential of oncolytic VACVs is characterized by their ability to efficiently infect, replicate in and lyse cancer cells [136, 222–224].

In order to select an efficient oncolytic virus strain for studies in murine GL261 glioma cells and tumors, the VACV strain LIVP 1.1.1, a replication-competent plaque purified wild-type isolate from LIVP and the more attenuated recombinant VACV strain GLV-1h68 based on the same parental virus strain were compared in cell culture studies [193].

Both VACVs have already been evaluated to efficiently infect and replicate in a great number of human, canine and feline cancer cells of different histological origin, including human glioblastoma cell lines [154, 155, 181, 218, 225–227]. However, so far there is not much data about VACV infection in murine cancer cells, which is necessary to study oncolytic VACV effects in immunocompetent mouse models.

To determine the percentage of VACV-infected cells over time, GL261 glioma cells infected with LIVP 1.1.1 or GLV-1h68 with an MOI of 1.0 were stained with anti-VACV antibody and Hoechst to detect cell nuclei 24, 48 and 72 h post infection (hpi). The stained slides were analyzed by fluorescence microscopy. As shown in Figure 10a, significantly more LIVP 1.1.1-infected GL261 glioma cells were detected 48 hpi and 72 hpi compared to GLV-1h68-infected GL261 glioma cells.

For analysis of viral replication, GL261 cells were infected with LIVP 1.1.1 and GLV-1h68 at an MOI of 1.0. Viral titers were determined 2, 8, 24, 48, 72 and 96 hpi in cells and supernatants by standard viral plaque assay. The initial virus titer was depicted as virus inoculum and active viral replication was assumed as an increase of the virus titer compared to the titer of the virus inoculum marked by the red line in Figure 10b, c. With a ~2-log increase in GLV-1h68-infected GL261 cells and a ~3-log increase in LIVP 1.1.1-infected GL261 cells within the first 48 h, the maximal virus titer was reached. After 48 hpi the virus titers declined indicating increased cell lysis or an inhibition of further replication. However, as shown in Figure 10b, the virus titer detected in GLV-1h68-infected cells was always below the initial virus inoculum. With the exception of the first time points (2 and 8 hpi), the GLV-1h68 virus titer was always higher in the cells than in the supernatants.

As shown in Figure 10c, the virus titer in the supernatant of LIVP 1.1.1-infected cells increased over time from 8 to 96 hpi indicating cell lysis in contrast to the virus titer in the supernatant of GLV-1h68-infected cells (Figure 10b), where no increase occurred.

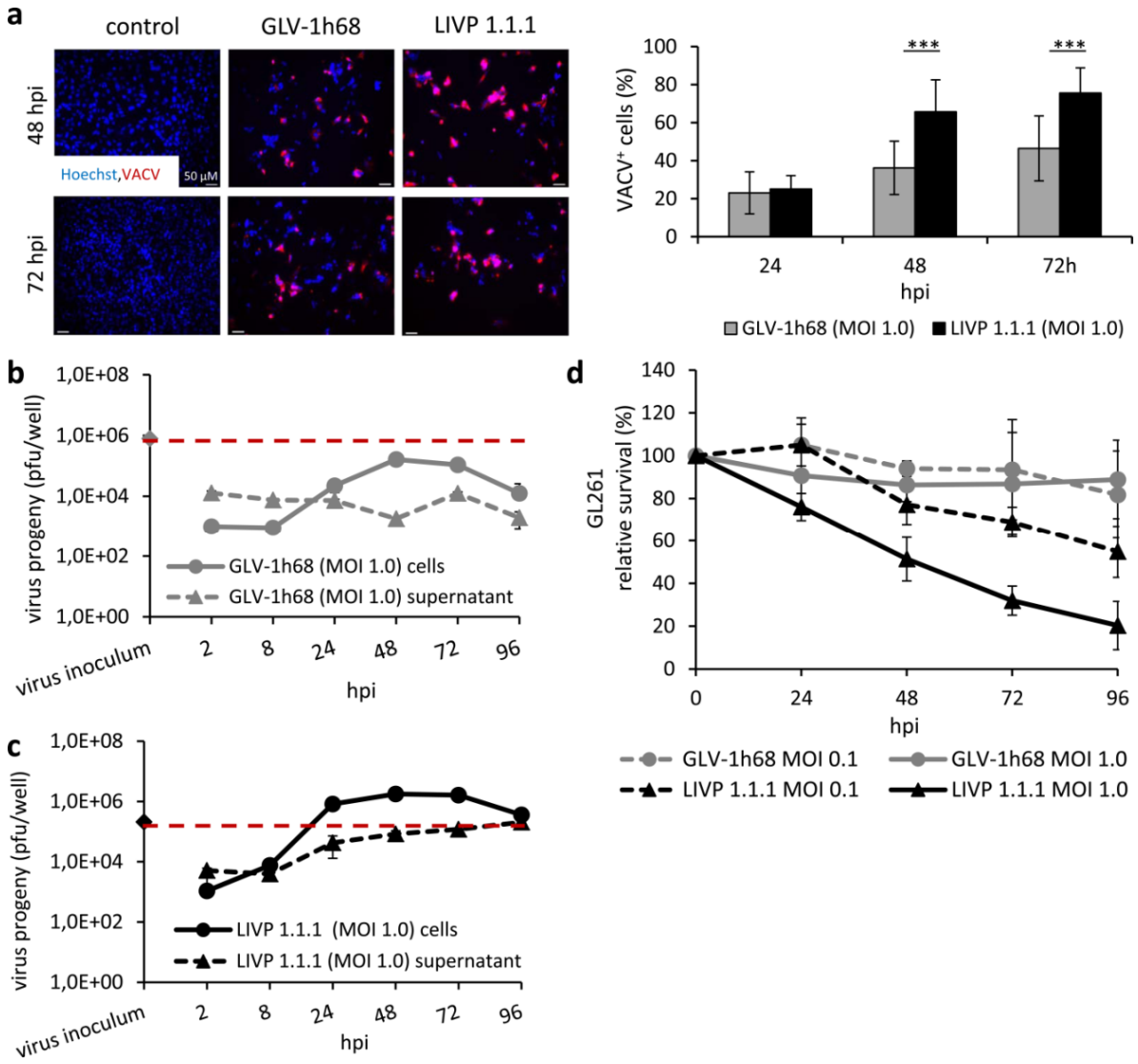

Figure 10: Comparison of GLV-1h68 and LIVP 1.1.1 infection, replication and lysis of GL261 cells in cell culture. Infection of GL261 cells with GLV-1h68 or LIVP 1.1.1 at an MOI of 1.0 was determined 24, 48 and 72 hpi. Representative overlay images of uninfected control, GLV-1h68- or LIVP 1.1.1-infected GL261 cells at 48 and 72 hpi are depicted. Cells were stained with α-VACV antibody (red) and Hoechst to stain cell nuclei (blue) and images were taken at a magnification of 20x. For calculation of the percentage of infected cells, 10 images per sample were taken and the number of Hoechst and VACV-positive cells counted**.** The bar chart shows mean values and standard deviation **(a)**. Viral replication in GL261 cells and supernatant infected with GLV-1h68 **(b)** or LIVP 1.1.1 **(c)** at an MOI of 1.0 was analyzed by standard viral plaque assay. The experiment was performed in triplicate and performed twice. MTT assay **(d)** was performed to detect the relative survival of GL261 cells after infection with GLV-1h68 or LIVP 1.1.1 (MOI 0.1, 1.0) Non-infected cells were used as control. Experiments were performed in triplicate and repeated two times in independent experiments.

As a third parameter, the effect of VACV infection on cell viability was tested by MTT assay. For this, cells were infected with LIVP 1.1.1 or GLV-1h68 at MOIs of 0.1 and 1.0 and relative survival was determined 24, 48, 72 and 96 hpi. Non-infected samples were used as references and were set 100% at every time point. As shown in Figure 10d, relative survival of GL261 cells after infection with LIVP 1.1.1 decreased with an MOI-dependent effect over the time course of the infection. At 96 hpi 20% of cells were alive after infection with an MOI of 1.0 and 55% with an MOI of 0.1. In line with the reduced number of infected cells and inefficient viral replication also virus-mediated cell death of GLV-1h68-infected cells was minimal. Relative survival in GL261 cells 96 h post GLV-1h68 infection was 89% (MOI 1.0) and 82% (MOI 0.1).

As for all three parameters (infection, replication and cell lysis) LIVP 1.1.1 showed stronger effects in GL261 cells than GLV-1h68, the wild-type isolate LIVP 1.1.1 was used for the following *in vivo* studies.

4.1.2 Investigation of tumor growth kinetics of subcutaneous GL261 tumors in three mouse strains before and after virus infection

$1x10^6$ GL261 cells were implanted subcutaneously in the left flank of Balb/c athymic, C57BL/6 wt and C57BL/6 athymic mice. At a tumor size between 200 and 400 mm^3, mice were injected intratumorally with either $5x10^6$ pfu/tumor LIVP 1.1.1 or PBS. The injection volume was 100 µl. The time point of injection was reached in the athymic mice after 11-13 days (Balb/c) and 12-13 days (C57BL/6) whereas it took about one week longer in the C57BL/6 wt mice with 17-21 days, respectively (Figure 11a). Tumor growth was monitored every second day. All three tumor models showed a very fast and aggressive tumor growth and needed to be euthanized after a short period of time (7-21 dpi) due to a tumor size of 4,000 mm^3.

In all three mouse models there was a slight tumor growth delay after infection with LIVP 1.1.1 (Figure 11b-d) but only in Balb/c athymic mice (Figure 11b) a significant tumor growth delay from 4 dpi to the end of the study in the LIVP 1.1.1 group could be detected. In addition, all tumor models showed edema formation at end stage disease at both treatment conditions - PBS and LIVP 1.1.1.

a	Balb/c athymic	C57BL/6 wt	C57BL/6 athymic
time of implantation	d0	d0	d0
time of injection (tumor volume between 200 and 400 mm^3)	11-13 dpimp	17-21 dpimp	12-13 dpimp
end-stage disease (tumor volume between 3000-4000 mm^3)	7-9 dpi	10-17 dpi	11-14 dpi
edema formation	yes	yes	yes

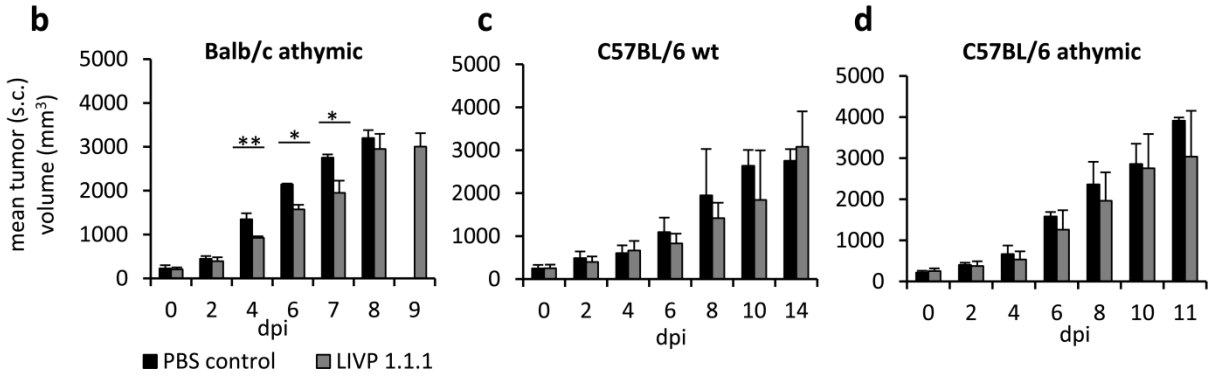

Figure 11: Tumor growth characteristics of subcutaneous GL261 gliomas before and after viral infection. Summary of tumor growth kinetics in three different mouse strains until the day of injection (d0) was reached, counted as days post implantation (dpimp). Summary of tumor growth kinetics until the end stage disease was reached counted as dpi (PBS and LIVP 1.1.1 groups). In addition, edema formation was monitored visually **(a)**. Balb/c athymic (n=3/4) **(b)**, C57BL/6 wt (n=5/6) **(c)** and C57BL/6 athymic (n=6) **(d)** mice with (s.c.) GL261 tumors were injected (i.t.) with $5x10^6$ pfu LIVP 1.1.1 or PBS at a tumor volume between 200-400 mm^3. Tumor growth post injection **(b-d)** was monitored by measuring the tumor every other day. Depicted are the mean values with standard deviation. Differences between virus-treated and PBS-treated groups were tested using two-sided t-test with unequal variances *p<0.05, **p<0.01.

4.1.3 Investigation of the time of virus injection in orthotopic GL261 tumors in Balb/c athymic and C57BL/6 wt mice

To establish orthotopic GL261 tumors for quantification of virus titers after intracranial infection, $1x10^5$ GL261 cells in a volume of 3 µl PBS were implanted intracranially into 5-6 week old female Balb/c athymic and C57BL/6 wt mice using a stereotactic apparatus.

Mice were monitored daily or every other day for indirect parameters of tumor formation including the general state of health, neurological dysfunctions such as impairment of movement, behavioral changes and weight loss (Figure 12a,c). In both, athymic and wild-type mice, a temporary weight loss was detected after anesthesia that was needed for tumor cell implantation, magnetic resonance imaging (MRI) and LIVP 1.1.1 injection and a constant weight loss was measured at end stage disease.

To identify the optimal time of virus injection and monitor tumor growth before and thereafter, mice were imaged by MRI.

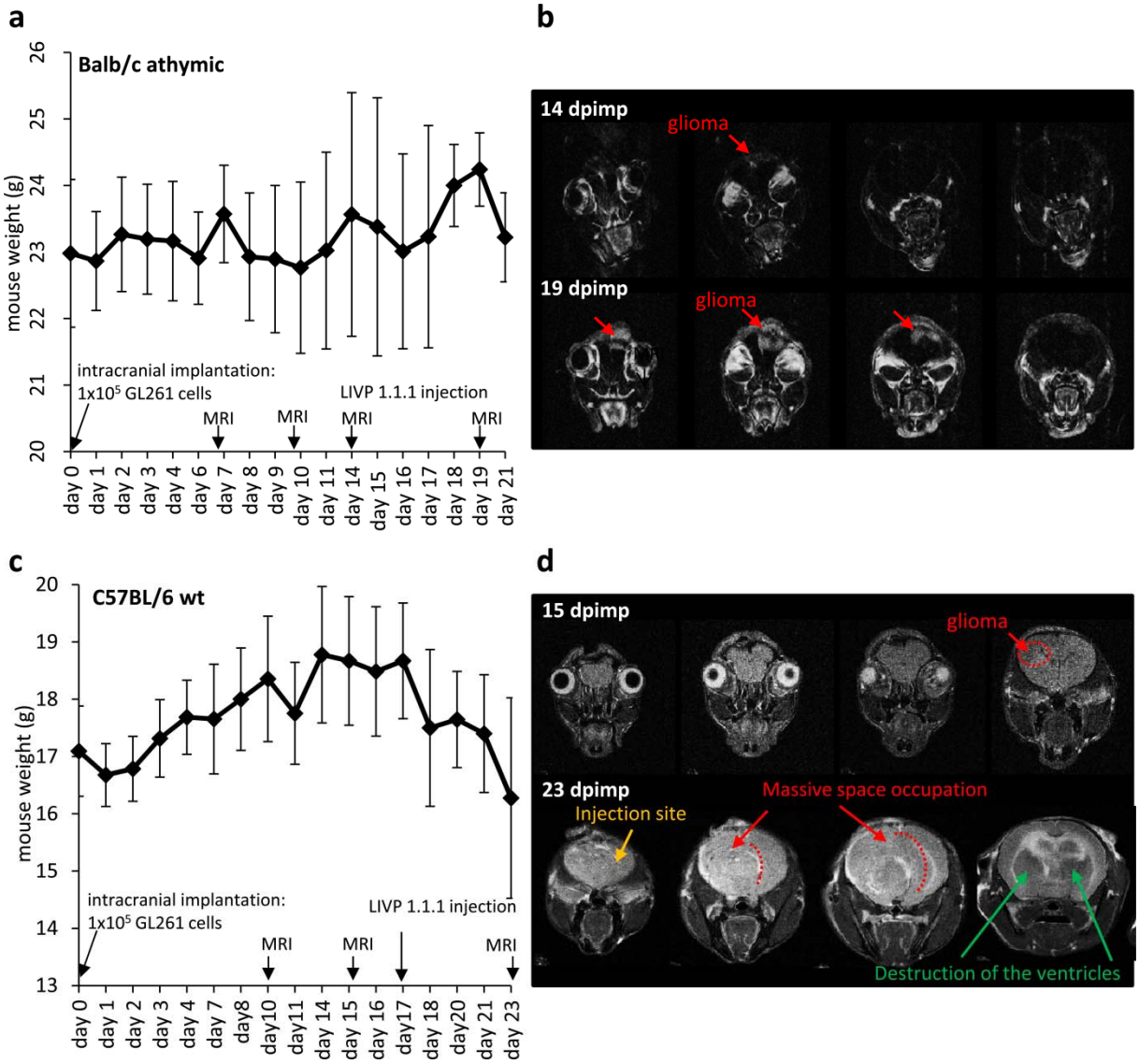

Figure 12: Monitoring of intracranial GL261 tumor growth by indirect parameters and MRI. 5-6 week old Balb/c athymic or C57BL/6 wt (n=5) mice were injected intracranially with $1x10^5$ GL261 cells. Mouse weight was monitored daily or every other day. Mean values and standard deviation of Balb/c athymic **(a)** and C57BL/6 wt mice **(c)** are depicted. Time point of MRI measurements and LIVP 1.1.1 injection ($5x10^6$ pfu LIVP 1.1.1 in 3 µl PBS) are marked by black arrows. MRI image series of one exemplarily chosen Balb/c athymic mouse brain (n=3) implanted with GL261 cells on day 14 and 19 post implantation (sectional plane: 24, 22, 21, 20 and 23, 22, 20, 19) **(b)**. For better resolution, mice were injected with the contrast agent Magnograf (300 µmol/kg body weight) prior to measurement. MRI image series without Magnograf of one exemplarily chosen C57BL/6 wt mouse brain (n=5) implanted with GL261 cells on day 15 and 23 post implantation (sectional plane: 34, 33, 32, 30 and 25, 24, 23, 21) **(d)**. Glioma formation and space occupation are marked with red arrows, destruction of the ventricles is marked in green and the injection site highlighted in yellow. (MRI measurement was performed in corporation with T.C. Basse-Lüsebrink; Department of Experimental Physics 5; University of Würzburg)

In Balb/c athymic mice, tumor formation was detected clearly at 14 days post implantation (Figure 12b) and this time point was thus chosen for LIVP 1.1.1 injection.

In C57BL/6 wt mice, first signs of tumor formation were detected 15 days post implantation (Figure 12d). As GL261 tumors were visible but slightly smaller than in Balb/c athymic mice at time of injection, tumors were allowed to grow for two more days and LIVP 1.1.1 injection was performed 17 days post implantation. At end stage disease massive space occupation and a destruction of the ventricles was observed.

4.1.4 Only Balb/c athymic mice bearing subcutaneous GL261 tumors showed efficient viral replication in contrast to all other mouse and tumor models

After the evaluation of the growth characteristics of the tumor models, the replication efficacy of LIVP 1.1.1 upon intratumoral injection in murine GL261 gliomas was tested.

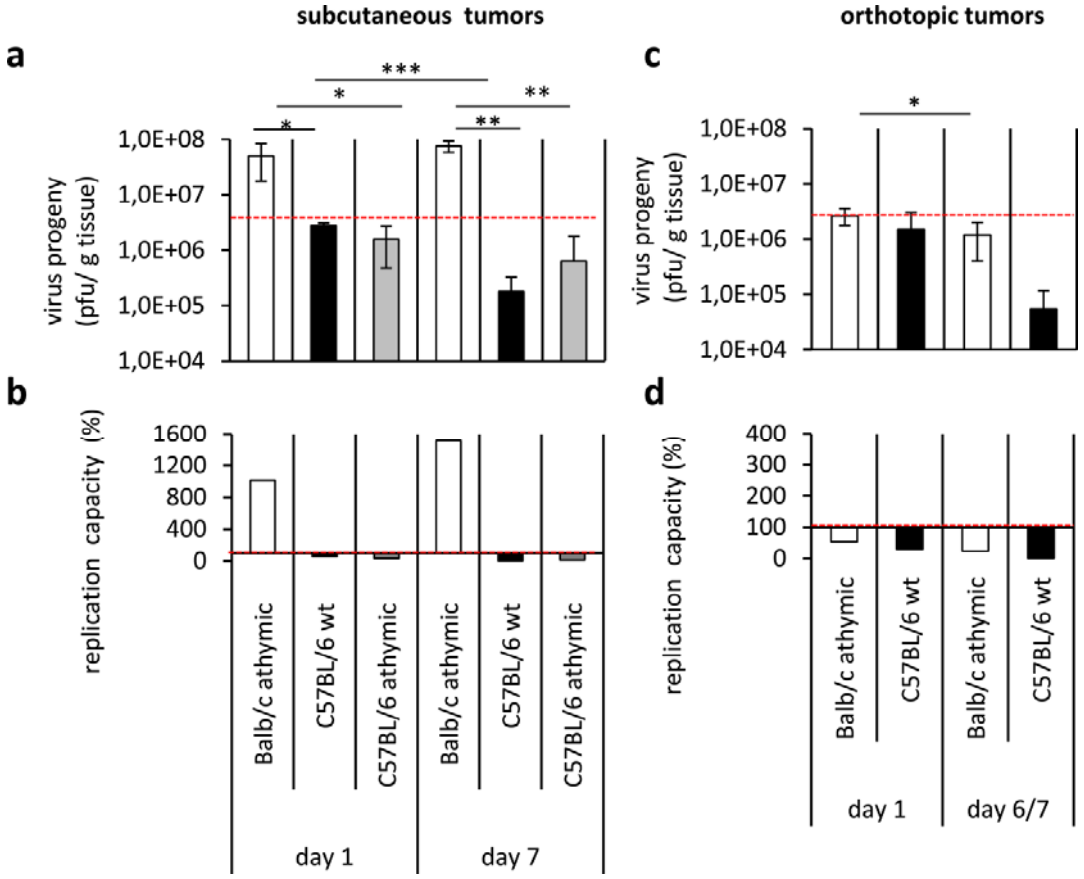

Figure 13: Detection of viral replication exclusively in Balb/c athymic nude mice with subcutaneous tumors but in none of the other mouse and tumor models. The bar charts show mean and standard deviation of LIVP 1.1.1 titers (pfu/g tissue) in subcutaneous **(a)** or orthotopic **(c)** GL261 tumors in Balb/c athymic, C57BL/6 wt or C57BL/6 athymic mice (n=5) at day 1 or 6/7 post virus injection. In addition, the replication capacity (%) of subcutaneous **(b)** or orthotopic tumor models **(d)** was calculated by dividing the actual virus titer by the initial virus inoculum multiplied by 100%. Viral titers and percentages of initially injected virus dose ($5x10^6$ pfu/mouse) were determined by standard viral plaque assay. The red line demonstrates the level of the virus inoculum of $5x10^6$ pfu/mouse or 100%. Differences of the virus titers in subcutaneous or orthotopic GL261 tumors were tested between mouse strains at 1 dpi and 6/7 dpi, respectively and within each mouse strain between 1 dpi and 6/7 dpi by using two-sided t-test with unequal variances *p<0.05, **p<0.01, ***p<0.001.

VACV replication was assumed as an increase of the viral titer compared to the initial injection dose of $5x10^6$ pfu/mouse. The virus was delivered intratumorally.

As depicted in Figure 13, the results revealed viral replication exclusively in Balb/c athymic mice bearing subcutaneous tumors with $5x10^7$ +/- $3x10^7$ pfu/g tissue 1 dpi and $8x10^7$ +/- $2x10^7$ pfu/g tissue 7 dpi (Figure 13a). In the other mouse models and tumor locations a decrease of LIVP 1.1.1 titers was detected during the observation time course. The replication capacity was up to 15-fold increased in subcutaneous tumors of Balb/c athymic mice at 7 dpi compared to a 28-fold and 8-fold decrease of the viral load in C57BL/6 wt mice and C57BL/6 athymic mice tumors, respectively (Figure 13b).

In the orthotopic brain tumors no replication was detected neither in Balb/c athymic mice ($1x10^6$ +/- $8x10^5$ pfu/g 7dpi) nor in the C57BL/6 wt mice ($6x10^4$ +/- $6x10^4$ pfu/g 7dpi) (Figure 13c). These findings coincide with a 4-fold decrease of the viral load in Balb/c athymic and 100-fold decrease in C57BL/6 wt mice at 7 dpi (Figure 13d).

Further it was analyzed whether viral particles were found exclusively in tumors or brains of the mice injected intratumorally with LIVP 1.1.1 ($5x10^6$ pfu) or whether viral particles were also found in other organs.

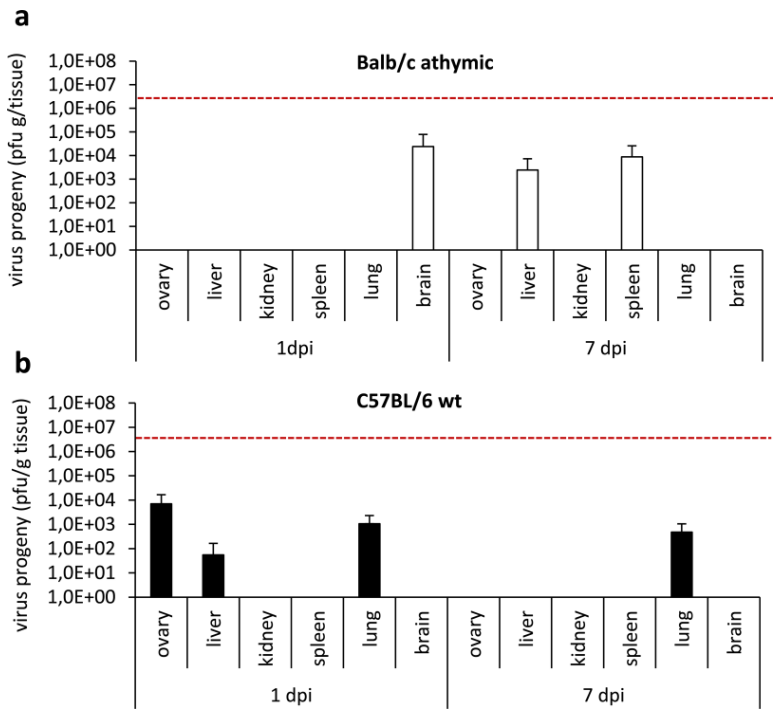

Figure 14: Viral distribution in Balb/c athymic (a) and C57BL/6 wt (b) mice with subcutaneous GL261 tumors at 1 and 7 dpi. Tissue homogenates were prepared and standard viral plaque assay was performed. The bar chart represents mean and standard deviation (n=5). The detection limit was 10^{-1}. The red lines mark the initially injected virus dose of $5x10^6$ pfu/mouse. No viral particles were detected in organs of mice with orthotopic GL261 tumors.

For this purpose tissue homogenates of different organs of tumor bearing mice 1 and 7 dpi were prepared and standard viral plaque assay was performed.

VACV was detected in some organs including brain (1 dpi), liver (1 dpi) and kidney (7 dpi) in case of Balb/c athymic mice with subcutaneous tumors (Figure 14a) or ovary (1 dpi), liver (1 dpi) and lung (1/7 dpi) in C57BL/6 wt mice (Figure 14b). However, the number of LIVP 1.1.1 virus particles was at least more than two log levels lower in the analyzed organs compared to the intratumorally injected virus titer of $5x10^6$ pfu and more than three log levels lower than in the tumor at the same time point.

In Balb/c athymic and C57BL/6 wt mice with orthotopic GL261 tumors that were injected with the virus intratumorally, no virus particles were detected in any organ tested (dilution factor 10^{-1}).

4.2 Characterization of the tumor microenvironment of subcutaneous GL261 tumors

Analyses of the replication capacity of LIVP 1.1.1 in the subcutaneous tumor models led to the question which immunological factors in the tumor microenvironment of Balb/c athymic nude mice support virus replication on the one hand and inhibit replication in mice with C57BL/6 genetic background on the other side (Figure 15).

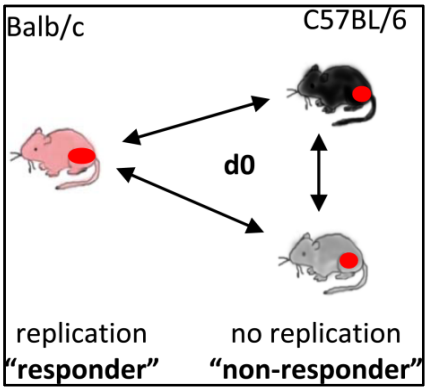

Figure 15: Schematic representation of the initial experimental situation

As the virus titer differed significantly already one day post injection the differences seem to exist already before virus injection on day 0 (day of injection). Therefore, initially a detailed characterization of the tumor microenvironment of the subcutaneous tumor models at the time of injection was performed. The experimental set-up consisted of a mouse immune-related antigen profiling including 59 biomarkers (4.2.1), an immune cell profiling of tumors, blood and spleens by FACS analysis (4.2.2) and an immunohistological analysis of the tumors (4.2.3).

4.2.1 Biomarker profiling in subcutaneous GL261 tumors on day of injection

To characterize the tumor microenvironment of the subcutaneous GL261 tumors at the day of injection, a subset of 59 biomarkers was tested using a mouse immune-related antigen profiling [228]. Of those 59 biomarkers, 19 biomarkers showed significant differences in the three

different mouse strains (Figure 16). In all those cases, highest biomarker concentrations were detected in C57BL/6 wt mice followed by C57BL/6 athymic nude and Balb/c athymic nude mice.

The study revealed that significant differences of the proinflammatory signature including proinflammatory cytokines and chemoattractants (Figure 16a, highlighted in light red) were all detectable between the C57BL/6 wt mice and both athymic nude mouse strains (C57BL/6 and Balb/c). No significant differences were observed between the C57BL/6 athymic nude and Balb/c athymic nude mice.

Proinflammatory cytokines that were significantly upregulated in C57BL/6 wt mice include interferon gamma-induced protein 10 (IP-10) (Figure 16b), IL-1α, IL-11 and macrophage inflammatory protein-1 beta (MIP-1 beta).

Chemoattractants significantly upregulated were: MCP-1 (Figure 16c), MCP-3 and MCP-5 that recruit mainly monocytes, macrophages, lymphocytes and eosinophils. MIP-2 and granulocyte chemoattractant protein-2 (GCP-2) attracting neutrophils and Lymphotactin and IP-10 recruiting lymphocytes [228].

Factors responsible for the proinflammatory signature (GCP-2, MIP-1 beta, MIP-2, MCP-3 and MCP-5) were mainly produced by macrophages.

Another factor which was almost 5-fold upregulated in the wild-type mice was VEGF-A a growth factor important for angiogenesis, vasculogenesis, and endothelial cell growth as well as CD40, which is a type I transmembrane glycoprotein of the TNF receptor superfamily associated in different signaling pathways including proliferation, cytokine production and inhibition of apoptosis. The only factor which showed significant differences between the two athymic mouse strains was tissue inhibitor of metalloproteinase (TIMP-1), highlighted in blue, that belongs to the group of factors associated with destruction of the extracellular matrix.

This analysis showed that implantation of the same tumor cells in different mouse strains resulted in a completely different tumor microenvironment with highest differences between immunodeficient and immunocompetent mice. It further demonstrated the influence of the adaptive immune system as main immune modulator.

a			Mouse strains			P-value * ** ***		
Biomarker profile	**Abbr.**	**unit**	**C57BL/6 wt**	**C57BL/6 athymic**	**Balb/c athymic**	**C57BL/6 wt : Balb/c athymic**	**C57BL/6 wt : C57BL/6 athymic**	**C57BL/6 athymic : Balb/c athymic**
Granulocyte Chemotactic Protein-2	GCP-2	ng/mL	0.2 +/- 0.03	0.1 +/- 0.02	0.1 +/- 0.01	0.005	0.004	0.220
Interferon gamma Induced Protein 10	IP-10	pg/mL	2940.0 +/- 602.2	921.0 +/- 1123.9	423.0 +/- 154.2	0.003	0.007	0.323
Interleukin-1 alpha	IL-1 alpha	pg/mL	1035.5 +/- 123.5	572.5 +/-158.6	438.8 +/- 218.3	0.002	0.004	0.266
Interleukin-11	IL-11	pg/mL	101.3 +/-17.9	70.8 +/- 6.2	n.d.	-	0.036	-
Leukemia Inhibitory Factor	LIF	pg/mL	775.0 +/- 112.9	533.8 +/- 167.1	452.3 +/- 71.5	0.006	0.037	0.378
Lymphotactin		pg/mL	879.5 +/- 201.4	516.2 +/- 267.6	188.0 +/- 32.0	0.006	0.053	0.051
Macrophage Inflammatory Protein-1 beta	MIP-1 beta	pg/mL	1457.5 +/- 281.2	294.2 +/- 164.5	171.0 +/- 15.9	0.003	0.001	0.170
Macrophage Inflammatory Protein-2	MIP-2	pg/mL	34.0 +/- 6.6	17.6 +/- 4.9	15.3 +/- 2.8	0.006	0.007	0.399
Monocyte Chemotactic Protein 1	MCP-1	pg/mL	436.8 +/- 122.1	160.3 +/- 51.3	115.8 +/- 44.0	0.010	0.014	0.183
Monocyte Chemotactic Protein 3	MCP-3	pg/mL	320.5 +/- 120.9	143.4 +/- 64.2	96.8 +/- 25.5	0.032	0.053	0.189
Monocyte Chemotactic Protein-5	MCP-5	pg/mL	184.5 +/- 38.9	94.8 +/- 38.2	87.6 +/- 33.0	0.007	0.012	0.758
T-Cell-Specific Protein RANTES	RANTES	pg/mL	0.3 +/- 0.1	0.1 +/- 0.1	0.03 +/- 0.01	0.017	0.020	0.226
Vascular Endothelial Growth Factor A	VEGF-A	pg/mL	9105.0 +/- 2539.6	1684.2 +/- 829.3	2230.0 +/- 600.3	0.011	0.007	0.271
von Willebrand factor	vWF	ng/mL	12.0 +/- 2.2	8.6 +/- 1.5	8.3 +/- 2.3	0.045	0.043	0.805
Stem Cell Factor	SCF	pg/mL	1380.0 +/- 175.7	791.6 +/-237.3	542.8 +/- 195.9	0.0003	0.004	0.110
CD40	CD40	pg/mL	724.8 +/-361.3	138.0 +/-51.7	154.6 +/-29.9	0.051	0.046	0.556
Tissue Inhibitor of Metallo-proteinases 1	TIMP-1	ng/mL	10.1 +/- 1.3	9.5 +/-1.9	5.9 +/- 1.6	0.003	0.654	0.011
Matrix Metalloproteinase-9	MMP-9	ng/mL	20.8 +/- 5.9	11.0 +/- 4.1	6.7 +/- 1.7	0.014	0.037	0.075

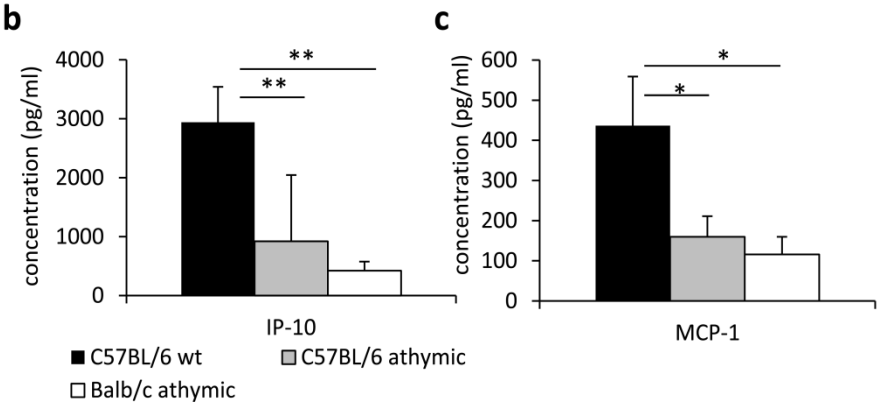

Figure 16: Identification of a proinflammatory signature in the GL261 tumor micromilieu of C57BL/6 wt mice. The mouse immune-related protein antigen profiling was performed by Myriad RBM. Mean values and standard deviation (n=5; C57BL/6 and Balb/c athymic and n=4 C57BL/6 wt) are listed in the table in **(a)**. Factors with significant differences between the mouse strains are shown. Differences between the mouse strains were analyzed using two-sided t-test with unequal variances *p<0.05 (yellow), **p<0.01 (green), ***p<0.001 (orange). Proinflammatory cytokines and chemoattractants are marked in light red; modulators of tissue homeostasis are marked in blue. IP-10 is shown exemplarily as proinflammatory cytokine **(b)** and MCP-1 **(c)** as chemoattractant.

4.2.2 Immune cell profiling of mice with subcutaneous GL261 tumors on day of injection

To see, whether major qualitative and/or quantitative differences in the immune cell populations of C57BL/6 wt, C57BL/6 athymic and Balb/c athymic mice with subcutaneous GL261 tumors at the day of injection exist, an immune cell profiling was performed. For this, single-cell suspensions of the tumors (n=3 mice per mouse strain) were prepared and FACS analysis was conducted.

As shown in Figure 17a, the majority of immune cells besides $CD3^+/CD4^+$ T-lymphocytes in the tumors of C57BL/6 wt mice that were significantly upregulated compared to the C57BL/6 and Balb/c athymic nude mice were immune cell subsets of the innate immune system. Such as $CD49^+$ NK cells, $CD11b^+/CD11c^+$ immature myeloid cells and cells of the monocyte/macrophage lineage ($CD45^+/CD11b^+$, $CD11b^+/MHCII^+$, $F4/80^+/MHCII^+$). This pattern underscores the result of the biomarker analysis shown in Figure 16a.

Analysis of single-cell suspensions of the blood in these mice (Figure 17b) showed that $CD3^+/CD4^+$ (17% +/-3%) and $CD3^+/CD8^+$ T-lymphocytes (17% +/-2%) were present exclusively in the wild-type mice. In addition, significantly more $CD19^+$ B-lymphocytes, $CD49^+$ NK cells, $CD11b^+/Ly6c^+$ DCs, $CD11b^+/CD11c^+$ immature myeloid cells and $CD11b^+/Gr1^+$ MDSCs were detected in the C57BL/6 athymic nude mice compared to the Balb/c athymic nude mice. The differences in the percentages were at least the double amount in the C57BL/6 athymic nude mice compared to both C57BL/6 wt and Balb/c athymic nude mice. In case of $CD49^+$ NK cells and $CD11b^+/CD11c^+$ immature myeloid cells the differences were also significant between C57BL/6 wt and C57BL/6 athymic nude mice.

Immune cell profiling of the spleens of the same mice (Figure 17c) revealed for T-lymphocytes the same findings as in the blood. In addition, a significant higher proportion of $CD49^+$ NK cells and $CD11b^+/CD11c^+$ immature myeloid cells was detected in C57BL/6 athymic nude mice compared to the Balb/c athymic nude mice.

The proportion of immature myeloid cells was in addition significantly higher in comparison to C57BL/6 wt mice. A higher number of $CD11b^+/Ly6G^+$ neutrophils were detected in Balb/c athymic nude mice compared to both C57BL/6 strains.

In summary, these results confirmed the biomarker profiling data and highlighted major differences due to the different immunological status of the mouse models.

	a tumor	Marker	C57BL/6 wt	C57BL/6 athymic	Balb/c athymic	C57BL/6 wt : C57BL/6 athymic	C57BL/6 wt : Balb/c athymic	C57BL/6 athymic : Balb/c athymic
adaptive	Lymphocytes	$CD3^+/CD4^+$	2.4 +/- 0.7	< 1	< 1	0.030	0.039	-
		$CD3^+/CD8^+$	< 1	< 1	< 1	-	-	-
		$CD19^+$	2.4 +/- 2.0	1.1 +/- 0.1	2.5 +/- 0.7	0.26	0.71	0.05
innate	NK cells	$CD49b^+$	5.5 +/- 0.3	1.9 +/-0.0	4.1 +/- 0.6	0.001	0.04	0.01
	Dendritic cells	$CD11b^+/Ly6c^+$	5.7 +/- 1.7	1.9 +/- 0.8	< 1	0.16	0.080	0.09
	Immature myeloid cells	$CD11b^+/CD11c^+$	4.7 +/- 0.9	3.3 +/- 1.1	1.5 +/- 0.4	0.04	0.03	0.08
	MDSC	$CD11b^+/Gr1^+$	< 1	1.7 +/- 0.5	< 1	0.03	-	0.12
	Neutrophils	$CD11b^+/Ly6G^+$	< 1	< 1	< 1	-	-	-
	Monocytes/ Macrophages	$CD45^+/CD11b^+$	8.8 +/- 1.1	3.5 +/- 0.1	2.3 +/- 0.5	0.01	0.004	0.04
		$CD11b^+/MHCII^+$	6.78 +/- 0.0	1.9 +/- 0.4	<1	0.0002	0.0004	0.03
		$CD68^+/MHCII^+$	3.5 +/-2.0	1.6 +/-0.8	1.0 +/- 0.3	0.22	0.161	0.37
		$F4/80^+/MHCII^+$	2.5 +/- 0.5	< 1	< 1	0.02	0.01	-

b blood	Marker	C57BL/6 wt	C57BL/6 athymic	Balb/c athymic	C57BL/6 wt : C57BL/6 athymic	C57BL/6 wt : Balb/c athymic	C57BL/6 athymic : Balb/c athymic
Lymphocytes	CD3+/CD4+	16.9 +/-3.0	< 1	< 1	0.01	0.01	-
	CD3+/CD8+	16.9 +/-2.0	< 1	< 1	0.006	0.006	-
	CD19+	52.2 +/- 5.0	61.2 +/- 1.9	44.6 +/- 3.1	0.10	0.01	0.02
NK cells	CD49+	10.0 +/- 2.4	29.1 +/- 3.0	13.1 +/- 0.7	0.001	0.03	0.002
Dendritic cells	CD11b+/Ly6c+	10.2 +/- 4.5	15.4 +/- 1.7	8.7 +/- 2.3	0.05	0.68	0.02
Immature myeloid cells	CD11b+/CD11c+	5.6 +/-1.1	19.3 +/-2.2	4.6 +/- 0.8	0.002	0.29	0.003
MDSC	CD11b+/Gr1+	5.5 +/-3.6	12.7 +/-2.1	6.4 +/-2.4	0.05	0.72	0.03
Neutrophils	CD11b+/Ly6G+	6.2 +/- 3.6	13.0 +/- 1.8	8.2 +/- 2.9	0.07	0.51	0.08
Monocytes/ Macrophages	CD11b+/MHCII+	4.2 +/- 1.3	5.6 +/- 1.6	7.0 +/-0.8	0.29	0.06	0.28
	F4/80+/MHCII+	1.0 +/- 0.2	1.5 +/- 0.3	3.3 +/- 0.2	0.04	0.002	0.004

c spleen	Marker	C57BL/6 wt	C57BL/6 athymic	Balb/c athymic	C57BL/6 athymic : Balb/c athymic	C57BL/6 wt : C57BL/6 athymic	C57BL/6 wt : Balb/c athymic
Lymphocytes	CD3+/CD4+	15.0 +/-1.0	< 1	< 1	0,19	0,001	-
	CD3+/CD8+	16.6 +/- 4.0	< 1	< 1	0,25	0,02	-
	CD19+	56.1 +/- 4.0	70.8 +/- 1.7	76.3 +/- 4.6	0,16	0,01	0,005
NK cells	CD49+	4.0 +/- 3.2	7.4 +/- 0.1	4.4 +/- 3.2	0,007	0,46	0,85
Dendritic cells	CD11b+/Ly6c+	6.8 +/- 1.7	5.1 +/- 0.7	4.8 +/- 0.5	0,64	0,22	0,17
Immature myeloid cells	CD11b+/CD11c+	4.7 +/- 0.9	7.9 +/- 0.9	3.4 +/- 0.6	0,004	0,010	0,09
MDSC	CD11b+/Gr1+	1.9 +/-0.7	3.2 +/- 0.6	3.0 +/- 1.1	0,76	0,06	0,22
Neutrophils	CD11b+/Ly6G+	2.0 +/- 0.3	2.0 +/-0.1	7.0 +/- 2.4	0,03	0,94	0,03
Monocytes/ Macrophages	CD11b+/MHCII+	6.9 +/-5.6	3.7 +/- 0.5	4.0 +/- 0.7	0,53	0,43	0,48
	F4/80+/MHCII+	3.1 +/- 1.5	5.2 +/- 0.6	6.9 +/- 0.1	0,03	0,11	0,40

* ** ***

Figure 17: Immune cell profiling and comparison of single-cell suspensions isolated from subcutaneous GL261 tumors (a), blood (b) and spleen (c) of C57BL/6 wt, C57BL/6 athymic and Balb/c athymic mice on d0. Shown are mean and standard deviation of 3 mice per group in percentages (%). Differences in marker expression between mouse strains were analyzed using two-sided t-test with unequal variances *p<0.05 (yellow), **p<0.01 (green), ***p<0.001 (orange). Highlighted in red is the mouse strain showing the highest percentage of a particular marker combination. Double stainings were performed to avoid false positive results. 10,000 events/sample and staining were measured by FACS analysis. Percentages below 1% are described as <1.

4.2.3 Identification of a diverse MHCII expression pattern in subcutaneous GL261 tumors on day of injection

An immunohistochemical analysis of subcutaneous GL261 tumor sections showed major differences in the expression of MHCII.

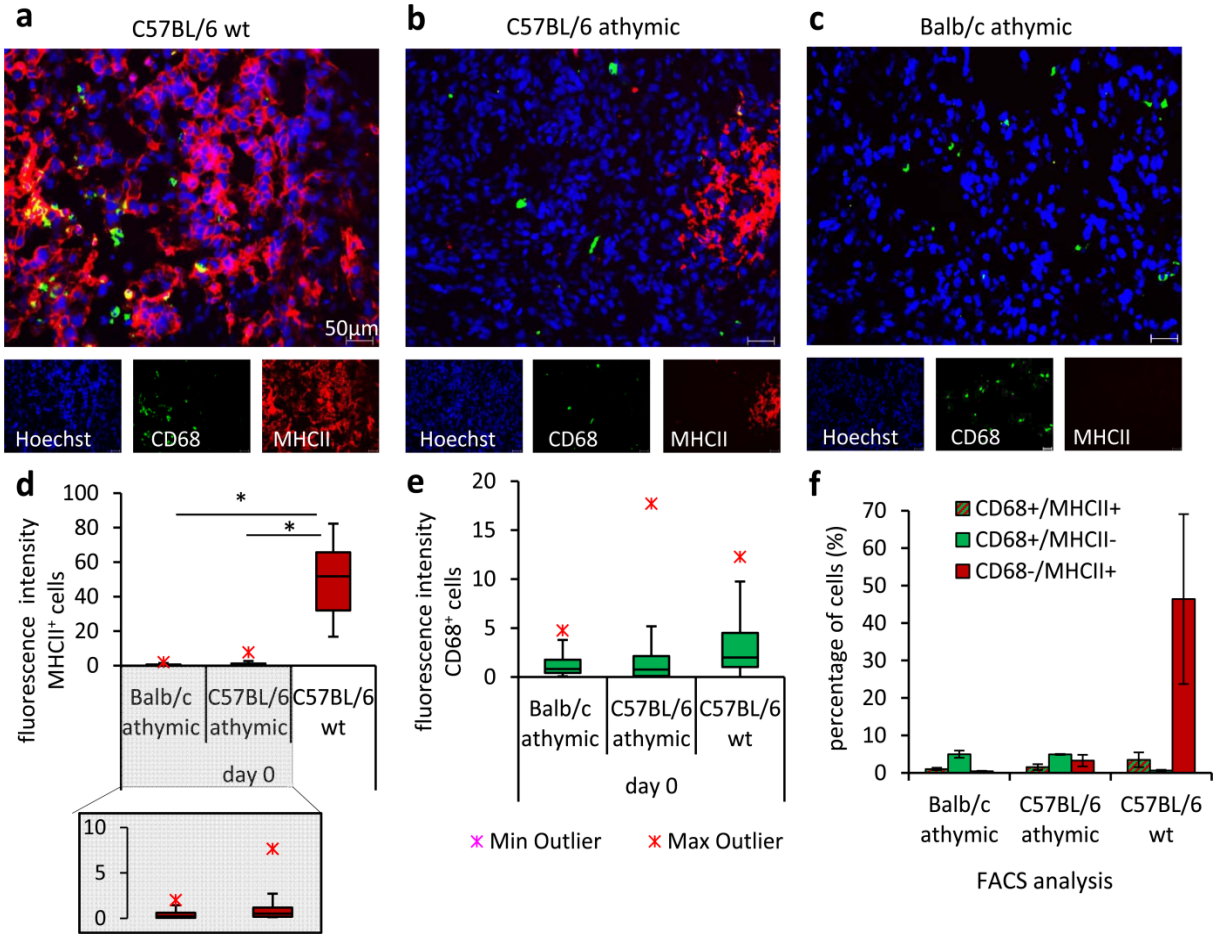

Figure 18: Qualitative and quantitative analyses of MHCII and CD68 marker gene expression in subcutaneous GL261 tumors of C57BL/6 wt, C57BL/6 athymic and Balb/c athymic mice on d0. Cryosections (10 µm) of subcutaneous GL261 tumors of C57BL/6 wt **(a)** C57BL/6 athymic **(b)** and Balb/c athymic mice **(c)** on d0 were stained with antibodies against CD68 (green) and MHCII (red). Hoechst 3342 was used to stain cell nuclei (blue). The depicted images are representative examples. Magnification 20x, scale bar 50 µm. The experiment was performed twice. The fluorescence intensities of MHCII **(d)** and CD68 **(e)** labelled subcutaneous tumor sections (tumor rim and tumor center) were determined in 10 images per tumor (n=3 mice/group) using ImageJ. Depicted are box and whisker charts calculated with a vertex42 template. Percentages of CD68 and MHCII double or single positive cells **(f)** were determined by FACS analysis of single-cell suspensions of subcutaneous GL261 tumors on d0 (n=3 mice per group). The bar chart shows mean and standard deviation. Differences in marker expression between mouse strains were analyzed using two-sided t-test with unequal variances *p<0.05.

MHCII expression was most pronounced and homogenously distributed throughout the tumor center and the tumor rim in subcutaneous tumors of C57BL/6 wt mice (Figure 18a). A patchy

distribution of MHCII positive cells was detected in tumors of C57BL/6 athymic mice (Figure 18b). In Balb/c athymic mice MHCII expression was hardly detectable (Figure 18c).

Interestingly, the expression of MHCII did not colocalize with CD68 an immune cell marker that typically is used to identify monocytes and macrophages (Figure 18a, b)[229].

Further, the morphology of the $MHCII^+/CD68^-$ cells was distinct from immune cell populations and resembled that of the GL261 glioma cells. This finding implicated the existence of a $MHCII^+$ non-macrophage population.

The quantitative evaluation of MHCII expression revealed a significant upregulation of MHCII in C57BL/6 wt mice compared to both athymic mouse strains (Figure 18d). The upregulation of MHCII in C57BL/6 athymic mice compared to Balb/c athymic mice was not significant. Additionally, amounts of $CD68^+$ immune cells were not significantly different in the three mouse strains (Figure 18e).

For further quantification and to ensure the results, FACS analysis was performed with the same marker combinations. The study revealed 46% +/- 23% $MHCII^+/CD68^-$ cells in C57BL/6 wt tumors, 3% +/- 2% $MHCII^+/CD68^-$ cells in tumors of C57BL/6 athymic mice and in Balb/c athymic mice the percentage of $MHCII^+/CD68^-$ cells was below the detection limit of 1% (Figure 18f).

4.2.4 Analysis of the influence of VACV infection on the microenvironment of subcutaneous GL261 tumors 1 dpi

In the next set of experiments it was analyzed, whether LIVP 1.1.1 does influence the specific MHCII and CD68 expression patterns observed on the day of injection in the three mouse models. For this, immunohistochemical analysis of GL261 subcutaneous tumors was performed. Determination of the fluorescence intensity of MHCII within the tumor sections revealed that intratumoral LIVP 1.1.1 administration had no impact on MHCII expression 1 dpi. There was no difference between the pattern seen on day 0 and 1 dpi in the different mouse models with no difference between the LIVP 1.1.1- and PBS-treated tumors (Figure 19a, b).

Analysis of CD68 marker gene expression 1 dpi showed no quantitative difference between LIVP 1.1.1- and PBS-injected tumors in none of the analyzed tumor models (Figure 19a, c). More CD68 positive cells were detected in the tumor rim than in the tumor center in all models and conditions, implicating that these are $CD68^+$-macrophages recruited to the tumor site (Figure 19c).

This immunohistochemical finding was supported by MRI 1H/19F *in vivo* images 3 dpi showing a weak 19F signal mainly at the tumor rim but not in the tumor center with no optical difference between LIVP 1.1.1- and PBS-treated groups and between C57BL/6 wt or Balb/c athymic mice

(Figure 19d, e). The colocalization of the 19F signal and CD68^{+} macrophages which demonstrates inflammatory processes was shown in detail by Weibel *et al.* [225].

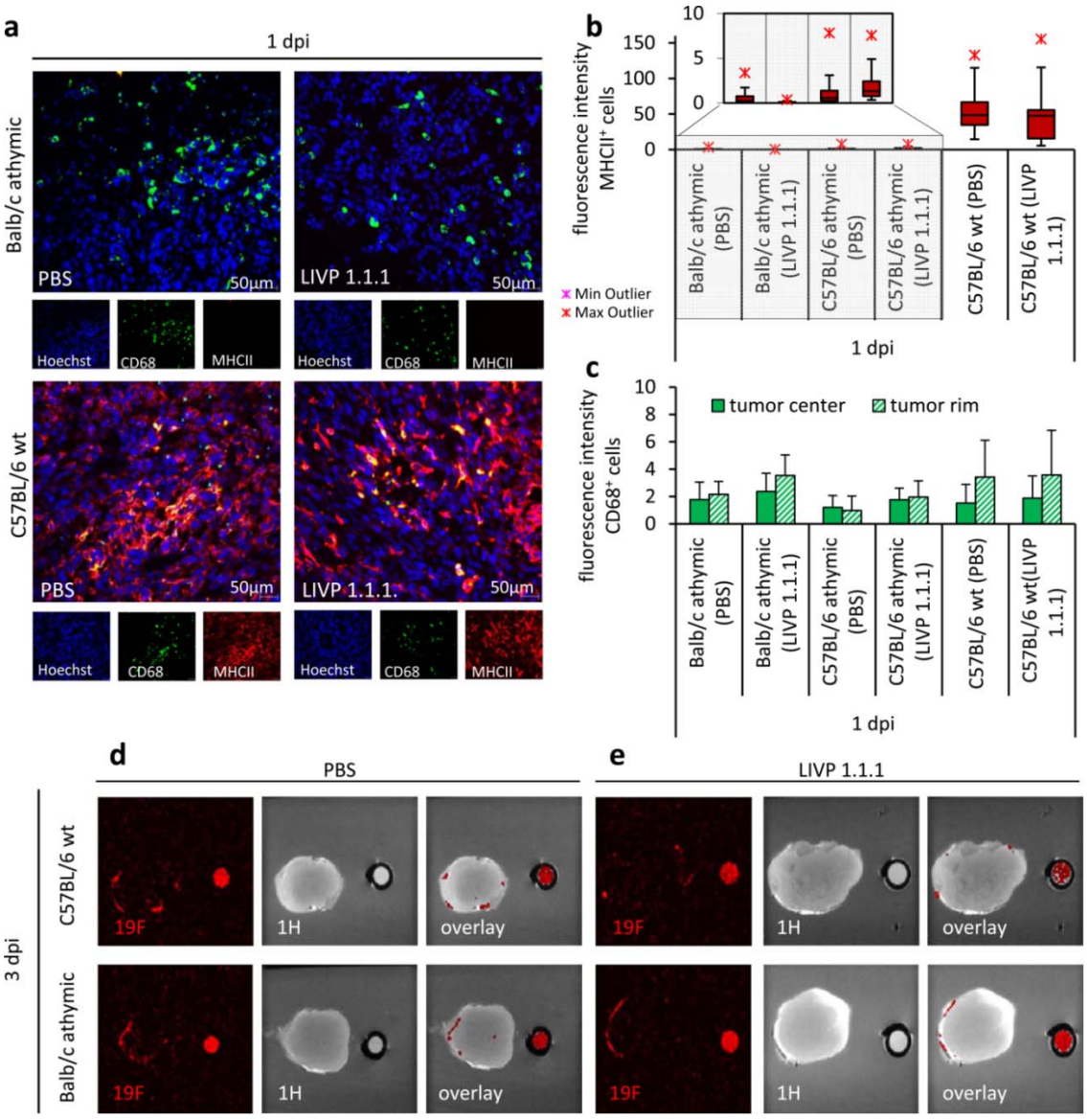

Figure 19: **VACV infection did not influence MHCII expression on non-monocytic cells.** Cryosections (10 µm) of subcutaneous GL261 tumors of Balb/c athymic, C57BL/6 athymic and C57BL/6 wt mice treated with LIVP 1.1.1 or PBS 1 dpi were stained with antibodies against CD68 (green) and MHCII (red). Hoechst 3342 was used to stain cell nuclei (blue). The depicted images are representative examples for stainings of Balb/c athymic and C57BL/6 wt mice (**a;** magnification 20x, scale bar 50 µm). The experiment was performed twice. The fluorescence intensity of MHCII **(b)** and CD68 **(c)** labelled tumor sections (tumor rim and tumor center) was determined in 10 images per tumor (n=3 mice/group) using ImageJ. Depicted are box and whisker charts calculated with a vertex42 template **(b)** and a bar chart with mean and standard deviation **(c)**. Representative 19F, 1H, and overlay 1H/19F *ex vivo* images of tumors of C57BL/6 wt or Balb/c athymic mice injected with PBS **(d)** or LIVP 1.1.1 **(e)** are depicted. Emulsified PFC was administered intravenously at the day of injection (LIVP 1.1.1 or PBS) into C57BL/6 wt or Balb/c athymic mice with subcutaneous GL261 tumors. 19F MRI measurement was performed by T. Basse-Lüssebrink and S. Weibel 3 days post infection. 19F signal was visible exclusively at the tumor rim.

4.2.5 Analysis of the influence of VACV infection on various immune cell populations at end stage disease

As described in 4.1.2 all three mouse strains showed a very fast and aggressive tumor growth and in addition, all tumor models were characterized by prominent edema formation at end stage disease.

a

mouse strain	PBS (µl)	LIVP 1.1.1 (µl)
Balb/c athymic	833 +/- 503	833 +/- 493
C57BL/6 wt	950 +/- 926	216 +/- 160
C57BL/6 athymic	1133 +/- 115	966 +/- 251

b

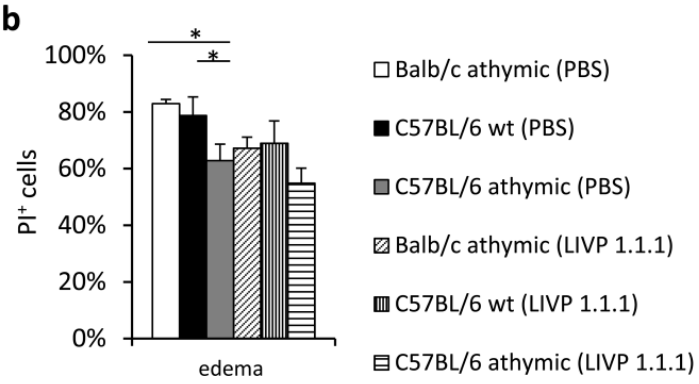

Figure 20: Analysis of edema fluid of tumor-bearing C57BL/6 wt, C57BL/6 athymic and Balb/c athymic mice at end stage disease. After mice were sacrificed, edema fluid was collected from end stage tumors and the amount was determined. Listed in **(a)** are the mean values and standard deviation (n=3). A single-cell suspension of the edema fluid was prepared and cells were stained with propidium iodide (PI) to detect dead cells **(b)**. Cells were analyzed by FACS analysis (10,000 events/sample) and mean values and standard deviation are shown (n=3). Two-sided t-test with unequal variances *p<0.05 was used.

For analysis of immune cell populations at end stage disease, edema fluid was analyzed separately in addition to the tumor. The amounts of edema fluid are listed in Figure 20a ranging from 216 µl +/- 160 µl in LIVP 1.1.1-treated C57BL/6 wt mice to 1133 µl +/-115 µl in PBS-treated C57BL/6 athymic mice. No significant difference in the amount of edema fluid was detectable between PBS- and LIVP 1.1.1-treated groups in none of the analyzed mouse models. FACS analysis revealed that, ~60-80% of isolated cells were PI^+-dead cells (Figure 20b) in the edema fluid. Most of these cells were immune cells (Figure 21). Significant more PI^+ cells were detected in Balb/c athymic mice compared to C57BL/6 athymic mice treated with PBS and the same was found for C57BL/6 wt mice compared to C57BL/6 athymic mice treated with PBS.

FACS analysis of tumors and edema fluid at end stage disease revealed that more than the double amount of $Ly6G^+$ neutrophils could be detected in the edema fluid compared to the tumor in all three mouse models at both treatment conditions - PBS and LIVP 1.1.1 (Figure 21a). Highest percentage of neutrophils was detectable in Balb/c athymic mice injected with LIVP 1.1.1 in tumor and edema fluid compared to mice with C57BL/6 background. The difference was significant in the tumor. As the percentage of $Ly6G^+$neutrophils was below the detection limit on the day of injection it can be concluded, that these cells were recruited to the tumor due to the increasing tumor volume and due to virus infection (higher percentage in LIVP 1.1.1-treated mice).

Similar to the results obtained for Ly6G more than the double amount of $CD45^+/CD11b^+$ cells (macrophages, granulocytes or MDSC) were detected in the edema fluid compared to the tumors of all three mouse models and both treatment conditions (Figure 21b). Significant more $CD45^+/CD11b^+$ cells were detectable in the edema fluid of C57BL/6 wt mice compared to Balb/c athymic mice, both treated with PBS. As shown in Figure 21b there was no significant difference in the tumors of the three mouse models and at both treatment conditions. For mature macrophages, this result was confirmed with similar findings obtained by immunohistochemical analysis and measurement of the fluorescence intensity of CD68 an alternative marker expressed on this cell type (Figure 21e).

In case of $CD11c^+$ DCs the percentage of cells was below 10% in edema fluid and tumors with no difference between the treatment conditions and mouse models (Figure 21c).

$F4/80^+/MHCII^+$-activated macrophages were significantly upregulated in C57BL/6 wt mice compared to C57BL/6 and Balb/c athymic mice in edema fluid and tumors with no difference between PBS and LIVP 1.1.1 treatment (Figure 21d).

Similar to the findings obtained at the day of injection and 1 dpi, quantification of the fluorescence intensity of $MHCII^+$ cells at end stage disease in the different mouse models showed a significantly higher fluorescence intensity in C57BL/6 wt mice treated with PBS than in Balb/c athymic mice (Figure 21f). MHCII in C57BL/6 athymic mice treated with PBS was in an intermediate state between Balb/c athymic and C57BL/6 wt mice but without significant difference. The fluorescence intensity of MHCII in the LIVP 1.1.1-treated group was lower than in the PBS-treated groups. Significant differences could be detected between Balb/c athymic and C57BL/6 wt mice and between Balb/c athymic and C57BL/6 athymic mice.

In addition it is important to note, that the amounts of CD3/CD4 and CD3/CD8 positive T-lymphocytes representing the adaptive immune system were below the detection limit at end stage disease not only in athymic mice were it was expected but also in wild-type mice.

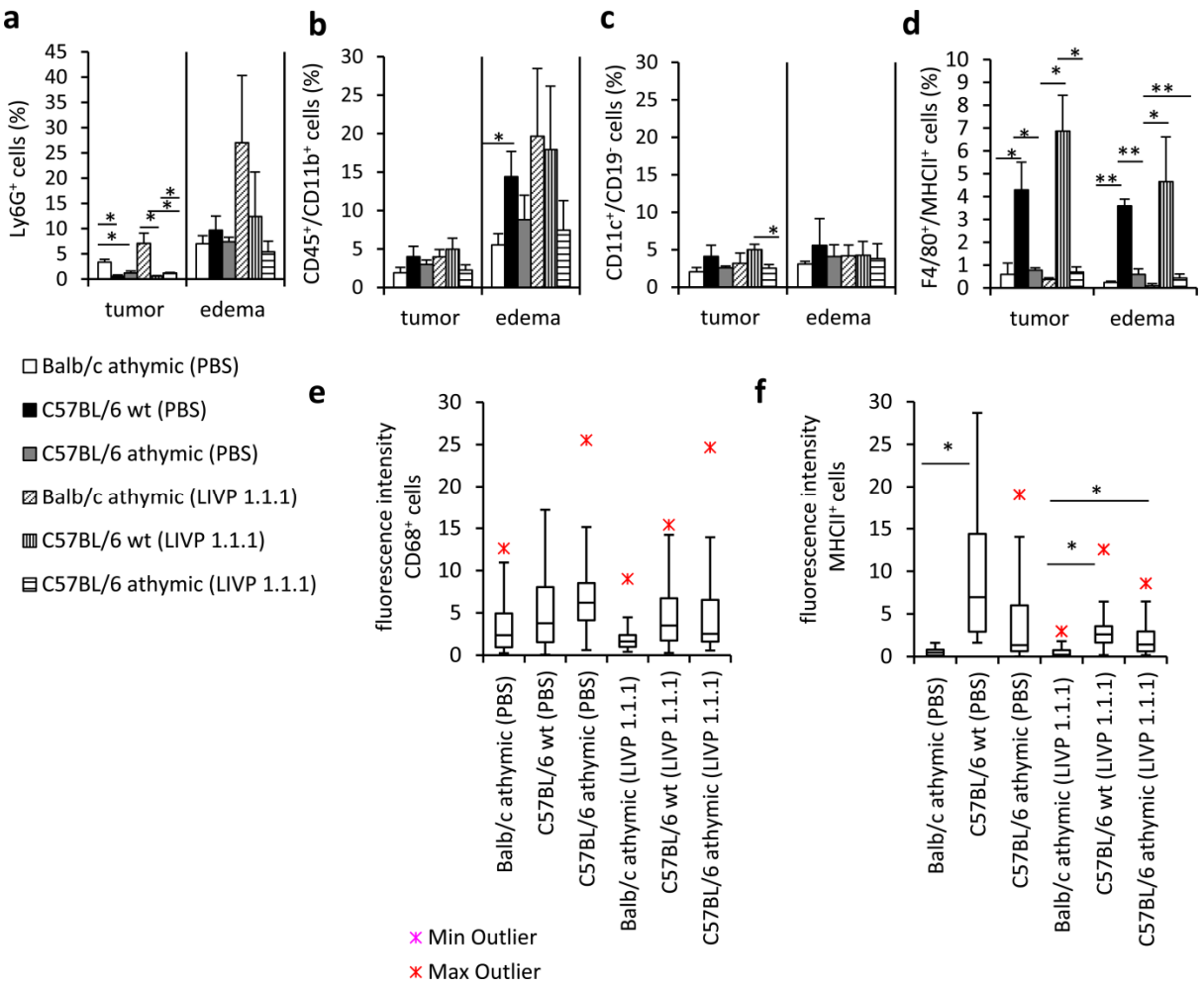

Figure 21: Immune cell profiling of end stage tumors and edema fluid in three mouse strains injected with LIVP 1.1.1 or PBS. Mice were sacrificed, edema fluid collected and tumors dissected. Single-cell suspensions were prepared and stained with fluorescence labeled antibody combinations against Ly6G **(a)**, CD45/CD11b **(b)**, CD11c/CD19 **(c)** and F4/80/MHCII **(d)**. Cells were analyzed by FACS analysis and mean values and standard deviation are shown (n=3). At end stage disease, the fluorescence intensity of CD68 **(e)** and MHCII **(f)** labelled tumor sections (tumor rim and tumor center) was determined using ImageJ (n=3 mice/group; 10 images per tumor). Depicted are box and whisker charts calculated with a vertex42 template. Differences in marker expression between mouse strains were analyzed using two-sided t-test with unequal variances *p<0.05, **p<0.01.

4.3 Approaches to modify the subcutaneous GL261 tumor microenvironment to improve oncolytic efficacy of LIVP 1.1.1 in C57BL/6 wt mice

After the detailed characterization of the subcutaneous GL261 tumor model in different mouse strains, it was elucidated whether therapeutic efficiency in the "non-responder" C57BL/6 wt mice could be improved. Based on differences detected in the biomarker- and immune cell profiling on day of injection between "responder" and "non-responder models" three different approaches were tested to improve the replication efficacy in non-responder C57BL/6 wt mice: Depletion of macrophages within the tumor microenvironment by clodronate liposomes (4.3.1), downregulation of the marker protein MHCII on cells within the tumor (4.3.3) and depletion of IFN-γ (4.3.4).

4.3.1 Phagocytic macrophages are not responsible for viral clearance in C57BL/6 wt mice

The biomarker profiling revealed a proinflammatory signature in C57BL/6 wt mice that was mainly produced by macrophages (Figure 16a). Furthermore, macrophages were recruited to subcutaneous GL261 tumors in C57BL/6 wt mice in comparison to athymic mice (Figure 17a).

To assess, whether macrophages were responsible for viral clearance in subcutaneous tumors of C57BL/6 wt mice the following experimental set-up was designed (Figure 22a): C57BL/6 wt mice were implanted subcutaneously with $5x10^6$ GL261 cells. At a tumor size between 200-300 mm^3, mice were injected intraperitoneal with 200 µl clodronate liposomes or PBS on three consecutive days. One day after the last clodronate/PBS injection, mice were injected intratumorally with LIVP 1.1.1 ($5x10^6$ pfu). The depletion efficiency was confirmed by FACS analysis with different marker combinations to identify monocytes/macrophages at 1 dpi (Figure 22b-e). In all marker combinations tested (CD11b/MHCII, CD11b/CD68, CD11b/Ly6c and CD11b/Gr1) a significant reduction in the clodronate treated group could be detected, althought the population was never below the detection limit. The percentage of monocytes/macrophages detected in subcutaneous GL261 tumors was 2-7%.

Standard viral plaque assay revealed that the virus titer at both treatment conditions (PBS or clodronate liposomes) did not differ significantly neither on day 1 nor on day 7 post infection (Figure 22f). There was a decrease of the virus titer from day 1 to day 7 and in both groups the virus titer was below the initial injection dose of $5x10^6$ pfu at both time points.

This experiment showed that macrophages could be excluded as factor responsible for the pronounced reduction of viral particles detected 1 dpi in this mouse strain and tumor model.

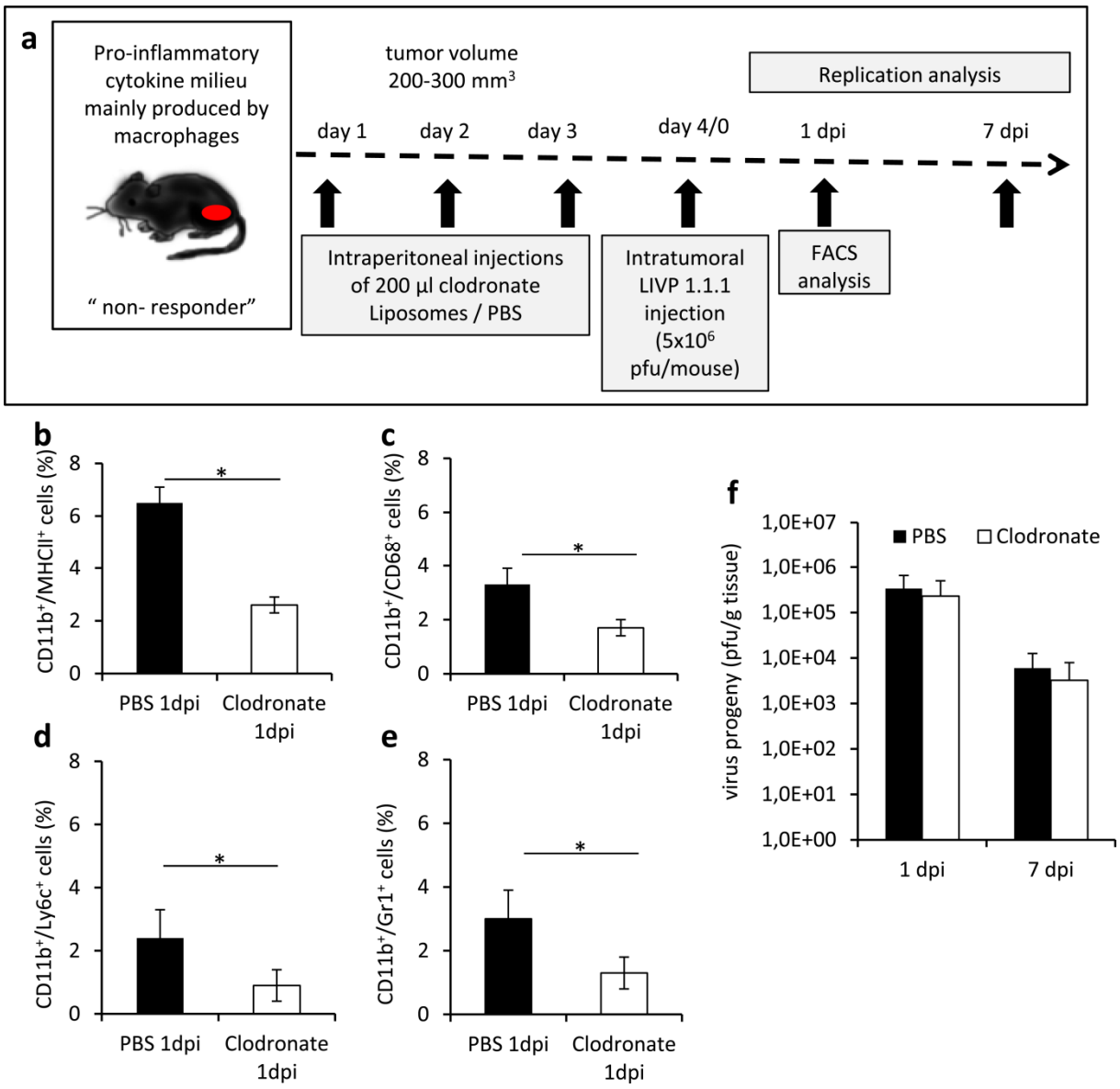

Figure 22: Macrophage depletion did not show an effect on virus replication in C57BL/6 wt mice with subcutaneous GL261 tumors. Schematic representation of the experimental set-up including time frame and applied methods **(a)**. C57BL/6 wt mice with subcutaneous GL261 tumors were injected (i.p.) with 200 µl PBS or clodronate liposomes on 3 consecutive days before LIVP 1.1.1 injection (i.t). FACS analysis was performed 1 dpi to confirm the macrophage depletion. For this, cell suspensions were stained with fluorescence-labeled antibody combinations against CD11b/MHCII **(b)**, CD11b/CD68 **(c)**, CD11b/Ly6c (**d)** and CD11b/Gr1 **(e)**. Shown are mean and standard deviation of 3 mice per group. Viral titers were determined by standard viral plaque assay 1 and 7 dpi **(f)**. Each time point represents the mean of at least 3 mice. Significant differences in marker gene expression and viral titers were tested with two-sided t-test with unequal variances (*$p<0.05$).

4.3.2 Pretreatment of GL261 glioma cells with IFN-γ results in diminished viral replication and MHCII upregulation in cell culture

The biomarker profiling revealed factors such as IP-10, MCP-1 or MIP-1β which were differentially expressed with highest concentrations in C57BL/6 wt mice, followed by C57BL/6 athymic and Balb/c athymic mice (Figure 16). The same pattern was found for the expression levels of MHCII detected in the subcutaneous GL261 tumors of all three mouse models (Figure 18). IP-10, MCP-1 or MIP-1β are known to be induced and upregulated by IFN-γ, a proinflammatory cytokine with immunomodulatory functions [230, 231]. Further, it is reported that IFN-γ does upregulate MHCII not only on professional APCs for antigen-specific $CD4^+$ T-lymphocyte activation but also on non-professional APCs such as tumor/glioma cells that do not express MHCII constitutively [231–234]. Several reports have shown, that GL261 glioma cells itself that under normal conditions do not express MHCII can upregulate this molecule after stimulation or overexpression with IFN-γ [234, 235].

In the next set of experiments it was analyzed whether the observed phenotypic change of the GL261 tumor cells may have an impact on viral replication or virus-mediated toxicity. For this, GL261 cells in cell cultures were either stimulated with recombinant murine (rm)-IFN-γ (10 ng/ml) or with rm-IL-4 (10 ng/ml) which are cytokines for induction of M1/M2 phenotypes in macrophages [236].

In accordance with the literature, stimulation of GL261 cells with IFN-γ for 24 h resulted in an increased amount of $MHCII^+$ GL261 cells from 0% to 31% +/- 1% which increased further to 80% +/- 5% at 72 h post stimulation. Mock (w/o) or IL-4 stimulated cells did not show MHCII expression on their surface (Figure 23a). Further it could be shown, that the upregulation of MHCII on the surface of GL261 glioma cells was time-dependent as there was an increase over time from 24 h to 72 h and it was dose-dependent with an increasing percentage of MHCII positive cells from 30 ng/ml to 100 ng/ml (Figure 23b).

FACS analysis using PI as a marker for cell death revealed that IFN-γ stimulation at a concentration of 10 ng/ml had no effect on cell viability compared to GL261 cells (w/o) or stimulated with 10 ng/ml IL-4 at 24 and 72 h post stimulation (Figure 23c, d). 72 h post stimulation proliferation of IFN-γ stimulated cells was significantly reduced compared to cells w/o stimulation or IL-4 stimulated (Figure 23d).

Replication analysis of the differentially stimulated GL261 tumor cells revealed that cells pre-incubated with IFN-γ were infected with LIVP 1.1.1, but the virus titers was more than 100-fold lower than in cells pre-incubated with IL-4 or w/o stimulation (Figure 23e). The virus titers at 24-

72 hpi of IFN-γ pre-incubated cells remained below the virus inoculum, implicating that no viral replication occurred in these cells. No difference was detectable between cells w/o stimulation or incubated with IL-4.

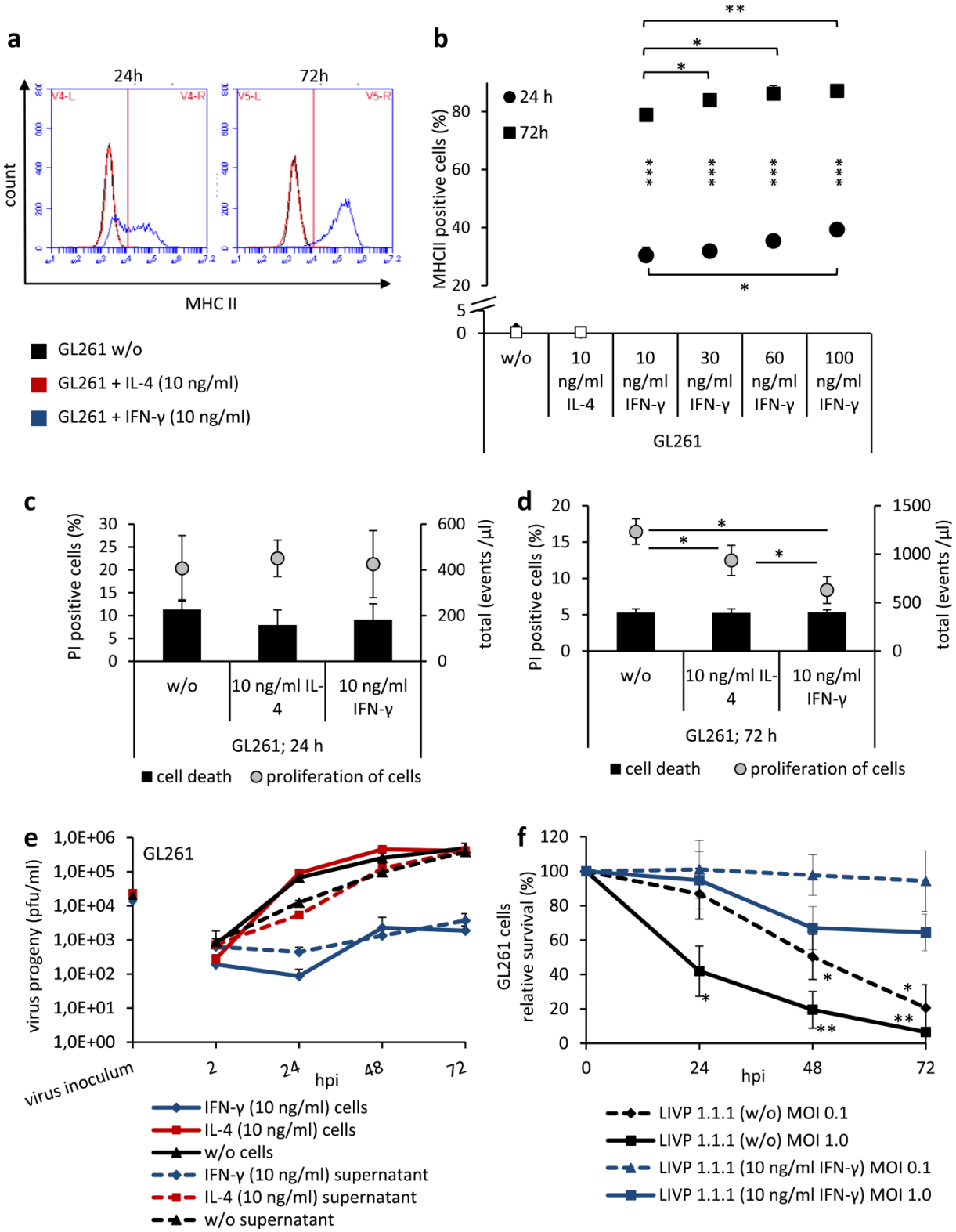

Figure 23: IFN-γ pretreatment upregulates MHCII, diminishes viral replication and reduces virus-mediated cytotoxicity in GL261 cells in cell culture. MHCII expression on GL261 cells w/o (without stimulation) or after stimulation with 10 ng/ml IL-4 or IFN-γ was analyzed by FACS analysis after 24 and 72

h **(a)**. MHCII expression on GL261 cells w/o or stimulated with 10 ng/ml IL-4 or 10, 30, 60, 100 ng/ml IFN-γ was measured by FACS analysis 24 and 72 h post stimulation **(b)**. Bar charts represent mean and standard deviation. Experiment was performed in triplicates and repeated in an independent experiment. Statistical significance was tested using two-sided t-test with unequal variances at each time point (24 and 72 h) between samples stimulated with 10 ng/ml IFN-γ and 30 ng/ml, 60 ng/ml or 100 ng IFN-γ, respectively, indicated by horizontal asterisk. In addition statistical significance was compared for each concentration between different time points, indicated by vertical asterisk. PI staining and thus measuring of cell death of GL261 cells w/o, or stimulated with 10 ng/ml IL-4 or IFN-γ for 24 h **(c)** and 72 h **(d)** was determined by FACS analysis. The bar charts represent the mean values and standard deviation of dead cells in percentage. Cell proliferation was determined by measuring the total events per µl. Cell debris was excluded from the measurement. GL261 cells w/o, or stimulated with 10 ng/ml IL-4 or 10 ng/ml IFN-γ for 24 h were infected with LIVP 1.1.1 at an MOI of 0.1 and viral titers were determined 2, 24, 48 and 72 hpi **(e)**. The chart shows the mean of triplicate samples and standard deviation. For MTT assay GL261 cells were infected with LIVP 1.1.1 (MOI 0.1 and 1.0) **(f)**. Experiment was repeated twice in triplicates. Statistical significance was tested using two-sided t-test with unequal variances between samples w/o stimulation or stimulated with 10 ng/ml IFN-γ (*p<0.05, **p<0.01, ***p<0.001).

Virus-mediated toxicity (MOI 1.0 and MOI 0.1) was significantly reduced in IFN-γ pre-incubated cells compared to cells without pre-incubation. In the unstimulated sample infected with an MOI of 0.1 only 20% +/- 14% of cells survived 72 hpi compared to 94% +/-18% in the IFN-γ pre-incubated samples (Figure 23f).

In summary, these results in cell culture revealed the capacity to up-regulate MHCII in the murine glioma cell line GL261 by INF-γ stimulation and highlighted an anti-viral state of the $MHCII^+$ GL261 tumor cells.

4.3.3 Analysis of the effect of Simvastatin on IFN-γ stimulated GL261 cells in cell culture and *in vivo*

Simvastatin (SV) is a lipid lowering agent belonging to the group of statins functioning as 3-hydroxy-3-methylglutaryl-coenzyme A (HMG-CoA) reductase inhibitor and is in the first instance used for treatment of dyslipidemia or the prevention of cardiovascular diseases. However, it also has immunosuppressive and immunomodulatory effects [237, 238]. SV is described to repress IFN-γ induced MHCII expression on target cells and thus T-lymphocyte activation [237, 238]. The effect could be shown on various cell types including astrocytes, the cell type of origin of GL261 glioma cells [237–239]. SV interacts and inhibits promotor IV of the MHCII transactivator CIITA which is responsible for the IFN-γ induced upregulation of MHCII and thus does not interact with the consecutive MHCII expression [237].

In cell culture, it could be shown that co-stimulation of GL261 glioma cells with 10 ng/ml IFN-γ and 4 or 6 µM SV for 72 h significantly reduced the percentage of MHCII-positive GL261 cells

compared to GL261 cells cultured with 10 ng/ml IFN-γ alone from 47% +/- 6% to 30% +/- 2% and 27% +/-2% (Figure 24a). The effect was dose-dependent.

PI staining of the cells as a parameter of cell viability revealed a toxic effect of SV in a dose-dependent manner. Co-stimulation of cells with 10 ng/ml IFN-γ and 4 or 6 µM Simvastatin for 72 h resulted in 18% +/- 1% or 32% +/- 12% of dead cells compared to 4% +/- 4% when cultured with IFN-γ alone (Figure 24b).

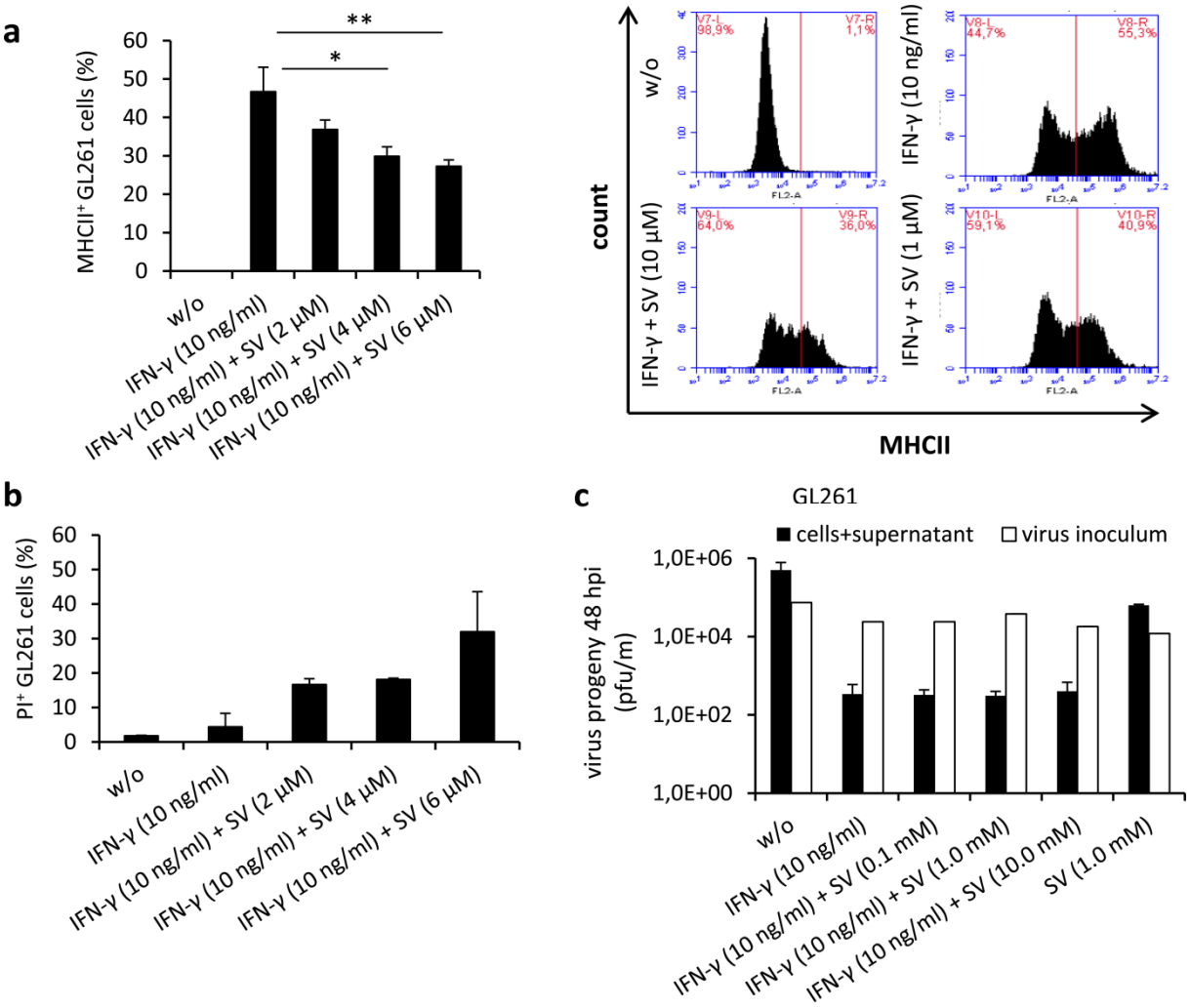

Figure 24: Simvastatin cannot restore IFN-γ induced reduction of viral replication in cell culture. MHCII expression **(a)** and PI-staining **(b)** of GL261 cells (w/o) stimulation or after stimulation with 10 ng/ml IFN-γ or after co-stimulation with 10 ng/ml IFN-γ and 2, 4 or 6 µM Simvastatin (SV) were analyzed by FACS analysis after 72 h. Bar charts represent mean and standard deviation. Images show representative analyses. Experiment was performed in triplicates and repeated in an independent experiment. GL261 cells stimulated for 72 h with IFN-γ (10 ng/ml), IFN-γ (10 ng/ml) + Simvastatin (2, 4, 6 µM), Simvastatin (6 µM) or (w/o) stimulation as control were infected with LIVP 1.1.1 at an MOI of 0.1 and viral titers were determined 48 hpi **(c)**. The chart shows the mean of triplicate samples and standard deviation. Statistical significance was tested using two-sided t-test with unequal variances *p<0.05, **p<0.01.

Replication analysis showed that SV independent of the concentration could not reverse the IFN-γ induced reduction of virus replication. There was no difference in the viral titer between GL261 cells treated with IFN-γ alone or in a combination of IFN-γ and SV. In both conditions the virus titer in non-stimulated cells was about 3-log levels higher than in stimulated cells. Taken together, in cell culture inhibition or down-regulation of MHCII on the cell surface had no effect on virus replication (Figure 24c).

It was further tested, whether application of SV would have an effect on MHCII expression levels in GL261 tumors of C57BL/6 wt mice or on the amount of virus progeny within these tumors.

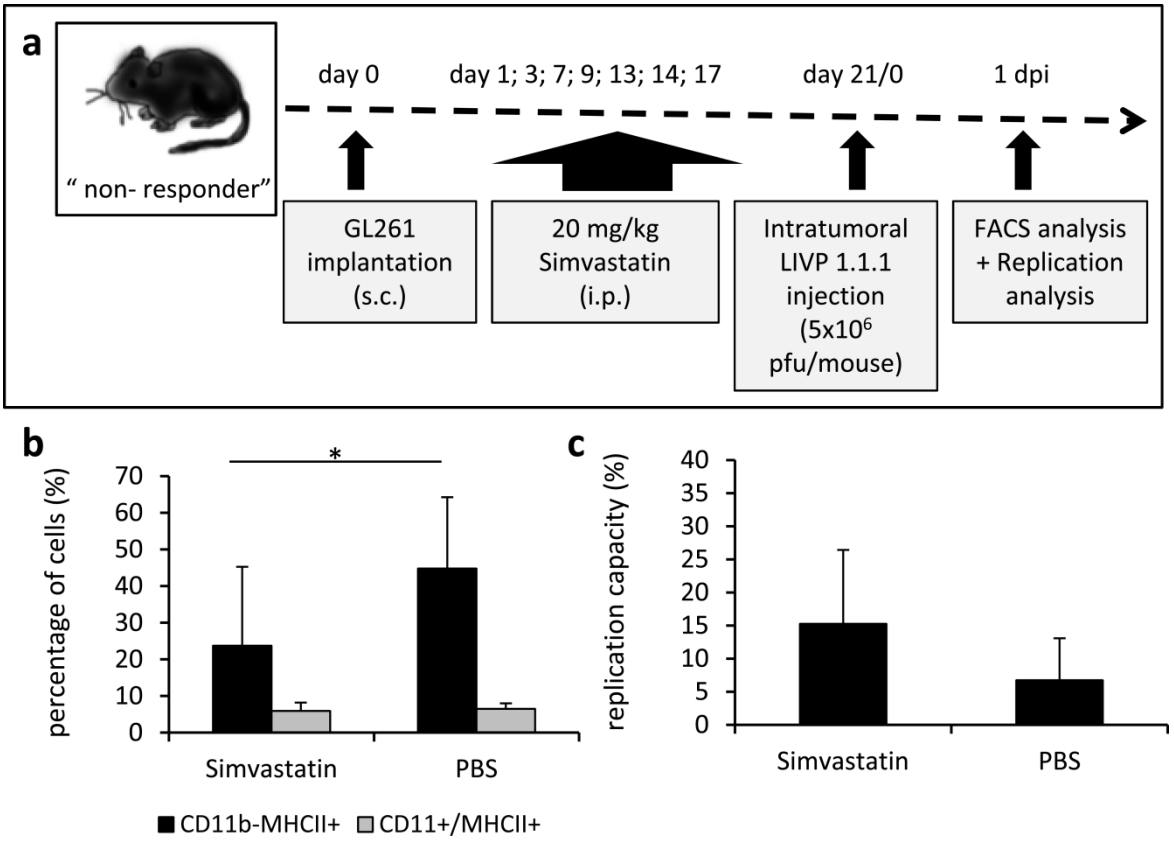

Figure 25: Simvastatin reduced MHCII expression in subcutaneous GL261 tumors in C57BL/6 wt mice, but the virus titer was not significantly increased. Schematic representation of the experimental design including time frame and applied methods **(a)**. C57BL/6 wt mice were implanted subcutaneously with $5x10^6$ GL261 cells and were injected (i.p.) with 100 µl PBS or Simvastatin (20 mg/kg) 1, 3, 7, 9, 13, 14, 17 dpimp. LIVP 1.1.1 ($5x10^6$ pfu) was injected (i.t) 21 dpimp. FACS and replication analysis was performed 1 dpi. For this, cell suspensions were stained with fluorescence-labeled antibody combinations against CD11b and MHCII **(b)**. Shown are mean and standard deviation of 4 mice per group. Viral titers were determined by standard viral plaque assay 1 dpi **(c)**. Statistical significance was tested using two-sided t-test with unequal variances *$p<0.05$.

To test whether SV treatment has an effect on viral replication in the subcutaneous GL261 tumor model in C57BL/6 wt mice, the following experimental approach was applied (Figure 25a): mice

were implanted subcutaneously with GL261 cells and 20 mg/kg SV was injected intraperitoneal 1, 3, 7, 9, 13, 14 and 17 days post implantation (dpimp). 21 dpimp LIVP 1.1.1 ($5x10^6$ pfu/mouse) was injected intratumorally and 1 dpi FACS and replication analysis were performed. As shown in Figure 25b, SV significantly reduced MHCII on $CD11b^-$ glioma cells to 24% +/- 21% in comparison to PBS-treated mice with 45% +/- 19% whereas no difference of $CD11b^+/MHCII^+$ immune cells (6% +/- 2% and 7% +/- 1%) was observed.

Replication analyses showed that the percentage of the initially injected virus dose at 1 dpi in the SV-treated group with 15% +/- 11% was slightly higher than in the PBS group with 7% +/- 6% but the difference was not significant (Figure 25c).

4.3.4 Endogenous IFN-γ levels were identified to upregulate MHCII on the surface of GL261 cells and to reduce viral replication in C57BL/6 wt mice

To affirm the finding that IFN-γ is responsible for the upregulation of MHCII on the surface of the tumor cells *in vivo* and the reduced viral replication in the C57BL/6 models, the MHCII expression and viral replication in subcutaneous GL261 tumors in C57BL/6 wt mice was compared with that of C57BL/6 IFN-γ knockout (KO) mice.

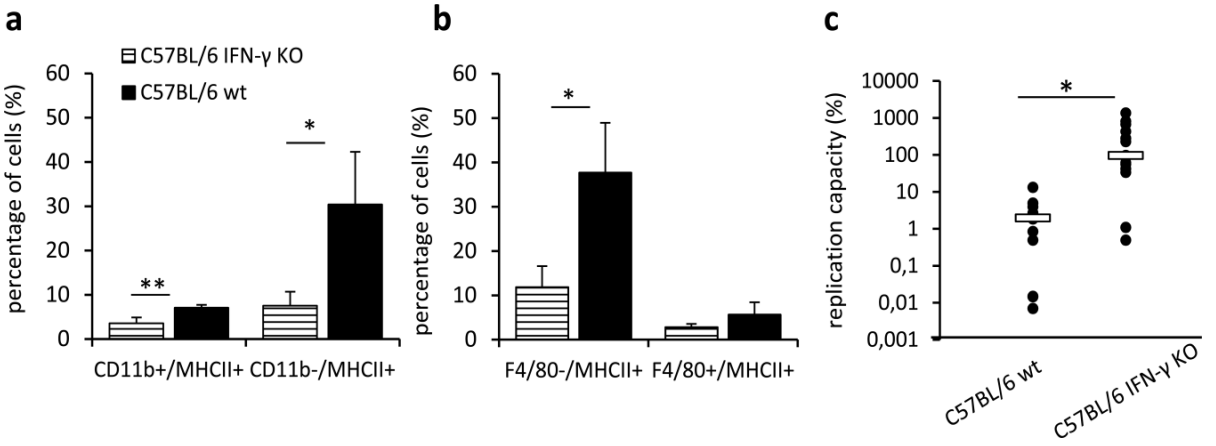

Figure 26: Impact of endogenous IFN-γ levels in C57BL/6 wt mice on viral infection. FACS analysis of single-cell suspensions isolated from subcutaneous GL261 tumors of C57BL/6 wt and C57BL/6 IFN-γ KO mice on d0 **(a, b)**. Shown are mean and standard deviation of 4 mice per group in percentages (%). Analysis was performed twice in independent experiments. Replication capacity (%) of subcutaneous GL261 tumors of C57BL/6 wt (n=14) and C57BL/6 IFN-γ KO mice (n=13) 1 dpi **(c)**. Viral titers were determined by standard viral plaque assay. The experiment was performed twice in two independent experiments. For the final calculations the experiments were taken together. Statistical power analysis of the experiment was performed. Differences between the mouse strains were tested using two-sided t-test with unequal variances (*$p<0.05$).

FACS analyses showed a significantly lower percentage of $CD11b^-/MHCII^+$ or $F4/80^-/MHCII^+$ -tumor cells in subcutaneous GL261 tumors of C57BL/6 IFN-γ KO mice compared to C57BL/6 wt

mice (Figure 26a, b). In addition, the replication capacity of LIVP 1.1.1 was significantly increased in C57BL/6 IFN-γ KO compared to the C57BL/6 wt mice (Figure 26c).

These findings confirmed the role of endogenous IFN-γ levels in C57BL/6 wt mice as candidate factor responsible for diminished VACV replication and as factor in charge for upregulation of MHCII on GL261 tumor cells in this particular mouse model.

4.3.5 IFN-γ induced antiviral state in GL261 cells is a reversible effect

As shown in 4.3.4, GL261 tumor cells which are initially in a $MHCII^-$ VACV-permissive status were modified or imprinted into a $MHCII^+$ VACV non-permissive status after implantation into C57BL/6 wt mice.

With the next experiments it was studied whether the modifications of the GL261 tumor cells in C57BL/6 wt mice were reversible or permanent effects.

For this, single-cell suspensions of subcutaneous GL261 tumors of C57BL/6 wt mice were prepared. As controls, GL261 tumors of Balb/c athymic mice were used since the status of those tumor cells was still $MHCII^-$-VACV-permissive (Figure 27a). By FACS analysis, it was shown that the number of $CD11b^-/MHCII^+$ tumor cells in the single-cell suspensions of tumor homogenates from C57BL/6 wt mice was reduced over time from day 0 to day 6 (Figure 27b, c).

By standard viral plaque assay of freshly isolated subcutaneous tumor homogenates from C57BL/6 wt mice that were cultivated *ex vivo* for 1 day and infected with LIVP 1.1.1 (MOI 0.1) it was shown that virus titers remained below the virus inoculum 24 hpi (Figure 27d). Tumor homogenates isolated from C57BL/6 wt mice or Balb/c athymic mice cultured for 6 days supported LIVP 1.1.1 (MOI 0.1) replication 24-72 hpi (Figure 27e) according to a loss of MHCII expression (Figure 27b, c).

In another experiment it was shown that tumor cells from both mouse strains cultivated *ex vivo* for 14 days, and being in a $MHCII^-$ status at this time point, upregulated MHCII on their cell surface with an increase from 24-72 h after stimulation with IFN-γ (Figure 27f).

These results demonstrated that imprinting of GL261 tumor cells by endogenous IFN-γ levels in C57BL/6 mice was not a permanent effect and tumor cells could be reset into the status before implantation after cultivation in cell cultures for an appropriate time period (Figure 27a).

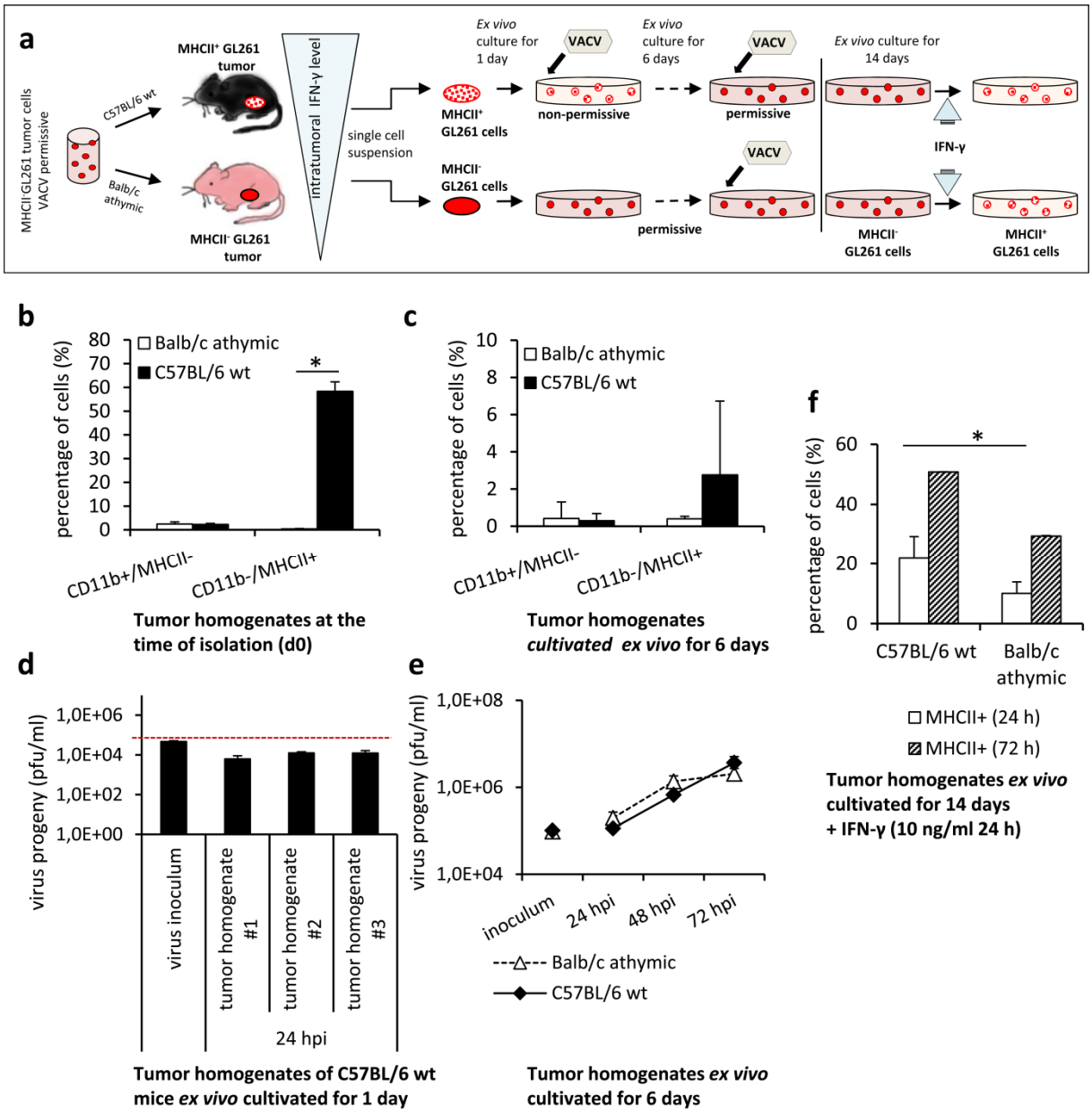

Figure 27: IFN-γ-induced antiviral state in GL261 glioma cells is a reversible effect. Schematic representation of the experimental set-up **(a)**. Single-cell suspension of s.c. GL261 tumors of C57BL/6 wt and Balb/c athymic mice were prepared and cells were cultured *ex vivo*. FACS analysis was performed on d0 **(b)** and after 6 days of *ex vivo* cultivation **(c)**. Shown are the mean values and standard deviation (n=3 mice) of the percentages of $CD11b^+/MHCII^+$ and $CD11b^-/MHCII^+$ immune and tumor cells. Tumor homogenates of s.c. GL261 xenografts isolated from C57BL/6 wt mice (n=3) were cultured in 24-well plates for 24 h and infected with LIVP 1.1.1 at an MOI of 0.1. Virus titers were analyzed by standard viral plaque assay **(d)**. Tumor homogenates of s.c. GL261 xenografts isolated from C57BL/6 wt or Balb/c athymic mice cultured *ex vivo* for 6 days (n=3) were infected with LIVP 1.1.1 (MOI 0.1) and analyzed by standard viral plaque assay in triplicate **(e)**. Shown are mean values and standard deviation. Tumor homogenates from C57BL/6 wt and Balb/c athymic mice were cultured *ex vivo* for 14 days and stimulated for 24 h with 10 ng/ml IFN-γ. Cells were analyzed by FACS analysis concerning MHCII expression 24 and 72 h post stimulation **(f)**. Shown are mean and standard deviation of 3 mice per group in percentages (%). Differences between the mouse strains were tested using two-sided t-test with unequal variances (*$p<0.05$).

4.3.6 MHCII expression – an indicator whether cancer cells are non-permissive for VACV infection

To test whether the upregulation of MHCII after stimulation of tumor cells with IFN-γ is a general glioma cell phenomenon four other human glioma cell lines (DBTRG-05MG, 42-MG-BA, U-138-MG and U87 MG) were analyzed in cell culture.

a

Cell line	tumor / cell type	origin	MHCII expression (%) w/o	MHCII expression (%) IFN-γ (10 ng/ml; 24 h)
DBTRG-05MG	glioblastoma	human	<1	<1
42-MG-BA	glioblastoma	human	<1	<1
U-138-MG	glioblastoma	human	<1	<1
U87	glioblastoma	human	<1	<1
GL261	glioma	murine (C57BL/6)	<1	31 +/- 1
IMA 2.1	astrocytes	murine (Balb/c)	<1	20 +/- 0.3
BV-2	microglia	murine (C57BL/6)	<1	26 +/- 0.6
J774	macrophages	murine (Balb/c)	<1	4 +/- 0.3

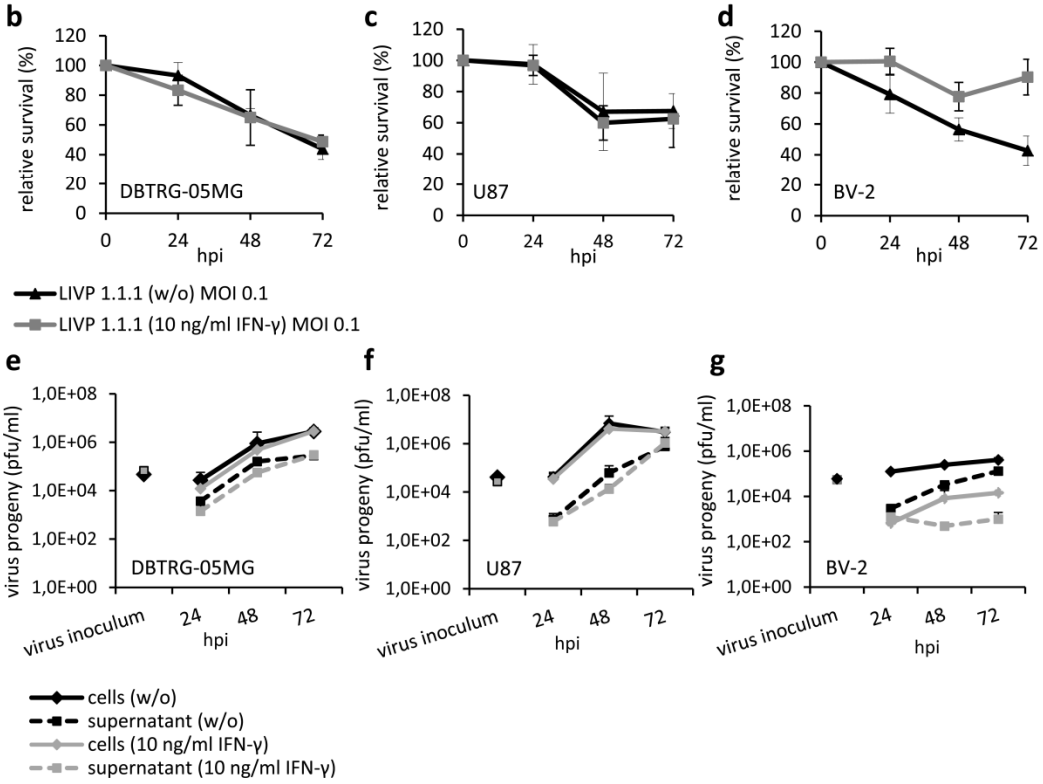

Figure 28: Upregulation of MHCII after stimulation with IFN-γ is a characteristic of immune cells, but also of GL261 tumor cells. Glioblastoma cells (DBTRG-05MG, 42-MG-BA, U87, GL261) and various immune/glia cells (IMA2.1, BV-2 and J774) were stimulated with 10 ng/ml IFN-γ for 24 h **(a)**. MHCII-expression was analyzed by FACS analysis after 24 h. MHCII expression levels below 1% are indicated as <1. Relative survival of DBTRG-05MG **(b)**, U87 **(c)** and BV-2 cells **(d)** w/o or stimulated with 10 ng/ml IFN-γ after infection with LIVP 1.1.1 (MOI 0.1, 1.0) were analyzed by MTT assay. Viral titers of DBTRG-05MG **(e)**, U87 **(f)** and BV-2 cells **(g)** were determined by standard viral plaque assay in triplicate. Cells were infected with LIVP 1.1.1 at an MOI of 0.1 and pre-incubated with 10 ng/ml IFN-γ or w/o for 24 h.

It was shown, that all four glioblastoma cell lines tested, did not upregulate MHCII after stimulation with recombinant human (rh)-IFN-γ (10 ng/ml; 24h; Figure 28a). Depicted here paradigmatically for two of them, non-stimulated DBTRG-05MG and U87 MG cells (w/o) and cells pre-incubated with IFN-γ did not show different responses to viral infection detected by MTT assay (Figure 28b, c) and standard viral plaque assay (Figure 28e, f). This suggests that DBTRG-05MG and U87 glioma cells in contrast to GL261 glioma cells were not responsive to IFN-γ and therefore the replication capacity of VACV is not affected in these cells.

In contrast, immune cells like BV-2 (murine microglia), IMA 2.1 (murine astrocytes) and J774 (murine macrophages) were able to upregulate MHCII after pre-incubation with IFN-γ (Figure 28a). In BV-2 cells virus-mediated cell death (Figure 28d) was reduced in the IFN-γ pre-incubated group and virus replication was impaired (Figure 28g). Macrophage/microglia-like behaviors of tumor cells are described in the context of gliomas and for other invasive glioma cell lines [240]. Furthermore, MHCII upregulation and expression could be seen as an indicator for cell lines not responsive to VACV infections.

4.4 Characterization of the tumor microenvironment of intracranial GL261 gliomas

In the next chapters the focus was set on the analysis of the tumor microenvironment of intracranial GL261 gliomas. In detail, the impact of two distinct cell populations besides the tumor cells, namely microglia/macrophages and astrocytes that are suspected to be involved in the clearing of viral particles in the early stages of antitumor therapy should be elucidated.

By different *in vitro* studies with various cell lines (4.5) and organotypic brain slice cultures (4.6) as well as *in vivo* findings (4.4.1 / 4.4.2) it was analyzed whether these glial cells are susceptible to VACV infection and whether VACV infection does affect the function of these cells.

Microglial cells are resident “macrophages” of the brain that react in the first instance to a whole range of pathologic stimuli such as virus infection and have important neuroprotective roles *e.g.* via phagocytosis of cellular debris after tissue injury [189, 241, 242]. Determined by the local environment microglia can exhibit either an acute inflammatory phenotype, referred to as classically activated or M1 microglia or a phenotype that mediates the humoral immune response, also called alternatively activated or M2 microglia [98, 243].

Astrocytes are the second cell type described to be recruited to the tumor site and involved in many aspects of brain functions and homeostasis *e.g.* the repair and scarring process following traumatic injuries [86, 104].

4.4.1 Orthotopic GL261 tumors showed pronounced upregulation of MHCII

As shown in Figure 13 viral replication was not supported in intracranial GL261 gliomas in C57BL/6 wt and Balb/c athymic mice. As both mouse models were "non-responders", most immunohistochemical analyses were performed only in C57BL/6 wt mice. In accordance with the findings within the subcutaneous GL261 tumor microenvironment in C57BL/6 wt mice, immunohistochemical analyses of orthotopic GL261 gliomas in these mice revealed that a large proportion of tumor cells expressed MHCII, 1 and 7 dpi in VACV- and PBS-injected tumors (red; Figure 29a-c). Tumor cells could be distinguished well from Iba-1-positive microglial cells (green). Taken together, this data implicated that expression of MHCII on GL261 tumor cells was not limited to subcutaneous tumors but also occurred in the orthotopic natural location of the tumor within the brains of these mice.

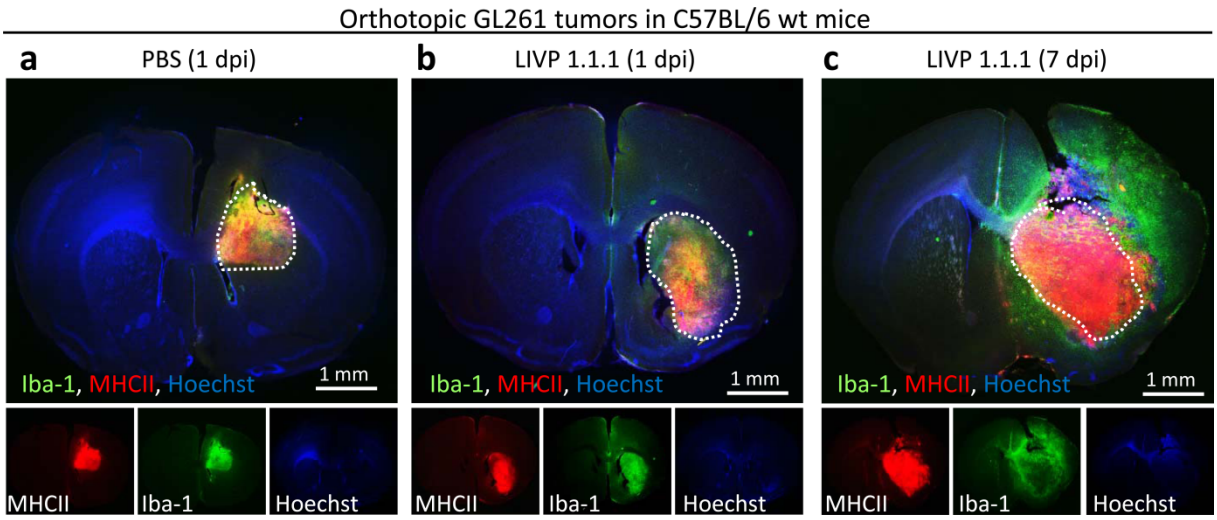

Figure 29: Detection of MHCII$^+$ tumor cells in orthotopic GL261 gliomas in C57BL/6 wt mice. Immunohistochemical staining and analysis of GL261 gliomas (white dotted line) in C57BL/6 wt mice injected intratumorally with PBS **(a)** or LIVP 1.1.1 (5x10^6 pfu) 1 dpi **(b)** or 7 dpi **(c)**. Sections were stained for MHCII (red), microglia (Iba-1$^+$, green) and cell nuclei (blue).

4.4.2 Recruitment of Iba1$^+$ microglia and GFAP$^+$ astrocytes to the tumor site is independent of LIVP 1.1.1 injection

As described in detail in 1.2.1, both microglia and astrocytes recruited and present in the glioma microenvironment have a crucial role in glioma growth and progression. In the next set of experiments, the recruitment of both immune cell types *i.e.* Iba-1$^+$ microglia and GFAP$^+$ astrocytes was analyzed in non-, mock- and LIVP 1.1.1-infected orthotopic GL261 gliomas in C57BL/6 wt mice.

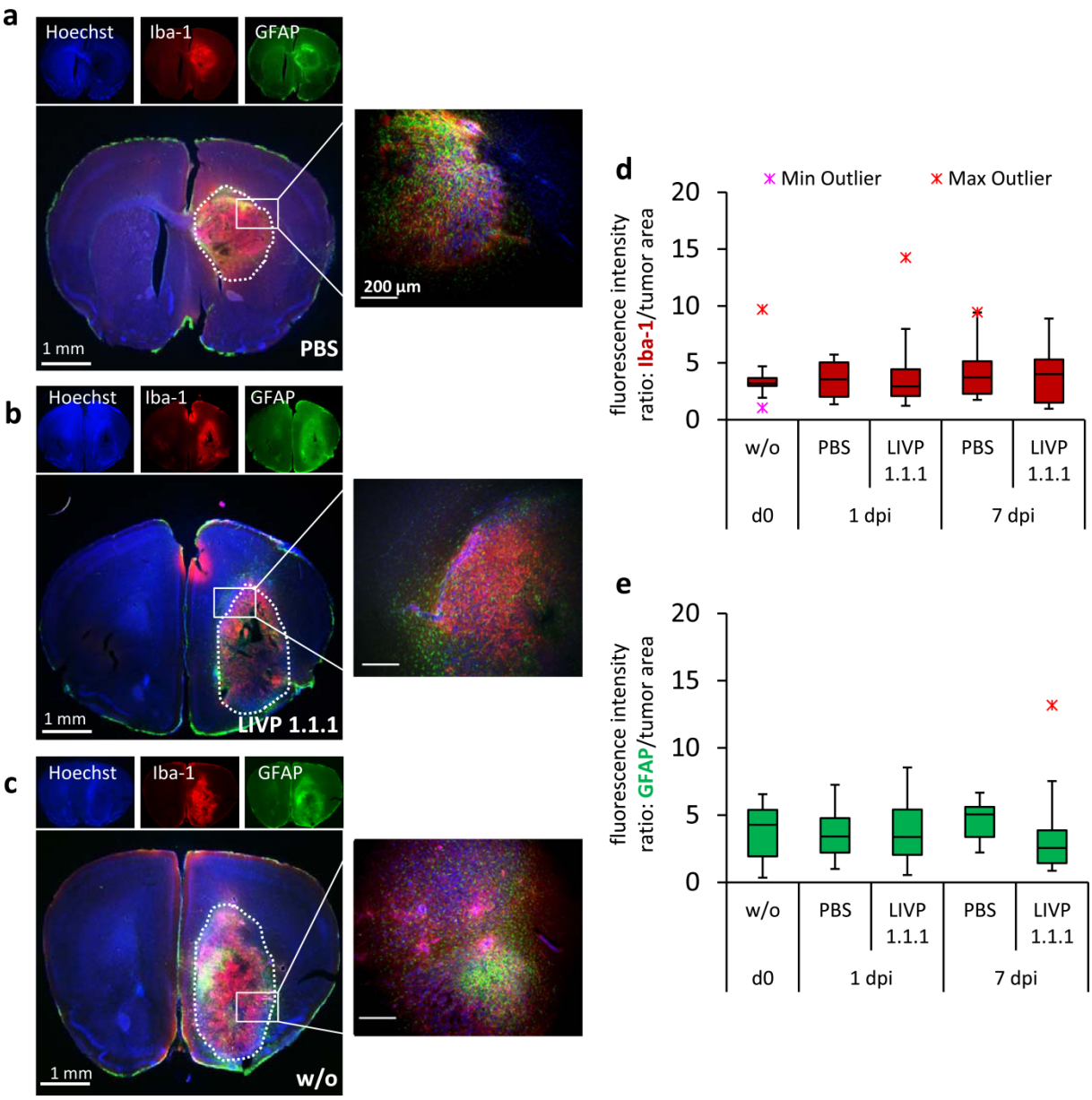

Figure 30: Intratumoral amounts and distribution of Iba1$^+$ microglia and GFAP$^+$ astrocytes in orthotopic GL261 gliomas in C57BL/6 wt mice is independent from intratumoral VACV injection. Immunohistochemical staining and analysis of GL261 gliomas in C57BL/6 wt mice injected intratumorally with PBS **(a)** or LIVP 1.1.1 (5x10^6 pfu) **(b)** or without injection (w/o) **(c)** at 1 dpi. Sections were stained for cell nuclei (Hoechst; blue), microglia (Iba-1$^+$, red) and astrocytes (GFAP$^+$, green). Quantitative analysis of microglia and astrocytes w/o injection and 1 and 7 days post PBS- or LIVP 1.1.1-injection (n=3; analyzed in duplicate). Fluorescence intensity and tumor area were measured with ImageJ and calculated as ratio: Iba-1$^+$ or GFAP$^+$/ tumor area (marked as white dotted line) **(d, e)**. For box plot diagrams a template from Vertex42 LLC has been used.

Immunohistochemical analysis of brain sections 1 dpi with PBS (Figure 30a) or LIVP 1.1.1 (Figure 30b) revealed a strong infiltration of the tumor with Iba-1$^+$ microglia and GFAP$^+$ astrocytes in both PBS- and LIVP 1.1.1-infected tumors. Surprisingly, tumors without injection showed a similar infiltration pattern (Figure 30c). Iba-1$^+$ microglial cells were distributed homogenously throughout the tumor (center and rim), whereas GFAP$^+$ astrocytes were located mainly at the

periphery of the tumors (Figure 30a-c). Quantitative analysis of glial cell infiltration during tumor growth revealed no difference in the amount of Iba-1^+ cells in untreated tumors compared to mock- or virus-injected tumors 1 and 7 days after infection (Figure 30d). Quantification of $GFAP^+$ astrocytes revealed almost the same pattern as seen for Iba-1 positive cells (Figure 30e). Taken together, these findings indicate that intratumoral amounts and distribution of $Iba1^+$ microglia and $GFAP^+$ astrocytes in GL261 gliomas is a consequence of the growing tumor [41, 96, 188, 189] and not of VACV-infection of the tumor.

4.5 Analysis of VACV-infections in murine GL261 glioma, microglial BV-2 and astrocytic IMA2.1 cells in cell culture

Next, it was analyzed whether there was a preferential uptake of viral particles into microglia and astrocytes that were identified to make up major proportion of the intracranial GL261 glioma mass (Figure 30). The experiments were performed in cell culture, using the following cell lines: the well-established microglia cell line BV-2, a frequently used substitute for primary microglia and for studies on astrocytes the cell line IMA2.1. BV-2 cells are primary murine microglial cells that were immortalized by stable transfection with v-raf/v-myc recombinant retrovirus displaying a phenotype functionally identical to native primary microglia [190, 191, 244].

IMA2.1 are immortalized murine cortical astrocytes that respond to certain stimuli similarly to primary astrocytes with upregulation of specific mRNA and expression of proteins [192].

To determine the replication capacity of LIVP 1.1.1 in cells of these cell lines, cells were infected at an MOI of 0.1 and 1.0 and standard viral plaque assay was performed.

The virus titer in BV-2 cells remained slightly below the initial infection dose, at all time points that were analyzed, except of the 48 hpi time point (Figure 31a).

In IMA2.1 cells, virus titer was far below the initial infection dose during the whole time course of the experiment (Figure 31b). No virus spreading was indicated by the complete lack of viral particles in the supernatant of infected IMA2.1 cells.

Data were compared with infection of GL261 glioma cells under the same culture conditions. As shown in Figure 31c, LIVP 1.1.1 efficiently replicated in GL261 tumor cells, determined by increasing cell-associated virus titers from 2 to 48 hpi and a plateau phase reached at 48 hpi at a virus dose of $2x10^6$ pfu/ml +/-$2x10^5$ pfu/ml. Already, 24 hpi virus titers were higher than the initial infection dose. Virus titers in the supernatant steadily increased over time, reaching a maximum at 96 hpi

Cell viability after LIVP 1.1.1-infection was examined by MTT assay at an MOI of 0.1 and 1.0. The assay showed that GL261 and BV-2 cells were lysed upon infection with LIVP 1.1.1 whereas IMA2.1 cells were intact with a slight decrease in the amount of living cells (Figure 31d-f).

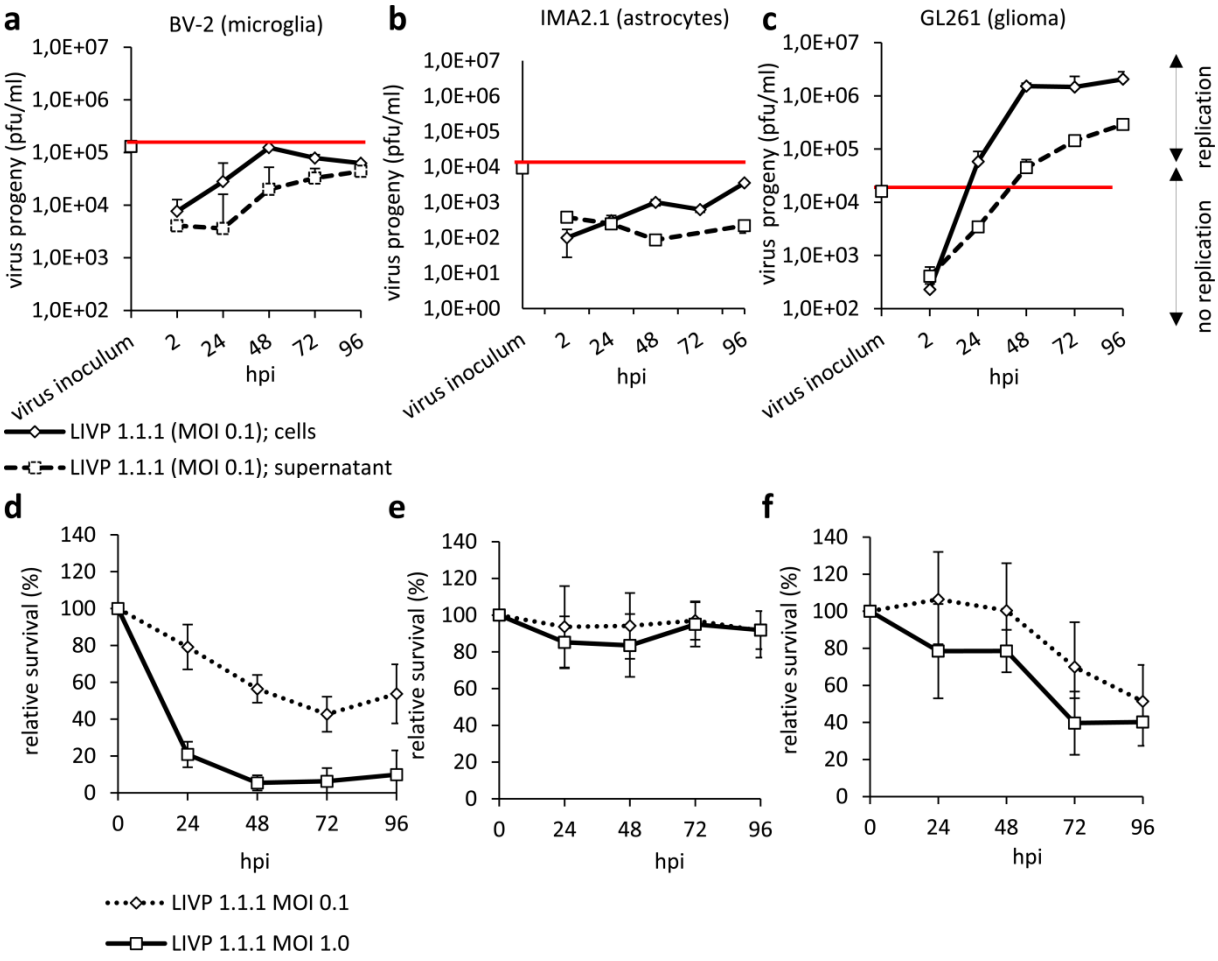

Figure 31: Comparison of LIVP 1.1.1 replication and lysis in BV-2, IMA 2.1 and GL261 cells in culture. Viral replication in BV-2 **(a)**, IMA2.1 **(b)** and GL261 **(c)** cells and supernatants, infected with LIVP 1.1.1 at an MOI of 0.1 was analyzed by standard viral plaque assay at 2, 24, 48, 72, 96 hpi. The experiment was performed in triplicate and performed twice. The virus concentration of the virus inoculum was used as reference to distinguish between active viral replication and no active replication (red line). MTT assay was performed to detect the percentage of surviving BV-2 **(d)**, IMA2.1 **(e)** and GL261 **(f)** cells after infection with LIVP 1.1.1 (MOI 0.1, 1.0). Experiments were performed in triplicate and repeated two times in independent experiments.

4.5.1 Analysis of cell death in BV-2 and GL261 cells

Since replication analysis of LIVP 1.1.1 in BV-2 and GL261 cells revealed a diverse efficacy in viral replication, but virus-mediated cell death was observed in both cell types, it was further investigated whether different mechanisms of cell death, apoptosis or necrosis appeared. VACV is known to induce either apoptosis or necrosis in different cell lines. Dependent on the infected cell type, apoptosis can be associated with reduced virus infection or replication [245].

To quantify late apoptosis, the proportion of the sub-G1 cell population was analyzed by FACS analysis and compared between the mock and virus-infected groups at 24, 48 and 72 hpi (Figure 32a, b). It was detected that the percentage of cells in the sub-G1 phase was higher in BV-2 cells than in GL261 cells at all time points. 40% of BV-2 cells were in the sub-G1 phase after 24 h and this amount of cells increased over time to 70% after 48 h and over 80% after 72 h. On the other hand, 24 hpi the amount of GL261 cells in the sub-G1 phase was around 10% and increased to 45% after 72 h. Additionally, distribution of PI-positive cells in PI-dim (apoptotic) and PI-bright (necrotic) cells [213, 214] revealed higher numbers of apoptotic cells in the VACV-infected BV-2 sample (Figure 32c) compared to infected GL261 cells (Figure 32d).

The data indicate that VACV-infection activates different cell death pathways and mechanisms in microglial BV-2 cells in contrast to GL261 tumor cells.

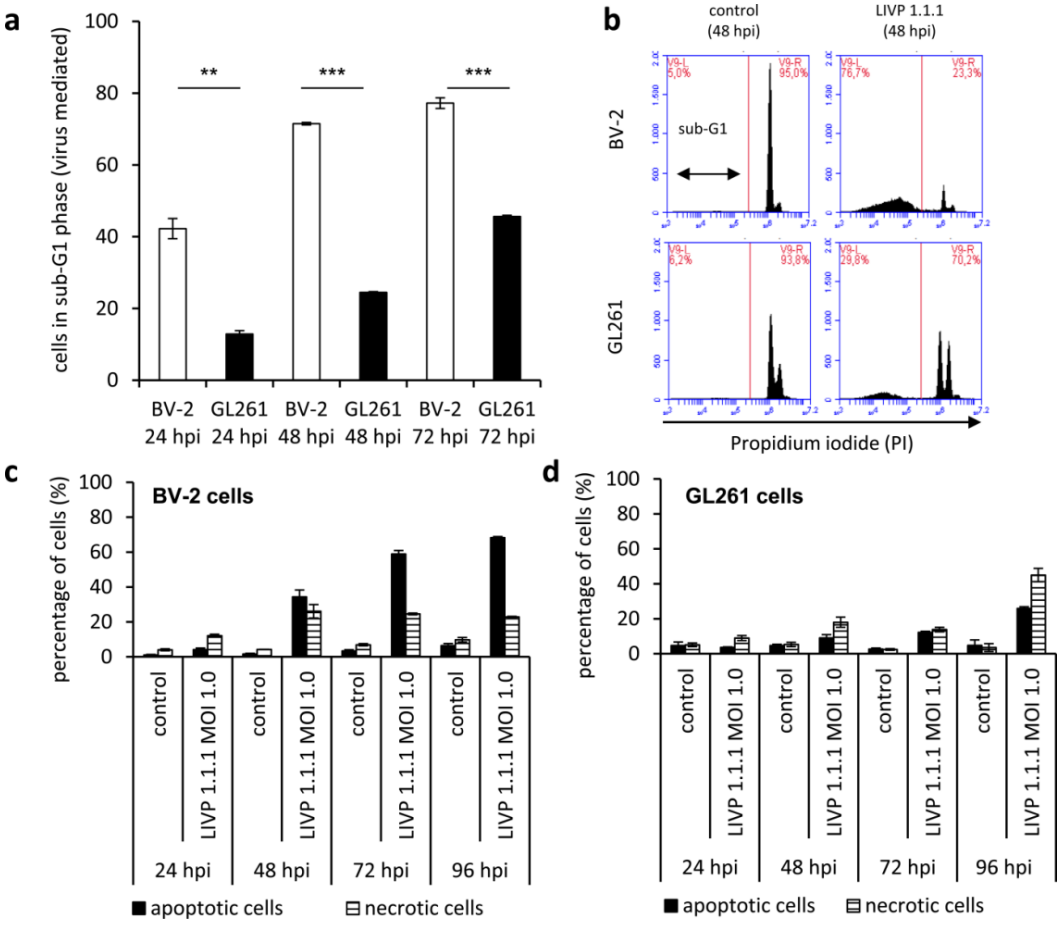

Figure 32: Different cell death characteristics of GL261 and BV-2 cells. Mean and standard deviation (n=3) of BV-2 or GL261 cells in sub-G1 phase 24, 48 or 72 h after viral infection (MOI 0.5) are shown in the bar chart in percentage relative to mock-infected samples **(a).** Cells that have lost part of their DNA due to DNA fragmentation in apoptosis are represented in sub-G1 peaks on DNA histograms. Representative examples 48 hpi for BV-2 and GL261 cells infected with LIVP 1.1.1 (MOI 0.5) or PBS are shown in **(b).** The percentages of PI-dim (apoptotic) and PI-bright (necrotic) cells in controls and LIVP 1.1.1-infected samples (MOI 1.0) are shown for BV-2 **(c)** and GL261 cells **(d)**. The experiments were performed in triplicate and repeated in an independent experiment.

4.5.2 Effects of BV-2 and IMA2.1 cells on VACV replication in GL261 glioma cells

The question that was addressed next was whether BV-2 and IMA2.1 cells indirectly or directly influence LIVP 1.1.1 replication in GL261 glioma cells.

For indirect co-culture experiments BV-2, IMA2.1 and GL261 cells were cultured for 48 h until semi confluence in cell culture flasks. The conditioned medium was collected and sterile filtered before use. For MTT cell survival assay or replication analysis BV-2 and IMA2.1 cells were either cultured in basic culture medium or in conditioned medium of GL261 cells for three days (Figure 33a, b; e, f). Alternatively, GL261 cells were either cultured in basic culture medium or in conditioned medium of BV-2 or IMA 2.1 cells for three days (Figure 33c, d; g, h).

As shown in Figure 33a, the relative survival of BV-2 microglial cells after infection with LIVP 1.1.1 (MOI 1.0) was significantly higher in BV-2 cells cultured in conditioned GL261 medium than in basic culture medium. There was no difference in relative survival of IMA2.1 cells cultured either in basic culture medium or conditioned GL261 medium (Figure 33b). Relative survival of GL261 cells after infection with LIVP 1.1.1 (MOI 1.0) cultured in conditioned BV-2 or IMA2.1 medium was slightly higher than in basic culture medium (Figure 33c, d). However, the difference was not significant.

Standard viral plaque assay revealed that the virus titer of LIVP 1.1.1 in BV-2 cells and supernatant cultured in GL261 conditioned medium was approximately 1 log-level lower than in BV-2 cells cultured in basic culture medium within the time frame of 24 h to 96 h (Figure 33e). In IMA2.1 the same result as in BV-2 could be detected, at 48-96 hpi (Figure 33f). The detected virus titer at both culture conditions in BV-2 and IMA 2.1 cells and supernatant was at all time points detected below the virus concentration of the initial virus inoculum. There was no difference in viral replication in GL261 cells and supernatant cultured either in basic or conditioned BV-2 or IMA2.1 medium (Figure 33g, h).

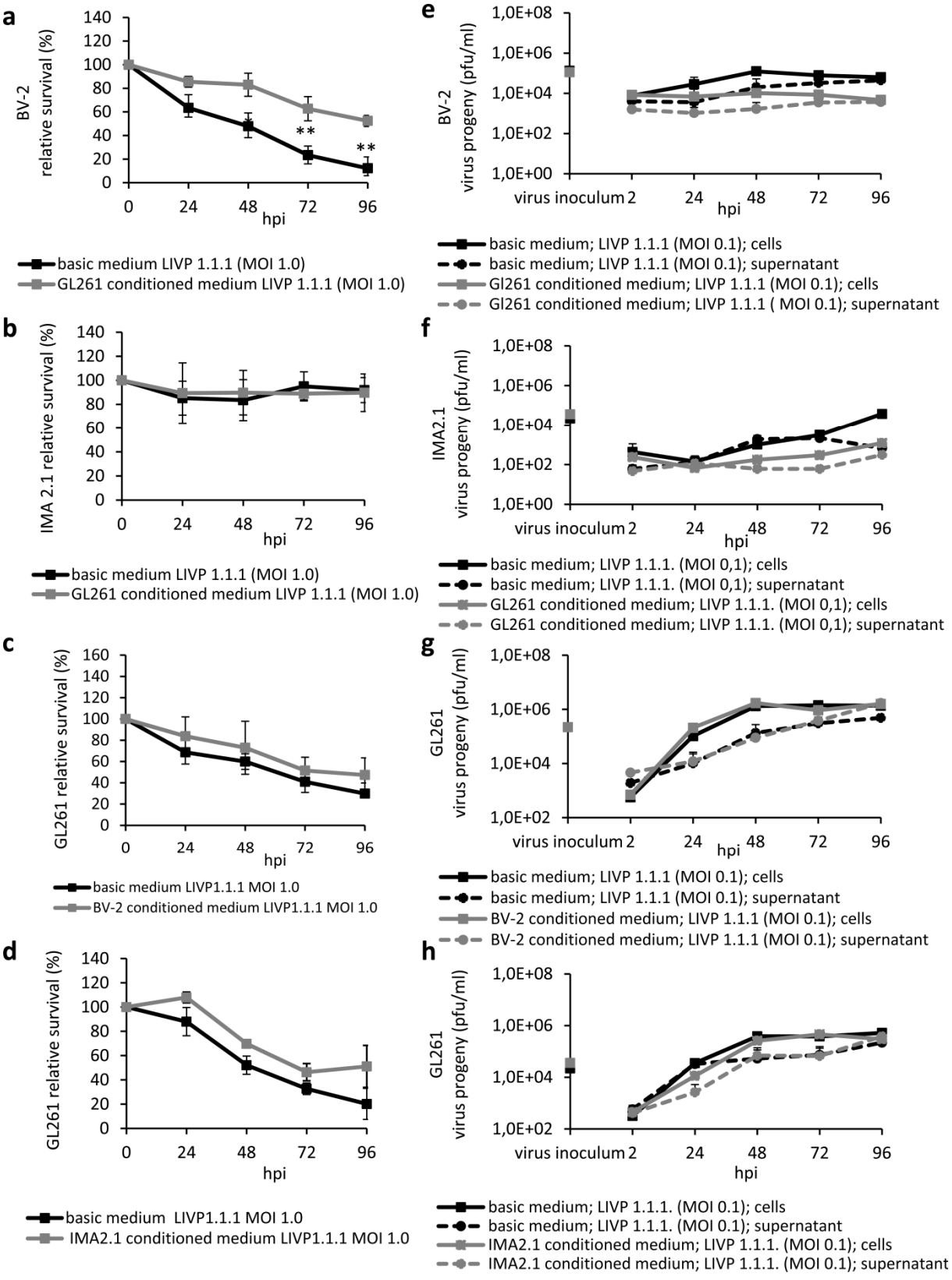

Figure 33: Analysis of viral progeny and virus-mediated cell death by indirect co-culture experiments with conditioned medium in BV-2, IMA2.1 and GL261 cells. For indirect co-culture experiments BV-2 and IMA2.1 were cultured in basic or sterile filtered conditioned GL261 medium for three days before infection with LIVP 1.1.1 (MOI 0.1 or 1.0). GL261 cells were cultured in basic or conditioned BV-2 or IMA2.1 cells. MTT assay was performed to detect the relative survival of BV-2 **(a)**, IMA2.1 **(b)** GL261 **(c, d)** cells after infection with LIVP 1.1.1 (MOI 1.0). Experiments were performed in triplicate and repeated in

independent experiments. Viral replication in BV-2 **(e)**, IMA2.1 (**f)** and GL261 **(g, h)** cells and supernatant, infected with LIVP 1.1.1 at an MOI of 0.1 was analyzed by standard viral plaque assay at 24, 48, 72, 96 hpi. The experiment was performed in triplicate and performed twice. The virus titer of the virus inoculum was used as reference to distinguish between active viral replication and no active replication.

To further analyze the competitive factors affecting virus replication and to determine which cell type was infected first, *i.e.* microglia or glioma cells, direct co-culture experiments were performed, where BV-2 and GL261 cells were cultured together at different proportions for 24 h.

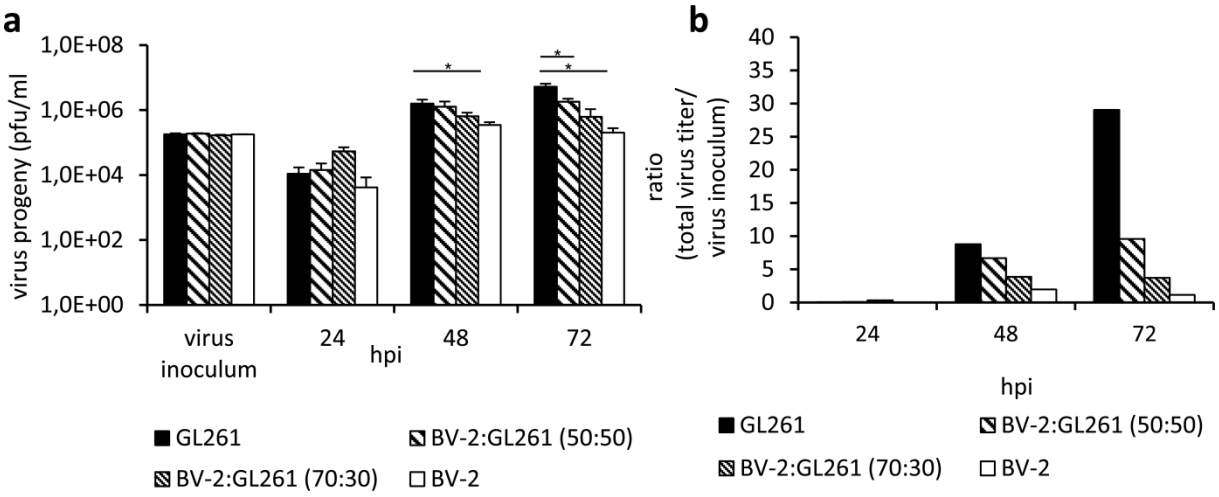

Figure 34: Analysis of a direct co culture experiment of BV-2 and GL261 cells. BV-2 and GL261 cells were cultured as direct co-cultures for 24 h in different proportions (50:50, 70:30, 100:0). For standard viral plaque assay, cells were infected with an MOI of 0.1 in triplicate. Bar charts represent mean and standard deviation **(a)**. Viral titers were related to the virus titer of the initial virus inoculum and illustrated as ratio (total virus titer / virus inoculum) **(b)**. Experiments were repeated in an independent experiment. Two-sided t-test with unequal variances was used for statistics (*p<0.05).

The results revealed a significant higher virus titer in GL261 cells that were cultured alone in contrast to a co-culture with 50% BV-2 cells 72 h after viral infection (Figure 34a, b).
In conclusion, these experiments showed that the more BV-2 cells were present in the co-culture the less viral particles were detected over time, suggesting that microglial BV-2 cells may compete for virus uptake in culture.

4.5.3 Impact of the immunologic phenotype of BV-2 and IMA2.1 cells on LIVP 1.1.1 infection in cell culture

There is a controversial discussion concerning the phenotype, function and role of microglia in malignant gliomas as reviewed by Wei *et al.* [246]. In literature a correlation between the presence of microglial cells with an M2 phenotype in gliomas and increasing tumor growth as well as a poor prognosis is described [246–248]. Cells with the M1 phenotype are expected to be present at injection sites and also during the initial phases of tumor growth [248–250]. According

to Glass and Synowitz [188], tumor-associated macrophages in gliomas have an aberrant immune type which shares both M1 and M2 features.

In the next set of experiments, both M1 and M2 phenotypes of BV-2 microglia were tested for their ability to take up and support LIVP 1.1.1 virus replication. The two different phenotypes M1 and M2 are dependent on exogenous addition of certain stimuli like IL-4 (10 ng/ml) for induction of the M2 phenotype, and IFN-γ (10 ng/ml) or LPS (10 µg/ml) or a combination of both for induction of the M1 phenotype [236]. LPS is known to induce nitric oxide (NO) production in BV-2 cells, a marker for the M1 phenotype [251, 252]. Cells were stimulated for 24 h with a respective reagent prior to infection.

Applying the Griess assay, a low NO production indicated by the measurement of nitrite was induced by treating BV-2 cells with IFN-γ or LPS alone (Figure 35a). However, when cells were treated with IFN-γ and LPS in combination, NO production was at the highest level as indirectly measured by the amount of nitrite. In addition, an up-regulation of the inducible isoform of nitric oxide synthase (iNOS) was detected by Western blot analysis of total proteins extracted from IFN-γ and LPS-treated BV-2 microglial cells (Figure 35b). Further, treatment of BV-2 cells with IL-4 or LPS both increased the expression of arginase 1, a marker for the M2 phenotype. Treatment of BV-2 cells with IFN-γ led to reduced arginase 1 expression (Figure 35b).

Furthermore, treatment with IFN-γ for 24 h resulted in high-level expression of MHCII molecules, an indicator for the M1 phenotype, whereas MHCII expression was not detectable in unstimulated or IL-4 stimulated cells detected by FACS analysis (Figure 35c).

LIVP 1.1.1 infection of cells stimulated with LPS, IFN-γ or a combination of both resulted in a reduction of virus progeny 24 hpi and 72 hpi (Figure 35d). In contrast, no differences in virus progeny were observed when comparing IL-4-stimulated BV-2 cells with unstimulated BV-2 cells.

In addition, around 50% of the cells which were stimulated with IFN-γ or LPS and IFN-γ were still alive 96 h after infection in growth medium with stimulating factors. The amount of living cells after LPS treatment was ~20%. It was less than 10% of living cells after IL-4 treatment or in the unstimulated cells (Figure 35e).

Further, BV-2 cells stimulated with IFN-γ and/or LPS proliferated to a lesser extent than unstimulated or IL-4-stimulated cells as determined by optical density measurement at 24 and 48 hpi (Figure 35f).

Based on standard viral plaque assay and MTT assay, these results indicate a higher amount of virus progeny in the M2 phenotype or unstimulated form of BV-2 cells in comparison to the M1 phenotype.

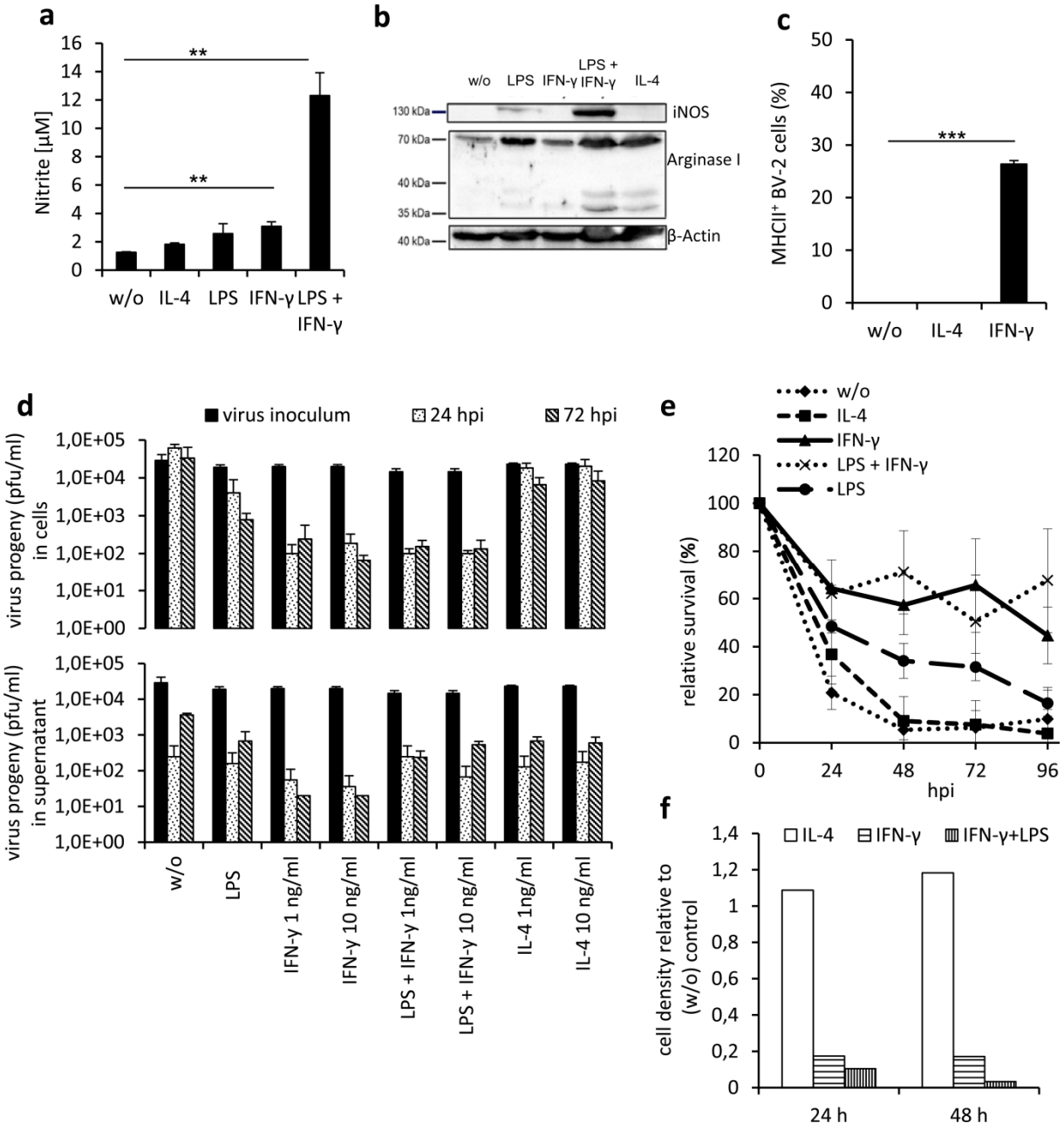

Figure 35: Reduction of virus progeny in BV-2 cells with M1 phenotype. BV-2 cells were stimulated with LPS (10 µg/ml), IFN-γ, (10 ng/ml), LPS + IFN-γ or IL-4 (10 ng/ml) for 24 h in medium with 2% FBS. Phenotypic characteristics of the cells were analyzed by Griess assay **(a)**, Western blot **(b)** and by detection of MHCII levels with FACS analysis **(c)**. Viral replication was analyzed by standard viral plaque assay in the presence of stimulating factors in different concentrations. Cells and supernatants were analyzed separately **(d)**. To detect the percentage of surviving cells after viral infection in the presence of stimulating factors a MTT assay was performed **(e)**. The proliferation efficiency of stimulated cells was detected via optical density measurement and calculated in proportion to unstimulated cells **(f)**. Two-sided t-test with unequal variances was used for statistics *p<0.05, **p<0.01, ***p<0.001. All experiments were performed in triplicate and repeated once in an independent experiment.

Polarization towards the M1 or M2 phenotypes is also known to occur in activated astrocytes [110]. The ability of different proinflammatory cytokines IL-4 (10 ng/ml), IFN-γ (10 ng/ml) and LPS (10 µg/ml) to induce NO production in IMA2.1 cells was analyzed by Griess assay. In addition,

the effect of bFGF (100 ng/ml) was tested, since this factor is described to enhance the proliferation of astrocytes similarly to IL-4 [253].

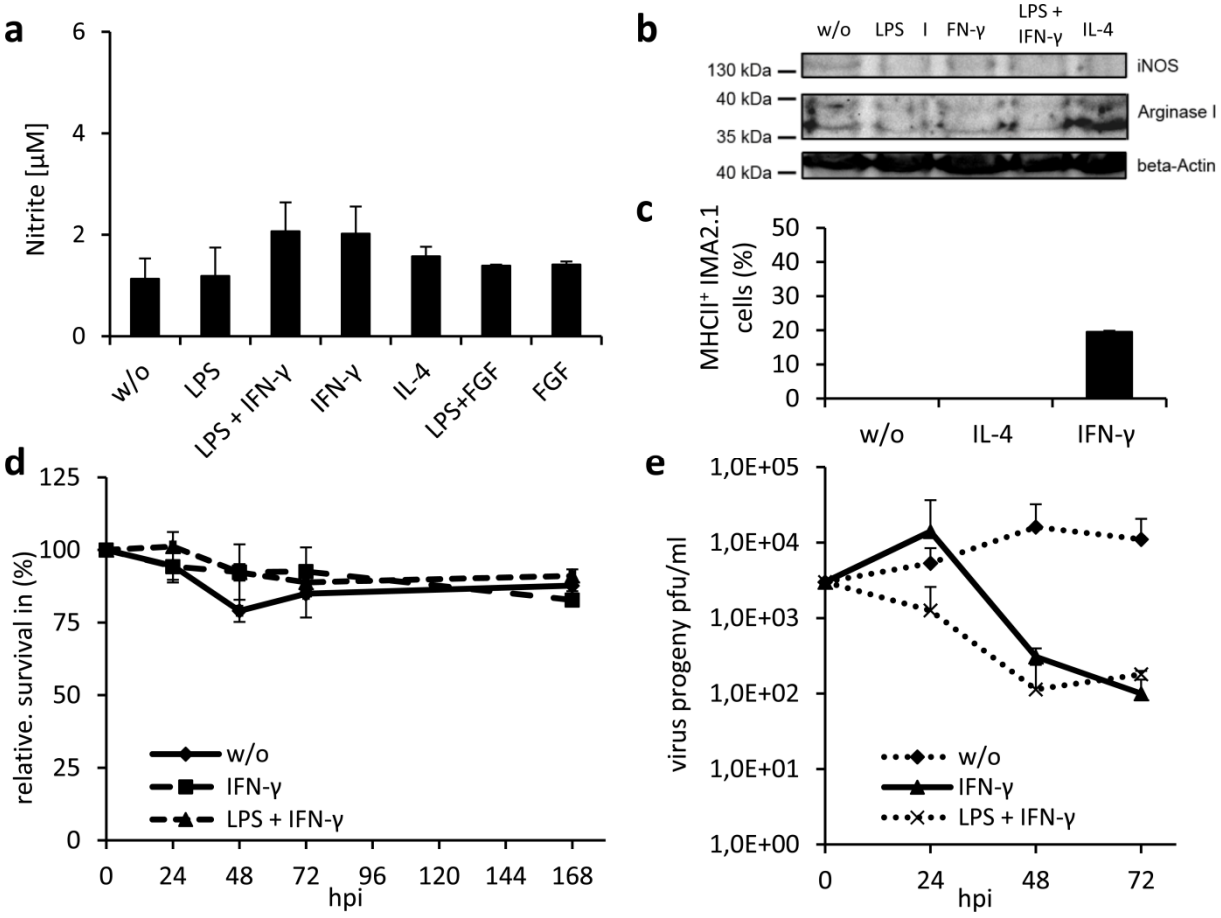

Figure 36: Stimulation of IMA 2.1 cells by various cytokines had no effect on relative survival after viral infection. IMA 2.1 cells were stimulated with LPS (10 µg/ml), IFN-γ, (10 ng/ml) LPS + IFN-γ, IL-4 (10 ng/ml) FGF (100 ng/ml) or FGF + LPS for 24 h in medium with 2% FBS. Phenotypic characteristics of cells were analyzed by Griess assay **(a)**, Western blot **(b)** and FACS analysis **(c)**. MTT assay was performed to detect the percentage of living cells in the presence of stimulating factors **(d)**. Viral replication was analyzed by standard viral plaque assay in the presence of stimulating factors **(e)**. All experiments were performed in triplicate.

The analysis of the Griess assay revealed no significant increase of the NO levels independent of the stimulation by LPS, IFN-γ, IL-4, FGF, or combinations of these (Figure 36a). By Western blot analysis iNOS expression levels were below the detection limit and no difference between the stimulating agents could be detected. Arginase 1, was detectable following IL-4 stimulation (Figure 36b). FACS analyses revealed increased MHCII expression levels in IMA2.1 cell cultures after stimulation with IFN-γ for 24 h (Figure 36c). Cells were tested negative for MHCII after stimulation with IL-4 or non-stimulated (w/o) for 24 h. There was no effect on virus mediated cell death when stimulated with IFN-γ or with a combination of IFN-γ and LPS in comparison to unstimulated cells, even after 168 hpi (Figure 36d). Infection of cells treated with IFN-γ or LPS

and IFN-γ resulted in a reduction of viral progeny compared to unstimulated cells (Figure 36e). Furthermore, under all treatment conditions the amount of viral progeny in cell cultures remained below the initial infection dose levels (time point 0).

Table 15 summarizes the results of the polarization experiments of both cell lines BV-2 and IMA 2.1 based on the determination of virus progeny and VACV-mediated cell death.

Table 15: Summary of treatment conditions on BV-2 and IMA2.1 cells and their effect on VACV infection.

Treatment condition		BV-2	IMA2.1	BV-2	IMA2.1
		(a) Replication capacity		(b) VACV-mediated cell death	
M2 phenotype	w/o	+	0	+	-
	IL-4	+	n.t.	+	-
M1 phenotype	IFN-γ	-	-	-	-
	IFN-γ+LPS	-	-	-	-
	LPS	-	-	-	-

Replication capacity (24 and 72 hpi) related to the virus concentration in the initial virus inoculum was determined by standard viral plaque assays **(a)**. **[+]** indicates an increase of the virus titer "high replication capacity", **[0]** virus titer at the same level as the initial virus inoculum "very low replication capacity", **[-]** virus titer below the initial virus inoculum; "absent/no replication". (**b**) VACV-mediated cell death was related to uninfected controls (24-72 hpi) and measured by MTT cell survival assays. **[+]** means more than 50% of cells are killed by LIVP 1.1.1, **[-]** means less than 50% of cells are killed by LIVP 1.1.1. Abbr. **[n.t.]** not tested, **[w/o]** without stimulation.

The use of LPS or IFN-γ alone, or LPS and IFN-γ in combination, all of which turn the cells into M1 phenotypes, resulted in a reduction of virus progeny in BV-2 cells. IFN-γ modulates a general microglial activation which increased MHCII expression. LPS and IFN-γ together had cumulative effects. In unstimulated cells virus progeny were detectable after 72 h, but the amount of virus progeny was below the amount of virus particles in the virus inoculum. Addition of IL-4 led to results similar to unstimulated BV-2 cells.

These data suggest that microglial cells can either be infected with LIVP 1.1.1 or the viral particles were phagocytized. Consequences are no further viral replication in cells with M1 phenotypes or abortive replication in cells with M2 phenotypes, respectively. In astrocytic IMA2.1 cells VACV infection was found to be independent from the status of polarization. The VACV LIVP 1.1.1 did not replicate in IMA2.1 cells.

4.6 Analysis of LIVP 1.1.1 infection in brain tumors using organotypic brain slice cultures

Besides direct and indirect co-culture (4.5.2) and polarization experiments (4.5.3), organotypic brain slice cultures (OSCs) were used to analyze, which cell types, *i.e.* microglia, astrocytes or glioma cells, are infected first or more efficiently by LIVP 1.1.1. OSCs represent an excellent experimental linkage between cell cultures and animal experiments as anatomical, morphological, and cellular functions of specific brain regions are maintained. The main advantage of OSCs is that factors such as cell-cell and cell-matrix interactions affecting viral entry or replication are preserved in the brain slice tumors [254].

4.6.1 Analysis of GL261 tumor growth and evaluation of VACV infection in organotypic brain slice cultures

First, viral replication of naïve OSCs prepared from C57BL/6 wt mice at the age of 3 days (young) or 7-8 weeks (adult) were compared. For infection, the VACV LIVP 1.1.1 or GLV-2b372 ($2x10^6$ pfu/slice) a virus construct derived from the parental LIVP 1.1.1 virus strain, which carries the TurboFP635 expression cassette under the control of the vaccinia synthetic early/late promoter at the *TK* locus, were used.

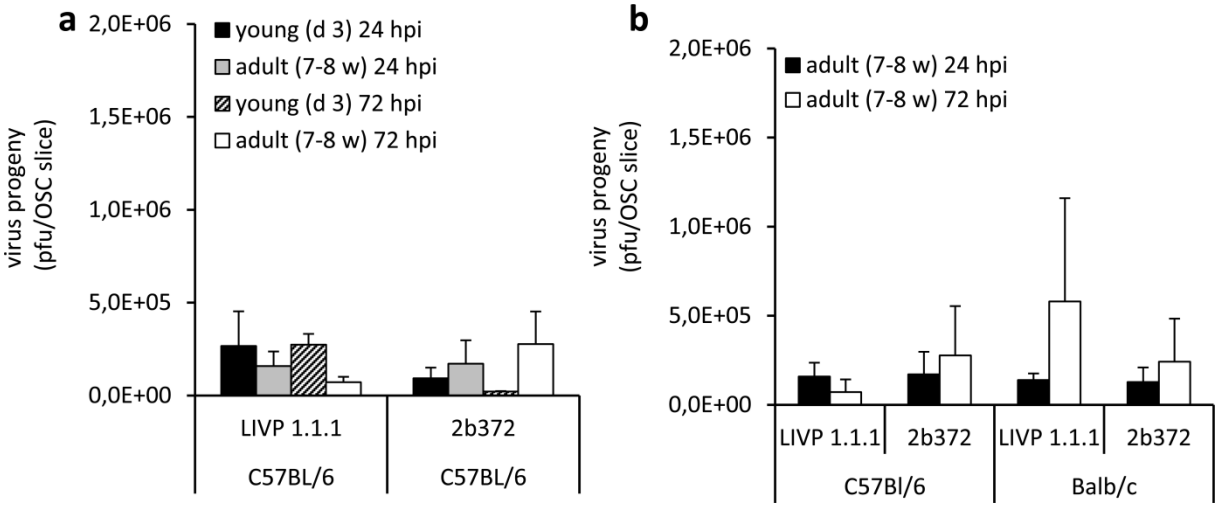

Figure 37: Replication analysis 24 and 72 hpi in naïve OSCs. OSCs from young (postnatal day 3) and adult (7-8 week) C57BL/6 wt mice were established. After 14 days in culture, OSCs were infected with $2x10^6$ pfu LIVP 1.1.1 or GLV-2b372/slice. Standard viral plaque assay was performed 24 and 72 hpi **(a)**. OSCs from adult (7-8 week) C57BL/6 wt and Balb/c wt mice were established. After 14 days in culture, OSCs were infected with $2x10^6$ pfu LIVP 1.1.1 or GLV-2b372/slice. Standard viral plaque assay was performed 24 and 72 hpi **(b)**.

Standard viral plaque assay revealed no significant difference between young and adult OSCs 24 hpi and 72 hpi for both VACV strains tested (Figure 37a). In addition, viral replication of LIVP 1.1.1 and GLV-2b372 in OSCs prepared from adult mice (7-8 weeks) of different genetic background, *i.e.* C57BL/6 wt and Balb/c wt, was compared. As shown in Figure 37b, there was an increase from 24 h to 72 h except in OSCs of C57BL/6 wt mice infected with LIVP 1.1.1. Significant differences between the mouse models were not observed, but virus titers were slightly higher in Balb/c wt compared to C57BL/6 wt mice. The virus titers remained below the initial infection dose of $2x10^6$ pfu/slice at all analyzed conditions and time points.

Next, GL261 tumor cell implantation into organotypic brain slice cultures (OSCs) was established. For this, OSCs of young C7BL/6 wt mice were prepared and cultured for 7 days. Then, $1x10^4$ GL261 glioma cells expressing red fluorescent protein (RFP) were implanted into the slices.

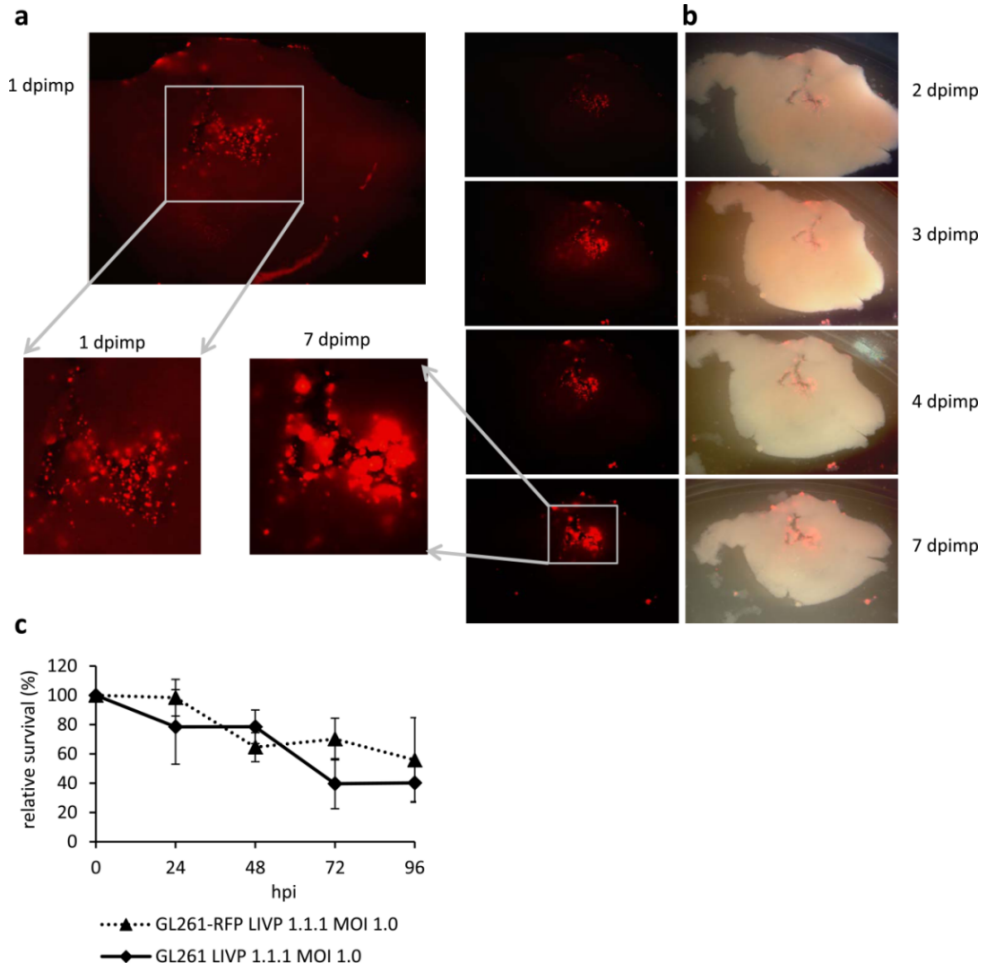

Figure 38: Visualization of proliferating GL261-RFP tumor cells implanted into OSCs. OSCs from young and adult C57BL/6 wt mice were established. After 7 days in culture, OSCs were implanted with $1x10^4$ GL261-RFP cells. Tumor cell proliferation indicated by an increase of the RFP signal from 1 dpimp to 7 dpimp was examined with a fluorescence microscope (Leica) **(a)**. Overlay pictures (phase contrast and RFP signal) of paradigmatically chosen OSCs of a young C57BL/6 wt mouse are shown in **(b)**. MTT assay was performed to compare LIVP 1.1.1 mediated cell death (MOI 1.0) in GL261 and GL261-RFP cells **(c)**.

Tumor cell proliferation indicated by an increase of the RFP signal from 1 dpimp to 7 dpimp could be detected as paradigmatically shown in a brain slice of a 15 day old C57BL/6 wt mouse (Figure 38a, b). The method could be established for both OSCs from young and adult 14 week old mice. By MTT assay no significant difference between GL261 and GL261-RFP cells was observed (Figure 38c).

For analysis of VACV infection of adult OSCs implanted with GL261-RFP tumor cells, immunohistochemical analysis was performed. LIVP 1.1.1 infection of the slices was carried out 7 days post GL261-RFP implantation and the analysis was conducted 24 hpi.

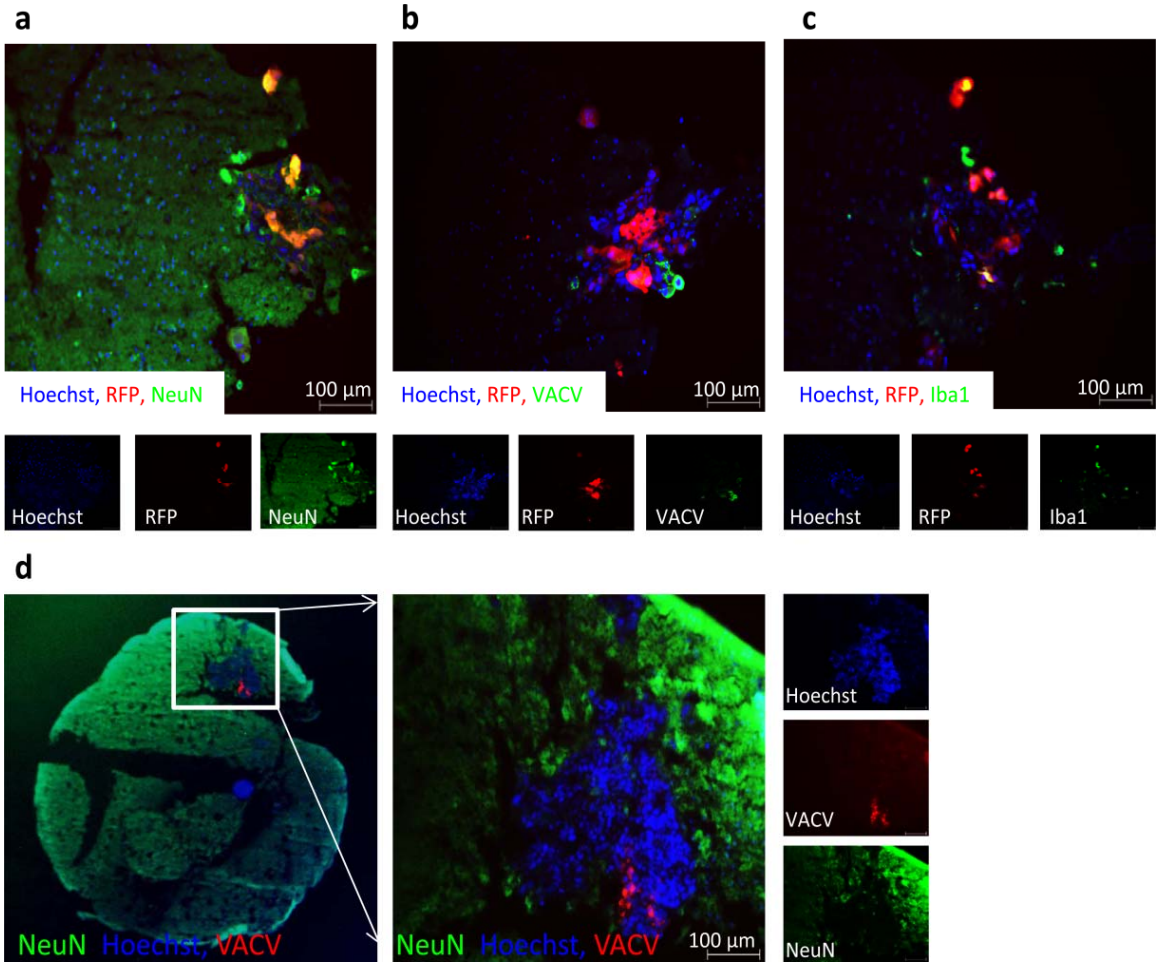

Figure 39: Localization of VACV infection within OSCs with implanted GL261 glioma cells. OSCs from adult mice were established and implanted with $1x10^4$ GL261-RFP cells **(a-c)** or GL261 cells **(d)**. 7 days after implantation OSCs were infected with $5x10^6$ pfu LIVP 1.1.1 **(a-c)** or GLV-2b372/6-well **(d)**. 24 h after infection RFP signal of GL261 tumor cells **(a-c)** or of VACV GLV-2b372 **(d)** was visualized and in addition, OSCs were stained with Hoechst (blue) **(a-d)**, anti-VACV **(b** green or **d** red**)**, anti-NeuN (green; **a**, **d**) or anti-Iba1 (green; **c**). Representative fluorescence images were taken at an Axiovert 200M inverse microscope at a magnification of 20x or a MZ16 FA Stereo-Fluorescence microscope.

Cell nuclei of implanted tumor cells were well distinguishable from the normal brain tissue since they were larger in size and in a close arrangement as indicated by Hoechst staining in blue (Figure 39a-d). NeuN depicted in green is a marker for neurons (Figure 39a, d).

As shown in Figure 39c, Iba1 positive microglial cells are stained in green and detectable around the tumor mass. VACV infection visible in green or in red in Figure 39b or 39d was detectable exclusively within the tumor mass.

4.6.2 LIVP 1.1.1 does not replicate efficiently in GL261 tumor spheres in organotypic brain slice cultures

In further experiments VACV infection of two different glioma cell lines implanted into adult OSCs was compared. Based on the results described so far, the murine GL261 glioma cell line can be viewed as syngeneic non-responder tumor model and the human U87 glioblastoma cell line in contrast as a responder model [180]. OSCs were implanted with either GL261-RFP or U87-RFP cells and the tumors were grown for 7 days. The OSCs with implanted tumor cells were infected with $5x10^6$ pfu LIVP 1.1.1. Standard viral plaque assay of OSCs with tumors revealed that OSCs with U87-RFP tumors showed over 10-fold higher amounts of virus progeny after 72 h in comparison to OSCs with GL261-RFP tumors **(Figure 40a)**.

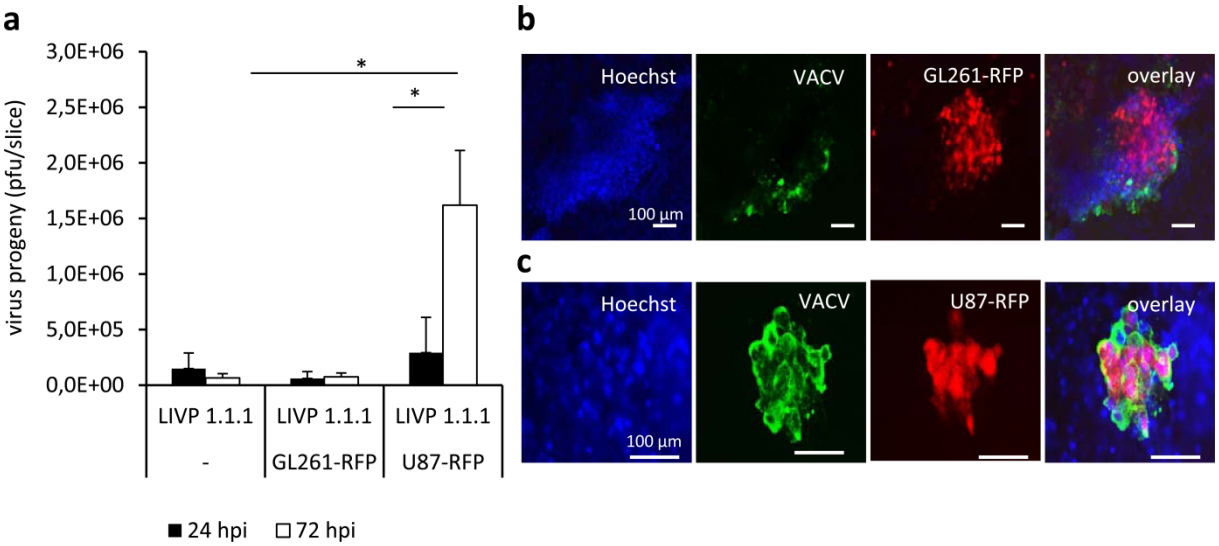

Figure 40: Analysis of VACV infection in OSCs with implanted glioma cells. OSCs from adult mice were established and implanted with $1x10^4$ GL261-RFP or U87-RFP cells. 7 days after implantation OSCs were infected with $5x10^6$ pfu LIVP 1.1.1 /6-well. Standard viral plaque assay was performed 24 h and 72 h after infection **(a)**. Two-sided t-test with unequal variances was used for statistics *$p<0.05$. 72 h after infection OSCs implanted with GL261-RFP **(b)** and U87-MG-RFP **(c)** cells were stained with Hoechst (blue) and anti-VACV antibody (green) to visualize infected tumor spheres marked in red. Representative florescence images were taken.

Immunohistochemical staining of tumor spheres confirmed that VACV infects GL261 tumors expressing RFP but viral particles were only detectable at the periphery of the tumor (Figure 40b). In contrast, OSCs with U87 tumors expressing RFP were completely infected 72 h after addition of the virus onto the slices (Figure 40c). Based on these results, it can be concluded that the findings obtained at intracranial implantation and infection experiments (Figure 13, Figure 30) were also confirmed in OSC tumors *ex vivo*. These observations suggest that there is a direct influence of the tumor milieu and the tumor cells on viral replication and on continued tumor growth.

4.6.3 Microglia could be protected from infection with VACV LIVP 1.1.1

Next, the role of phagocytic microglia in mouse brain tumors was determined in OSCs. GL261-RFP cells were implanted into OSCs and allowed to establish for 7 days. In a second step, microglial BV-2 cells either non-stimulated or stimulated for 24 h with IFN-γ were added onto OSCs. One day after addition of BV-2 microglial cells, OSCs were infected with VACV LIVP 1.1.1 for 24 h.

As shown in Figure 41a, unstimulated BV-2 cells (green) located around the tumor cells were infected with LIVP 1.1.1 (blue) whereas the GL261-RFP tumor cells (red) were only partially infected. Similar results were obtained for BV-2 cells pre-incubated with IL-4.

Interestingly, BV-2 cells stimulated with IFN-γ (green) for 24 h prior VACV (blue) application were not infected, but on the contrary the GL261-RFP tumor cells (red) were intensively infected (Figure 41b).

From these results demonstrating the capability to modulate the infection of the tumor cells and infiltrating immune cells it can be concluded that OSCs represent a suitable approach to model *ex vivo* interactions of conditioned immune cells, intracellular pathogens and tumor cells for the understanding of interactions in the tumor microenvironment.

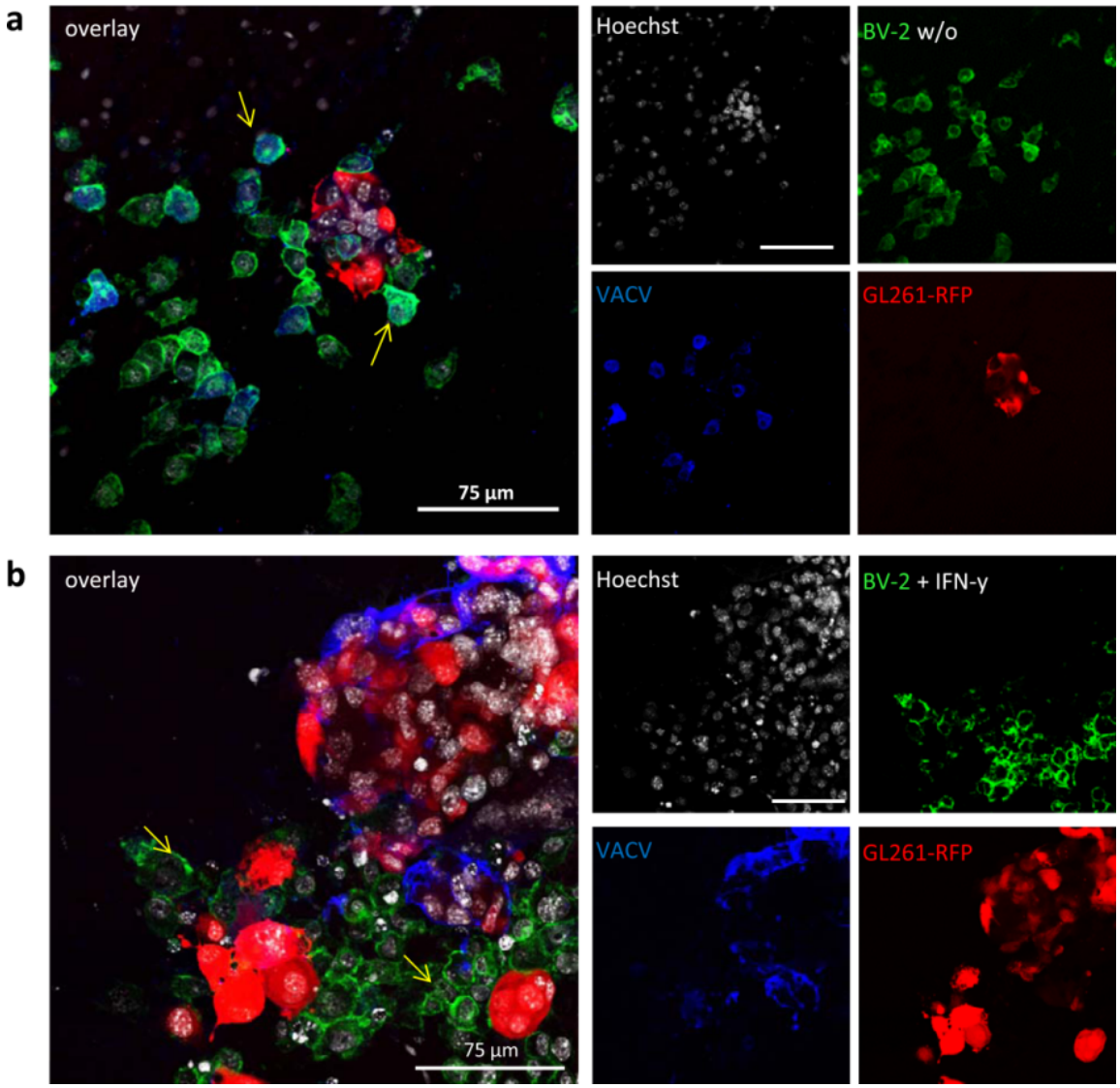

Figure 41: Stimulation with IFN-γ prevented BV-2 cells from infection with LIVP 1.1.1 in OSCs. OSCs from adult mice were established and implanted with $1x10^4$ GL261-RFP cells. 7 days after implantation, unstimulated (w/o) **(a)** or IFN-γ-stimulated **(b)** BV-2 cells were applied directly onto the implanted OSCs. 24 h later OSCs were infected with LIVP 1.1.1. OSCs were stained after additional 24 h with FITC-IB4 (BV-2; green), Hoechst (white) and anti-VACV (blue). Representative fluorescence images were taken at a spectral confocal & multiphoton system (Leica TCS SP2). Yellow arrows mark infected and uninfected BV-2 cells, respectively.

Part 2: Characterization of the anti-apoptotic factor AVEN in the context of oncolytic VACV therapy

[The majority of the results in part 2 are part of a manuscript "Cecil et al., Genetic variations of tumor cell lines and their specific differences in apoptotic pathways when confronted with the oncolytic vaccinia virus GLV-1h68" (in preparation).]

4.7 Analysis of the role and function of AVEN in different human tumor cell lines for oncolytic VACV therapy

Factors of the tumor microenvironment such as IFN-γ or specific cell types, like microglia or astrocytes, influencing the success of oncolytic virotherapy in malignant GL261 gliomas were analyzed in part 1 of this study. In part 2, the specific role and interference of molecules and factors which are part of the apoptotic cell death pathways such as the apoptosome complex were analyzed in the context of oncolytic virotherapy. For this part of the study, the oncolytic VACV GLV-1h68 and various human cancer cell lines have been used.

In order to understand why some tumor cells are able to survive an infection by the oncolytic VACV GLV-1h68, the data of gene expression from infected and non-infected cells of the melanoma cell lines (888-MEL, 1936-MEL), the breast cancer cell line GI-101A, as well as the colon adenocarcinoma cells HT-29 were evaluated (J. Reinboth; unpublished data). The acquired gene expression data was then visualized by heatmapping. In addition, boolean modeling of the apoptosis network was performed and the significant gene expression changes were mapped onto the models (A. Cecil; unpublished data). Based on these data, a special focus was set on the anti-apoptotic protein AVEN and its expression and function in different cancer cell lines.

AVEN, was recently identified by Chau *et al.* [255] and is a ubiquitous protein which is expressed in a great number of adult tissues and cell lines [255, 256]. It binds to Bcl-xL strengthening its anti-apoptotic activity and also interacts with APAF-1 suppressing the APAF-1-mediated activation of caspase-9 [255]. Furthermore, AVEN binds and activates the cell cycle-regulating ataxia-telangiectasia (ATM) protein kinase, a critical regulator of the G2/M DNA damage checkpoint in the DNA damage response pathway [257, 258].

In this study it should be elucidated whether there is a specific role or function of AVEN for successful infection and replication of GLV-1h68 in the four different tumor cell lines and thus, whether therapeutic success or failure is dependent on AVEN levels in the cancer cells. For this, a

number of different biological assays such as MTT assay, replication analysis, FACS analysis or siRNA knockdown experiments were performed.

4.7.1 Characterization of GLV-1h68 permissiveness in various human tumor cell lines

First, an MTT assay was performed to compare GLV-1h68-induced cell death in 888-MEL, 1936-MEL, GI-101A and HT-29 (Figure 42a-d). Analysis was carried out at different MOIs (0.01, 0.1, 1.0) and a time course from 24 to 72 hpi.

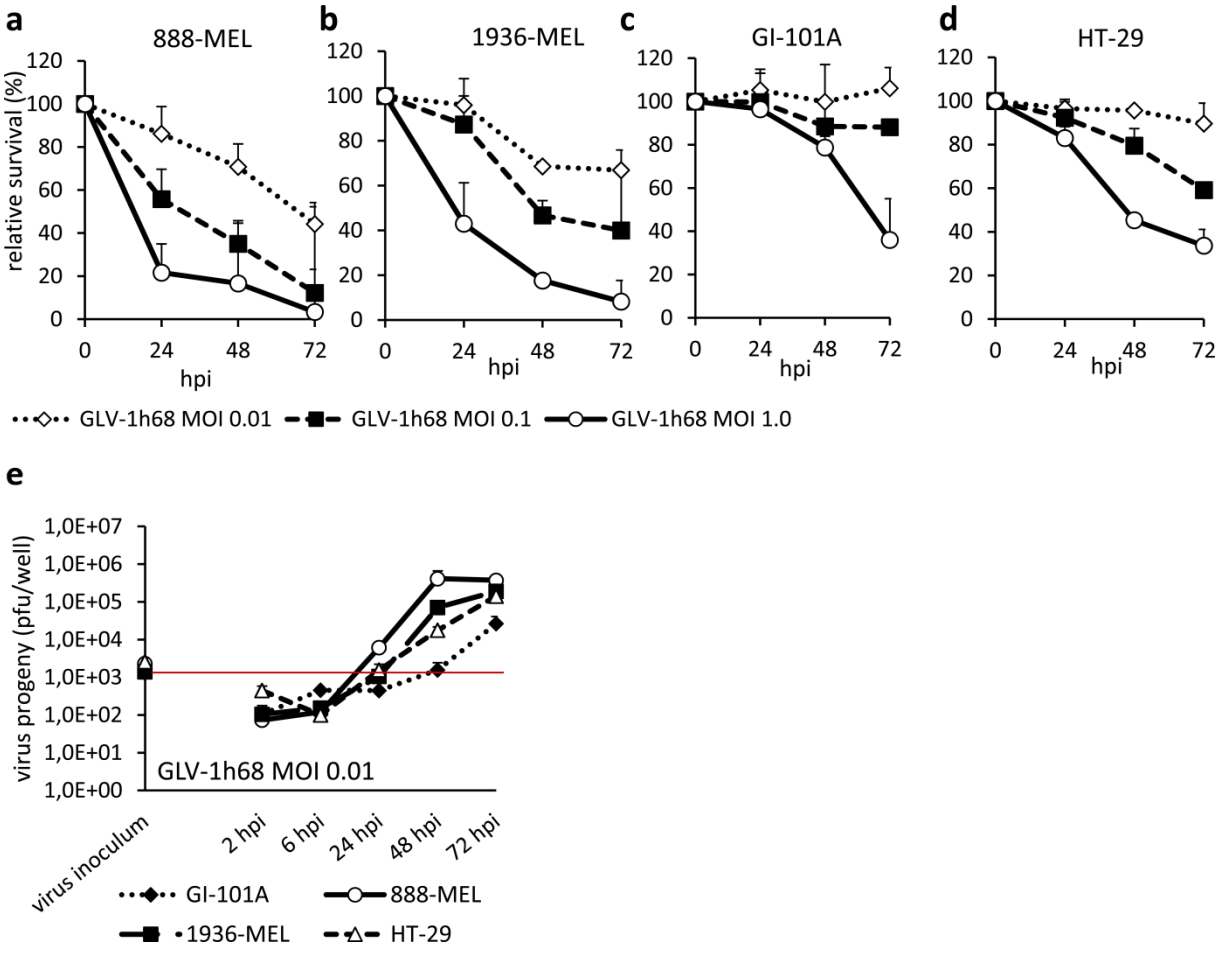

Figure 42: Differences in GLV-1h68 infection in various human tumor cell lines. MTT assay was performed to detect the percentage of dead cells after viral infection with GLV-1h68 (MOI 0.01, 0.1 and 1.0) in 888-MEL **(a)**, 1936-MEL **(b)**, GI101A **(c)** and HT-29 **(d)** in a time frame of 24-72 hpi.
Viral replication in 888-MEL, 1936-MEL, GI-101A, HT-29 cells, infected with GLV-1h68 at an MOI of 0.01 was analyzed by standard viral plaque assay in triplicate **(e)**. The red line separates active replication from no replication efficiency.

888-MEL and 1936-MEL cells showed a more pronounced virus-induced cell death than the HT-29 and GI-101A cells at all MOIs tested.

By standard viral plaque assay (MOI 0.01) it was demonstrated that all four cell lines were permissive for viral replication. This was indicated by an increase of the virus titer (pfu/ml) in

cells and supernatants from the virus titer of the initial virus inoculum (Figure 42e). Virus replication was most prominent in 888-MEL with a virus titer higher than the initial virus inoculum already 24 hpi. Weakest viral replication was detected in GI-101A where active viral replication started for the first time at 72 hpi.

Taken together, the infection/replication pattern of GLV-1h68 is different in all four cell lines analyzed and does not correspond with the *in vivo* T.I. classification of responder (888-MEL and GI-101A) and non-responder (1936-MEL and HT-29) cell lines [149].

4.7.2 Analysis of *AVEN* gene expression levels in cells of four human tumor cell lines

As described by Chau *et al.* [255] AVEN is found ubiquitously expressed in various cell lines and tissues. This should be verified for 888-MEL, 1936-MEL, GI-101A and HT-29. *AVEN* gene expression was tested on RNA level by culturing cells for 24 and 48 h.

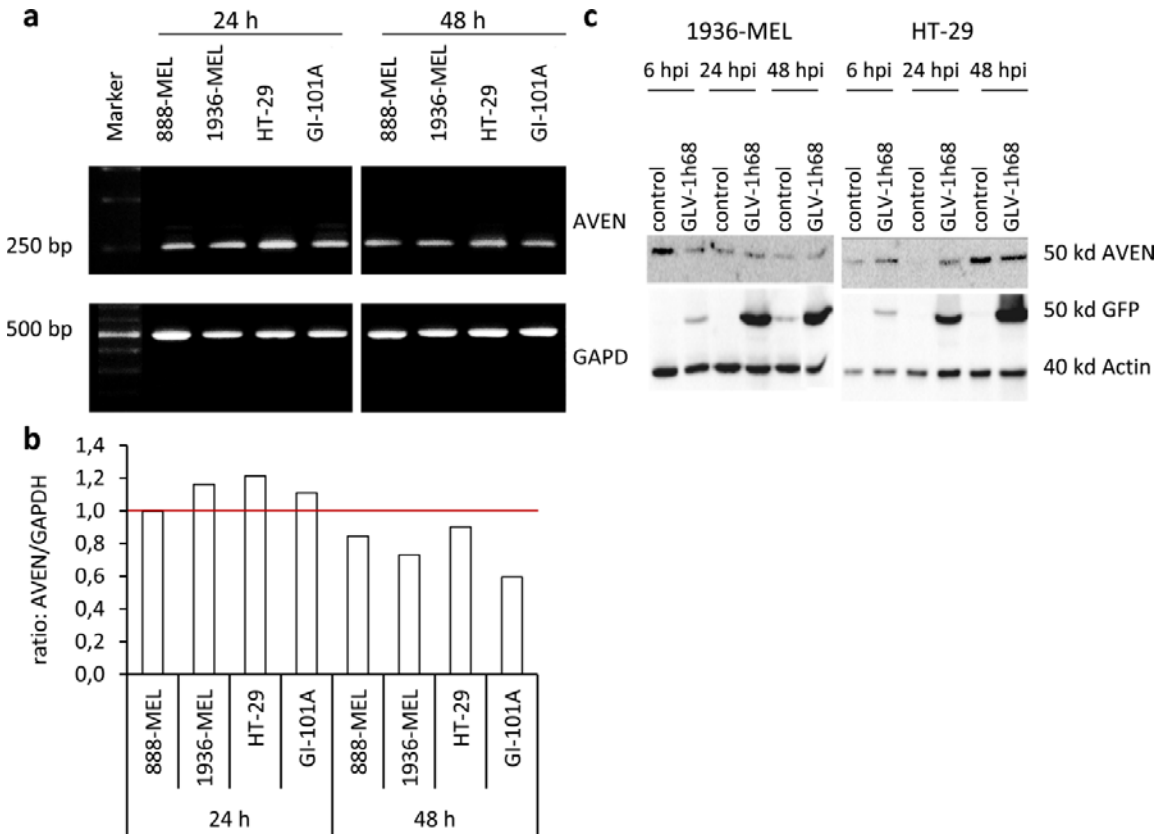

Figure 43: Analysis of AVEN expression on RNA and protein level in human tumor cell lines. *AVEN* mRNA expression in 888-MEL, 1936-MEL, GI-101A and HT-29 cultured for 24 or 48 h was analyzed by PCR **(a)**. PCR reactions were performed on templates of cDNA from the corresponding human cancer cell lines using a set of primers for *AVEN* and *GAPDH* as internal control. The bar chart represents the ratio between *AVEN* expression and *GAPDH* expression in the analyzed cell lines at 24 and 48 h. The red line marks a ratio of 1.0 **(b)**. The protein expression of AVEN and GAPDH in HT-29 and 1936-MEL cells infected with GLV-1h68 (MOI 1.0) at 6, 24 and 48 hpi. Mock-infected cells were used as control. GFP expression represents viral infection **(c)**.

AVEN mRNA could be detected in all four cell lines cultured for 24 and 48 h, respectively (Figure 43a). *GAPDH*, a house-keeping gene, was used as control. The ratio of the end point measurement between *AVEN* and *GAPDH* gene expression levels revealed a ratio >1 (higher *AVEN* gene expression) after 24 h than after 48 h (ratio <1) in culture (Figure 43b) which could be due to increasing cell densities. The *AVEN/GAPDH* ratio was highest in HT-29 compared to the other cell lines. This is in accordance with the gene expression data of J. Reinboth (unpublished data), were upregulation of *AVEN* was only detected in HT-29 cells and in none of the other cell lines.

Testing AVEN on protein level paradigmatically shown for HT-29 and 1936-MEL revealed that it was expressed in all cell lines 6, 24 and 48 hpi in control and GLV-1h68-infected samples (Figure 43c).

4.7.3 AVEN interference in HT-29 cells enhanced apoptotic characteristics and reduced GLV-1h68 infection

Furthermore, it was analyzed whether the anti-apoptotic factor AVEN affects the permissiveness of the weak/non-responder cell line HT-29 to GLV-1h68 infection. For this, siRNA targeting *AVEN* was utilized in HT-29 cells. Cells were transfected for 48 to 72 h with the siRNA which targets *AVEN* (si-AVEN) and as control a scrambled RNA (si-control) was used. As shown in Figure 44a, *AVEN* gene expression was down-regulated in HT-29 cells compared to cells transfected with si-control. DNA fragmentation was tested as one characteristic to distinguish apoptotic from necrotic cell death [211] and to verify whether the knockdown of AVEN does enhance apoptotic characteristics in the cancer cells. It was shown that down-regulation of the anti-apoptotic factor AVEN in HT-29 cells revealed a significant increase of DNA fragmentation, detected as an increase of cells in sub-G1 phase in si-AVEN transfected cells compared to si-control transfected cells (Figure 44b). Detection of $Annexin^+/7AAD^-$ (apoptotic) or $Annexin^-/7AAD^+$ (necrotic) cells revealed no significant difference between si-control and si-AVEN transfected HT-29 cells (Figure 44c).

Western blot analysis revealed the expression of procaspase-3 (32 kDa) in both si-AVEN and si-control transfected cells whereas the cleaved and activated form of the effector caspase-3 was not detected (Figure 44d). In accordance with the literature, down-regulation of AVEN results in an activation and cleavage of the initiator caspase-9 (35 kd). GAPDH was used as loading control.

In addition, replication of GLV-1h68 (MOI 1.0) and the percentage of GFP^+ cells and thus the infection rate was evaluated in HT-29 cells treated with si-AVEN or si-control. As shown in Figure 44e, a significant reduction of the virus titer and a significantly smaller number of GFP^+ cells

(Figure 44g) were detected in si-AVEN transfected cells compared to si-control transfected cells. Percentage of cells in sub-G1 phase 24 hpi was significantly enhanced in GLV-1h68-infected si-AVEN transfected HT-29 cells compared to si-control transfected and infected HT-29 cells (Figure 44f).

Taken together, these results showed that down-regulation of AVEN results in an increase of apoptosis in HT-29 cells, a reduced infection rate (GFP^+ cells) and an impaired viral replication.

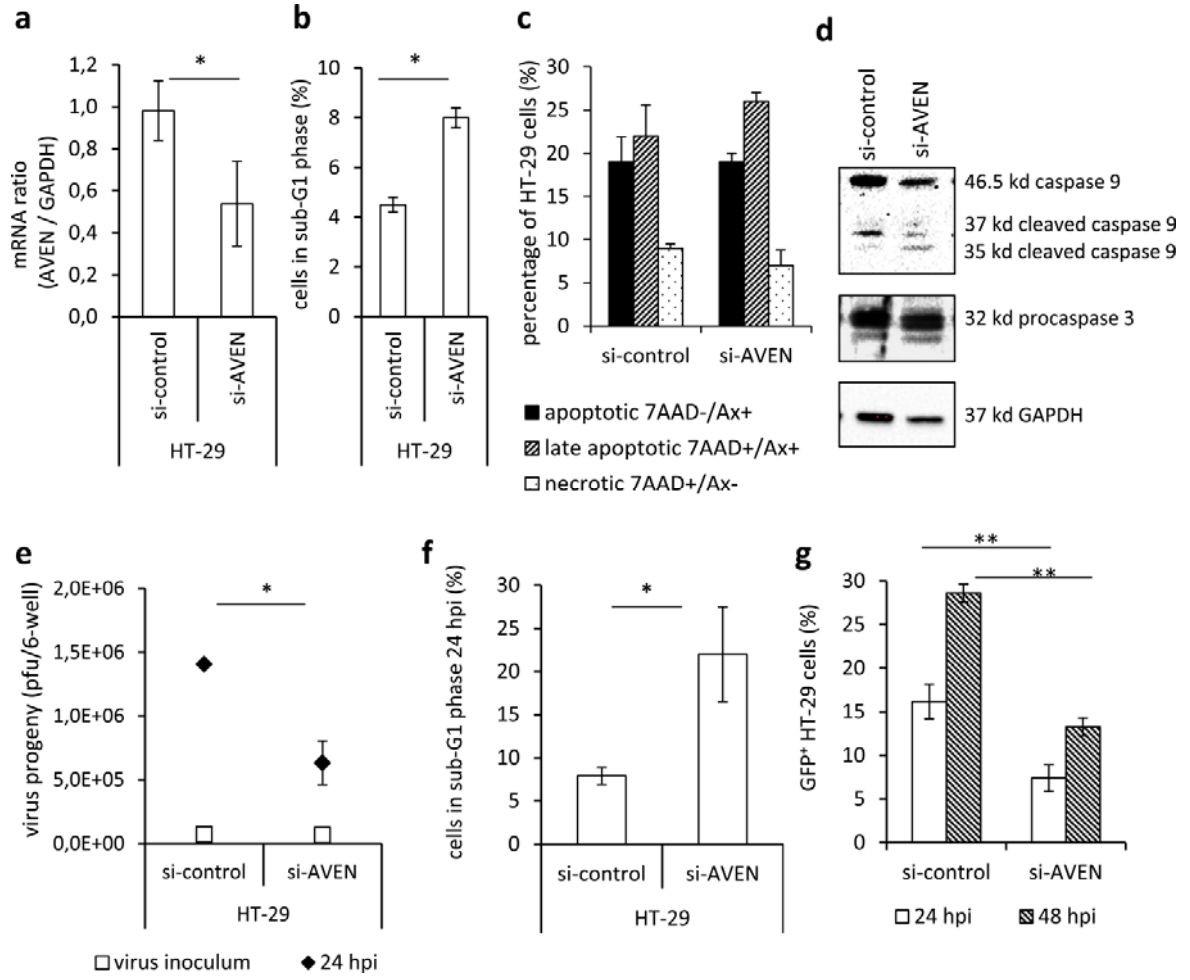

Figure 44: Characterization of knockdown of AVEN in HT-29 cells. Down-regulation of *AVEN* mRNA expression for 72 h in HT-29 cells transfected with AVEN siRNA (si-AVEN) or scrambled control siRNA (si-control) **(a)**. The percentage of si-control or si-AVEN transfected HT-29 cells in sub-G1 phase indicating DNA fragmentation measured by FACS analysis **(b)**. For analyzing cell membrane permeability, transfected cells were stained with the vital dye 7AAD and Annexin (Ax) and were subsequently analyzed by FACS analysis **(c)**. Protein expression levels of caspase-9 and caspase-3 were analyzed in si-control and si-AVEN transfected HT-29 cells by Western blot analysis. GAPDH was used as loading control **(d)**. Viral replication of GLV-1h68 (MOI 1.0) was analyzed in si-control and si-AVEN transfected HT-29 cells by standard viral plaque assay 24 hpi **(e)**. Percentage of transfected and infected HT-29 cells in sub-G1 phase were analyzed by FACS analysis **(f)**. In parallel to the virus titer, the infection rate of the samples was determined by measuring the percentage of GFP^+ cells by FACS analysis 24 and 48 hpi **(g)**. All transfection experiments were performed in 6-well plates in triplicate and repeated in an independent experiment. Two-sided t-test with unequal variances was used for statistics *p<0.05, **p<0.01.

4.7.4 AVEN interference in 1936-MEL cells enhanced apoptotic characteristics and reduced GLV-1h68 infection

To study, whether the effects of AVEN on VACV GLV-1h68 infection are a general phenomenon or unique for the non-responder cell line HT-29, knockdown of AVEN was also analyzed in the weak responder cell line 1936-MEL.

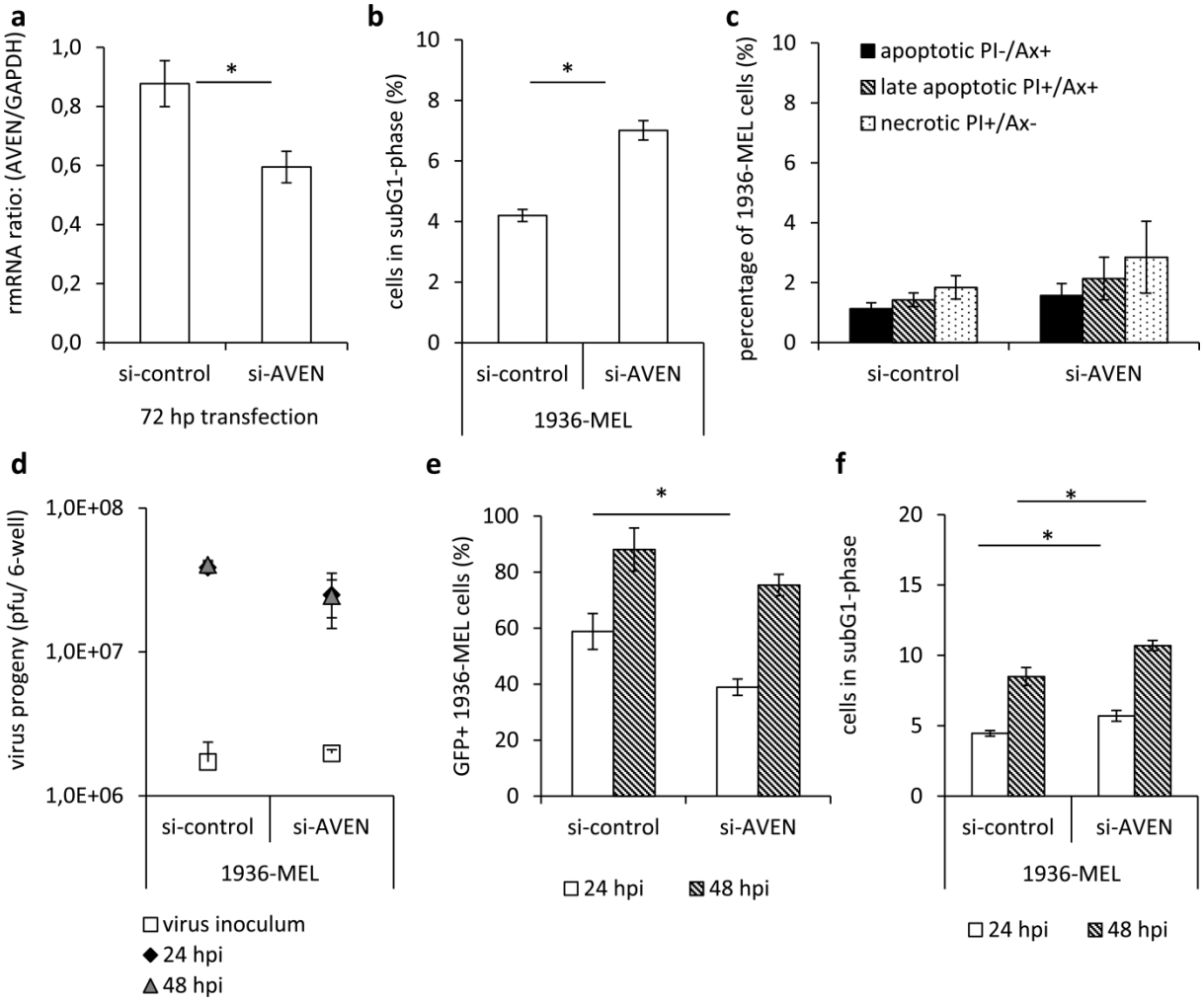

Figure 45 Knockdown of AVEN results in reduced infection of GLV-1h68 in 1936-MEL cells. Transfection of 1936-MEL with si-AVEN or si-control for 72 h and determination of AVEN gene expression levels by PCR **(a)**. Quantitative differences were determined by Image J. The percentage of si-control or si-AVEN transfected 1936-MEL cells in sub-G1 phase indicating DNA fragmentation was measured by FACS analysis **(b)**. For analyzing cell membrane permeability, transfected cells were stained with PI and Annexin (Ax) and were subsequently analyzed by FACS analysis **(c)**. Viral replication of GLV-1h68 (MOI 0.5) was analyzed in si-control and si-AVEN transfected 1936-MEL cells by standard viral plaque assay 24 and 48 hpi **(d)**. The infection rate of the samples was determined by measuring the percentage of GFP^+ cells by FACS analysis 24 and 48 hpi **(e)**. Transfected 1936-MEL cells in sub-G1 phase 24 hpi and 48 hpi were analyzed by FACS analysis **(f)**. All transfection experiments were performed in 6 well plates in triplicate and repeated two times. Two-sided t-test with unequal variances was used for statistics *p<0.05, **p<0.01, ***p<0.001.

Consistently, cells were transfected with si-AVEN or si-control for 72 h resulting in a down-regulation of *AVEN* on mRNA level (Figure 45a). DNA fragmentation was significantly increased in si-AVEN transfected cells compared to si-control transfected cells (Figure 45b). Detection of $Annexin^{+}/7AAD^{-}$ (apoptotic) or $Annexin^{-}/7AAD^{+}$ (necrotic) cells revealed no significant difference between si-control and si-AVEN transfected 1936-MEL cells (Figure 45c). Replication analysis of si-AVEN transfected 1936-MEL cells compared to si-control transfected 1936-MEL cells revealed no significant difference in the VACV titer (Figure 45d). However, the percentage of GFP^{+} 1936-MEL cells was significantly reduced in si-AVEN transfected cells compared to si-control transfected cells 24 hpi (Figure 45e). Percentage of cells in sub-G1 phase was significantly enhanced in GLV-1h68-infected si-AVEN transfected 1936-MEL cells compared to si-control transfected 1936-MEL cells 24 and 48 hpi (Figure 45f). The same experiments were performed with the responder cell line 888-MEL and showed similar results (data not shown).

5 Discussion

Glioblastoma multiforme (GBM) is one of the most frequent gliomas in the adult population and also the most malignant form of brain cancer (WHO IV). Even though extensive pre-clinical and clinical research has been performed, the prognosis and survival time of GBM patients post diagnosis with less than 15 month is still fatal and has not improved much in recent years [63]. Standard of care for GBM is maximal surgical resection followed by radiation and adjuvant and concomitant Temozolomide chemotherapy [113, 116]. Difficulties and challenges of GBM treatment and reasons for treatment failure include amongst others: the highly infiltrative and aggressive growth characteristics of the tumor and the heterogeneity of the disease. In addition, the blood brain barrier that prevents most therapeutics to reach the tumor site. Further the high recurrence rate of the tumor, and the existence of glioma stem cells as well as the immune-specialized location of the tumor within the brain, and the highly immune suppressive tumor microenvironment [70, 259, 260].

There are a great number of alternative therapeutical approaches for the treatment of GBM currently under investigation in preclinical and clinical studies. Those are ranging from molecular targeted therapy, immune and gene therapeutic approaches to oncolytic virotherapy [119, 120, 122, 123]. Focussing on oncolytic virotherapy in this thesis – replication-competent oncolytic viruses are defined to selectively target, infect and destroy cancer cells while leaving healthy non-transformed cells and tissues unharmed. In addition, genetically modified oncolytic viruses may serve as viral vectors delivering genetic materials with anti-cancer or proinflammatory activities to the cancer site. Oncolytic viruses may also function as cancer vaccines that indirectly kill tumor cells by initiation of an antitumor immune response [134, 136, 137, 260]. Currently, there are a great number of oncolytic virus families under investigation for their use as anti-cancer therapeutics and some of them have been tested in clinical trials [133, 138, 139].

One promising candidate for oncolytic virotherapy belonging to the subfamily of *chordopoxvirinae* is VACV. VACV has a great safety potential demonstrated during its use as vaccine virus in the immunization against smallpox. It is a double-stranded DNA virus with the unique characteristic to only replicate in the cytoplasm without integration into the host genome [261].

Although oncolytic viruses in most cases kill tumor cells with high efficiency in cell culture, there are several tumor xenografts that only show reduced replication capacity in animal models [142, 254]. In addition, promising preclinical findings in the context of GBM, but also other malignancies could not be translated to the clinic so far. The oncolytic viruses have been shown

to be safe, however, the therapeutic efficiency remained below the expectations, to date [142, 182, 183].

As reviewed by Dey *et al.* [183] the preclinical models are one explanation for the observed dichotomy between preclinical and clinical findings in the context of oncolytic virotherapy. Most studies have been performed in immunodeficient athymic nude mice implanted with human tumor xenografts where the influence of the adaptive immune system has not been taken into account. To date several factors have been identified to be responsible for reduced therapeutic efficiency: virus neutralization by factors in the blood, inefficient virus spreading in the tumor tissues due to stromal barriers, high interstitial pressure and virus elimination by components of the immune system [134].

One successful approach to improve the outcome of oncolytic virotherapy could be the concept of personalized medicine. Here, the therapeutic efficiency is maximized by screening the cancer patients for specific molecular or immunological factors whereby the most promising therapeutic option is chosen [186, 187]. Biomarkers for identification of patients that respond to a particular therapy is thus overriding [35, 58].

Based on the preclinical and clinical trial failures it became obvious that for development of a successful oncolytic virotherapy or combinatorial approaches a detailed analysis of the tumor and its heterogeneity, the interactions of the oncolytic virus and the tumor microenvironment as well as the impact of the immune system and host defence mechanisms need to be understood [142].

5.1 Oncolytic VACV therapy for GL261 gliomas

The aim of the study was to identify potential physiological factors of the tumor microenvironment and immune system interfering with oncolytic VACV LIVP 1.1.1 in subcutaneous or intracranial murine GL261 glioma models. For this, a comparative experimental approach was investigated with respect to the genetic background (C57BL/6 vs. Balb/c) and immunologic status (immunocompetent wild-type vs. immunodeficient athymic) of the host.

5.1.1 Comparison of the VACV GLV-1h68 and LIVP 1.1.1 for oncolytic VACV therapy of GL261 gliomas

In initial cell culture experiments VACV replication and relative survival of GL261 glioma cells after infection with LIVP 1.1.1 an attenuated VACV wild-type isolate of the LIVP strain and the even more attenuated VACV GLV-1h68 were compared. Sequencing studies demonstrated that both VACVs have a disruption in the Tk gene locus (Chen, *et al.* personal communication)

resulting in enhanced tumor specificity and reduced virulence [193, 194]. As expected, the less attenuated wild-type isolate LIVP 1.1.1 showed a better infectivity, replication capacity and virus-mediated tumor cell killing in an MOI-dependent manner compared to the triple mutant GLV-1h68. The observed differences between LIVP 1.1.1 and GLV-1h68 can be explained by observations of Chen *et al.* [262], demonstrating that the number of inserted foreign expression cassettes correlated with the efficiency of virus replication in different cell lines. The less expression cassettes were included, the more virus replication took place. For both VACVs the intracellular virus titers were higher 24-72 hpi than the titers detected in the supernatants. This indicates that the amount of assembled IMVs within the host cells and cell membrane associated CEVs are higher than the number of secreted EEV and IMV particles in the supernatant.

It is important to note, that although the GL261 glioma cells were infected with GLV-1h68 (20-40%), the virus titer of GLV-1h68-infected cells and supernatants was far below the virus titer of the initial virus inoculum at all time points. The results further indicate that GL261 cells are susceptible for infection with LIVP 1.1.1 and thus for all future experiments this oncolytic virus has been used.

5.1.2 Establishment of subcutaneous and intracranial GL261 tumor models

As reviewed by Stylli *et al.* [263] an optimal preclinical murine glioma model is characterized by the following properties: invasive and angiogenic tumor growth, cellular heterogeneity, genetic and histologic similarities to human gliomas, an orthotopic location allowing tumor-stroma interactions, and not being immunogenic in immunocompetent hosts. Finally the model should be reproducible, predictable and it should imitate the therapeutic responsiveness.

The GL261 glioma model which was chosen for this study is termed the “gold standard model” for glioma research [234]. GL261 is a syngeneic GBM mouse model which allows studies in immune competent C57BL/6 wt mice [264]. The model was initially developed by Seligman and Shear by intracranial implantation of 20 methylcholanthrene pellets into mouse brains [265]. The morphology of GL261 cells is described to be similar to human GBM cells and there are several markers and mutations which the cells do have in common [264]. GL261 tumor growth is infiltrative and invasive with areas of necrosis, and further, the model is characterized as non- or moderate immunogenic [234, 264, 266].

Due to the purpose of this study the tumor cells were implanted either at subcutaneous or orthotopic location and in different mouse strains. All of the present models showed efficient gliomagenesis (~60-100%) with major differences between athymic and wild-type mice as well as reproducible tumor growth rates before and after treatment which was in line with the

literature [266]. In the subcutaneous models, tumor growth was monitored with a digital caliper and in the orthotopic models by indirect parameters or MRI. The study revealed that subcutaneous tumors of athymic mice reached the "time of injection" which was defined as point when a tumor volume of 200-400 mm^3 was detected, about 7 days faster in comparison to C57BL/6 wt mice. The time of injection in Balb/c athymic mice was 11-13 dpimp, in C57BL/6 athymic mice 12-13 dpimp and in C57BL/6 wt mice 17-21 dpimp. One possible explanation for the decelerated tumor growth could be the residual immunogenicity in these mice. Though, as the GL261 glioma cells are syngeneic with the genetic background of the C57BL/6 wt mice it is assumed that this effect is only minimal. As reviewed in detail by Manjili [267] another explanation could be the different endogenous IFN-γ levels of the host that support or inhibit tumor formation: High endogenous IFN-γ levels as in wild-type mice prevent tumor formation whereas mice with low endogenous IFN-γ levels like athymic nude or SCID mice are described to be more susceptible for tumor formation. As described in 1.1.4, IFN-γ is a major component of the cancer immunoediting concept. Here, IFN-γ is involved mainly in the first two phases "elimination" and "equilibrium" by forcing the immunogenic phenotype of developing tumors [49, 50]. In the orthotopic model the time of injection was reached after 14 days in athymic mice and after 17 days in wild-type mice.

5.1.3 Assessment of factors influencing the outcome of VACV infection and replication in the various mouse models

Viral replication was exclusively supported in subcutaneous tumors of Balb/c athymic mice termed as "responder" but in none of the C57BL/6 tumor models termed as "non-responder" (Figure 46).

The analysis of the tumor microenvironment by immunohistochemistry and FACS analysis revealed a significant upregulation of MHCII on GL261 tumor cells in C57BL/6 wt mice in comparison to Balb/c athymic mice. In literature there is evidence that GL261 glioma cells upregulate this molecule after stimulation with or overexpression of IFN-γ. Under normal conditions they do not express MHCII [234, 235]. By stimulating GL261 tumor cells with IFN-γ an upregulation of MHCII on the cell surface was confirmed in cell culture in this study. This phenotypic change was associated with reduced virus replication and reduced virus-mediated cell death after infection with VACV LIVP 1.1.1. In addition, the comparison of MHCII expression and virus replication in C57BL/6 wt mice and C57BL/6 IFN-γ KO mice revealed that also *in vivo* GL261 tumor cells were sensitive to IFN-γ: In C57BL/6 IFN-γ KO mice there was a significant reduction of MHCII expression, but on the other hand virus replication was significantly

improved in comparison to C57BL/6 wt mice. Besides, experiments with tumor homogenates isolated from Balb/c athymic and C57BL/6 wt mice demonstrated that the IFN-γ mediated effects on the IFN-γ sensitive GL261 glioma cells were reversible.

It can be concluded that in the subcutaneous tumor milieu of Balb/c athymic mice the threshold level of IFN-γ was too low to induce a $MHCII^+$/VACV non-permissive status of the GL261 tumor cells.

The comparison of the tumor microenvironment of the three mouse strains revealed that the C57BL/6 athymic mice were in an "intermediate state" between C57BL/6 wt and Balb/c athymic mice (Figure 46). However, the results were controversial. The biomarker profiling revealed that all biomarker concentrations were in between the C57BL/6 wt and Balb/c athymic mice although not significantly different to the latter. Flow cytometry analysis revealed that in the tumors highest immune cell concentrations were found in C57BL/6 wt mice. In the blood significantly more $CD19^+$ B-lymphocytes, $CD49^+$ NK cells, $CD11b^+/Ly6c^+$ dendritic cells, $CD11b^+/CD11c^+$ immature myeloid cells and $CD11b^+/Gr1^+$ MDSCs were detected in C57BL/6 athymic mice compared to the Balb/c athymic mice. The quantification of the MHCII levels in tumors of these mice was not significantly different between C57BL/6 athymic and Balb/c athymic mice but the histological analysis indeed represented an intermediate state with a patchy-like distribution of MHCII expression in C57BL/6 athymic mice, absent MHCII expression in Balb/c athymic mice and massive expression of MHCII in C57BL/6 wt mice. However, analysis of the replication capacity with only 13% of the initial virus inoculum left 7 dpi in C57BL/6 athymic mice revealed in contrast similarities to the C57BL/6 wt mice and significant differences to Balb/c athymic mice.

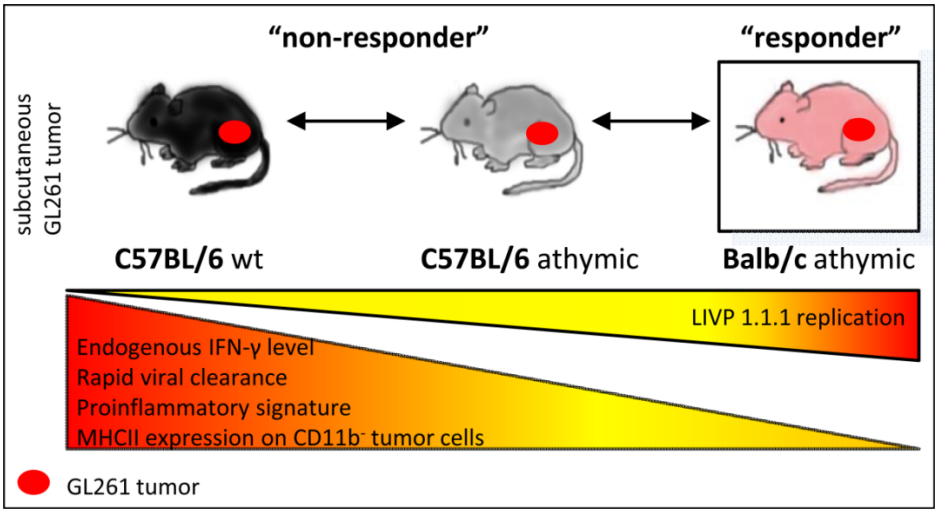

Figure 46: Schematic overview on factors influencing VACV LIVP 1.1.1 replication in subcutaneous GL261 glioma models.

It can be assumed that based on the genetic background of these mice and although the IFN-γ levels were lower in the athymic mice than in the wild-type mice the threshold level of IFN-γ was high enough to change the phenotype of the tumor cells resulting in a VACV non-permissive state. The differences between the two C57BL/6 mouse strains can be explained by the source of IFN-γ production which in the first instance are $CD4^+$ T-lymphocytes, $CD8^+$ T-lymphocytes and NK-cells but also B-cells, NKT-cells and professional antigen-presenting cells (APCs) [231].

It is well known that the outcome of diseases in mice infected with several intracellular pathogens (*e.g. Leishmania major* or bacterial septic peritonitis) is dependent on the genetic background and an individual T_H1/T_H2 balance [268–270]. C57BL/6 is classically defined as prototypical T_H1 mouse strain and Balb/c is defined as T_H2 mouse strain [268, 269, 271, 272]. In addition, innate immune cells such as macrophages, also show different characteristics in the two mouse strains especially in response to certain pathogenic stimuli [269, 271–273].
In line with the findings observed for VACV replication in this study, are the results of studies on the disease mechanism of ectromelia virus (ECTV) infection, the causative agent of mousepox [268, 270]. In case of mousepox disease, C57BL/6 mice are termed resistant and Balb/c mice as susceptible mouse strain [268, 270, 274].
The strain-dependent resistance is controlled by different gene complexes: paradigmatic examples are the fifth component of complement C5, the MHC gene complex, NK cell gene complex and a gene complex of selectin. The strain-dependent resistance is further dependent on the capacity and time frame of T_H1 cytokine production (IFN-γ, IL-2 and IL-12) and antiviral cytotoxic T-lymphocyte response [268, 270]. Further, inhibition of IFN-γ with monoclonal neutralizing antibodies in the resistant C57BL/6 mice has been demonstrated to result in diminished NK and CTL responses and in the development of fulminant mousepox with a course of disease comparable to susceptible Balb/c mice [268, 274]. Taken together and with regard to the subcutaneous tumor models the genetic background of the host was affirmed to have a major impact on VACV LIVP 1.1.1 replication [219].

Reasons for the observed difference of LIVP 1.1.1 replication in the Balb/c athymic mice at subcutaneous and orthotopic locations and the finding that there was no significant difference in the orthotopic GL261 gliomas of C57BL/6 wt and Balb/c athymic mice might be the following: An explanation for the reduced virus yield in the orthotopic model in addition to the IFN-γ sensitivity of the tumor cells could be the different and special microenvironment of the tumor within the brain tissues. The brain in contrast to the periphery is defined as an immune privileged or immune specialized organ [126, 275–277]. The differences between the immune

system in the brain and the periphery include a reduced number of antigen-presenting cells, a restricted number of activated lymphocytes that can enter the brain tissues, no traditional lymphatic system present in the brain and the fact that engrafted tissues in the CNS are slower rejected than transplants elsewhere in the body [126, 275–277].

Factors different to the subcutaneous tumor microenvironment are further microglia and astrocytes that are recruited to the tumor site. This finding is in line with the literature describing that gliomas are heavily infiltrated by microglia but also astrocytes [41, 86, 96, 104, 188, 189]. In addition, those cell types are the first line of defense in case of CNS injury or infection [189, 241, 242]. It therefore can be supposed that microglia and astrocytes are the first cells that interact with the injected oncolytic VACV. Based on this, microglia and astrocytes in the context VACV infections were extensively analyzed in the present study. The hypothesis that microglia and astrocytes might function as VACV decoys was supported by the following findings: In cell culture it was shown that IMA 2.1 astrocytes and BV-2 microglia become infected by VACV but do not further support active viral replication. In direct co-cultures of BV-2 microglia and GL261 glioma cells the presence of BV-2 cells reduced the virus titer of the culture in comparison to cultures with GL261 glioma cells only. This indicates that microglia and glioma cells compete for virus uptake in this cell culture setting. Further glioma and microglia cells are interacting with each other as demonstrated by indirect co-culture experiments that revealed factors released by GL261 glioma cells that inhibited the VACV replication and VACV-mediated cell death of the BV-2 microglial cells. In addition, BV-2 microglia and GL261 glioma cells showed different cell death characteristics with more BV-2 cells undergoing apoptosis whereas the major proportion of GL261 glioma cells showed necrotic characteristics after virus infection.

Based on these findings it can be concluded that besides the IFN-γ sensitivity of the tumor cells which influences the final outcome of VACV replication in the individual microenvironment, microglia and astrocytes in the orthotopic tumor location are the most important additional factors that do prevent viral replication in the GL261 glioma model. IFN-γ concentrations in the orthotopic location were not measured directly so far, however, measurement of MHCII as indirect parameter by immunohistochemistry revealed that at least gliomas implanted in C57BL/6 wt mice were positive for this molecule similar to tumors implanted at the subcutaneous location in these mice.

5.1.4 Occurrence of individual tumor microenvironments in the individual Gl261 glioma models

The comparative experimental setup applied in this study mimics the clinical situation that different patients suffering on the same disease display individual tumor microenvironments due to individual immunologic and genetic backgrounds. The therapeutic outcomes may also be different which have led to the concept of personalized medicine. Subcutaneous or orthotopic implantation of glioma cells (GL261) into mouse strains with different genetic (C57BL/6 *vs*. Balb/c) and immunologic (wt *vs*. athymic) backgrounds resulted in individual tumor microenvironments that respond to oncolytic VACV therapy with different outcomes. In the context of the tumor microenvironment the genetic background of the host including genetic polymorphisms of cytokine receptors or the tumor itself are described as factors responsible for a diverse immune cell infiltration and activation [221]. Additionally, tumor-host interactions are controlled by soluble factors released from the cells in the tumor micromilieu and the tumor cells [29, 187].

5.1.4.1 The tumor microenvironment in the subcutaneous tumor models and the role of IFN-γ in this context

Endogenous IFN-γ present or absent in the GL261 tumor microenvironment of C57BL/6 wt or C57BL/6 IFN-γ KO mice was identified as factor responsible for VACV LIVP 1.1.1 inhibition in the wild-type model. IFN-γ is a proinflammatory cytokine that together with type I IFNs (IFN-α, β) plays a crucial role in the control of intracellular pathogens [231]. Intracellular defense mechanisms in case of VACV infection include the effector enzymes iNOS and IDO, activated downstream of the IFN-γ receptor, that are responsible for direct blocking of VACV replication [278, 279]. Further, IFN-γ blocks preferentially late gene transcription and VACV genome replication in mouse fibroblasts [280]. It also targets genes of the transcription factor interferon regulatory factor 1 (IRF-1) that are crucial for induction of an antiviral state. In addition to the direct IFN-γ induced antiviral effects, IFN-γ also induces pro-apoptotic and anti-proliferative effects, that negatively influence viral replication [231].

The interplay between viruses and the interferon system as well as an overview on various resistance mechanisms including a soluble IFN-γ receptor expressed by VACV or IFN-γ-binding proteins are reviewed in detail by Schroder *et al.* [231], Chesler *et al.* [281] and Randall *et al.* [282]. However, it is interesting to note that there are major differences between oncolytic

viruses, as for example oncolytic adenovirus was found to be efficacious in GL216, despite inducing IFN-γ in the tumors [283].

In the actual study, induction of tumor cell death by IFN-γ was excluded as reason for impaired virus replication in IFN-γ pre-incubated GL261 glioma cells in cell culture. Flow cytometry revealed a reduced proliferation of IFN-γ-stimulated cells (72 hours), however, no significant differences between GL261 cells cultured with IFN-γ, IL-4 (10 ng/ml) or without stimulation were detected.

IFN-γ is described to be a factor not only modulating innate, but also adaptive immunity [231]. Besides a major role in T_H1 immune response as described in 1.1.3, IFN-γ is involved in recruitment of immune cells to sites of inflammation by expression of adhesion molecules and chemokines. Factors upregulated by IFN-γ are *e.g.* IP-10, MCP-1 or MIP-1β [230, 231].

The biomarker profiling of the subcutaneous tumors on the day of infection in the three different mouse models revealed that all of these factors were differentially expressed with highest concentrations in C57BL/6 wt mice, followed by C57BL/6 athymic and Balb/c athymic mice. The expression levels of IFN-γ were determined at the tumor sites as well, however, the differences were not statistically different. Therefore, IP-10 was used as surrogate marker for IFN-γ induction. As described by Rossi and Zlotnik [284], chemokines such as IP 10 are relatively resistant to inactivation, and have a long half-life *in vivo*. In addition, the half-life of IFN-γ is limited to 7-9 hours but its effect on the target cells is present for up to for 4 weeks [285]. The diagnostic advantage of IP 10 compared to IFN-γ is that as an induced protein, its release is not undulating and staged and it has a higher *in vivo* and *ex vivo* stability [286].

In addition, the diverse expression pattern of MHCII which was detected on the GL261 tumor cells in these models correlated with the concentration gradient of IP-10 and further IFN-γ induced chemokines.

To solve the question whether MHCII expression in GL261 cells is only a marker of IFN-γ exposure or directly relevant to the lack of virus replication detected *in vivo,* Simvastatin a factor known to repress IFN-γ induced MHCII expression on target cells was applied [237, 238]. The study revealed that Simvastatin reduced MHCII on IFN-γ pre-treated GL261 glioma cells but the reduced virus titer of IFN-γ pre-incubated cells could not be reversed by Simvastatin treatment. Treatment of C57BL/6 wt mice with multiple intraperitoneal injections of Simvastatin prior to virus infection did not significantly increase the virus titer in comparison to mice not treated with Simvastatin. But MHCII expression levels on $CD11b^-$ tumor cells were significantly reduced.

In literature it is described that IFN-γ upregulates MHCII not only on professional APCs for antigen-specific $CD4^+$ T-lymphocyte activation, but also on nonprofessional APCs such as tumor

cells that do not express MHCII constitutively [231]. In case of glioma cells, upregulation of MHCII on the cell surface is described in detail in [232, 287].

Based on this, the responsiveness and capability of murine and human tumor and immune cells to upregulate MHCII following stimulation with recombinant IFN-γ was investigated. It is known, that most cancer cells have deficient IFN responsive pathways or develop mutations resulting in IFN-γ-insensitivity [288, 289]. However, in the present study besides immune cell lines such as BV-2, IMA2.1 and J774, GL261 glioma cells were the only cancer cell line that showed the capability to upregulate MHCII and thus to be sensitive to IFN-γ exposure. Huysentruyt *et al.* [290] describes highly invasive or metastatic tumors, such as GBM, which contain neoplastic cells with mesenchymal/macrophage/microglia like properties including phagocytosis or antigen expression.

Taking together the findings of the analysis of the tumor microenvironment in GL261 tumors of C57BL/6 wt mice with an up-regulation of MHCII on the tumor cell surface associated with a highly "proinflammatory signature" revealed that these tumors are in an immunologically active state. There are several reports describing the presence of two immunologically distinct cancer phenotypes – an immunologically silent form and an immunologically active form.

The immunologically active form is associated with immune effector functions resulting in immune mediated tissue destruction and tumor rejection. Tumors that are diagnosed to be in an immunologically active state display a better prognosis and treatment response - especially in case of cancer immunotherapy [58, 221, 291]. Central to the inflammatory active status is the IFN-γ-signal transducer and activator of transcription (STAT-1)- IRF-1 axis [291]. The nuclear transcription factor IRF-1 induced by IFN-γ is associated with inflammation, cell proliferation and apoptosis [292]. In a study of Murtas *et al*. [291], the authors showed a strong correlation between IFN-γ and TNF-α induced IRF-1 activation and nuclear translocation in connection with different intrinsic properties of the cancer cells. The authors concluded that different cancer cells have a different threshold to respond to stimulation with cytokines. As a result they used the induction of IRF-1 by IFN-γ in tumor cells *in vitro* to make predictions about the responsiveness of the tumor cells in the tumor microenvironment *in vivo* [291]. Kaplan *et al.* [289] demonstrated that one of the major targets of IFN-γ induced anti-tumor actions are the tumor cells themselves by enhancing their immunogenicity.

Translating these findings to the actual study with GL261 glioma cells, it was assumed that the same is true for the sensitivity of these tumor cells and their responsiveness to diverse concentrations of endogenous IFN-γ levels in the tested mouse models [219].

In summary the actual study is in line with research findings by Yu-Ping Liu *et al.* [288], describing the induction of a constitutive antiviral state in tumor cells by a constitutively low secretion of type I IFNs by tumor infiltrating cells. In addition, Monsurrò *et al.* [293] described an intrinsic anti-viral state and thus two distinct molecular phenotypes of pancreatic adenocarcinoma cells based on a diverse expression profile of interferon-stimulated genes in these cells.

5.1.4.2 The tumor microenvironment in the orthotopic tumor models and the capacity of microglia and astrocytes to function as VACV decoys

In the present study it was shown that orthotopic non-infected GL261 gliomas were heavily infiltrated by microglia and astrocytes. Additionally the amounts of microglia and astrocytes were not significantly different between PBS- and LIVP 1.1.1-injected GL261 gliomas. These findings are in line with the literature describing that glioma cells do release factors to attract immune cells, in the first instance microglial cells, to the tumor sites [85, 97, 246]. The results further indicate that microglia and astrocytes are not recruited to the tumor due to virus infection, but rather as a consequence of the tumor or the injection. This finding is in line with a study of Geletneky *et al*. [294], demonstrating the same is true for intracranial parvovirus H-1 (H-1PV) injection of a RG-2 glioma model in immunocompetent rats.

As those cell types are known to be the first line of defense in case of CNS injury or infection it is assumed that they are the first cell types interacting with VACV after injection [189, 241, 242]. Analysis of BV-2 microglial cells and IMA 2.1 astrocytes in cell culture revealed that virus replication in these cells was at all analyzed time points below the initial virus inoculum. This implicates that virus infection was abortive and productive replication was not supported in these cells. Further as the virus titer in the supernatant increased only slightly in BV-2 cells but not a bit in IMA 2.1 cells it can be concluded that no virus spreading occurred.

Surprisingly, despite minimal virus replication in BV-2 microglial cells it was shown that infection of these cells with LIVP 1.1.1 resulted in cell lysis in cell culture. Analysis of several cell death characteristics like membrane permeability and DNA fragmentation to distinguish between apoptotic and necrotic cell death, it was shown that LIVP 1.1.1 induced apoptosis in murine BV-2 cells in contrast to Gl261 tumor cells that in majority exhibited the necrotic cell death characteristics.

In literature it is described that oncolytic viruses kill cancer cells by direct oncolysis which is usually a combination of apoptosis, necrosis, pyroptosis or autophagic cell death with an individual virus specific preference [135]. Necrotic cell death is classically termed as immunogenic cell death associated with release of proinflammatory factors and immune

activating mediators, whereas apoptosis is classically termed non-immunogenic. However, recent findings observed also forms of immunogenic apoptosis, *e.g.* following chemotherapy [134]. Poxviruses including VACV are described to cause a lytic infection resulting in necrotic cell death and they are known to encode for proteins that inhibit the apoptotic pathway [245, 295, 296]. This is comprehensible as apoptosis is a crucial non-specific anti-viral effect as an early death of an infected cell results in a significant reduction of virus progeny, increased phagocytosis of virus particles and reduced virus spread [297]. There are several examples where apoptosis was detected mainly in immune cell types *e.g*. in macrophages and in most cases it was associated with an abortive VACV infection like for Chinese hamster ovary cells, for B-lymphocytes, dendritic cells or monocytes [245, 298, 299]. As described by Taylor *et al.* [295] induction of apoptosis in immune cells following VACV infection could be an immune evasion strategy of the virus, or in contrast an anti-viral mechanism initiated by the infected cell. In a recent review by Woller *et al.* [134] it was discussed that oncolytic viruses induced programed apoptosis, necroptosis or necrosis-like programed cell death with characteristics of both apoptosis and necrosis in contrast to the classical cell death modalities.

The mutual interaction and influence of microglia cells and glioma cells is described in detail in 1.2.1.1. Glioma cells do release factors that suppress the immune functions of microglia and force the shift to the M2 phenotype of these immune cells [85, 246]. However, the debate about the composition and amount of M1 and M2 microglia within gliomas is controversial and it is assumed that the predominance of one phenotype is time dependent [98, 101, 102, 123, 246]. Glass and Synowitz [188] observed that tumor-associated macrophages in gliomas have an aberrant immune type which shares both M1 and M2 features.

Broder *et al.* [300] reported that human primary macrophages do not support productive infection of VACV which is consistent with results from primary mouse and rabbit macrophages.

In a study of Byrd *et al.* [298] it was demonstrated that primary human monocyte derived macrophages (MDMs) with either M1- (GM-CSF-stimulated) or M2- (M-CSF-stimulated) phenotype do support VACV replication in contrast to AB-serum-derived MDMs.

In the actual study, both phenotypes, M1 and M2, induced in the microglial cell line BV-2 were analyzed for VACV infection, replication and VACV-mediated cell death. The results have been summarized in Table 15. The study revealed, that the use of LPS or IFN-γ or a combination of both, inducing the M1 phenotype resulted in an abortive infection of LIVP 1.1.1 by further reducing the virus yield. Treatment with IL-4 leading to the induction of the M2 phenotype showed similar results when compared to unstimulated BV-2 cells, however, infection was very

weak or abortive. Activation of BV-2 cells with LPS and IFN-γ or combination treatment had negative effects on cell proliferation as observed in the MTT assay.

In astrocytic IMA2.1 cells, VACV infection was found to be independent from the status of polarization. IMA2.1 cells were infected by VACV LIVP 1.1.1, however, the infection was abortive. It can be concluded that due to the abortive infection in both astrocytes and microglia, these cells function as VACV decoys and thus prevent efficient oncolytic VACV replication in malignant GL261 gliomas.

5.1.5 Implementation of organotypic brain slice cultures as alternative model for glioblastoma multiforme

Organotypic brain slice cultures (OSCs) represent an optimal link between monolayer cell culture approaches and animal models. OSCs display a preserved cytoarchitecture and cell heterogeneity that allows morphological, biochemical, physiological or pharmaceutical studies and screenings [203, 207, 243]. As an intermediary cell-based system organotypic brain slice cultures were established from both young and adult mice.

There are major differences between young and adult OSCs as described by Mewes *et al*. [203]. Comparison of VACV infection in OSCs prepared from young and adult mouse brains of C57BL/6 wt mice revealed no significant difference. The same was true for the comparison between adult OSCs prepared either from Balb/c or C57BL/6 wt mice. The titers of LIVP 1.1.1 were slightly higher 72 hpi in slices of Balb/c mice which might be due to lower IFN-γ levels in the T_H2-dominant Balb/c mouse strain.

Tumor formation and tumor-specific virus infection was proved by immunohistochemistry and fluorescence microscopy.

Infection of OSCs implanted with GL261-RFP cells resulted not in active viral replication and it was shown that the cells of GL261-RFP tumors were infected initially at the rim of the tumor, but no further progression of the infection was detected at later time. This data resembles the results that were obtained from *in vivo* experiments in mice with intracranial tumors. In comparison, OSCs implanted with U87-RFP cells showed active virus replication and the tumor spheres were well-infected. This is in accordance with a recent study published by Buckel *et al.* [180], demonstrating that LIVP 1.1.1 injection eradicated U87 tumors in subcutaneous xenograft models. It was further shown that this cell line does infiltrate brain slice cultures in an *in vivo*-like manner [204, 254, 301].

Further, the application of BV-2 cells pre-treated with IFN-γ to OSCs implanted with GL261 glioma cells revealed that 24 hpi the glioma cells were stained positive for VACV in contrast to

BV-2 cells. The opposite was true if BV-2 cells were applied to the slice without pre-treatment. This initial finding suggests that the preference of VACV infection in gliomas might be altered by pre-stimulation of microglial cells so that in consequence tumor cells would be infected in the first instance. Taken together, this method supported the *in vitro* and *in vivo* research findings.

5.1.6 Possible therapeutic perspectives and approaches

A possible therapeutic approach to overcome the non-productive infection of microglial and astrocytic cells in glioblastoma treatment could be the application of multiple virus doses to saturate microglia and astrocytes or even a much higher virus dose at the beginning. The route of virus application may also be very important: Intratumoral application causes an injury leading to further recruitment of microglial cells. However, a systemic virus injection may not be sufficient in glioblastoma therapy and it needs to be elucidated whether a particular virus is able to cross the blood brain barrier as paradigmatically described for parvovirus 1 [182, 294]. Another promising approach tested preclinically is the systemic administration of infected carrier cells such as neural, mesenchymal or adipose derived stem cells with a natural tumor tropism. The use of these carrier cells shield the oncolytic viruses from serum host factors and help to circumvent the host-antiviral immune response and serve in addition as virus factories on the way to the tumor site. However, to date there are major limitations to overcome before clinical application [182, 183, 302, 303]. The intranasal route is another possibility which is discussed for delivery of therapeutic agents, including oncolytic viruses, to the tumor site in the brain. It is with regard to clinical application practicable, painless, non-invasive and it circumvents the blood brain barrier [182].

As discussed and reviewed by Koks *et al.* [182] there is a major change in the field of oncolytic virus research: There is a shift from the assumption that the immune system is exclusively an inhibitory factor, but rather can be used as supportive component. Several studies with immunocompetent hosts revealed evidence that the proinflammatory antitumor immune response might be improved by application of oncolytic viruses. And this in consequence improves the overall therapeutic efficiency. However, it needs to be elucidated in detail in future studies.

The same is true for possible treatment schedules combining oncolytic viruses with immunostimulatory, -modulatory or -inhibitory agents. As described by Fulci *et al.* [304, 305] glioma-bearing rats that received cyclophosphamide (CPA) a chemotherapeutic agent with immunosuppressive function, before injection of the oncolytic virus (HSV-1 derivative), had a

significantly improved survival time compared to animals without pre-administration of CPA. CPA has been shown to improve viral replication, oncolysis and reduced the amount of microglia, macrophages and IFN-γ in the tumors. Therefore, it could be a very interesting approach to further study the GL261 glioma model in combination with the oncolytic VACV LIVP 1.1.1, as well. In another approach the authors depleted phagocytes with clodronate liposomes by systemic delivery and *ex vivo* in brain slice cultures. The data indicated that tumor infiltrating microglia and macrophages directly affected clearance of an oncolytic virus derived from HSV 1. However, in the present study, with the subcutaneous GL261 model, depletion of phagocytic cells had no impact on VACV replication. However, the composition of macrophages/microglia in intratumoral and subcutaneous tumors is diverse.

5.2 Impact of the anti-apoptotic factor AVEN on oncolytic VACV GLV-1h68 infection of cancer cells

Apoptosis is besides the necrotic and autophagic cell death classified as a typical cell death mechanism [306]. Apoptosis is essential for tissue homeostasis and development and thus, was for long described as non-immunogenic cell death in contrast to necrotic cell death [134]. However, also apoptosis-induced immunogenic cell death events have been reported.

Apoptotic cell death is a highly controlled process, characterized by the activation of the caspase cascade, morphological changes, formation of apoptotic bodies, loss of mitochondrial membrane integrity and DNA fragmentation [134]. The caspase cascade is either activated by an extrinsic or an intrinsic pathway resulting in apoptosis [307, 308]. A central part of the intrinsic pathway is the apoptosome complex. The formation of this complex is the result of a Bcl-2 family-regulated release of cytochrome C from the mitochondria into the cytosol that binds to the apoptosis protease activating factor 1 (APAF-1). A conformational change of APAF-1 results finally in the binding of the initiator procaspase-9 following activation of several effector caspases [309, 310]. A number of endogenous apoptosome regulators has been described including the anti-apoptotic factor AVEN [311].

In contrast, necrotic cell death is a less controlled and coordinated process which is characterized by swelling of organelles and cytoplasm, fracturing of the cell membrane and release of components of the cytoplasm inducing inflammation [134].

Viruses have evolved diverse strategies to block many different cell death mechanisms as virus replication is dependent on host cell factors and needs to be completed before lysis. Induction of cell death is facilitated after completion of the infection cycle to release virus progeny [306].

In the present study, the expression and function of the anti-apoptotic protein AVEN in different cancer cell lines was analyzed. Aim was to elucidate whether there is a specific role or function of AVEN for successful infection and replication of GLV-1h68 in tumor cells of different histological background (888-Mel, 1936-MEL, GI-101A, HT-29). Initially virus-mediated cell death and replication was tested in these cells. It was shown that 888-MEL and 1936-MEL were responder cell lines whereas virus-mediated cell death in GI-101A and HT-29 was impaired. However all cell lines showed active viral replication after 24 hpi (888-MEL, 1936-MEL, HT-29) and 48 hpi (GI-101A). Taken together, many aspects of oncolytic virotherapy have already been studied in these cells and the results of the present study were in line with the literature [146, 149, 150, 153, 225, 312–315].

AVEN as target gene has been chosen based on gene expression data (unpublished data, J. Reinboth) and based on Boolean models (A. Cecil, unpublished data). In addition, there are actual studies described in literature showing that elevated AVEN gene expression levels were found in adult acute leukemia patients with worse prognosis [217]. Further, Eißmann *et al.* found an oncogenic potential of AVEN during the evolution of hematopoietic neoplasms [316]. Based on a microarray study, Kutuk *et al.* [317] described decreased nuclear AVEN gene expression levels in breast cancer tissue compared to healthy breast tissues associated with resistance to apoptosis in the cancer tissue induced by DNA damage.

In the present study, AVEN was ubiquitously expressed in cells of all four human tumor cell lines which is in accordance with the literature [255].

SiRNA knockdown of AVEN in HT-29 cells revealed an upregulation of apoptotic characteristics with an increase of DNA fragmentation and activation of caspase 9. In addition, the analysis revealed that down-regulation of AVEN resulted in a significant lower percentage of GFP^+ VACV-infected HT-29 cells compared to cells pre-incubated with si-control. Furthermore, the replication was significantly reduced. Similar results were obtained for si-RNA knockdown of 1936-MEL.

It is important to note, that these were initial experiments and further biochemical assays need to be performed in future studies to elucidate the mechanisms behind the reduced virus replication in those cells that showed enhanced apoptotic characteristics. However, this study is in line with the literature demonstrating that poxviruses developed mechanisms to actively suppress apoptotic cell death [245, 295, 296]. AVEN was detected as factor in the tumor cells which is able to modify the outcome of VACV infection. It is suggested to develop an oncolytic VACV which will be supportive for VACV replication in cancer cells that express elevated levels of the anti-apoptotic factor AVEN. The resulting oncolytic VACV might express a siRNA gene against AVEN induced by a very late promoter which would be activated after efficient virus replication

and which would further support cell death of the cancer cells. It is assumed that this would significantly support tumor shrinkage *in vivo*.

5.3 Conclusion

Within this work the interactions between tumor cells and VACV have been analyzed. Furthermore the impact of the immune system with regard to the capacity of VACV replication in cell culture and therapeutic efficiency in mouse models has been studied. In summary, it has been shown that GL261 glioma cells are sensitive for IFN-γ stimulation. As a consequence, dependent on the endogenous IFN-γ levels in the tumor microenvironment, an antiviral state in the tumor cells was induced, preventing efficient VACV replication in the corresponding tumor model. In addition, IP 10 and MHCII have been identified as prognostic markers, correlating with endogenous IFN-γ levels and the respective capacity of VACV replication. In the highly aggressive GL261 glioma model, the IFN-γ-induced anti-tumor effects described for the immunological active phenotype were not prominent enough to lead to a therapeutic success. In addition, in the orthotopic tumor location microglia and astrocytes have been identified to function as VACV traps, preventing virus infection of the tumor cells. Finally, it has been shown that VACV replication was negatively influenced after down-regulation of the anti-apoptotic factor AVEN in various tumor cells.

Taken together, important host factors that have major impact on the therapeutic efficiency of VACV infection were identified in the present study. The knowledge about parameters that prevent efficient virus replication will help to further improve oncolytic VACV therapy for example by the development of combination treatments or design of alternative VACV strains. Further, for successful therapy development, the testing of patients prior to therapy with regard to the genetic and immunologic background is highly recommended and thereby as consequence translates the concept of personalized medicine into the future of oncolytic virus therapy. Although more comprehensive studies in the clinic are needed, the endogenous IFN-γ level, IFN-γ sensitivity of cancer cells or MHCII expression on cancer cells might be used as possible biomarkers for oncolytic VACV therapy in future trials.

6 References

1. Ferlay J, Soerjomataram I, Ervik M, Dikshit R, Eser S, Mathers C, Rebelo M, Parkin DM, Forman D, Bray F: **GLOBOCAN 2012 v1.0, Cancer Incidence and Mortality Worldwide**. *IARC Cancer Base No 11 [Internet] Available from http//globocan.iarc.fr, accessed 25/06/2015* 2013.

2. Ferlay J, Soerjomataram I, Dikshit R, Eser S, Mathers C, Rebelo M, Parkin D., Forman D, Bray F: **Cancer incidence and mortality worldwide : Sources , methods and major patterns in GLOBOCAN 2012**. *Int J Cancer* 2015, **386**:359–386.

3. **http://www.who.int/mediacentre/factsheets/fs297/en/#**

4. Weinberg R: **How Cancer Arises**. *Sci Am* 1996, **275**:62–70.

5. Tian T, Olson S, Whitacre JM, Harding A: **The origins of cancer robustness and evolvability.** *Integr Biol (Camb)* 2011, **3**:17–30.

6. Merlo LMF, Pepper JW, Reid BJ, Maley CC: **Cancer as an evolutionary and ecological process.** *Nat Rev Cancer* 2006, **6**(December):924–935.

7. Polyak K, Haviv I, Campbell IG: **Co-evolution of tumor cells and their microenvironment**. *Trends Genet* 2009, **25**(December):30–38.

8. Grivennikov SI, Greten FR, Karin M: **Immunity, Inflammation, and Cancer**. *Cell* 2010, **140**:883–899.

9. Tlsty TD, Coussens LM: **Tumor stroma and regulation of cancer development.** *Annu Rev Pathol* 2006, **1**:119–150.

10. **http://www.iarc.fr/en/publications/pdfs-online/wcr/2003/wcr-3.pdf**

11. Futreal PA, Coin L, Marshall M, Down T, Hubbard T, Wooster R, Rahman N, Stratton MR: **A census of human cancer genes.** *Nat Rev Cancer* 2004, **4**(March):177–183.

12. Weir B, Zhao X, Meyerson M: **Somatic alterations in the human cancer genome**. *Cancer Cell* 2004, **6**(November):433–438.

13. Knudson AG: **Two genetic hits (more or less) to cancer.** *Nat Rev Cancer* 2001, **1**(November):157–162.

14. Loeb KR, Loeb LA: **Significance of multiple mutations in cancer.** *Carcinogenesis* 2000, **21**:379–385.

15. Balmain A, Gray J, Ponder B: **The genetics and genomics of cancer.** *Nat Genet* 2003, **33 Suppl**(march):238–244.

16. Fearon ER, Vogelstein B: **A genetic model for colorectal tumorigenesis.** *Cell* 1990, **61**:759–767.

17. Hanahan D, Weinberg RA: **The Hallmarks of Cancer**. *Cell* 2000, **100**:57–70.

18. Anand P, Kunnumakara AB, Sundaram C, Harikumar KB, Tharakan ST, Lai OS, Sung B, Aggarwal BB: **Cancer is a preventable disease that requires major lifestyle changes**. *Pharm Res* 2008, **25**:2097–2116.

19. Aggarwal BB, Vijayalekshmi R V., Sung B: **Targeting inflammatory pathways for prevention and therapy of cancer: Short-term friend, long-term foe**. *Clin Cancer Res* 2009, **15**:425–430.

20. Hanahan D, Weinberg RA: **Hallmarks of cancer: the next generation.** *Cell* 2011, **144**:646–74.

21. Visvader JE: **Cells of origin in cancer.** *Nature* 2011, **469**:314–322.

22. Rejniak KA, McCawley LJ: **Current trends in mathematical modeling of tumor-microenvironment interactions: a survey of tools and applications.** *Exp Biol Med* 2010, **235**:411–423.

23. Kitano H: **Cancer as a robust system: implications for anticancer therapy.** *Nat Rev Cancer* 2004, **4**(March):227–235.

24. Wong KM, Hudson TJ, McPherson JD: **Unraveling the genetics of cancer: genome sequencing and beyond.** *Annu Rev Genomics Hum Genet* 2011, **12**:407–430.

25. Marusyk A, Polyak K: **Tumor heterogeneity: Causes and consequences**. *Biochim Biophys Acta - Rev Cancer* 2010, **1805**:105–117.

26. Babayan A, Hannemann J, Spötter J, Müller V, Pantel K, Joosse SA: **Heterogeneity of Estrogen Receptor Expression in Circulating Tumor Cells from Metastatic Breast Cancer Patients**. *PLoS One* 2013, **8**:1–11.

27. Eroles P, Bosch A, Alejandro Pérez-Fidalgo J, Lluch A: **Molecular biology in breast cancer: Intrinsic subtypes and signaling pathways**. *Cancer Treat Rev* 2012, **38**:698–707.

28. Goubran HA, Kotb RR, Stakiw J, Emara ME, Burnouf T: **Regulation of tumor growth and metastasis: the role of tumor microenvironment.** *Cancer Growth Metastasis* 2014, **7**:9–18.

29. Allen M, Louise Jones J: **Jekyll and Hyde: the role of the microenvironment on the progression of cancer.** *J Pathol* 2011, **223**:162–76.

30. Egeblad M, Nakasone ES, Werb Z: **Tumors as organs: Complex tissues that interface with the entire organism**. *Dev Cell* 2010, **18**:884–901.

31. Kalluri R, Zeisberg M: **Fibroblasts in cancer.** *Nat Rev Cancer* 2006, **6**(May):392–401.

32. Carmeliet P, Jain RK: **Angiogenesis in cancer and other diseases.** *Nature* 2000, **407**:249–257.

33. Bergers G, Benjamin LE: **Tumorigenesis and the angiogenic switch.** *Nat Rev Cancer* 2003, **3**:401–410.

34. Fridman WH, Pagès F, Sautès-Fridman C, Galon J: **The immune contexture in human tumours: impact on clinical outcome.** *Nat Rev Cancer* 2012, **12**:298–306.

35. Angell H, Galon J: **From the immune contexture to the Immunoscore: the role of prognostic and predictive immune markers in cancer.** *Curr Opin Immunol* 2013, **25**:261–7.

36. Mantovani A, Romero P, Palucka AK, Marincola FM: **Tumour immunity: effector response to tumour and role of the microenvironment**. *Lancet* 2008, **371**:771–783.

37. Fridlender ZG, Sun J, Kim S, Kapoor V, Cheng G, Ling L, Worthen GS, Albelda SM: **Polarization of Tumor-Associated Neutrophil Phenotype by TGF-??: "N1" versus "N2" TAN**. *Cancer Cell* 2009, **16**:183–194.

38. Kerkar SP, Restifo NP: **Cellular constituents of immune escape within the tumor microenvironment**. *Cancer Res* 2012, **72**:3125–3130.

39. Banchereau J, Steinman RM: **Dendritic cells and the control of immunity.** *Nature* 1998, **392**:245–252.

40. Vivier E, Tomasello E, Baratin M, Walzer T, Ugolini S: **Functions of natural killer cells.** *Nat Immunol* 2008, **9**:503–510.

41. Watters JJ, Schartner JM, Badie B: **Microglia function in brain tumors.** *J Neurosci Res* 2005, **81**:447–55.

42. Lin W, Karin M: **A cytokine-mediated link between innate immunity , inflammation , and cancer**. *J Clin Investig* 2007, **117**:1175–1183.

43. Ben-Baruch A: **Inflammation-associated immune suppression in cancer: The roles played by cytokines, chemokines and additional mediators**. *Semin Cancer Biol* 2006, **16**:38–52.

44. Li N, Grivennikov SI, Karin M: **The Unholy Trinity: Inflammation, Cytokines, and STAT3 Shape The Cancer Microenvironment**. *Cancer Cell* 2011, **19**:429–431.

45. Bonecchi R, Locati M, Mantovani A: **Chemokines and Cancer: A Fatal Attraction**. *Cancer Cell* 2011, **19**:434–435.

46. Mantovani A, Allavena P, Sica A, Balkwill F: **Cancer-related inflammation.** *Nature* 2008, **454**:436–44.

47. Dunn GP, Bruce AT, Ikeda H, Old LJ, Schreiber RD: **Cancer immunoediting : from immunosurveillance to tumor escape**. *Nat Immunol* 2002, **3**:991–998.

48. Shankaran V, Ikeda H, Bruce AT, White JM, Swanson PE, Old LJ, Schreiber RD: **IFNgamma and lymphocytes prevent primary tumour development and shape tumour immunogenicity.** *Nature* 2001, **410**:1107–11.

49. Ikeda H, Old LJ, Schreiber RD: **The roles of IFN gamma in protection against tumor development and cancer immunoediting.** *Cytokine Growth Factor Rev* 2002, **13**:95–109.

50. Schreiber RD, Old LJ, Smyth MJ: **Cancer immunoediting: Integrating immunity's roles in cancer suppression and promotion.** *Science (80-)* 2011, **331**:1565–70.

51. Dunn GP, Old LJ, Schreiber RD: **The three Es of cancer immunoediting.** *Annu Rev Immunol* 2004, **22**:329–60.

52. Burnet F: **The concept of immunological surveillance**. *Prog Exp Tumor Res* 1970, **13**:1–27.

53. Thomas L: **On immunosurveillance in human cancer**. *Yale J Biol Med* 1982, **55**:329–333.

54. Vesely MD, Kershaw MH, Schreiber RD, Smyth MJ: **Natural innate and adaptive immunity to cancer.** *Annu Rev Immunol* 2011, **29**:235–71.

55. Teng MWL, Swann JB, Koebel CM, Schreiber RD, Smyth MJ: **Immune-mediated dormancy: an equilibrium with cancer.** *J Leukoc Biol* 2008, **84**:988–993.

56. Galon J, Costes A, Fatima S-C, Amos K, Mlecnik B, Lagorce-Pages C, Tosolini M, Camus M, Berger A, Matthieu C, Berger A, Wind P, Zinzindohoue F, Bruneval P, Cugnenc P-H, Trajanoski Z, Friedman W-

H, Pagès F: **Type, Density, and Location of Immune Cells Within Human Colorectal Tumors Predict Clinical Outcome**. *Science (80-)* 2006, **313**(September):1960–1965.

57. Galon J, Fridman WH, Pages F: **The adaptive immunologic microenvironment in colorectal cancer: A novel perspective**. *Cancer Res* 2007, **67**:1883–1886.

58. Galon J, Angell HK, Bedognetti D, Marincola FM: **The continuum of cancer immunosurveillance: prognostic, predictive, and mechanistic signatures.** *Immunity* 2013, **39**:11–26.

59. Galon J, Pagès F, Marincola FM, Angell HK, Thurin M, Lugli A, Zlobec I, Berger A, Bifulco C, Botti G, Tatangelo F, Britten CM, Kreiter S, Chouchane L, Delrio P, Arndt H, Asslaber M, Maio M, Masucci G V, Mihm M, Vidal-Vanaclocha F, Allison JP, Gnjatic S, Hakansson L, Huber C, Singh-Jasuja H, Ottensmeier C, Zwierzina H, Laghi L, Grizzi F, et al.: **Cancer classification using the Immunoscore: a worldwide task force.** *J Transl Med* 2012, **10**:205.

60. **Brain, other CNS and intracranial tumours incidence statistics**

61. Mehta M, Vogelbaum MA, Chang S, Patel N: **Neoplasms of the Central Nervous System**. In *Cancer Princ Pract Oncol (9th ed)*; 2011:2022–2032.

62. Louis DN, Ohgaki H, Wiestler OD, Cavenee WK, Burger PC, Jouvet A, Scheithauer BW, Kleihues P: **The 2007 WHO classification of tumours of the central nervous system.** *Acta Neuropathol* 2007, **114**:97–109.

63. Ostrom QT, Gittleman H, Lioa P, Rouse C, Chen Y, Dowling J, Wolinsky YP, B.A CK, Barnholtz-Sloan J: **CBTRUS Statistical Report: Primary Brain and Central Nervous System Tumors Diagnosed in the United States in 2007–2011**. *Neuro Oncol* 2014, **16**:(suppl 4): iv1–iv63.

64. Huse JT, Holland EC: **Targeting brain cancer: advances in the molecular pathology of malignant glioma and medulloblastoma.** *Nat Rev Cancer* 2010, **10**:319–331.

65. Omuro A: **Glioblastoma and Other Malignant Gliomas**. *Jama* 2013, **310**:1842.

66. Miller CR, Perry A: **Glioblastoma Morphologic and Molecular Genetic Diversity**. *Arch Pathol Lab Med* 2007.

67. Bondy ML, Scheurer ME, Malmer B, Barnholtz-Sloan JS, Davis FG, Il'yasova D, Kruchko C, McCarthy BJ, Rajaraman P, Consortium JAS on behalf of the BTE: **Brain Tumor Epidemiology: Consensus from the Brain Tumor Epidemiology Consortium (BTEC)**. *Cancer* 2010, **113**(7 Suppl.):1953–1968.

68. Corle C, Makale M, Kesari S: **Cell phones and glioma risk: A review of the evidence**. *J Neurooncol* 2012, **106**:1–13.

69. Preusser M, de Ribaupierre S, Wöhrer A, Erridge SC, Hegi M, Weller M, Stupp R: **Current concepts and management of glioblastoma.** *Ann Neurol* 2011, **70**:9–21.

70. Wen PY, Kesari S: **Malignant gliomas in adults.** *N Engl J Med* 2008, **359**:1850.

71. Ray-Chaudhury A: **Pathology of Glioblastoma Multiforme in Glioblastoma,**. In *Glioblastoma Mol Mech Pathog Curr Ther Strateg*; 2010:77–84.

72. Louis DN: **Molecular pathology of malignant gliomas.** *Annu Rev Pathol* 2006, **1**:97–117.

73. Dunn GP, Rinne ML, Wykosky J, Genovese G, Quayle SN, Dunn IF, Agarwalla PK, Chheda MG, Campos B, Wang A, Brennan C, Ligon KL, Furnari F, Cavenee WK, Depinho RA, Chin L, Hahn WC: **Emerging insights into the molecular and cellular basis of glioblastoma**. *Genes Dev* 2012, **26**:756–784.

74. Hoffman HJ, Duffner PK: **Extraneural metastases of central nervous system tumors.** *Cancer* 1985, **56**(7 Suppl):1778–1782.

75. Armstrong TS: **Head's up on the treatment of malignant glioma patients.** *Oncol Nurs Forum* 2009, **36**:E232–40.

76. Bleeker FE, Molenaar RJ, Leenstra S: **Recent advances in the molecular understanding of glioblastoma**. *J Neurooncol* 2012, **108**:11–27.

77. Ohgaki H, Kleihues P: **The definition of primary and secondary glioblastoma**. *Clin Cancer Res* 2013, **19**:764–772.

78. Ohgaki H, Kleihues P: **Genetic pathways to primary and secondary glioblastoma.** *Am J Pathol* 2007, **170**:1445–53.

79. Humphrey PA, Wong AJ, Vogelstein B, Zalutsky MR, Fuller GN, Archer GE, Friedman HS, Kwatra MM, Bigner SH, Bigner DD: **Anti-synthetic peptide antibody reacting at the fusion junction of deletion-mutant epidermal growth factor receptors in human glioblastoma.** *Proc Natl Acad Sci U S A* 1990, **87**:4207–4211.

80. Carrabba G, Mukhopadhyay D, Guha A: **Aberrant Signalling Complexes in GBMs: Prognostic and Therapeutic Implications**. In *Glioblastoma*; 2010:95–129.

81. Parsons DW, Jones S, Zhang X, Lin JC-H, Leary RJ, Angenendt P, Mankoo P, Carter H, Siu I-M, Gallia GL, Olivi A, McLendon R, Rasheed BA, Keir S, Nikolskaya T, Nikolsky Y, Busam D a, Tekleab H, Diaz LA, Hartigan J, Smith DR, Strausberg RL, Marie SKN, Shinjo SMO, Yan H, Riggins GJ, Bigner DD, Karchin R, Papadopoulos N, Parmigiani G, et al.: **An integrated genomic analysis of human glioblastoma multiforme.** *Science* 2008, **321**:1807–1812.

82. Molenaar RJ, Verbaan D, Lamba S, Zanon C, Jeuken JWM, Boots-Sprenger SHE, Wesseling P, Hulsebos TJM, Troost D, van Tilborg AA, Leenstra S, Vandertop WP, Bardelli A, van Noorden CJF, Bleeker FE: **The combination of IDH1 mutations and MGMT methylation status predicts survival in glioblastoma better than either IDH1 or MGMT alone.** *Neuro Oncol* 2014, **16**(January):1–11.

83. Watanabe T, Nobusawa S, Kleihues P, Ohgaki H: **IDH1 mutations are early events in the development of astrocytomas and oligodendrogliomas.** *Am J Pathol* 2009, **174**:1149–1153.

84. Verhaak RG, Hoadley KA, Purdom E, Wang V, Qi Y, Wilkerson MD, Miller CR, Ding L, Golub T, Mesirov JP, Alexe G, Lawrence M, O'Kelly M, Tamayo P, Weir BA, Gabriel S, Winckler W, Gupta S, Jakkula L, Feiler HS, Hodgson JG, James CD, Sarkaria JN, Brennan C, Ka and TCGARN: **An integrated genomic analysis identifies clinically relevant subtypes of glioblastoma characterized by abnormalities in PDGFRA, IDH1, EGFR and NF1**. *Cancer* 2010, **19**:38–46.

85. Charles NA, Holland EC, Gilbertson R, Glass R, Kettenmann H: **The brain tumor microenvironment.** *Glia* 2011, **59**:1169–80.

86. Lorger M: **Tumor microenvironment in the brain.** *Cancers (Basel)* 2012, **4**:218–43.

87. Chen S, Parney IF: **Immune Response: Glioma-Associated Immunosuppression**. In *Glioma Cell Biol*; 2014:221–239.

88. Kruse C, Liau L, Prins R, Antonios J, Ha E, Kasahara N, Soto H, Yang I: **Chronic inflammation drives glioma growth: cellular and molecular factors responsible for an immunosuppressive microenvironment**. *Neuroimmunol Neuroinflammation* 2014, **1**:66.

89. Yang I, Han SJ, Kaur G, Crane C, Parsa AT: **The role of microglia in central nervous system immunity and glioma immunology.** *J Clin Neurosci* 2010, **17**:6–10.

90. Graeber MB, Streit WJ: **Microglia: biology and pathology.** *Acta Neuropathol* 2010, **119**:89–105.

91. Saijo K, Glass CK: **Microglial cell origin and phenotypes in health and disease.** *Nat Rev Immunol* 2011, **11**:775–87.

92. Kaminska B, Sielska and M: **Characteristics of Phenotype and Pro-Tumorigenic Roles of Glioma Infiltrating Microglia/Macrophages**. *J Neurol Neurophysiol* 2011, **S5**:1–8.

93. Kettenmann H, Hanisch U, Noda M, Verkhratsky A: **Physiology of Microglia**. *Physiol Rev* 2011, **91**:461–553.

94. Luo X-G, Chen S-D: **The changing phenotype of microglia from homeostasis to disease.** *Transl Neurodegener* 2012, **1**:9.

95. Colton CA: **Heterogeneity of microglial activation in the innate immune response in the brain.** *J neuroimmune Pharmacol* 2009, **4**:399–418.

96. Roggendorf W, Strupp S, Paulus W: **Distribution and characterization of microglia/macrophages in human brain tumors.** *Acta Neuropathol* 1996, **92**:288–93.

97. Badie B, Schartner J: **Role of microglia in glioma biology.** *Microsc Res Tech* 2001, **54**:106–13.

98. Kaminska B, Gabrusiewicz K, Sielska M: **Characteristics of Phenotype and Pro-Tumorigenic Roles of Glioma Infiltrating Microglia/Macrophages**. *J Neurol Neurophysiol* 2011:1–8.

99. Morantz RA, Wood GW, Foster M, Clark M, Gollahon K: **Macrophages in experimental and human brain tumors. Part 2: studies of the macrophage content of human brain tumors.** *J Neurosurg* 1979, **50**:305–311.

100. Graeber MB, Scheithauer BW, Kreutzberg GW: **Microglia in brain tumors.** *Glia* 2002, **40**:252–9.

101. Li W, Graeber MB: **The molecular profile of microglia under the influence of glioma.** *Neuro Oncol* 2012, **14**:958–78.

102. Voisin P, Bouchaud V, Merle M, Diolez P, Duffy L, Flint K, Franconi J-M, Bouzier-Sore A-K: **Microglia in close vicinity of glioma cells: correlation between phenotype and metabolic alterations.** *Front Neuroenergetics* 2010, **2**(October):131.

103. Liu W, Tang Y, Feng J: **Cross talk between activation of microglia and astrocytes in pathological conditions in the central nervous system.** *Life Sci* 2011, **89**:141–6.

104. Zhang Y, Barres BA: **Astrocyte heterogeneity: an underappreciated topic in neurobiology.** *Curr Opin Neurobiol* 2010, **20**:588–94.

105. Matyash V, Kettenmann H: **Heterogeneity in astrocyte morphology and physiology.** *Brain Res Rev* 2010, **63**:2–10.

106. Barres BA: **The Mystery and Magic of Glia: A Perspective on Their Roles in Health and Disease**. *Neuron* 2008, **60**:430–440.

107. Buffo A, Rolando C, Ceruti S: **Astrocytes in the damaged brain: Molecular and cellular insights into their reactive response and healing potential**. *Biochem Pharmacol* 2010, **79**:77–89.

108. Ridet JL, Malhotra SK, Privat a., Gage FH: **Reactive astrocytes: Cellular and molecular cues to biological function**. *Trends Neurosci* 1997, **20**:570–577.

109. John GR, Lee SC, Brosnan CF: **Cytokines: powerful regulators of glial cell activation.** *Neuroscientist* 2003, **9**:10–22.

110. Jang E, Kim J-H, Lee S, Kim J-H, Seo J-W, Jin M, Lee M-G, Jang I-S, Lee W-H, Suk K: **Phenotypic polarization of activated astrocytes: the critical role of lipocalin-2 in the classical inflammatory activation of astrocytes.** *J Immunol* 2013, **191**:5204–19.

111. Bechmann I, Steiner B, Gimsa U, Mor G, Wolf S, Beyer M, Nitsch R, Zipp F: **Astrocyte-induced T cell elimination is CD95 ligand dependent**. *J Neuroimmunol* 2002, **132**:60–65.

112. Persano L, Rampazzo E, Basso G, Viola G: **Glioblastoma cancer stem cells: Role of the microenvironment and therapeutic targeting.** *Biochem Pharmacol* 2012:1–11.

113. Stupp R, Roila F: **Malignant glioma: ESMO clinical recommendations for diagnosis, treatment and follow-up.** *Ann Oncol* 2009, **20**(Supplement 4):126–8.

114. Patel M, Kim J, Ruzevick J, Li G, Lim M: **The Future of Glioblastoma Therapy: Synergism of Standard of Care and Immunotherapy**. *Cancers (Basel)* 2014, **6**:1953–1985.

115. Laperriere N, Zuraw L, Cairncross G: **Radiotherapy for newly diagnosed malignant glioma in adults: a systematic review.** *Radiother Oncol* 2002, **64**:259–73.

116. Stupp R, Mason WP, van den Bent MJ, Weller M, Fisher B, Taphoorn MJB, Belanger K, Brandes A a, Marosi C, Bogdahn U, Curschmann J, Janzer RC, Ludwin SK, Gorlia T, Allgeier A, Lacombe D, Cairncross JG, Eisenhauer E, Mirimanoff RO: **Radiotherapy plus concomitant and adjuvant temozolomide for glioblastoma.** *N Engl J Med* 2005, **352**:987–96.

117. Stupp R, Hegi ME, Mason WP, van den Bent MJ, Taphoorn MJ, Janzer RC, Ludwin SK, Allgeier A, Fisher B, Belanger K, Hau P, Brandes A a., Gijtenbeek J, Marosi C, Vecht CJ, Mokhtari K, Wesseling P, Villa S, Eisenhauer E, Gorlia T, Weller M, Lacombe D, Cairncross JG, Mirimanoff RO: **Effects of radiotherapy with concomitant and adjuvant temozolomide versus radiotherapy alone on survival in glioblastoma in a randomised phase III study: 5-year analysis of the EORTC-NCIC trial**. *Lancet Oncol* 2009, **10**:459–466.

118. Weller M: **Novel diagnostic and therapeutic approaches to malignant glioma.** *Swiss Med Wkly* 2011, **141**(May):w13210.

119. Adamson C, Kanu OO, Mehta AI, Di C, Lin N, Mattox AK, Bigner DD: **Glioblastoma multiforme: a review of where we have been and where we are going.** *Expert Opin Investig Drugs* 2009, **18**:1061–83.

120. Selznick LA, Shamji MF, Fecci P, Gromeier M, Friedman AH, Sampson J: **Molecular strategies for the treatment of malignant glioma-genes, viruses, and vaccines.** *Neurosurg Rev* 2008, **31**:141–55.

121. Sathornsumetee S, Rich JN: **Designer therapies for glioblastoma multiforme.** *Ann N Y Acad Sci* 2008, **1142**:108–32.

122. Jhanwar-Uniyal M, Labagnara M, Friedman M, Kwasnicki A, Murali R: **Glioblastoma: Molecular Pathways, Stem Cells and Therapeutic Targets**. *Cancers (Basel)* 2015, **7**:538–555.

123. Lima FRS, Kahn SA, Soletti RC, Biasoli D, Alves T, da Fonseca ACC, Garcia C, Romão L, Brito J, Holanda-Afonso R, Faria J, Borges H, Moura-Neto V: **Glioblastoma: Therapeutic challenges, what lies ahead.** *Biochim Biophys Acta* 2012, **1826**:338–49.

124. Clarke J, Butowski N, Chang S: **Recent advances in therapy for glioblastoma.** *Arch Neurol* 2010, **67**:279–83.

125. Rolle CE, Sengupta S, Lesniak MS: **Challenges in Clinical Design of Immunotherapy Trials for Malignant Glioma**. *Neurosurg Clin N Am* 2011, **21**:201–214.

126. Daga A, Bottino C, Castriconi R, Gangemi R, Ferrini S: **New perspectives in glioma immunotherapy.** *Curr Pharm Des* 2011, **17**:2439–67.

127. Liu T-C, Galanis E, Kirn D: **Clinical trial results with oncolytic virotherapy: a century of promise, a decade of progress.** *Nat Clin Pract Oncol* 2007, **4**:101–17.

128. Kelly E, Russell SJ: **History of oncolytic viruses: genesis to genetic engineering.** *Mol Ther* 2007, **15**:651–659.

129. Russell S, Peng K-W, Bell JC: **Oncolytic virotherapy**. *Nat Biotechnol* 2014, **30**:1–29.

130. Wollmann G, Ozduman K, van den Pol AN: **Oncolytic virus therapy for glioblastoma multiforme: concepts and candidates.** *Cancer J* 2012, **18**:69–81.

131. Chen NG, Szalay AA: *Cancer Management in Man: Chemotherapy, Biological Therapy, Hyperthermia and Supporting Measures*. Springer; 2011.

132. Dave R V., Jebar AHS, Jennings VA, Adair RA, West EJ, Errington-Mais F, Toogood GJ, Melcher AA: **Viral warfare! Front-line defence and arming theimmune system against cancer using oncolytic vaccinia and other viruses**. *Surgeon* 2014, **12**:210–220.

133. Pol J, Bloy N, Obrist F, Eggermont A, Galon J, Cremer I, Erbs P, Limacher J-M, Preville X, Zitvogel L, Kroemer G, Galluzzi L: **Trial Watch: Oncolytic viruses for cancer therapy.** *Oncoimmunology* 2014, **3**(April):e28694.

134. Woller N, Gürlevik E, Ureche C-I, Schumacher A, Kühnel F: **Oncolytic Viruses as Anticancer Vaccines**. *Front Oncol* 2014, **4**(July):1–13.

135. Bartlett DL, Liu Z, Sathaiah M, Ravindranathan R, Guo Z, He Y, Guo ZS: **Oncolytic viruses as therapeutic cancer vaccines.** *Mol Cancer* 2013, **12**:103.

136. Chen NG, Szalay AA: **Oncolytic Virotherapy in Cancer.** In *Cancer Manag Man Chemother Biol Ther Hyperth Support Meas*. Edited by Minev BR. New York, NY: Springer New York; 2011:295–316.

137. Kaufmann JK, Chiocca EA: **Glioma virus therapies between bench and bedside**. *Neuro Oncol* 2014, **16**:334–351.

138. Ilkow CS, Swift SL, Bell JC, Diallo JS: **From Scourge to Cure: Tumour-Selective Viral Pathogenesis as a New Strategy against Cancer**. *PLoS Pathog* 2014, **10**.

139. Sze DY, Reid TR, Rose SC: **Oncolytic virotherapy**. *J Vasc Interv Radiol* 2013, **24**:1115–1122.

140. Gujar SA, Lee PWK: **Oncolytic Virus-Mediated Reversal of Impaired Tumor Antigen Presentation.** *Front Oncol* 2014, **4**(April):77.

141. Patel MR, Kratzke RA: **Oncolytic virus therapy for cancer: The first wave of translational clinical trials**. *Transl Res* 2013, **161**:355–364.

142. Bell J, McFadden G: **Viruses for tumor therapy**. *Cell Host Microbe* 2014, **15**:260–265.

143. Forbes NE, Krishnan R, Diallo J-S: **Pharmacological modulation of anti-tumor immunity induced by oncolytic viruses.** *Front Oncol* 2014, **4**(July):191.

144.Sagonowsky E: **Amgen wins FDA panel nod for T-Vec in melanoma**. *http://www.fiercevaccines.com/story/amgen-wins-fda-panel-nod-t-vec-melanoma/2015-04-29* 2015.

145. Jefferson A, Cadet VE, Hielscher A: **The mechanisms of genetically modified vaccinia viruses for the treatment of cancer**. *Crit Rev Oncol Hematol* 2015:1–10.

146. Zhang Q, Yu YA, Wang E, Chen N, Danner RL, Munson PJ, Marincola FM, Szalay AA: **Eradication of solid human breast tumors in nude mice with an intravenously injected light-emitting oncolytic vaccinia virus.** *Cancer Res* 2007, **67**:10038–46.

147. Izmailyan R, Chang W: **Vaccinia virus WR53.5/F14.5 protein is a new component of intracellular mature virus and is important for calcium-independent cell adhesion and vaccinia virus virulence in mice.** *J Virol* 2008, **82**:10079–10087.

148. Yu Z, Li S, Brader P, Chen N, Yu YA, Zhang Q, Szalay AA, Fong Y, Wong RJ: **Oncolytic vaccinia therapy of squamous cell carcinoma.** *Mol Cancer* 2009, **8**:45.

149. Worschech A, Chen N, Yu YA, Zhang Q, Pos Z, Weibel S, Raab V, Sabatino M, Monaco A, Liu H, Monsurró V, Buller RM, Stroncek DF, Wang E, Szalay AA, Marincola FM: **Systemic treatment of xenografts with vaccinia virus GLV-1h68 reveals the immunologic facet of oncolytic therapy.** *BMC Genomics* 2009, **10**:301.

150. Wang H, Chen NG, Minev BR, Szalay AA: **Oncolytic vaccinia virus GLV-1h68 strain shows enhanced replication in human breast cancer stem-like cells in comparison to breast cancer cells.** *J Transl Med* 2012, **10**:167.

151. Seubert CM, Stritzker J, Hess M, Donat U, Sturm JB, Chen N, von Hof JM, Krewer B, Tietze LF, Gentschev I, Szalay AA: **Enhanced tumor therapy using vaccinia virus strain GLV-1h68 in combination with a β-galactosidase-activatable prodrug seco-analog of duocarmycin SA.** *Cancer Gene Ther* 2011:42–52.

152. Hofmann E, Weibel S, Szalay AA: **Combination treatment with oncolytic Vaccinia virus and cyclophosphamide results in synergistic antitumor effects in human lung adenocarcinoma bearing mice.** *J Transl Med* 2014, **12**:197.

153. Ehrig K, Kilinc MO, Chen NG, Stritzker J, Buckel L, Zhang Q, Szalay AA: **Growth inhibition of different human colorectal cancer xenografts after a single intravenous injection of oncolytic vaccinia virus GLV-1h68.** *J Transl Med* 2013, **11**:79.

154. Gentschev I, Müller M, Adelfinger M, Weibel S, Grummt F, Zimmermann M, Bitzer M, Heisig M, Zhang Q, Yu YA, Chen NG, Stritzker J, Lauer UM, Szalay AA: **Efficient colonization and therapy of human hepatocellular carcinoma (HCC) using the oncolytic vaccinia virus strain GLV-1h68.** *PLoS One* 2011, **6**:e22069.

155. Donat U, Weibel S, Hess M, Stritzker J, Härtl B, Sturm JB, Chen NG, Gentschev I, Szalay AA: **Preferential colonization of metastases by oncolytic vaccinia virus strain GLV-1h68 in a human PC-3 prostate cancer model in nude mice.** *PLoS One* 2012, **7**:e45942.

156. Galanis E: **Cancer: Tumour-fighting virus homes in.** *Nature* 2011, **477**:40–41.

157. Zemp FJ, Corredor JC, Lun X, Muruve DA, Forsyth PA: **Oncolytic viruses as experimental treatments for malignant gliomas: using a scourge to treat a devil.** *Cytokine Growth Factor Rev* 2010, **21**:103–17.

158. Modrow S, Falke D, Truyen U, Schätzl H: *Molekulare Virologie*. 3rd edition. Spektrum; 2010.

159. Chalikonda S, Bartlett DL: **Vaccinia and Pox-Virus**. In *Cancer Drug Discov Dev Gene Ther Cancer*. Edited by Hunt K, Vorburger S, Swisher S.; 2007:73–85.

160. Shen Y, Nemunaitis J: **Fighting cancer with vaccinia virus: teaching new tricks to an old dog.** *Mol Ther* 2005, **11**:180–95.

161. Broyles SS: **Vaccinia virus transcription**. *J Gen Virol* 2003, **84**:2293–2303.

162. Moss B, Earl PL: **Overview of the Vaccinia Virus Expression System**. *Curr Protoc Mol Biol* 2002, **Supplement**:16.15.1–5.

163. Jacobs BL, Langland JO, Kibler K V, Denzler KL, White SD, Holechek SA, Wong S, Huynh T, Baskin CR: **Vaccinia virus vaccines: past, present and future.** *Antiviral Res* 2009, **84**:1–13.

164. Moss B: **Regulation of Vaccinia Virus Transcription**. *Annu Rev Biochem* 1990.

165. Roberts KL, Smith GL: **Vaccinia virus morphogenesis and dissemination.** *Trends Microbiol* 2008, **16**:472–9.

166. Schmidt FI, Bleck CKE, Mercer J: **Poxvirus host cell entry**. *Curr Opin Virol* 2012, **2**:20–27.

167. Moss B: **Poxvirus cell entry: How many proteins does it take?** *Viruses* 2012, **4**:688–707.

168. Liu L, Cooper T, Howley P, Hayball J: **From Crescent to Mature Virion: Vaccinia Virus Assembly and Maturation**. *Viruses* 2014, **6**:3787–3808.

169. Smith GL, Law M: **The exit of vaccinia virus from infected cells.** *Virus Res* 2004, **106**:189–97.

170. Tolonen N, Doglio L, Schleich S, Krijnse Locker J: **Vaccinia virus DNA replication occurs in endoplasmic reticulum-enclosed cytoplasmic mini-nuclei.** *Mol Biol Cell* 2001, **12**:2031–2046.

171. Pogo BG-T, Melana SM, Blaho J: **Poxvirus infection and apoptosis.** *Int Rev Immunol* 2004, **23**:61–74.

172. Smith GL, Murphy BJ, Law M: **Vaccinia virus motility.** *Annu Rev Microbiol* 2003, **57**:323–342.

173. Essajee S, Kaufman HL: **Poxvirus vaccines for cancer and HIV therapy.** *Expert Opin Biol Ther* 2004, **4**:575–88.

174. Guse K, Cerullo V, Hemminki A: **Oncolytic vaccinia virus for the treatment of cancer.** *Expert Opin Biol Ther* 2011, **11**:595–608.

175. Kirn DH, Thorne SH: **Targeted and armed oncolytic poxviruses: a novel multi-mechanistic therapeutic class for cancer.** *Nat Rev Cancer* 2009, **9**:64–71.

176. McFadden G: **Poxvirus Tropism**. *Nat Rev Microbiol* 2005, **3**:201–213.

177. Lun XQ, Jang J-H, Tang N, Deng H, Head R, Bell JC, Stojdl DF, Nutt CL, Senger DL, Forsyth PA, McCart JA: **Efficacy of systemically administered oncolytic vaccinia virotherapy for malignant gliomas is enhanced by combination therapy with rapamycin or cyclophosphamide.** *Clin Cancer Res* 2009, **15**:2777–88.

178. Lun X, Chan J, Zhou H, Sun B, Kelly JJP, Stechishin OO, Bell JC, Parato K, Hu K, Vaillant D, Wang J, Liu T-C, Breitbach C, Kirn D, Senger DL, Forsyth PA: **Efficacy and safety/toxicity study of recombinant vaccinia virus JX-594 in two immunocompetent animal models of glioma.** *Mol Ther* 2010, **18**:1927–36.

179. Advani SJ, Buckel L, Chen NG, Scanderbeg DJ, Geissinger U, Zhang Q, Yu YA, Aguilar RJ, Mundt AJ, Szalay AA: **Preferential replication of systemically delivered oncolytic vaccinia virus in focally irradiated glioma xenografts.** *Clin cancer Res* 2012, **18**:2579–90.

180. Buckel L, Advani SJ, Frentzen A, Zhang Q, Yu YA, Chen NG, Ehrig K, Stritzker J, Mundt AJ, Szalay AA: **Combination of fractionated irradiation with anti-VEGF expressing vaccinia virus therapy enhances tumor control by simultaneous radiosensitization of tumor associated endothelium.** *Int J cancer* 2013, **133**:2989–99.

181. Duggal R, Geissinger U, Zhang Q, Aguilar J, Chen NG, Binda E, Vescovi AL, Szalay AA: **Vaccinia virus expressing bone morphogenetic protein-4 in novel glioblastoma orthotopic models facilitates enhanced tumor regression and long-term survival.** *J Transl Med* 2013, **11**:155.

182. Koks C a. E, De Vleeschouwer S, Graf N, Van Gool SW: **Immune Suppression during Oncolytic Virotherapy for High-Grade Glioma; Yes or No?** *J Cancer* 2015, **6**:203–217.

183. Dey M, Auffinger B, Lesniak MS, Ahmed AU: **Antiglioma oncolytic virotherapy: unattainable goal or a success story in the making?** *Futur Virol* 2012, **29**:997–1003.

184. Ning J, Wakimoto H, Rabkin SD: **Immunovirotherapy for glioblastoma.** *Cell Cycle* 2014, **13**:175–6.

185. Dey M, Ulasov I V, Tyler M a, Sonabend AM, Lesniak MS: **Cancer stem cells: the final frontier for glioma virotherapy.** *Stem Cell Rev* 2011, **7**:119–29.

186. Kaur B, Chiocca EA: **Personalizing oncolytic virotherapy?** *Mol Ther* 2007, **15**:6–7.

187. Ogino S, Galon J, Fuchs CS, Dranoff G: **Cancer Immunology - Analysis of Host and Tumor Factors for Personalized Medicine**. *Nat Rev clin Oncol* 2012, **8**:617–632.

188. Glass R, Synowitz M: **CNS macrophages and peripheral myeloid cells in brain tumours.** *Acta Neuropathol* 2014, **128**:347–62.

189. Markovic DS, Glass R, Synowitz M, Rooijen N Van, Kettenmann H: **Microglia stimulate the invasiveness of glioma cells by increasing the activity of metalloprotease-2.** *J Neuropathol Exp Neurol* 2005, **64**:754–62.

190. Blasi E, Barluzzi R, Bocchini V, Mazzolla R, Bistoni F: **Immortalization of murine microglial cells by a v-raf/v-myc carrying retrovirus.** *J Neuroimmunol* 1990, **27**:229–37.

191. Bocchini V, Mazzolla R, Barluzzi R, Blasi E, Sick P, Kettenmann H: **An immortalized cell line expresses properties of activated microglial cells**. *J Neurosci Res* 1992, **31**:616–621.

192. Schildknecht S, Kirner S, Henn A, Gasparic K, Pape R, Efremova L, Maier O, Fischer R, Leist M: **Characterization of mouse cell line IMA 2.1 as a potential model system to study astrocyte functions.** *ALTEX* 2012, **29**:261–74.

193. Zhang Q, Liang C, Yu YA, Chen N, Dandekar T, Szalay AA: **The highly attenuated oncolytic recombinant vaccinia virus GLV-1h68: comparative genomic features and the contribution of F14.5L inactivation.** *Mol Genet Genomics* 2009, **282**:417–35.

194. Mccart JA, Ward JM, Lee J, Hu Y, Alexander HR, Libutti SK, Moss B, Bartlett DL: **Systemic Cancer Therapy with a Tumor-selective Vaccinia Virus Mutant Lacking Thymidine Kinase and Vaccinia Growth Factor Genes Systemic Cancer Therapy with a Tumor-selective Vaccinia Virus Mutant Lacking Thymidine Kinase and Vaccinia Growth Factor Genes**. *Cancer Res* 2001:8751–8757.

195. Gentschev I, Adelfinger M, Josupeit R, Rudolph S, Ehrig K, Donat U, Weibel S, Chen NG, Yu YA, Zhang Q, Heisig M, Thamm D, Stritzker J, Macneill A, Szalay AA: **Preclinical evaluation of oncolytic vaccinia virus for therapy of canine soft tissue sarcoma.** *PLoS One* 2012, **7**:e37239.

196. Gerson RJ, Macdonald JS, Albertsa AW, Kornbrusta DJ, Majka DVMJA, Stubbs RJ, Bokelman DL: **Animal safety and toxicology of simvastatin and related hydroxy-methylglutaryl-coenzyme a reductase inhibitors**. *Am J Med* 1989, **87**:S28–S38.

197. Sadeghi MM, Collinge M, Pardi R, Bender JR: **Simvastatin modulates cytokine-mediated endothelial cell adhesion molecule induction: involvement of an inhibitory G protein.** *J Immunol* 2000, **165**:2712–8.

198. Leung BP, Sattar N, Crilly A, Prach M, McCarey DW, Payne H, Madhok R, Campbell C, Gracie JA, Liew FY, McInnes IB: **A novel anti-inflammatory role for simvastatin in inflammatory arthritis.** *J Immunol* 2003, **170**:1524–30.

199. Berridge M V, Tan AS, Mccoy KD, Wang R: **The Biochemical and Cellular Basis of Cell Proliferation Assays That Use Tetrazolium Salts**. *BIOCHEMICA* 1996:4–9.

200. Dulbecco R, Vogy M: **Some problems of animal virology as studied by the plaque technique.** *Cold Spring Harb Symp Quant Biol* 1953, **18**:273–279.

201. Müller HC, Hellwig K, Rosseau S, Tschernig T, Schmiedl A, Gutbier B, Schmeck B, Hippenstiel S, Peters H, Morawietz L, Suttorp N, Witzenrath M: **Simvastatin attenuates ventilator-induced lung injury in mice.** *Crit Care* 2010, **14**:R143.

202. Pampaloni F, Reynaud EG, Stelzer EHK: **The third dimension bridges the gap between cell culture and live tissue**. 2007, **8**(october):839–845.

203. Mewes A, Franke H, Singer D: **Organotypic brain slice cultures of adult transgenic P301S mice-a model for tauopathy studies.** *PLoS One* 2012, **7**:e45017.

204. Aaberg-Jessen C, Nørregaard A, Christensen K, Pedersen CB, Andersen C, Kristensen BW: **Invasion of primary glioma- and cell line-derived spheroids implanted into corticostriatal slice cultures.** *Int J Clin Exp Pathol* 2013, **6**:546–60.

205. Chuang H-N, Lohaus R, Hanisch U-K, Binder C, Dehghani F, Pukrop T: **Coculture system with an organotypic brain slice and 3D spheroid of carcinoma cells.** *J Vis Exp* 2013:2–6.

206. Braun E, Zimmerman T, Hur T Ben, Reinhartz E, Fellig Y, Panet A, Steiner I: **Neurotropism of herpes simplex virus type 1 in brain organ cultures Printed in Great Britain**. *J Gen Virol* 2006:2827–2837.

207. Sundstrom L, Iii BM, Bradley M, Pringle A: **Organotypic cultures as tools for functional screening in the CNS**. *Drug Discov Today* 2005, **10**:993–1000.

208. Stoppini L, Buchs PA, Muller D: **A simple method for organotypic cultures of nervous tissue.** *J Neurosci Methods* 1991, **37**:173–82.

209. Paxinos G, Franklin KBJ: *The Mouse Brain in Stereotaxic Coordinates*. 2nd edition. Academic press; 2001.

210. Bergold PJ, Casaccia-Bonnefil P: **Preparation of Organotypic Hippocampal Slice Cultures Using the Membrane Filter Method**. In *Neurotransmitter Methods*. Edited by Rayne RC. Springer New York; 1997:pp 15–22.

211. Krysko D V, Vanden Berghe T, D'Herde K, Vandenabeele P: **Apoptosis and necrosis: detection, discrimination and phagocytosis.** *Methods* 2008, **44**:205–21.

212. Darzynkiewicz Z, Juan G, Li X, Gorczyca W, Murakami T, Traganos F: **Cytometry in cell necrobiology: analysis of apoptosis and accidental cell death (necrosis).** *Cytometry* 1997, **27**:1–20.

213. Zamai L, Canonico B, Luchetti F, Ferri P, Melloni E, Guidotti L, Cappellini a, Cutroneo G, Vitale M, Papa S: **Supravital exposure to propidium iodide identifies apoptosis on adherent cells.** *Cytometry* 2001, **44**:57–64.

214. Huang H, Xiao T, He L, Ji H, Liu X-Y: **Interferon-β-armed oncolytic adenovirus induces both apoptosis and necroptosis in cancer cells.** *Acta Biochim Biophys Sin (Shanghai)* 2012, **44**:737–45.

215. Sun J, Zhang X, Broderick M, Fein H: **Measurement of Nitric Oxide Production in Biological Systems by Using Griess Reaction Assay**. *Sensors* 2003, **3**:276–284.

216. Griess P: **Bemerkungen zu der abhandlung der H.H. Weselsky und Benedikt "Ueber einige azoverbindungen**. *Chem Ber* 1879, **12**:426.

217. S.Paydas, Tanriverdi K, Yavuz S, Disel U, Sahin B, Burgut R: **Survivin and aven: two distinct antiapoptotic signals in acute leukemias**. *Ann Oncol* 2003, **14**:1045–1050.

218. Gentschev I, Donat U, Hofmann E, Weibel S, Adelfinger M, Raab V, Heisig M, Chen N, Yu YA, Stritzker J, Szalay AA: **Regression of human prostate tumors and metastases in nude mice following treatment with the recombinant oncolytic vaccinia virus GLV-1h68.** *J Biomed Biotechnol* 2010, **2010**:11.

219. Kober C, Weibel S, Rohn S, Kirscher L, Szalay AA: **Intratumoral INF-γ triggers an antiviral state in GL261 tumor cells: a major hurdle to overcome for oncolytic vaccinia virus therapy of cancer**. *Mol Ther — Oncolytics* 2015, **2**:1–14.

220. Kober C, Rohn S, Weibel S, Geissinger U, Chen NG, Szalay AA: **Microglia and astrocytes attenuate the replication of the oncolytic vaccinia virus LIVP 1.1.1 in murine GL261 gliomas by acting as vaccinia virus traps**. *J Transl Med* 2015, **13**:216.

221. Ascierto ML, De Giorgi V, Liu Q, Bedognetti D, Spivey TL, Murtas D, Uccellini L, Ayotte BD, Stroncek DF, Chouchane L, Manjili MH, Wang E, Marincola FM: **An immunologic portrait of cancer.** *J Transl Med* 2011, **9**:146.

222. Liu T-C, Kirn D: **Systemic efficacy with oncolytic virus therapeutics: clinical proof-of-concept and future directions.** *Cancer Res* 2007, **67**:429–32.

223. Bourke MG, Salwa S, Harrington KJ, Kucharczyk MJ, Forde PF, de Kruijf M, Soden D, Tangney M, Collins JK, O'Sullivan GC: **The emerging role of viruses in the treatment of solid tumours.** *Cancer Treat Rev* 2011, **37**:618–32.

224. Ferguson MS, Lemoine NR, Wang Y: **Systemic delivery of oncolytic viruses: Hopes and Hurdles.** *Adv Virol* 2012, **2012**:14.

225. Weibel S, Basse-Luesebrink TC, Hess M, Hofmann E, Seubert C, Langbein-Laugwitz J, Gentschev I, Sturm VJF, Ye Y, Kampf T, Jakob PM, Szalay AA: **Imaging of intratumoral inflammation during oncolytic virotherapy of tumors by 19F-magnetic resonance imaging (MRI).** *PLoS One* 2013, **8**:e56317.

226. Weibel S, Hofmann E, Basse-Luesebrink TC, Donat U, Seubert C, Adelfinger M, Gnamlin P, Kober C, Frentzen A, Gentschev I, Jakob PM, Szalay AA: **Treatment of malignant effusion by oncolytic virotherapy in an experimental subcutaneous xenograft model of lung cancer.** *J Transl Med* 2013, **11**:106.

227. Donat U, Rother J, Schäfer S, Hess M, Härtl B, Kober C, Langbein-Laugwitz J, Stritzker J, Chen NG, Aguilar RJ, Weibel S, Szalay AA: **Characterization of Metastasis Formation and Virotherapy in the Human C33A Cervical Cancer Model.** *PLoS One* 2014, **9**:e98533.

228. **http://rbm.myriad.com/products-services/biomarker-detail/**

229. **http://www.ncbi.nlm.nih.gov/gene/968**

230. Boehm U, Klamp T, Groot M, Howard JC: **Cellular responses to interferon-gamma.** *Annu Rev Immunol* 1997, **15**:749–95.

231. Schroder K, Hertzog PJ, Ravasi T, Hume DA: **Interferon-γ: an overview of signals, mechanisms and functions**. *J Leukoc Biol* 2004, **75**:163–89.

232. Soos JM, Krieger JI, Stüve O, King CL, Patarroyo JC, Aldape K, Wosik K, Slavin a J, Nelson P a, Antel JP, Zamvil SS: **Malignant glioma cells use MHC class II transactivator (CIITA) promoters III and IV to direct IFN-gamma-inducible CIITA expression and can function as nonprofessional antigen presenting cells in endocytic processing and CD4(+) T-cell activation.** *Glia* 2001, **36**:391–405.

233. Akbasak A, Oldfield EH, Saris SC: **Expression and modulation of major histocompatibility antigens on murine primary brain tumor in vitro.** *J Neurosurg* 1991, **75**:922–9.

234. Maes W, Van Gool SW: **Experimental immunotherapy for malignant glioma: lessons from two decades of research in the GL261 model.** *Cancer Immunol Immunother* 2011, **60**:153–60.

235. Szatmári T, Lumniczky K, Désaknai S, Trajcevski S, Hídvégi EJ, Hamada H, Sáfrány G: **Detailed characterization of the mouse glioma 261 tumor model for experimental glioblastoma therapy.** *Cancer Sci* 2006, **97**:546–53.

236. Weisser SB, van Rooijen N, Sly LM: **Depletion and reconstitution of macrophages in mice.** *J Vis Exp* 2012, **66**:1–7.

237. Kwak B, Mulhaupt F, Myit S, Mach F: **Statins as a newly recognized type of immunomodulator.** *Nat Med* 2000, **6**:1399–402.

238. Kwak B, Mulhaupt F, Veillard N, Pelli G, Mach F: **The HMG-CoA reductase inhibitor simvastatin inhibits IFN-gamma induced MHC class II expression in human vascular endothelial cells.** *Swiss Med Wkly* 2001, **131**:41–6.

239. Zeinstra E, Wilczak N, Chesik D, Glazenburg L, Kroese FGM, De Keyser J: **Simvastatin inhibits interferon-gamma-induced MHC class II up-regulation in cultured astrocytes.** *J Neuroinflammation* 2006, **3**:16.

240. Huysentruyt LC, Akgoc Z, Seyfried TN: **Hypothesis: are neoplastic macrophages/microglia present in glioblastoma multiforme?** *ASN Neuro* 2011, **3**:183–193.

241. Markovic DS, Vinnakota K, Chirasani S, Synowitz M, Raguet H, Stock K, Sliwa M, Lehmann S, Kälin R, van Rooijen N, Holmbeck K, Heppner FL, Kiwit J, Matyash V, Lehnardt S, Kaminska B, Glass R, Kettenmann H: **Gliomas induce and exploit microglial MT1-MMP expression for tumor expansion.** *Proc Natl Acad Sci U S A* 2009, **106**:12530–5.

242. Olson JK, Miller SD: **Microglia Initiate Central Nervous System Innate and Adaptive Immune Responses through Multiple TLRs**. *J Immunol* 2004, **173**:3916–3924.

243. Ajmone-Cat MA, Mancini M, De Simone R, Cilli P, Minghetti L: **Microglial polarization and plasticity: evidence from organotypic hippocampal slice cultures.** *Glia* 2013, **61**:1698–711.

244. Henn A, Lund S, Hedtjärn M, Schrattenholz A, Pörzgen P, Leist M: **The suitability of BV2 cells as alternative model system for primary microglia cultures or for animal experiments examining brain inflammation.** *ALTEX* 2009, **26**:83–94.

245. Liskova J, Knitlova J, Honner R, Melkova Z: **Apoptosis and necrosis in vaccinia virus-infected HeLa G and BSC-40 cells.** *Virus Res* 2011, **160**:40–50.

246. Wei J, Gabrusiewicz K, Heimberger A: **The controversial role of microglia in malignant gliomas.** *Clin Dev Immunol* 2013, **2013**:12.

247. Komohara Y, Ohnishi K, Kuratsu J, Takeya M: **Possible involvement of the M2 anti-inflammatory macrophage phenotype in growth of human gliomas.** *J Pathol* 2008, **216**:15–24.

248. Kennedy BC, Showers CR, Anderson DE, Anderson L, Canoll P, Bruce JN, Anderson RCE: **Tumor-associated macrophages in glioma: friend or foe?** *J Oncol* 2013, **2013**:11.

249. Kigerl KA, Gensel JC, Ankeny DP, Alexander JK, Donnelly DJ, Popovich PG: **Identification of two distinct macrophage subsets with divergent effects causing either neurotoxicity or regeneration in the injured mouse spinal cord.** *J Neurosci* 2009, **29**:13435–44.

250. Girard S, Brough D, Lopez-Castejon G, Giles J, Rothwell NJ, Allan SM: **Microglia and macrophages differentially modulate cell death after brain injury caused by oxygen-glucose deprivation in organotypic brain slices.** *Glia* 2013, **61**:813–24.

251. Fenn AM, Henry CJ, Huang Y, Dugan A, Godbout JP: **Lipopolysaccharide-induced interleukin (IL)-4 receptor-α expression and corresponding sensitivity to the M2 promoting effects of IL-4 are impaired in microglia of aged mice.** *Brain Behav Immun* 2012, **26**:766–77.

252. Karlstetter M, Walczak Y, Weigelt K, Ebert S, Van den Brulle J, Schwer H, Fuchshofer R, Langmann T: **The novel activated microglia/macrophage WAP domain protein, AMWAP, acts as a counter-regulator of proinflammatory response.** *J Immunol* 2010, **185**:3379–90.

253. Abschuetz A, Kehl T, Geibig R, Leuchs B, Rommelaere J, Régnier-vigouroux A: **Oncolytic murine autonomous parvovirus , a candidate vector for glioma gene therapy , is innocuous to normal and immunocompetent mouse glial cells**. *Cell Tissue Res* 2006, **325**:423–426.

254. Fulci G, Passer B: **Analysis of HSV Oncolytic Virotherapy in Organotypic Cultures**. In *Gene Ther Cancer Methods Mol Biol*. *Volume 542*. Edited by Walther W, Stein US. Totowa, NJ: Humana Press; 2009:75–87. [*Methods in Molecular Biology™*]

255. Chau BN, Cheng EH, Kerr D a, Hardwick JM: **Aven, a novel inhibitor of caspase activation, binds Bcl-xL and Apaf-1.** *Mol Cell* 2000, **6**:31–40.

256. Robert G. Hawley, Yuzhong Chen, Irene Riz and CZ: **An Integrated Bioinformatics and Computational Biology Approach Identifies New BH3-Only Protein Candidates**. *Open Biol J* 2012:6–16.

257. Guo JY, Yamada A, Kajino T, Wu JQ, Tang W, Freel CD, Feng J, Chau BN, Wang MZ, Margolis SS, Yoo HY, Wang X-F, Dunphy WG, Irusta PM, Hardwick JM, Kornbluth S: **Aven-dependent activation of ATM following DNA damage.** *Curr Biol* 2008, **18**:933–42.

258. Gross A: **A new Aven-ue to DNA-damage checkpoints.** *Trends Biochem Sci* 2008, **33**:514–6.

259. Kroeger KM, Muhammad AKMG, Baker GJ, Assi H, Wibowo MK, Xiong W, Yagiz K, Candolfi M, Lowenstein PR, Castro MG: **Gene therapy and virotherapy: novel therapeutic approaches for brain tumors.** *Discov Med* 2010, **10**:293–304.

260. Auffinger B, Ahmed AU, Lesniak MS: **Oncolytic virotherapy for malignant glioma: translating laboratory insights into clinical practice.** *Front Oncol* 2013, **3**:1–13.

261. Chen NG, Szalay AA: **Oncolytic vaccinia virus: a theranostic agent for cancer**. *Future Virol* 2010, **5**:763–784.

262. Chen NG, Yu YA, Zhang Q, Szalay AA: **Replication efficiency of oncolytic vaccinia virus in cell cultures prognosticates the virulence and antitumor efficacy in mice.** *J Transl Med* 2011, **9**:164.

263. Stylli SS, Luwor RB, Ware TMB, Tan F, Kaye AH: **Mouse models of glioma**. *J Clin Neurosci* 2015, **22**:619–626.

264. Jacobs VL, Valdes PA, Hickey WF, De Leo JA: **Current review of in vivo GBM rodent models: emphasis on the CNS-1 tumour model.** *ASN Neuro* 2011, **3**:e00063.

265. Seligman A, Shear M: **Studies in Carcinogenesis: VIII. Experimental Production of Brain Tumors in Mice with Methylcholanthrene**. *Am J Cancer* 1939.

266. Candolfi M, Curtin JF, Nichols WS, Muhammad AKMG, King D, Pluhar GE, Mcniel EA, Ohlfest JR, Freese AB, Moore F, Lerner J, Lowenstein PR, Castro MG, Candolfi M, Curtin JF, King GD, Lerner J, Lowenstein PR, Castro MG: **Intracranial glioblastoma models in preclinical neuro-oncology: neuropathological characterization and tumor progression**. *JNeuroonc* 2008, **85**:133–148.

267. Manjili HM: **Revisiting cancer immunoediting by understanding cancer immune complexity**. *J Pathol* 2011, **224**:5–9.

268. Karupiah G: **Type 1 and type 2 cytokines in antiviral defense.** *Vet Immunol Immunopathol* 1998, **63**:105–9.

269. Watanabe H, Numata K, Ito T, Takagi K, Matsukawa A: **Innate Immune Response in Th1- and Th2-Dominant Mouse Strains**. *Shock* 2004, **22**:460–466.

270. Szulc L, Gieryńska, Małgorzata Winnicka A, Martyniszyn L, Boratyńska-Jasińska, Anna Niemiałtowski M: **T cell cytokine synthesis at the single-cell level in BALB/c and C57BL/6 mice infected with ectromelia virus**. *Postep Hig Med Dosw* 2012, **3**:222–230.

271. Kuroda E, Kito T, Yamashita U: **Reduced Expression of STAT4 and IFN- in Macrophages from BALB/c Mice**. *J Immunol* 2002, **168**:5477–5482.

272. Kuroda E, Noguchi J, Doi T, Uematsu S, Akira S, Yamashita U: **IL-3 is an important differentiation factor for the development of prostaglandin E2-producing macrophages between C57BL/6 and BALB/c mice.** *Eur J Immunol* 2007, **37**:2185–95.

273. Mills CD, Kincaid K, Alt JM, Michelle J, Hill AM: **M-1/M-2 Macrophages and the Th1/Th2 Paradigm**. *J Immunol* 2000, **164**:6166–6173.

274. Chaudhri G, Panchanathan V, Buller RML, van den Eertwegh AJM, Claassen E, Zhou J, de Chazal R, Laman JD, Karupiah G: **Polarized type 1 cytokine response and cell-mediated immunity determine genetic resistance to mousepox.** *Proc Natl Acad Sci U S A* 2004, **101**:9057–62.

275. Galea I, Bechmann I, Perry VH: **What is immune privilege (not)?** *Trends Immunol* 2007, **28**:12–18.

276. Sloan DJ, Wood MJ, Charlton HM: **The immune response to intracerebral neural grafts**. *Trends Neurosci* 1991, **14**:341–346.

277. Wraith D, Nicholson L: **The adaptive immune system in diseases of the central nervous system**. *J Clin …* 2012, **122**.

278. Karupiah G, Xie Q, Buller RML, Nathan C, Duarte C, Macmicking JD: **Inhibition of Viral Replication by Interferon-y-Induced Nitric Oxide Synthase**. *Science (80-)* 1993, **261**(September):1445–1448.

279. Terajima M, Leporati AM: **Role of Indoleamine 2,3-Dioxygenase in Antiviral Activity of Interferon-gamma Against Vaccinia Virus.** *Viral Immunol* 2005, **18**:722–9.

280. Trilling M, Le VTK, Zimmermann A, Ludwig H, Pfeffer K, Sutter G, Smith GL, Hengel H: **Gamma interferon-induced interferon regulatory factor 1-dependent antiviral response inhibits vaccinia virus replication in mouse but not human fibroblasts.** *J Virol* 2009, **83**:3684–95.

281. Chesler DA, Reiss CS: **The role of IFN-gamma in immune responses to viral infections of the central nervous system.** *Cytokine Growth Factor Rev* 2002, **13**:441–54.

282. Randall RE, Goodbourn S: **Interferons and viruses: an interplay between induction, signalling, antiviral responses and virus countermeasures.** *J Gen Virol* 2008, **89**(Pt 1):1–47.

283. Jiang H, Clise-Dwyer K, Ruisaard KE, Fan X, Tian W, Gumin J, Lamfers ML, Kleijn A, Lang FF, Yung WKA, Vence LM, Gomez-Manzano C, Fueyo J: **Delta-24-RGD oncolytic adenovirus elicits anti-glioma immunity in an immunocompetent mouse model**. *PLoS One* 2014, **9**.

284. Rossi D, Zlotnik A: **The biology of chemokines and their receptors.** *Annu Rev Immunol* 2000, **18**:217–242.

285. **http://www.anticancer.net/en/gamma_interferon/**

286.**http://www.imd-berlin.de/en/fachinformationen/diagnostics-information/ip-10-a-new-marker-to-detect-cellular-immune-activation.html**

287. Saito T, Tanaka R, Yoshida S, Washiyama K, Kumanishi T: **Immunohistochemical analysis of tumor-infiltrating lymphocytes and major histocompatibility antigens in human gliomas and metastatic brain tumors.** *Surg Neurol* 1988, **29**:435–42.

288. Liu Y-P, Suksanpaisan L, Steele MB, Russell SJ, Peng K-W: **Induction of antiviral genes by the tumor microenvironment confers resistance to virotherapy.** *Sci Rep* 2013, **3**:1–20.

289. Kaplan DH, Shankaran V, Dighe AS, Stockert E, Aguet M, Old, Lloyd J. Schreiber RD: **Demonstration of an interferon γ-dependent tumor surveillance system in immunocompetent mice**. *Proc Natl Acad Sci USA* 1998, **95**:7556–7561.

290. Huysentruyt LC, Akgoc Z, Seyfried TN: **Hypothesis: are neoplastic macrophages/microglia present in glioblastoma multiforme?** *ASN Neuro* 2011, **3**:183–193.

291. Murtas D, Maric D, De Giorgi V, Reinboth J, Worschech a, Fetsch P, Filie a, Ascierto ML, Bedognetti D, Liu Q, Uccellini L, Chouchane L, Wang E, Marincola FM, Tomei S: **IRF-1 responsiveness to IFN-γ predicts different cancer immune phenotypes.** *Br J Cancer* 2013, **109**:76–82.

292. Kröger A, Köster M, Schroeder K, Hauser H, Mueller PP: **Activities of IRF-1**. *J Interf cytokine Res* 2002, **22**:5–14.

293. Monsurrò V, Beghelli S, Wang R, Barbi S, Coin S, Di Pasquale G, Bersani S, Castellucci M, Sorio C, Eleuteri S, Worschech A, Chiorini JA, Pederzoli P, Alter H, Marincola FM, Scarpa A: **Anti-viral state segregates two molecular phenotypes of pancreatic adenocarcinoma: potential relevance for adenoviral gene therapy**. *J Transl Med* 2010, **8**:1–11.

294. Geletneky K, Kiprianova I, Ayache A, Koch R, Herrero M, Deleu L, Sommer C, Thomas N, Rommelaere J: **Regression of advanced rat and human gliomas by local or systemic treatment with oncolytic parvovirus H-1 in rat models**. *Neuro Oncol* 2010, **12**:804–814.

295. Taylor JM, Barry M: **Near death experiences: Poxvirus regulation of apoptotic death**. *Virology* 2006, **344**:139–150.

296. Kalbacova M, Spisakova M, Liskova J, Melkova Z: **Lytic infection with vaccinia virus activates caspases in a Bcl-2-inhibitable manner.** *Virus Res* 2008, **135**:53–63.

297. Shisler JL, Moss B: **Immunology 102 at poxvirus U: avoiding apoptosis.** *Semin Immunol* 2001, **13**:67–72.

298. Byrd D, Shepherd N, Lan J, Hu N, Amet T, Yang K, Desai M, Yu Q: **Primary human macrophages serve as vehicles for vaccinia virus replication and dissemination.** *J Virol* 2014(April).

299. Humlová Z, Vokurka M, Esteban M, Melková Z: **Vaccinia virus induces apoptosis of infected macrophages.** *J Gen Virol* 2002, **83**(Pt 11):2821–32.

300. Broder CC, Kennedy PE, Michaels F, Berger EA: **Expression of foreign genes in cultured human primary macrophages using recombinant vaccinia virus vectors.** *Gene* 1994, **142**:167–174.

301. De Boüard S, Herlin P, Christensen JG, Lemoisson E, Gauduchon P, Raymond E, Guillamo J-S: **Antiangiogenic and anti-invasive effects of sunitinib on experimental human glioblastoma.** *Neuro Oncol* 2007, **9**:412–23.

302. Power AT, Bell JC: **Taming the Trojan horse: optimizing dynamic carrier cell/oncolytic virus systems for cancer biotherapy.** *Gene Ther* 2008, **15**:772–9.

303. Willmon C, Harrington K, Kottke T, Prestwich R, Melcher A, Vile R: **Cell carriers for oncolytic viruses: Fed Ex for cancer therapy.** *Mol Ther* 2009, **17**:1667–76.

304. Fulci G, Breymann L, Gianni D, Kurozomi K, Rhee SS, Yu J, Kaur B, Louis DN, Weissleder R, Caligiuri MA, Chiocca EA: **Cyclophosphamide enhances glioma virotherapy by inhibiting innate immune responses.** *Proc Natl Acad Sci U S A* 2006, **103**:12873–8.

305. Fulci G, Dmitrieva N, Gianni D, Fontana EJ, Pan X, Lu Y, Kaufman CS, Kaur B, Lawler SE, Lee RJ, Clay B, Brat DJ, Rooijen N Van, Rachamimov AS, Fred H, Weissleder R, Martuza RL, Chiocca EA: **Depletion of Peripheral Macrophages and Brain Microglia Increases Brain Tumor Titers of Oncolytic Viruses**. *Cancer Res* 2010, **67**:9398–9406.

306. Workenhe ST, Mossman KL: **Oncolytic Virotherapy and Immunogenic Cancer Cell Death: Sharpening the Sword for Improved Cancer Treatment Strategies**. *Mol Ther* 2013, **22**:251–256.

307. Taylor RC, Cullen SP, Martin SJ: **Apoptosis: controlled demolition at the cellular level.** *Nat Rev Mol Cell Biol* 2008, **9**:231–41.

308. Ledgerwood EC, Morison IM: **Targeting the apoptosome for cancer therapy.** *Clin Cancer Res* 2009, **15**:420–4.

309. Bao Q, Shi Y: **Apoptosome: a platform for the activation of initiator caspases.** *Cell Death Differ* 2007, **14**:56–65.

310. Brenner D, Mak TW: **Mitochondrial cell death effectors.** *Curr Opin Cell Biol* 2009, **21**:871–7.

311. Bratton SB, Salvesen GS: **Regulation of the Apaf-1-caspase-9 apoptosome.** *J Cell Sci* 2010, **123**(Pt 19):3209–14.

312. Ascierto ML, Worschech A, Yu Z, Adams S, Reinboth J, Chen NG, Pos Z, Roychoudhuri R, Di Pasquale G, Bedognetti D, Uccellini L, Rossano F, Ascierto PA, Stroncek DF, Restifo NP, Wang E, Szalay AA, Marincola FM: **Permissivity of the NCI-60 cancer cell lines to oncolytic Vaccinia Virus GLV-1h68.** *BMC Cancer* 2011, **11**:451.

313. Reinboth J, Ascierto ML, Chen NG, Zhang Q, Yu YA, Aguilar RJ, Carretero R, Worschech A, Zhao Y, Wang E, Marincola FM, Szalay AA: **Correlates between host and viral transcriptional program associated with different oncolytic vaccinia virus isolates.** *Hum Gene Ther Methods* 2012, **23**:285–96.

314. Weibel S, Raab V, Yu YA, Worschech A, Wang E, Marincola FM, Szalay AA: **Viral-mediated oncolysis is the most critical factor in the late-phase of the tumor regression process upon vaccinia virus infection.** *BMC Cancer* 2011, **11**:68.

315. Chen NG, Yu YA, Zhang Q, Szalay AA: **Replication efficiency of oncolytic vaccinia virus in cell cultures prognosticates the virulence and antitumor efficacy in mice**. *J Transl Med* 2011, **9**:164.

316. Eißmann M, Melzer IM, Fernández SBM, Michel G, Hrabě de Angelis M, Hoefler G, Finkenwirth P, Jauch A, Schoell B, Grez M, Schmidt M, Bartholomae CC, Newrzela S, Haetscher N, Rieger MA, Zachskorn C, Mittelbronn M, Zörnig M: **Overexpression of the anti-apoptotic protein AVEN contributes to increased malignancy in hematopoietic neoplasms.** *Oncogene* 2013, **32**:2586–91.

317. Kutuk O, Temel SG, Tolunay S, Basaga H: **Aven blocks DNA damage-induced apoptosis by stabilising Bcl-xL.** *Eur J Cancer* 2010, **46**:2494–505.

7 Appendices

7.1 List of Abbreviations

%	percent
°C	degree Celsius
µ	micro
2D	two-dimensional
3D	three-dimensional
AKT	protein kinase B
APAF-1	apoptosis protease activating factor 1
APC	allophycocyanin
APCs	antigen-presenting cells
APS	ammonium persulfate
ATRX	thalassemia/mental-retardation-syndrome-X-linked
Balb/c athymic nude	Hsd:Athymic Nude-Foxn1^{nu}
bp	base pair
BSS	Balanced Salt Solution
$C_3H_3NaO_3$	sodium pyruvate
C57BL/6 athymic nude	B6.Cg/NTac-*FoxN1*^{nu}
C57BL/6 IFN-γ KO	B6.129S7-*Ifngtm1Ts*/J
C57BL/6 wt	C57BL/6JOlaHsd
CAFs	cancer-associated fibroblasts
CDKN2A	cyclin-dependent kinase inhibitor 2A
cDNA	complementary DNA
CEV	cell-associated enveloped virion
cm	centimeter
CMC	carboxymethylcellulose
CNS	central nervous system
CPA	cyclophosphamide
CTLA-4	cytotoxic T-lymphocyte-associated protein 4
DAMP	damage-associated molecular pattern
DCs	dendritic cells
dd	double distilled
DMEM	Dulbecco's Modified Eagle Medium
DMSO	dimethyl sulfoxide
dpimp	days post implantation
e.g.	*exempli gratia* (for example)
ECL	enhanced chemiluminescence
ECM	extracellular matrix
ECTV	ectromelia virus
EDTA	ethylenediaminetetraacetic acid
EEV	extracellular enveloped virion
EGF, EGFR	epidermal growth factor/ receptor
EGFRL	epidermal growth factor receptor ligand
ER	endoplasmic reticulum

et al.	*et alii* (masuculine), *et aliae* (feminine)
FACS	flow cytometry
FBS	fetal bovine serum
FGF	fibroblast growth factor
FITC	fluorescein isothiocyanate
FSC	forward scatter
g	gram
GAPDH	glyceraldehyde 3-phosphate dehydrogenase
GBM	glioblastoma multiforme
GCP	granulocyte chemoattractant protein
G-CSF	granulocyte colony-stimulating factor
GCV	ganciclovir
GDNF	glial cell-derived neurotrophic factor
GFP	green fluorescent protein
GITR	glucocorticoid-induced tumor necrosis factor receptor related protein
GM-CSF	granulocyte macrophage colony-stimulating factor
GusA	β-glucuronidase
h	hour
h.i.	heat inactivated
H_2O_2	hydrogen peroxide
HGF/SF	hepatocyte growth factor/scatter factor
HMG-CoA	3-hydroxy-3-methylglutaryl-coenzyme A
hpi	hours post infection
HSV	Herpes simplex virus
i.e.	*it est* (in other words, it/that is)
i.p.	intraperitoneal
i.t.	intratumoral
i.v.	intravenous
ICAM	intercellular adhesion molecule
IEV	intracellular enveloped virion
IF	immunofluorescence
IFN	interferon
Ig	immunoglobulin
IL	interleukin
ILB4	Griffonia simplicifolia isolectin B4
IMV	intracellular mature virion
IP-10	interferon gamma-induced protein 10
IRF-1	interferon regulatory factor 1
IV	immature virion
K_3PO_4	tripotassium phosphate
KCl	potassium chloride
KH_2PO_4	monopotassium phosphate
$KHCO_3$	potassium bicarbonate
l	liter
LacZ	β-galactosidase
LOH	loss of heterozygosity
LPS	lipopolysaccharide

m	milli
M	molar
M1	classically activated macrophages/microglia
M2	alternatively activated macrophages/microglia
MCP	monocyte chemotactic protein
M-CSF	macrophage colony-stimulating factor
MDM2	mouse double minute 2 homolog
MDM	monocyte derived macrophage
MDSC	myeloid-derived suppressor cell
MeOH	methanol
$MgCl_2$	magnesium chloride
MGMT	O6-methylguanine-DNA methyltransferase
MHC	major histocompatibility complex
min	minute
MIP	macrophage inflammatory protein
MMP	matrix metalloproteinase
MOI	multiplicity of infection
MRI	magnetic resonance imaging
mTor	mammalian target of rapamycin
MTT	3-(4,5-dimethylthiazol-2-yl)-2,5-diphenyltetrazolium bromide
MV	measles virus
MΦ	macrophage
n.d.	not detectable
$Na_2HPO_4x12H_2O$	disodium phosphate hydrate
NaCl	sodium chloride
NaH_2PO_4	monosodium phosphate
$NaHCO_3$	sodium bicarbonate
NaN_3	sodium azide
NaOH	sodium hydroxide
NDV	Newcastle disease virus
NED	N-1-naphthyl-ethylenediamine dihydrochloride
NF-kB	nuclear factor kappa-light-chain-enhancer of activated B cells
NH_4Cl	ammonium chloride
NK cell	natural killer cell
nm	nanometer
NO	nitric oxide
NOS	nitric oxide synthases
OSC	organotypic brain slice culture
OV	oncolytic virus
PAMP	pathogen-associated molecular pattern
PBS	Phosphat Buffered Saline
PD-1	programmed cell death protein 1
PDGF, PDGFR	platelet-derived growth factor/ receptor
PE	phycoerythrin
PerCP	peridinin-chlorophyll proteins
pfu	plaque forming unit
PGE2	prostaglandin E2

pH	negative decimal logarithm of the hydrogen ion activity
PI	propidium iodide
PIP3	phosphatidylinositol (3,4,5)-trisphosphate
pro-MMP2	pro-matrixmetalloproteinase
PTEN	phosphatase and tensin homolog
P-TRITC	phalloidin tetramethylrhodamine in MeOH
Rb	retinoblastoma protein
rh	recombinant human
rm	recombinant murine
rpm	rounds per minute
RPMI	Roswell Park Memorial Institute
RT-PCR	reverse transcription polymerase chain reaction
RUC-GFP	Renilla luciferase – Aequorea green fluorescent protein
s	second
s.c.	subcutaneous
SCF	stem cell factor
SDF-1	stromal cell-derived factor-1
SDS	sodium dodecyl sulfate
SSC	sideward scatter
STATs	signal transducer and activator of transcription
TAA	tumor-associated antigen
TAM	tumor-associated macrophage
TEMED	N,N,N',N'-Tetramethylethylendiamin
TGF-β	tumor growth factor beta
T_H	T-helper cell
TIMP	tissue inhibitor of metalloproteinase
TK	thymidine kinase
TMZ	Temozolomide
TNF-α	tumor necrosis factor alpha
TRAIL	TNF-related apoptosis-inducing ligand
TReg	regulatory T cell
uPA	plasminogen activator
VACV	vaccinia virus
VCAM1	vascular cell adhesion protein 1
VEGF	vascular endothelial growth factor
vWF	von Willebrand factor
w/o	without
WB	Western blot
WHO	World Health Organization
wt	wild-type
α	alpha
α-	anti-
β	beta
γ	gamma

7.2 List of Tables

7.3 List of Figures

7.5 Publication List

Cecil A*, **Kober C***, Rohn S, Reinboth J, Weibel S, Schmidt J, Szalay AA, Dandekar T
Genetic variations of tumor cell lines and their specific differences in apoptosic pathways when confronted with the oncolytic vaccinia virus GLV-1h68
(to be submitted) *authors contributed equally

Kober C*, Rohn S*, Weibel S, Geissinger U, Chen NG, Szalay AA
Microglia and astrocytes attenuate the replication of the oncolytic vaccinia virus LIVP 1.1.1 in murine GL261 gliomas by acting as vaccinia virus traps
Journal of Translational Medicine (2015), 13:216; doi: 10.1186/s12967-015-0586-x
*authors contributed equally

Kober C, Weibel S, Rohn S, Kirscher L, Szalay AA
Intratumoral INF-γ triggers an anti-viral state in GL261 tumor cells: A major hurdle to overcome for oncolytic virotherapy of cancer
Molecular Therapy-Oncolytics (2015) 2, 15009; doi:10.1038/mto.2015.9

Kirscher L, Deán-Ben XL, Scadeng M, Zaremba A, Zhang Q, **Kober C**, Fehm TF, Razansky D, Ntziachristos V, Stritzker J, Szalay AA
Doxycycline Inducible Melanogenic Vaccinia Virus as Theranostic Anti-Cancer Agent
Theranostics 2015; 5(10):1045-1057. (doi:10.7150/thno.12533)

Donat U, Rother J, Schäfer S, Hess M, Härtl B, **Kober C**, Langbein-Laugwitz J, Stritzker J, Chen NG, Aguilar RJ, Weibel S, Szalay AA
Characterization of Metastasis Formation and Virotherapy in the Human C33A Cervical Cancer Model
PLOS one, 2014 Jun 2;9(6):e98533. (doi:10.1371/journal.pone.0098533)

Wong CC, Martincorena I, Rust AG, Rashid M, Alifrangis C, Alexandrov LB, Tiffen JC, **Kober C**; Chronic Myeloid Disorders Working Group of the International Cancer Genome Consortium, Green AR, Massie CE, Nangalia J, Lempidaki S, Döhner H, Döhner K, Bray SJ, McDermott U,Papaemmanuil E, Campbell PJ, Adams DJ.
Inactivating CUX1 mutations promote tumorigenesis
Nature Genetics, 2014 Jan; 46(1):33-8.(doi: 10.1038/ng.2846)

Weibel S, Hofmann E, Basse-Luesebrink TC, Donat U, Seubert C, Adelfinger M, Gnamlin P, **Kober C**, Frentzen A, Gentschev I, Jakob PM, Szalay AA
Treatment of malignant effusion by oncolytic virotherapy in an experimental subcutaneous xenograft model of lung cancer
J. Transl. Med., 2013 May 1;11:106. (doi:10.1186/1479-5876-11-106)

7.6 Conferences / Poster presentations

Kober C, Rohn S, Weibel S, Chen N.G, Szalay A.A
Endogenous IFN-γ levels and infiltration of microglia and astrocytes determine the efficacy of oncolytic vaccinia virus replication in murine GL261 glioma models
9th International Conference on Oncolytic Virus Therapeutics 2015, Boston (MA) (Abstract No. P-76)

Kober C, Rohn S, Weibel S, Chen N.G, Szalay A.A
Characterization of murine GL261 glioma models for oncolytic vaccinia virus therapy
13th Annual Meeting of the Association for Cancer Immunotherapy CIMT 2015, Mainz, (CIMT Abstracts No. 258)

Kober C, Rohn S, Weibel S, Chen N.G, Szalay A.A
Characterization of murine GL261 glioma models for oncolytic vaccinia virus therapy
9th International GSLS Students' Symposium (EUREKA!) 2014, Würzburg

17th International Vascular Biology Meeting 2012, Wiesbaden (attended)

7th International GSLS Students' Symposium 2012, Würzburg (attended)

7.7 Eidesstattliche Erklärung

Erklärung gemäß §4 Absatz 3 der Promotionsordnung der Fakultät für Biologie der Julius-Maximilians-Universität Würzburg:

Hiermit erkläre ich die vorgelegte Dissertation selbständig angefertigt zu haben und keine anderen als die von mir angegebenen Quellen und Hilfsmittel verwendet zu haben.

Des Weiteren erkläre ich, dass die vorliegende Arbeit weder in gleicher noch in ähnlicher Form bereits in einem anderen Prüfungsverfahren vorgelegt wurde.

Zuvor habe ich neben den akademischen Graden „Bachelor of Science“ und „Master of Science“ keine akademischen Grade erworben oder zu erwerben versucht.

Würzburg, den _____ _____

(Christina Kober)

7.8 Acknowledgements / Danksagung

An dieser Stelle möchte ich mich bei allen bedanken, die mir beim Erstellen dieser Arbeit mit Rat und Tat zur Seite standen.

Mein Dank gilt Herrn Prof. Dr. Aladar Szalay, der es mir ermöglichte meine Doktorarbeit in seiner Arbeitsgruppe am Lehrstuhl für Biochemie, am Biozentrum der Universität Würzburg zu absolvieren und zu beenden. Ich möchte mich für seine Unterstützung meiner wissenschaftlichen Ideen und sein Interesse an meiner Arbeit bedanken und dass er es mir ermöglicht hat an der 9. Internationalen Konferenz „Oncolytic Virus Therapeutics“ in Boston teilzunehmen.

Weiterhin möchte ich mich bei Herrn Prof. Dr. Frieder Grummt für das Korrekturlesen und sein Interesse an meiner Arbeit bedanken. Herrn Prof. Dr. Thomas Dandekar danke ich herzlich für die Übernahme des Zweitgutachtens.

Ein ganz besonderer Dank gilt Dr. Stephanie Weibel, die an der Planung dieses so spannenden Gliom-Projekts maßgeblich beteiligt war. Sie hat durch viele Gespräche und Diskussionen mit wichtigen Impulsen zum Fortschritt dieser Arbeit beigetragen und mich immer wieder mit Ihren Ideen inspiriert. Ich möchte Ihr dafür danken, dass Sie mich und meine Arbeit nicht vergessen hat und mich weiter unterstützt hat, auch nachdem Sie nicht mehr Teil dieser Arbeitsgruppe war. Das hat mit mir sehr viel bedeutet.

Ich möchte mich bei allen Kollegen der AG Szalay für die gute Zusammenarbeit und für die gemeinsame Zeit bedanken. Ich durfte interessante Menschen kennenlernen und es sind in dieser Zeit Freundschaften entstanden, die ich nicht mehr missen möchte.

Im Einzelnen gilt mein Dank Dr. Barbara Härtl, die vor allem im letzten Jahr eine sehr große Unterstützung für mich war. Ich danke Ihr, dass Sie die Zeit aufgewendet hat, meine Arbeit kritisch zu lesen und dadurch zu verbessern, für Ihre Hilfe bei allen Belangen rund um die Tieranträge und für die vielen Gespräche und Momente die wir zusammen verbracht haben.

Bei PD Dr. Ivaylo Gentschev möchte ich mich für seine Unterstützung, viele wissenschaftliche Diskussionen und Gespräche bedanken. Dr. Susanne Rohn danke ich für Ihre Mitarbeit bei meinem Gliom-Projekt und für Ihre praktische Unterstützung im AVEN-Projekt. Dr. Alexander Cecil danke ich für die gute Zusammenarbeit im AVEN-Projekt. Ich möchte mich bei Dr. Marion Adelfinger für die Hilfe rund um das FACS Gerät oder die Mäuse betreffend bedanken und die Gespräche während der gemeinsamen Mittagspausen. Ein großer Dank gebührt auch Johanna Langbein-Laugwitz für die reibungslose Organisation rund um das Labor, die Herstellung der Kryoschnitte, die vielen Aufmunterungen und Gespräche auch über das Labor hinaus. Ich

bedanke mich bei Dr. Thomas Basse-Lüsebrink für die gute Zusammenarbeit bei den MRT Messungen und die netten Gespräche nebenbei.

Ein besonderer Dank geht natürlich an meine Doktorandenkollegen, die entweder bis zum Schluss oder ein Teil des Weges an meiner Seite waren. Lorenz dir danke ich für dein optimistisches, positives und fröhliches Wesen, welches die Tage öfters mal wieder heller gemacht hat. Danke für die vielen Gespräche, in denen du mich aufgemuntert hast und deine konstruktiven Vorschläge bei meinen Projekten. Und auch dir Juliane, wir haben dieses Projekt (fast) zusammen angefangen und werden es zusammen beenden! Danke für die gute Zusammenarbeit, dass du meine Zumba Partnerin geworden bist und deine Freundschaft darüber hinaus. Sandeep, I appreciated it very much to work with you. It was really nice meeting you.

Ich möchte mich bei Johanna Schmidt bedanken, für Ihre Mithilfe beim AVEN-Projekt und die tolle Erfahrung ihre Bachelor-Betreuerin gewesen sein zu dürfen.

Mein Dank gilt auch Dr. Ulrike Donat, Dr. Carolin Seubert, Dr. Elisabeth Hoffmann, Dr. Ulrike Geissinger, Meike Müller die nun andere Wege gehen, deren Wissen und Methoden aber Teil dieser Gruppe sind. Ein weiterer Dank gebührt Jason Aguilar und Nanhai Chen (Genelux Corporation, San Diego) für die Produktion und Bereitstellung der Vaccinia Viren. Außerdem bedanke mich bei Dr. Stefan Schildknecht (Universität Konstanz) für die Bereitstellung der IMA2.1 Zellen, Dr. Marcus Karlstetter (Universitätsklinik Köln) für die BV-2 Microglia and Prof. Axel Pagenstecher (Universitätsklinik Marburg) für die Bereitstellung der GL261 Zellen.

Außerdem möchte ich mich bei Herrn Prof. Dr. Utz Fischer und den Mitarbeitern seines Lehrstuhls für das kollegiale Arbeitsverhältnis bedanken, vor allem Tanja Dambach für Ihre Hilfe bei allen bürokratischen Belangen.

Frau Dr. Ljubica Lozo danke ich für Ihr offenes Ohr und Ihren Beistand im Rahmen des Mentoring Programms und Frau Gisela Kaiser stellvertretend für die Unterstützung beim Beantragen und der Bewilligung meines Promotionsabschlussstipendiums.

Ich danke meinen Freunden, die immer wieder an mich gedacht haben und da waren während dieser Zeit.

Mein größter Dank gilt meinen Eltern, meinen beiden Schwestern, meiner wunderbaren Familie, auf die ich mich immer verlassen kann und konnte. Danke dass Ihr an meiner Seite seid, ich immer zu euch kommen kann und Ihr an mich glaubt.

Vor allem aber danke ich dir lieber Tobias. Danke dass du immer für mich da bist, dich für mich freust, mich aufmunterst, mich unterstützt, mich ablenkst, meine Sachen liest obwohl du sie nicht verstehst und dabei immer genau weißt was davon gerade nötig ist.